OPTIMIZED DIGITAL SIGNAL PROCESSING ALGORITHMS APPLIED TO RADIO COMMUNICATIONS

by

Alan James Auchmuty Carter

November, 1992.

Submitted in fulfilment of the academic requirements for the degree of Doctor of Philosophy in the Department of Electronic Engineering at the University of Natal.

OPTIMIZED DIGITAL SIGNAL PROCESSING ALGORITHMS APPLIED TO RADIO COMMUNICATIONS

by

Alan James Auchmuty Carter.

ABSTRACT

The application of digital signal processing to radio communications has come of age with the advent of low power, high speed microprocessors and over the past five years, various transceiver architectures, utilizing this new technology have been extensively researched. Due to the flexible nature of a software based transceiver, a myriad of possible applications exist and currently the emphasis is on the development of suitable algorithms.

The principal aim of this research is the derivation of optimized digital signal processing algorithms applicable to three separate areas of radio communications. Optimized, as used by the author within this dissertation, implies a reasonable compromise between performance, complexity and numerical processing efficiency. This compromise is necessary since the algorithms are applied to a portable transceiver where power consumption, size and weight are limited.

The digital signal processing algorithms described by this research is as follows:-

1. The derivation and assessment of a multirate speech amplitude modulation demodulator which exhibits low distortion (typically less than 2%) for a wide range of modulation indices, carrier frequency offsets and deviations. The demodulator is processing efficient and requires only five multiplications and five decisions for every output sample.

2. The derivation and assessment of a low sampling rate speech frequency modulation demodulator for signals whose bandwidth exceed quarter the sampling frequency. The demodulator exhibits low distortion (typically less than 2%) and is processing efficient requiring eighteen multiplications and three decisions for every output sample.

3. The derivation and assessment of a multirate single-sideband suppressed carrier automatic frequency control system which is a combination of a simple second order adaptive line enhancer and a digital phase-locked loop. The processing efficient automatic frequency control system is suited for low signal to noise power conditions, in both stationary and mobile communication channels.

PREFACE.

The Oxford dictionary [Swannell, 1986, pg. 180] defines engineering as the "application of science for control and use of power in machines; road-building etc." while the origin of the word engineer can be traced to the late Latin word ingenium meaning "ingenious invention" [Partridge, 1966, pg. 251].

In the mid-1980's a team of engineers at Grinaker Electronics in Pretoria, South Africa embarked upon the ambitious development of a wideband (20 to 400 MHz), multimode, portable **digital signal processing** (DSP) transceiver [Pengelley, 1992]. Each member of the team was responsible for a particular technology; Matthias Schmitz and Les Brand the analogue **reciter** (receiver/exciter), Danie Lindeque the frequency synthesizer, Paul Straub the power amplifier, Franswa Spies the control microprocessor and Alan Carter the low intermediate frequency DSP reciter. To solve the many practical problems within the different technology sectors ingenious solutions had to be found and developed, and working as a team, each member had of necessity to consider the effect that their part would have on the total system. This dissertation, which outlines solutions to some of the practical DSP problems, pays tribute to the team, of which the author was honoured to be part.

Since three unrelated problems and their solutions are discussed in this dissertation, the author has subdivided the body of the work into four separate chapters. Chapter two reviews suitable DSP techniques required for the development of the algorithms; while chapters three, four and five discuss the derivation of the three separate algorithms. The general structure of these three chapters is to first discuss previous research, outlining limitations and problems. An optimized solution is then presented making use of the DSP techniques outlined in chapter two. The chapter is then concluded by assessing the implementation of the solution.

The experimental and theoretical research described in this dissertation was carried out by the author in the DSP laboratory at Grinaker Electronics Limited, Pretoria, South Africa. The study was undertaken from February 1989 to December 1992 under the supervision of Professor A.D. Broadhurst of the University of Natal, Durban.

This research represents original work by the author and has not been submitted in any form to another University for any degree. Where use has been made of work carried out by others, it has been duly acknowledged in the text.

Signed: 

Date: 14th March, 1993.

ACKNOWLEDGEMENTS.

The following persons and organizations have been essential to this research and to them I extend my sincere thanks.

Professor A.D. Broadhurst for his patient guidance and caring supervision through the major part of my university career.

Dr. H.J. Coetzee and Mr. J.M. Harris who provided valuable assistance in reviewing this dissertation.

Mr. W.B. Wolmarans who provided the essential drafting support.

Mr. K.L. Bell, a technical director of Grinaker Electronics Ltd. who constantly advocated and supported this ambitious project.

The TR 600 team; Messrs. L.T. Brand, D.R. Lindeque, P.J. Straub, F.J. Spies and M.M.A. Schmitz without whom the DSP transceiver would not have become a reality.

Grinaker Electronics Ltd. and Denel (Pty) Ltd. for equipment and funding.

My Spiritual Father, my Mother, Father, David and friends who have supported me through the years of interesting and dynamic work.

To my wife Cindy, for her loyalty and unwavering support.

TABLE OF CONTENTS.

LIST OF FIGURES

LIST OF TABLES

LIST OF SYMBOLS.

A_c	Peak amplitude of carrier signal (volts).
$A_c(t)$	Time varying envelope of carrier signal (volts).
A_{IF}	Peak amplitude of local oscillator signal (volts).
A_m	Peak amplitude of modulating signal (volts).
A_o	Peak amplitude of demodulated signal (volts).
A_{ot}	True peak amplitude of demodulated signal (volts).
$A_c \cos \omega_c t$	A carrier signal (volts).
$A_{IF} \cos \omega_{IF} t$	A local oscillator signal (volts).
$A_m \cos \omega_m t$	A modulating signal (volts).
$a_1, a_2 \ldots$	Filter coefficients.
B_L	The noise bandwidth of PLL (hertz).
$b_1, b_2 \ldots$	Filter coefficients.
C_E	Complex envelope correlation.
C_i	Input carrier signal power (watts).
$E[n]$	Frequency estimate sample (volts).
$f(t)$	Continuous-time signal.
f_{AIF}	The IF frequency after sampling (hertz).
f_b	Modulation signal bandwidth (hertz).
f_{BIF}	The IF frequency before sampling (hertz).
f_{BW}	The -3 dB power bandwidth of a filter (hertz).
f_c	The carrier frequency (hertz).
f_D	Doppler frequency (hertz).
f_{FM}	The bandwidth of a FM signal (hertz).
f_{IF}	The IF frequency (hertz).

f_l	The lower frequency limit (hertz).
f_m	The modulating frequency (hertz).
f_{osc}	The local oscillator frequency (hertz).
f_{PD}	Peak Doppler frequency (hertz).
f_r	The resonance frequency (hertz).
f_s	The sampling frequency (hertz).
f'_s	Sampling frequency after decimation (hertz).
f_u	The upper frequency limit (hertz).
$F(s)$	The Laplace transform of $f(t)$.
$F(\omega)$	The Fourier transform of $f(t)$.
$F(z)$	The z transform of $f(t)$.
$F(\exp j\omega T_s)$	The Fourier transform of sampled $f(t)$.
f_{-6BW}	The -6 dB power bandwidth of a filter (hertz).
G_{ACT}	NCO/TCXO actual gain.
G_{UNI}	NCO/TCXO unity gain.
$H(\omega)$	The Fourier transform of $h(t)$.
$H_{PLL}(s)$	Closed-loop PLL transfer function.
$H(z)$	The z transform of $h(t)$.
$H_{BP}(\exp j\omega T_s)$	Sampled bandpass filter's response.
i	Iteration counter.
$I[n]$	The nth sample of the in-phase signal (volts).
$I(t)$	The continuous-time in-phase signal (volts).
$Im\{\ \}$	The imaginary part of a signal.
k	An integer value.
K	FM modulator constant.
K_o	Voltage controlled oscillator gain.
K_d	Phase detector gain.
K_{DC}	DC loop gain of a PLL.

l	An integer value.
m	The AM modulation index (ratio).
M	Maximum of either I or Q vector.
$m(t)$	A modulating time dependant signal (volts).
n	An integer value.
N	Minimum of either I or Q vector.
N_i	Input noise power (watts).
N_o	Output noise power (watts).
$p(A_c)$	Pdf of the envelope of a fading signal.
P_{IM}	Error image signal power (watts).
P_o	Output signal power (watts).
P_m	Total power in AM sidebands (watts).
P_{md}	Total power in the modulation signal (watts).
q	Number of bits of accuracy.
$Q[n]$	The nth sample of the quadrature signal (volts).
$Q(t)$	The continuous-time quadrature signal (volts).
r	IIR-ALE's filter coefficient.
R	The magnitude of a complex number (volts).
$Re\{\ \}$	The real part of a signal.
$r(t)$	A general amplitude modulating signal (volts).
$S(t)$	Switching function.
S_o	Output signal power (watts).
T_{Dt}	Urban time delay spread (seconds).
T_{ds}	Sampling time difference (seconds).
T_n	The nth sample period (seconds).

T_p	Wave propagation time (seconds).
T_s	Sampling period (seconds).
T'_s	Sampling period after decimation (seconds).
v_m	Mobile unit's velocity (meters per second).
$V_i(t)$	Time dependant input signal (volts).
$\overline{V}_i(t)^2$	Mean squared value of signal (volts^2).
$V_o(t)$	Time dependant output signal (volts).
$V_{dt}(t)$	The differentiated signal (volts).
$w[n]$	IIR-ALE's adaptive filter coefficient.
$w_{IIR}[n]$	The steady state value of $w[n]$.
$x(t)$	Continuous-time signal (volts).
$\|x\|$	The absolute value of x.
$X[n]$	The nth sample of the input signal (volts).
$X(z)$	The z transform of the input signal.
X_o	Integer to be square rooted.
$X(\exp j\omega T_s)$	The Fourier transform of sampled $x(t)$.
y_{i-1}	An iteration variable.
Y_{q-1}	Square root of X_o.
$Y(z)$	The z transform of the output signal.
$Y[n]$	The nth sample of the output signal (volts).
$Y(\exp j\omega T_s)$	The Fourier transform of sampled $y(t)$.
z^{-1}	The unit delay operator.
Z	Complex vector.
$\%D_{dt}$	Differentiator percentage harmonic distortion.
$\%D_{HIL}$	Hilbert transform percentage harmonic distortion.

$\%D_{MOD}$	Modulus function percentage harmonic distortion.
$\%D_{QUAD}$	I and Q gain/phase error percentage distortion.
$\%D_{SL}$	Square law demodulator % harmonic distortion.
$\%THD_{AM}$	AM demodulator percentage total harmonic distortion.
$\%THD_{FM}$	FM demodulator percentage total harmonic distortion.
α	Amplitude error ratio between the I and Q signals.
$\alpha_{IIR}[n]$	Gradient of the error function.
$\alpha_{MIIR}[n]$	Modified gradient of the error function.
β	FM modulation index (ratio).
β_F	The IIR-ALE's forgetting factor.
γ	The phase error between the I and Q signals.
$\Gamma_c(\omega)$	VCO input noise spectral density (volts^2/Hz).
$\Gamma_n(\omega)$	Input noise spectral density (volts^2/Hz).
Δf	Peak frequency deviation (hertz).
$\Delta\omega$	A frequency step (radians/sec).
$\Delta\dot{\omega}$	A frequency ramp (radians/sec^2).
ϵ_{dt}	Differentiator's fractional error function.
ϵ_{HIL}	Hilbert transformer's fractional error function.
$\epsilon_{IIR}[n]$	IIR-ALE error function.
ϵ_{MOD}	Modulus function's fractional error function.
ϵ_{Pdt}	Differentiator's peak fractional error (ratio).
ϵ_{PHIL}	Hilbert transform's peak fractional error (ratio).
ϵ_{PMOD}	Modulus function's peak fractional error (ratio).
ζ	Damping factor of second order loop.

θ	Phase angle of a transformed vector (radians).
θ_a	Acceleration error (radians).
θ_D	Angle of incidence (radians).
θ_v	Static phase error (radians).
κ	A constant value.
λ_c	Wavelength of carrier.
μ	The AM transmission efficiency (ratio).
ξ	A subsector's constant.
ρ	A subsector's constant.
σ	Standard deviation of a Gaussian distribution.
Σ	Summation of two or more signals.
τ_1, τ_2	PLL loop filter time constants (seconds).
τ'_1, τ'_2	DPLL loop filter time constants.
τ_{RC}	Time constant of RC filter.
υ	IIR-ALE convergence parameter.
$\phi(t)$	Time dependant phase angle (radians).
ϕ	Phase angle (radians).
χ	Subsector's starting phase angle (radians).
ψ	Phase angle of subsector (radians).
$\psi_{MIIR}[n]$	Power of modified error gradient vector.

ω	Angular frequency in radians per second.
ω_b	The -3 dB angular frequency bandwidth.
ω_c	Angular frequency of carrier.
ω_{cs}	RF angular frequency separation.
ω_{IF}	Angular frequency of local oscillator.
ω_m	Angular frequency of modulating signal.
ω_n	Second order PLL natural angular frequency.
ω'_n	Prewarped PLL natural angular frequency.
ω_s	Angular sampling frequency.

LIST OF ABBREVIATIONS.

+/-	plus or minus.
A/D	Analogue-to-digital converter.
AFC	Automatic frequency control.
AGC	Automatic gain control.
ALE	Automatic line enhancement.
AM	Amplitude modulation.
AR	Autoregressive.
ARMA	Autoregressive-moving average.
bit	Binary digit.
bits/s/Hz	Bits per seconds per Hertz.
CNR	Carrier to noise power ratio (dB).
CNR_i	Input carrier to noise power ratio (dB).
CORDIC	Coordinate rotation digital computer.
CPM	Continuous-phase modulation.
CW	Carrier wave.
dB	The ratio of $10\log X/Y$.
dBV	The ratio of $20\log(V_{RMS}/1V_{RMS})$.
DC	Direct current.
DEMOD	Demodulator.
DFT	Discrete Fourier transform.
DHT	Discrete Hilbert transform.
DPLL	Digital phase-locked loop.
DPSK	Differential phase-shift keying.
DPTCT	Dual-pilot tone calibration.
DSB-SC	Double-sideband suppressed carrier.

DSP	Digital signal processing.
DTL	Digital tanlock loop.
D/A	Digital-to-analogue converter.
EKF	Extended Kalman filter.
FFT	Fast Fourier transform.
FIR	Finite impulse response.
FM	Frequency modulation.
FSK	Frequency-shift keying.
GG	Gradient gain of AFC system.
GMSK	Gaussian-filtered minimum shift keying.
GTFM	Generalized tamed frequency modulation.
HF	High frequency; typically 2 to 30 MHz.
Hz	Hertz (cycles per second).
I and Q	In-phase and quadrature signal pair.
IF	Intermediate frequency.
IIR	Infinite impulse response.
IIR-ALE	Infinite impulse response adaptive line enhancer.
Kbits/s	Kilobits per second.
kHz	Kilohertz.
KSPS	Kilosamples per second.
LMR	Land mobile radio, which include radiotelephones, packet radios and radio paging systems.
LMS	Least mean square.
LO	Local oscillator.
LP	Linear prediction.
LSB	Lower sideband.

MA	Moving average.
MAP	Maximum a posteriori.
MHz	Megahertz.
MIC	Microphone input.
ML	Maximum likelihood.
MRLMS	Modified normalized recursive least mean squares.
MSE	Mean square error.
MSPS	Megasamples per second.
MUSIC	Multiple signal classification.
MUX	Multiplexer.
MV	Minimum variance.
NCO	Numerically controlled oscillator.
NRLMS	Normalized recursive least mean squares.
PC	Pilot carrier.
pdf	Probability density function.
PEP	Peak envelope power.
PLL	Phase-locked loop.
ppm	Parts per million.
PSAM	Pilot symbol assisted modulation.
PSK	Phase-shift keying.
%	Percent.
%THD	Percentage total harmonic distortion.
QAM	Quadrature amplitude modulation.
QPSK	Quadrature phase-shift keying.
Reciter	Receiver/ exciter.
RF	Radio frequency.
RLS	Recursive least squares.
RLMS	Recursive least mean squares.
ROM	Read only memory.
Rx	Receive.

SD	Standard deviation.
sec	Second.
S/H	Sample and hold.
SNR	Signal to noise power ratio (dB).
SNR_i	Input signal to noise power ratio (dB).
SNR_o	Output signal to noise power ratio (dB).
Squelch	Speech in noise detection.
SSB	Single-sideband.
SSB-SC	Single-sideband suppressed carrier.
TCXO	Temperature compensated crystal oscillator.
THD	Total harmonic distortion.
TAB	Tone-above-band.
TIB	Tone-in-band.
TTIB	Transparent tone-in-band.
Tx	Transmit.
UHF	Ultra high frequency; typically 200 to 400 MHz.
USB	Upper sideband.
VCO	Voltage controlled oscillator.
VHF	Very high frequency; typically 30 to 200 MHz.
VLSI	Very large scale integrated.
V/UHF	Very to ultra high frequency; typically 30 to 400 MHz.

CHAPTER 1

INTRODUCTION AND OVERVIEW OF RESEARCH.

Historically, as integrated circuit technology progressed, many developments took advantage of the improvements offered. Radio transceivers were no exception and over the last five years there has been a significant increase in products incorporating **digital signal processing** (DSP) integrated circuits. Typically, DSP offers numerous advantages over conventional analogue techniques, which include; software flexibility, multi-functionality, previous generation compatibility, ease of manufacture and improved performance.

In the mid-1980s Rockwell International Corporation in the United States of America, announced their HF-2050 DSP receiver which is capable of operation in the very low to **high frequency** (HF) bands [Anderson & Whikehart, 1985]. The receiver detects a number of modulation types, which include **single-sideband** (SSB), **carrier wave** (CW) and **amplitude modulation** (AM). Figures 1.1 (a) and (b) give the block diagram of both the receiver, and the sampling rates used at each of the stages. Due to the processing speed limitations of the digital technology which prevents sampling at the antenna, the design combines analogue and DSP **intermediate frequency** (IF) stages to demodulate the signal.

The first DSP IF stage is at 3 MHz and the wide, linear, dynamic range is obtained by an oversampling technique described by Claasen, Mecklenbrauker, Peck & van Hurck [1980]. The IF signal is oversampled which spreads the sample noise (due to the finite resolution of the **analogue-to-digital converter** (A/D)) over a far greater bandwidth than that of the modulated IF signal. The wideband signal is then filtered, before processing, to increase the **signal to noise power**

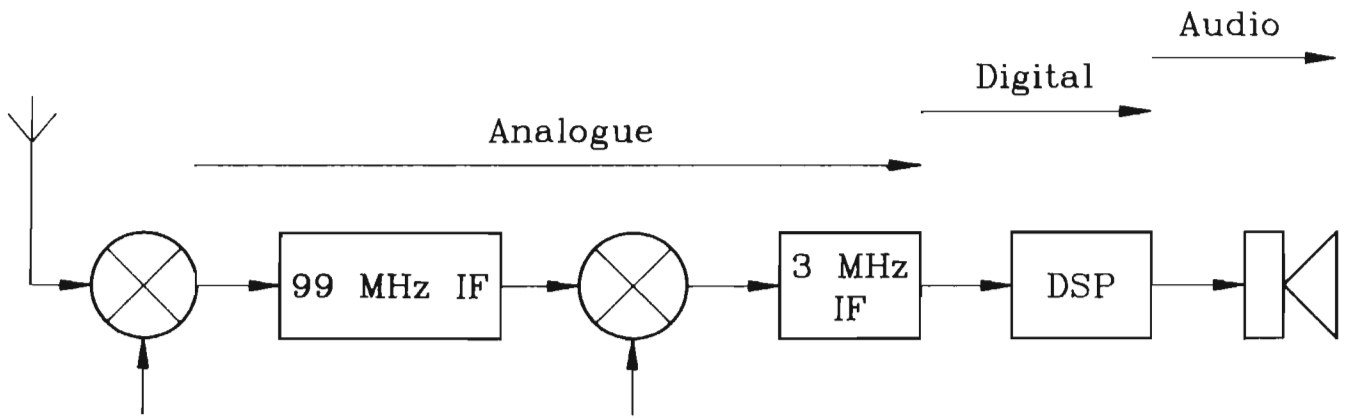

Figure 1.1(a) The HF-2050 block diagram showing the DSP integration.

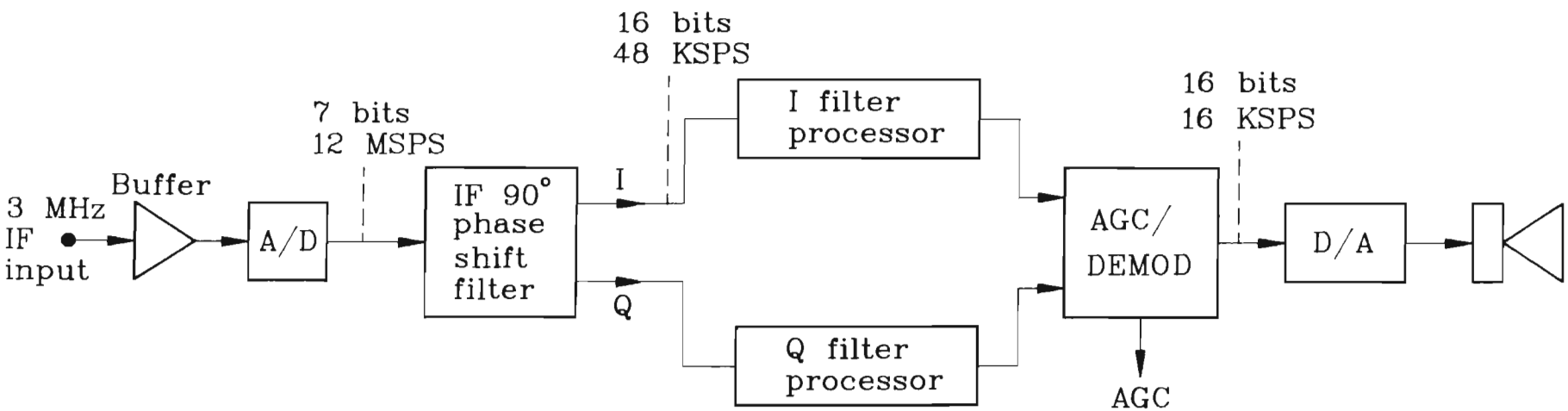

Figure 1.1(b) The DSP section of the HF-2050 showing processing rates.

ratio (SNR) and thus the dynamic range. The final IF stage is a baseband (or zero Hz), quadrature structure which also controls the gain of the analogue amplifiers.

Although the dynamic performance of the HF-2050 is impressive, four DSP microprocessors are required to demodulate and control the signal due to the high sampling rates and selection of IF frequency. This approach is prohibitive for the low current, light weight requirement of a portable transceiver.

Harris Corporation, in the United States of America, in 1989, introduced the vehicle mounted RF-5000 HF SSB digital radio system. It is reported that the transceiver includes a DSP IF, Linear Predictive Vocoder and various low to high speed modem options however, little has been published on the techniques used within the transceiver [Hayes, 1987]. Wideband and multimode operation are two of the current transceiver design trends in military and para-military communications, although conventionally, due to the practical implementation of transceivers, the spectrum has been broken into three bands with different speech modulation modes for each. The convention being, SSB and AM in the HF band, **frequency modulation** (FM) in the **very high frequency** (VHF) band and AM in the **ultra high frequency** (UHF) band.

Although new technology, due to high cost and risk, is often first developed by the military it is noteworthy that DSP is already being applied to commercial radio communications. Kenwood in Japan, have recently announced the TS-950S digital HF transceiver [Hart, 1990] which is aimed at amateur radio users. The TS-950S employs DSP techniques to generate the SSB, CW, **frequency-shift keying** (FSK), and AM signals on transmit while on receive the DSP unit provides an audio filtering function.

Increases in data transmission and system capacity requirements, combined with the need for security has resulted in the development of a **very large scale integrated** (VLSI) DSP demodulator circuit for land mobile radio applications [Saulnier, Puckette, Gaus, Dunki-Jacobs & Theil, 1990]. This circuit interfaces at a high IF (4 MHz) and requires bandpass filtering before sampling. By using an undersampling technique, generally known as subharmonic sampling, the high IF is frequency translated to a lower frequency where the new IF frequency is one quarter of the final sampling frequency. Being commercial and requiring high fidelity, FM is the preferred speech modulation scheme and consequently digital FM techniques are normally utilized. Digital FM techniques include **Gaussian-filtered minimum shift keying** (GMSK), **generalized tamed frequency modulation** (GTFM) and **continuous-phase modulation** (CPM) [Ohno & Adachi, 1990]. Since anticipated production volumes for land mobile radios are large it is preferable to design dedicated, limited functionality, VLSI integrated circuits, which affects the structure of the demodulator as the objective is to reduce the complexity and size of the circuit [Saulnier & Rafferty, 1990]. Although DSP microprocessors have the advantage of software flexibility and are thus used for specialized applications, they are often more costly and incur the added expense of software development.

1.1 A DISCUSSION ON DIGITAL SIGNAL PROCESSING RADIO ARCHITECTURES.

When applying DSP to radio communications two different receiver architectures have been adopted; the baseband IF and the low frequency IF. The baseband IF (see figure 1.2) is implemented by mixing the **radio frequency** (RF) signal to baseband with 90 degree phase shifted local oscillators at the RF signal's frequency. The dual channel, baseband **in-phase and quadrature signal pair** (I and Q) signals are then sampled by two analogue-to-digital converters whose outputs are used in the detection of phase and amplitude modulated signals.

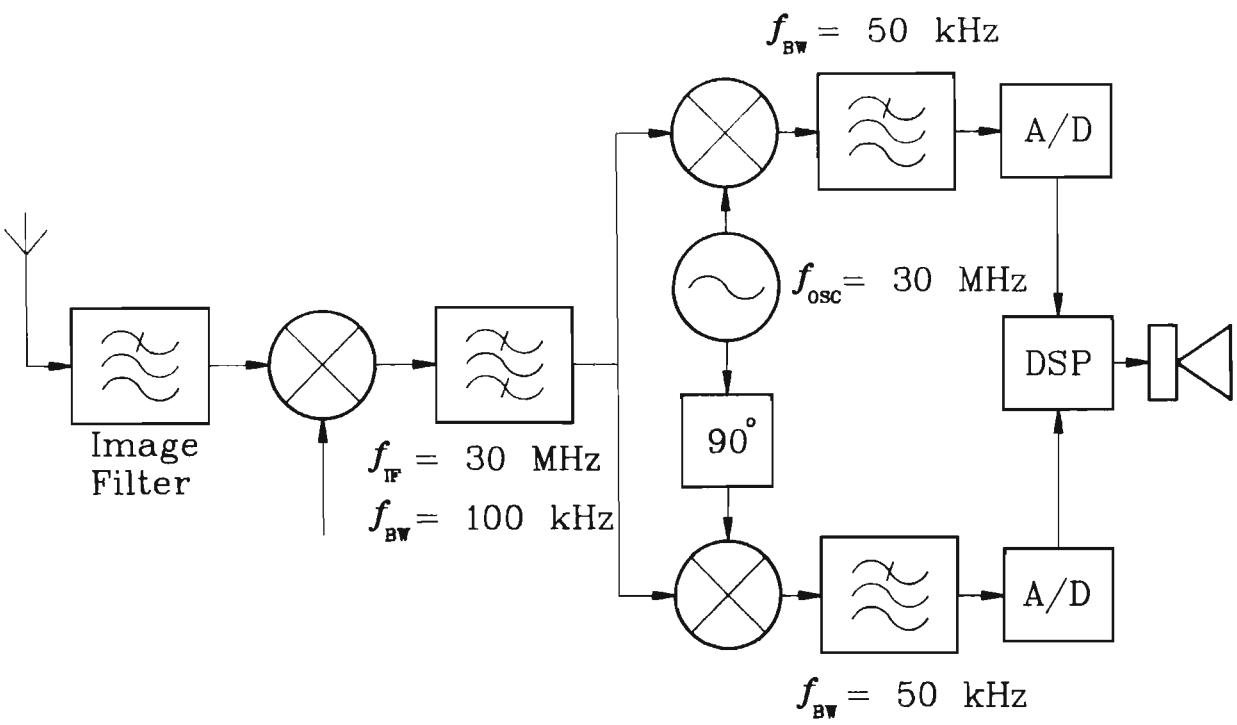

Figure 1.2 DSP applied to a baseband architecture.

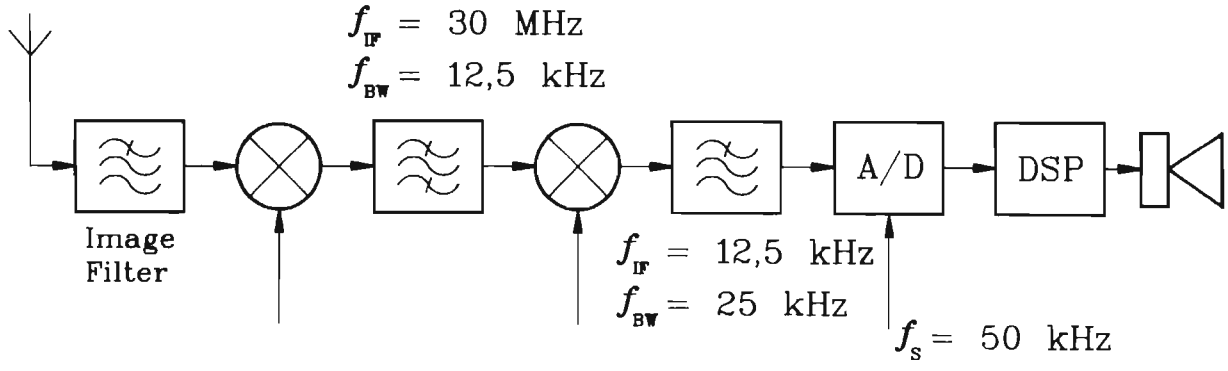

Figure 1.3 DSP applied to a low frequency IF.

This architecture is useful as baseband sampling implies a slower sampling rate and is typically used in wideband applications, for example, surveillance receivers [Roome & Griffin, 1991]. A baseband IF architecture suffers from numerous practical implementation problems which include various effects caused by the local oscillator [Hamilton, 1991] for example; mismatches in amplitude and phase between the I and Q signals and **direct current** (DC) offsets [Brown, Dewey & Collier, 1986]. These practical problems were experienced by Kruger [1986] in the implementation of a digital receiver utilizing sampled analogue I and Q signals followed by digital demodulation implemented within a DSP microprocessor. Churchill, Ogar & Thompson [1981] suggest a numerical technique to correct for these errors, although this requires extra processing. Alternatively, Loper [1990] suggests using a novel tri-phase baseband receiver where the extra channel is employed to correct for any phase and amplitude mismatches. This approach however, implies a complex analogue interface where three signals need to be sampled simultaneously.

As an alternative solution to these problems numerous researchers have suggested the concept of a low frequency DSP IF and a typical block diagram of this architecture is shown in figure 1.3. Early references to this architecture include a prototype receiver developed at the University of Birmingham, United Kingdom [Bagwell & Considine, 1985] and a prototype transceiver designed at Grinaker Electronics, South Africa [Carter, 1986]. Typically the low DSP IF tends to be in the region of 10 to 30 kHz. In a effort to move the digital processing closer to the antenna in receivers, there has been a trend to undersample analogue bandlimited high IF stages (> 400 kHz) to allow digital interfacing at these higher frequencies. Restrictions in the aperture uncertainty of the A/D's preceding sample and hold [Masterton, Benn, Dolman, Roberts, Breakenridge & Rambaut, 1991] tends to limit the conversion resolution at the higher frequencies. Similarly, if in a transmitter the same high IF interface is required; instead of frequency mixing, this could be achieved by filtering out one of the sampling

harmonic lobes caused by the **digital-to-analogue converter** (D/A). As with undersampling however, this approach is also limited due to the roll off of the higher frequency lobes and the consequent degradation in the transmitted SNR; therefore in the design of a digital transceiver it is often simpler to use the same low IF for both receive and transmit [Carter, 1988].

Although the low DSP IF solves the problems associated with a baseband IF less processing time is available due to the faster sampling rates inherently required by this architecture. To emphasize the problem consider the processing required for **single-sideband** (SSB) reception in the **very to ultra high frequency** (V/UHF) range. This modulation mode requires SSB detection, **automatic gain control** (AGC), **automatic frequency control** (AFC), **speech in noise detection** (squelch) and serial communications with a host controller all in real-time. Although extensive research has to date been conducted on the optimum selection of a DSP IF architecture, the need to research and assess the dynamic performance of efficient DSP transceiver software algorithms still exists.

1.2 A DISCUSSION OF A PORTABLE DIGITAL SIGNAL PROCESSING TRANSCEIVER.

Figure 1.4 is a block diagram of a typical portable DSP transceiver where the last low frequency IF stage is digitized. The block diagram, depending on synthesizer and IF frequency selection, is applicable to a wide frequency range of operation, however, for the purpose of this dissertation it is assumed that the multimode transceiver operates within the V/UHF (30 to 400 MHz) band. Furthermore, it is assumed that the following general parameters apply to the transceiver:-

1. The choice of the DSP IF frequency is 12,5 kHz which is a combination of the bandwidth of the anti-aliasing filter and synthesizer resolution.

2. The second analogue IF stages includes a crystal filter. The crystal filter is the anti-aliasing filter on Rx and removes the sampling harmonics on Tx.

3. The -3 **decibel** (dB) power bandwidth of the crystal filter is 15 kHz which is a function of the maximum permissible transmission bandwidth allowed for FM by the transceiver.

4. The -3 dB audio power bandwidth is 300 Hz to 2,7 kHz.

5. The sampling rate, to prevent aliasing of the IF signal, is 50 kHz, which is four times the DSP IF. This implies that 20 microseconds of processing time is available between IF samples. However, since a four times decimation or undersampling is sometimes employed in demodulation, typically 80 microseconds occurs between each of the final demodulated signal's samples.

6. Since the transceiver is portable, power consumption and weight is minimized. This implies that the DSP IF hardware is limited to a single, fixed point DSP microprocessor with 8 kilowords of external program and data memory and a single low power A/D converter. Any other integrated circuits are assumed to have a negligible effect on the total current consumption.

Figure 1.4 A block diagram of a typical portable wideband transceiver.

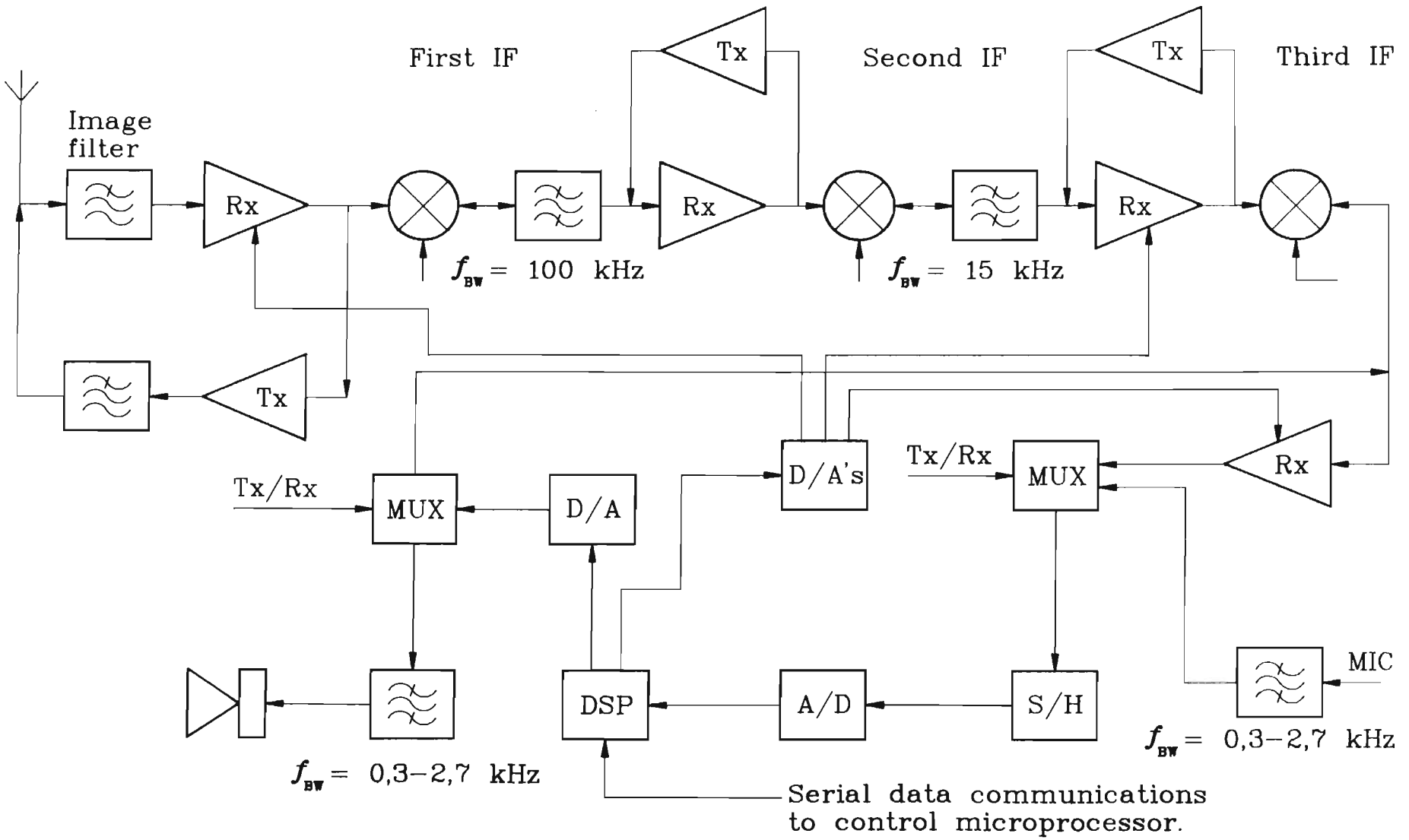

1.3 AN OUTLINE OF THIS DISSERTATION AND THE AUTHOR'S PERSONAL CONTRIBUTION.

The principle aim of the author's research has been to derive optimized DSP algorithms applicable to radio communications. Optimized as used by the author is a suitable compromise between performance, complexity and numerical processing efficiency. Originality is claimed by the author for the following contributions to digital signal processing applied to radio communications:-

1. The derivation and assessment of a multirate speech amplitude modulation demodulator which exhibits low distortion (typically less than 2%) for a wide range of modulation indices, carrier frequency offsets and deviations.

2. The derivation and assessment of a low sampling rate speech frequency modulation demodulator for signals whose bandwidth exceed quarter the sampling frequency. The demodulator which is processing efficient exhibits low distortion (typically less than 2%) for a wide range of frequency deviations.

3. The derivation and assessment of a multirate **single-sideband suppressed carrier** (SSB-SC) AFC system which involves the combination of a simple second order **infinite impulse response adaptive line enhancer** (IIR-ALE) and a **digital phase-locked loop** (DPLL). The processing efficient automatic frequency control system is suited for low signal to noise power conditions, in both stationary and mobile communication channels.

This dissertation is divided into four main chapters to address each of the author's originality claims. In chapter 2 suitable DSP techniques required for the derivation of the three separate algorithms are reviewed. The techniques are introduced in the order required by subsequent chapters.

Chapter 3 is the derivation and assessment of the multirate AM demodulator and chapter 4, the low sampling rate FM demodulator. Furthermore, chapter 5 discusses the derivation and assessment of the multirate IIR-ALE/DPLL AFC algorithm for speech SSB-SC communications. Each of these chapters is subdivided into three sections:-

1. An introduction discussing previous research and outlining limitations and problems.

2. The optimized solution to the problem addressed by the chapter, which typically utilizes various DSP techniques as outlined in chapter 2.

3. An analysis and evaluation of a fixed point, real-time implementation of the solution.

Chapter 6 concludes this dissertation with various recommendations and further proposed areas of research.

CHAPTER 2

A COLLECTION OF DSP TECHNIQUES APPLIED TO RADIO COMMUNICATIONS.

This dissertation concerns the derivation and evaluation of three different DSP algorithms and their application to radio communications. The three algorithms are, a multirate AM demodulator, a low sampling rate FM demodulator and a SSB-SC AFC system. This chapter introduces background concepts and principles used by each of these algorithms. Although the algorithms are different, occasionally they make use of common DSP techniques and therefore it is not possible to categorize the different techniques according to the algorithm they support. Consequently the author has elected to discuss the techniques in the sequential order required by subsequent chapters. Each separate technique begins with a motivation for its inclusion, and its relationship to the proposed algorithms.

2.1 TECHNIQUES FOR CREATING QUADRATURE SIGNALS.

By splitting a real signal into two 90 degree phase shifted signals, a quadrature signal pair is created. This is a complex signal, which has the advantage that it can be utilized to obtain both the amplitude and phase of the original carrier and consequently, is often used in the demodulation of AM and FM signals [Kruger, 1986].

This section reviews the techniques for creating quadrature signals. It is expedient to simultaneously extend the review to consider the types of errors (phase, amplitude and group delay) caused, and structural limitations of the various techniques. There are three groups of techniques for creating baseband I and Q signals described

by the current literature. The three groups are, mixing, sampling and filtering. Often the techniques are combined with decimation in order to match the sampling rate with the bandwidth of the modulating signal.

2.1.1 Mixing techniques to create I and Q signals.

The conventional mixing approach, as shown in figure 2.1, is to use analogue processes. Mixers with 90 degree phase shifted local oscillators are used to phase shift the signal. This is followed by lowpass filters to remove the double frequency terms. Separate, synchronized A/D's, then sample the two channels which results in digitized baseband I and Q signals. As outlined in chapter 1 the problems associated with this method are; difficulty in accurately balancing the phase and amplitude between the different local oscillators and an inflexible double channel IF structure. However in the situation where a wide bandwidth is required ie: surveillance receivers [Roome & Griffin, 1991] this technique is used to minimize the processing requirement.

A more recent technique described by Liu, Ghafoor & Stockmann [1989], has a structure as shown in figure 2.2. The signal is down converted to a minimum IF frequency whose frequency is dependant on the modulation bandwidth. Following the down conversion the signal is sampled and mixed with synthesized quadrature local oscillators, which results in the I and Q signals. Furthermore, Liu et al. [1989] describe a simple technique of creating the quadrature local oscillator signals which does not suffer from the analogue mismatch problems. However, since their primary function is to use the I and Q signals for frequency domain processing it is unnecessary to filter the double frequency component as it can simply be ignored. This is not possible for time

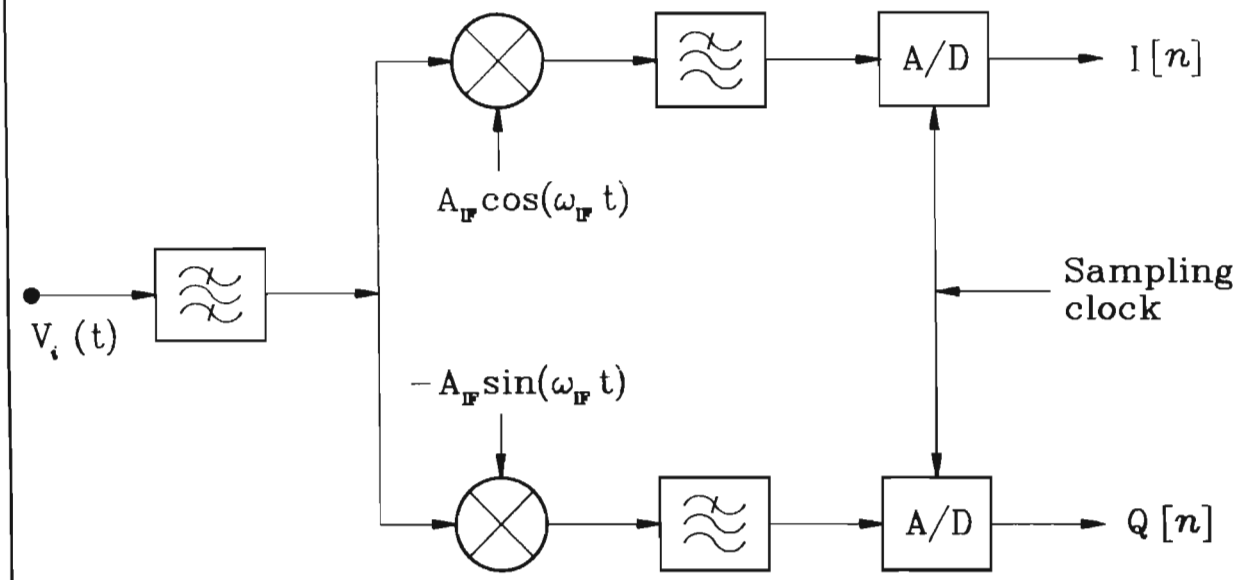

Figure 2.1 Analogue technique to obtain I and Q signals.

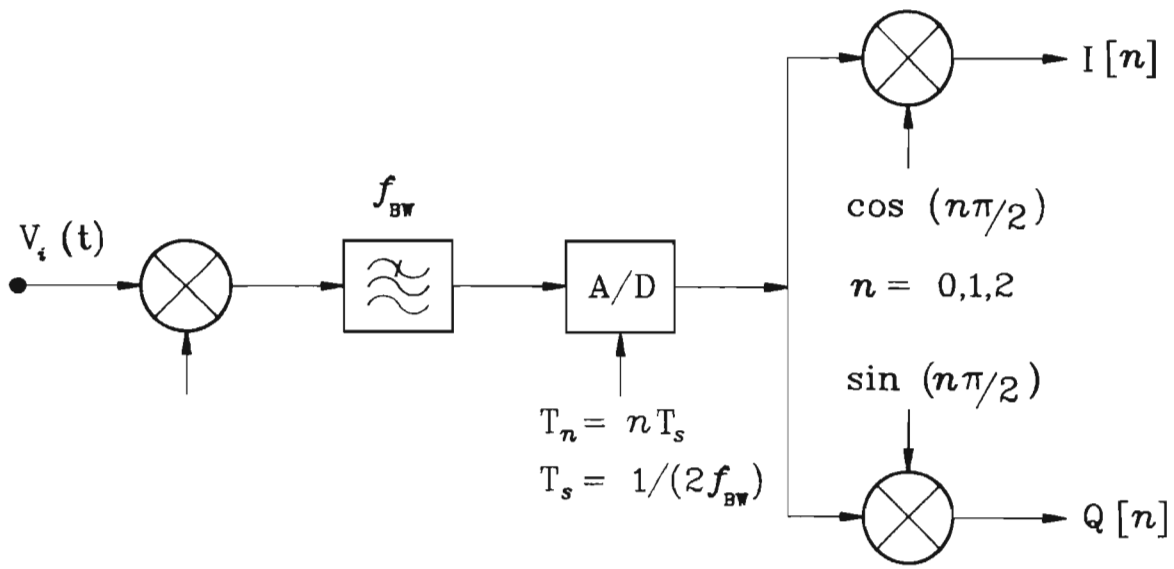

Figure 2.2 Liu et al.'s [1989] digital technique of creating I and Q signals.

domain processing and two filters are required to remove the double frequency terms. This implies further processing which can be avoided by using a sampling or filtering approach to I and Q signal creation.

2.1.2 Sampling techniques to create I and Q signals.

The fundamental relationship between the spectrum of the continuous-time signal and its sampled counterpart, is given by

$$F(\exp j\omega T_s) = \frac{1}{T_s} \sum_{n=-\infty}^{\infty} F(\omega + n\omega_s) \ , \qquad (2\text{-}1)$$

where ω_s is the angular sampling frequency. T_s is the sampling period and $F(\omega)$ is the Fourier transform of the continuous-time signal $f(t)$.

From this expression it is apparent that sampling causes a frequency translation or modulation and it is therefore reasonable to suspect that sampling could be employed to create I and Q signals. The concept of quadrature sampling of a bandpass signal has been extensively reviewed in the literature and two approaches are described; second order [Kohlenberg, 1953; Grace & Pitt, 1968, 1970] and more recently, first order sampling [Brown, 1979, 1980, 1983]. Second order sampling implies that the sample periods, although repetitive, are not equal, while first order sampling implies repetitive and equal sampling periods. An excellent summary of the theory of bandpass sampling and its associated implementation problems, is provided by Vaughan, Scott and White [1991] while Liu et al. [1989] describe how to apply quadrature sampling to frequency domain processing, typically the discrete Fourier transform.

A bandpass signal is defined as a deterministic signal with non zero portions of its spectrum confined to the frequency region of $\omega_c - \omega_b/2 \leq |\omega| \leq \omega_c + \omega_b/2$. Second order sampling involves sampling the

bandpass signal $x(t)$ and its quarter wavelength translation $x(t-1/4f_c)$ at a rate dependant on the position and bandwidth of the IF signal. The relationship of possible sampling rates relative to the position and bandwidth of the IF signal is given by [Grace & Pitt, 1970]

$$T_s = \frac{l}{2f_c} \leq \frac{1}{2f_b} \quad , \tag{2-2}$$

where $l = 1,2,3, \ldots$. The carrier frequency is f_c and f_b is the signal bandwidth, both in **hertz** (Hz). The resultant sampling time difference between the I and Q signals is given by

$$T_{ds} = \frac{1}{4f_c} + nT_s \quad , \tag{2-3}$$

where $n = \ldots -1,0,+1 \ldots$. Specifically these conditions apply to an IF frequency of 12,5 kHz, with an IF bandwidth $(2f_b)$ of 25 kHz whose I and Q signals are both sampled at a frequency of 25 kHz. Figure 2.3 is a block diagram of this specific second order quadrature sampler, the sampling rate is 40 microseconds and the quarter wavelength time delay is 20 microseconds.

First order sampling of bandpass signals is a derivative of second order sampling and its structure is shown in figure 2.4. The difference equations of the I and Q channels derived by Brown [1980] are given by

$$I[2nT_s] = (-1)^n X[2nT_s] \tag{2-4}$$

and

$$Q[(2n-1)T_s] = (-1)^{n+1} X[(2n-1)T_s] \quad , \tag{2-5}$$

where T_s is the sample time of 20 microseconds, for the specific example of a 12,5 kHz IF with a 25 kHz bandwidth.

From the above difference equations it is apparent that the I and Q samples are obtained at different time instants, which results in a timing misadjustment between the signals. The misadjustment error being a function of the IF bandwidth and inverse

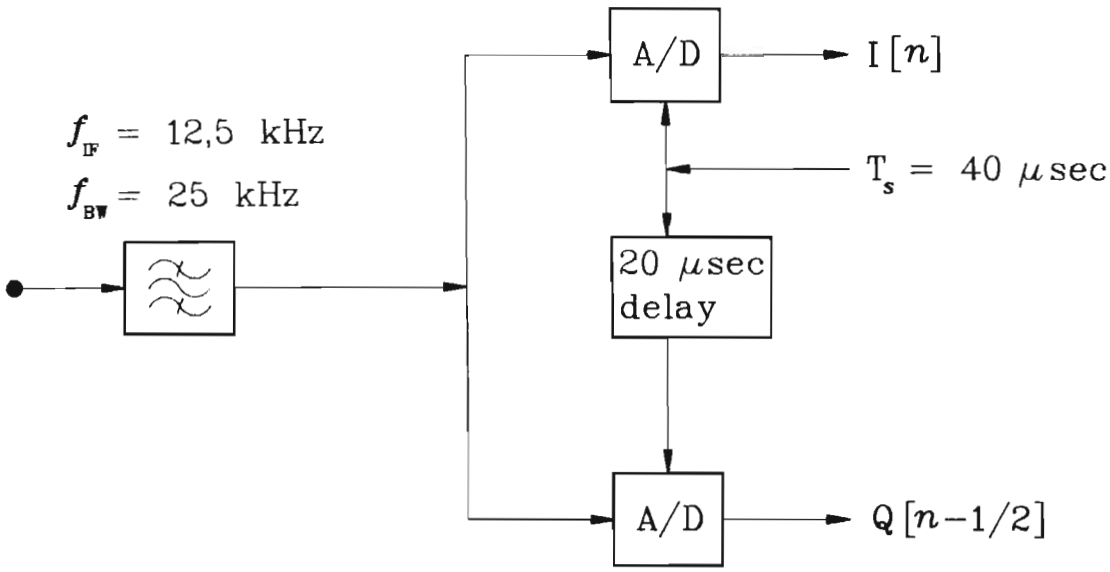

Figure 2.3 A second order quadrature sampler.

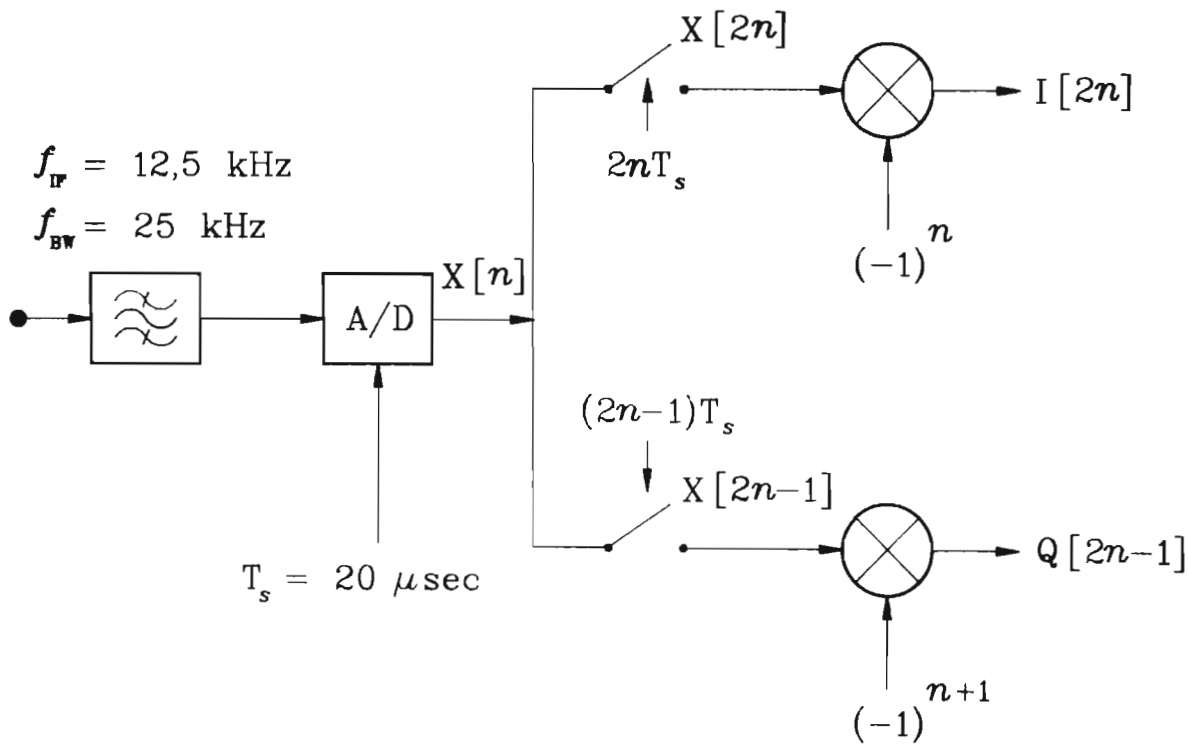

Figure 2.4 A first order quadrature sampler.

function of the sampling rate. Saulnier et al. [1990] describe a technique of interpolation between samples to overcome the timing misadjustment, however the accuracy of the technique is dependant on the sampling rate and typically a high degree of over sampling is required. Hence in the specific application where the signal bandwidth approaches a quarter of the sampling frequency, wideband filtering techniques are needed to obtain the necessary accuracy.

2.1.3 Filtering techniques to create I and Q signals.

Filtering techniques to create I and Q signals are based on the **discrete Hilbert transform** (DHT) which ideally has the following Fourier transform $H(\omega)$, where

$$H(\omega) = \begin{cases} -j & \text{for } 0 \le \omega < \pi \\ +j & \text{for } -\pi \le \omega < 0 \end{cases} . \qquad (2\text{-}6)$$

There are two general structures that can be employed in the design of a DHT firstly the **finite impulse response** (FIR) filter and secondly the **infinite impulse response** (IIR) filter. The FIR filter is a pure zero filter while the IIR filter incorporates poles and zeros.

Design techniques of FIR discrete Hilbert transforms include windowing, frequency sampling and equiripple approximations. Practical design results in the truncation of the infinite FIR DHT which causes amplitude ripple, but no phase error in the passband [Oppenheim & Schafer, 1975, pg. 361-363]. Furthermore, since the impulse response of a FIR DHT is symmetrical about the midpoint of the sample window it has a linear phase response and a constant group delay [Antoniou, 1979, pg. 218-221]. To minimize the amplitude ripple the order of the FIR DHT is normally large. The implementation and performance of these high order DHT FIR filters have been described by Rice & Wu [1982].

There have been two techniques described in the literature which can be employed to improve the processing requirements of the FIR DHT. Saulnier et al. [1990] have derived simple second and third order FIR DHT filters which are utilized when the signal is over sampled. This approach is employed in VLSI dedicated integrated circuits where the objective is to limit the number of multiplications. In the application where system flexibility is important and it is not possible to use a dedicated VLSI component for each modulation mode Mitchell's [1989] approach is more suitable. Mitchell's technique is to centre the FIR DHT passband evenly at $f_s/4$, where f_s is the sampling frequency. Designing an odd order filter results in zero valued even coefficients which reduces the number of multiplications and accumulations required (see figure 2.5). Although this offers a significant improvement, due to the pipelined architecture and instruction sets of VLSI DSP microprocessors, decimating IIR filters have a processing and memory advantage.

The use of IIR discrete Hilbert transforms is less common due to the more complex design procedure, however there are two approaches which have been described in the literature. Gold & Rader [1969] propose using Jacobian elliptic functions combined with the bilinear transform to design a pair of IIR allpass networks (see figure 2.6) whose phase difference is the closest possible approximation to 90 degrees over an interval of frequencies. While Ansari [1987] describes a different procedure of designing IIR Hilbert transformers from halfband filters using elliptic functions. This results in a single filter network rather than a differential filter network.

In a specific example, Rader [1984] derives the coefficients for a wideband IIR 90 degree network which operates over the frequency range of $\pi/4 < \omega < 3\pi/4$ with a phase error of less than 0,1145 degrees. He

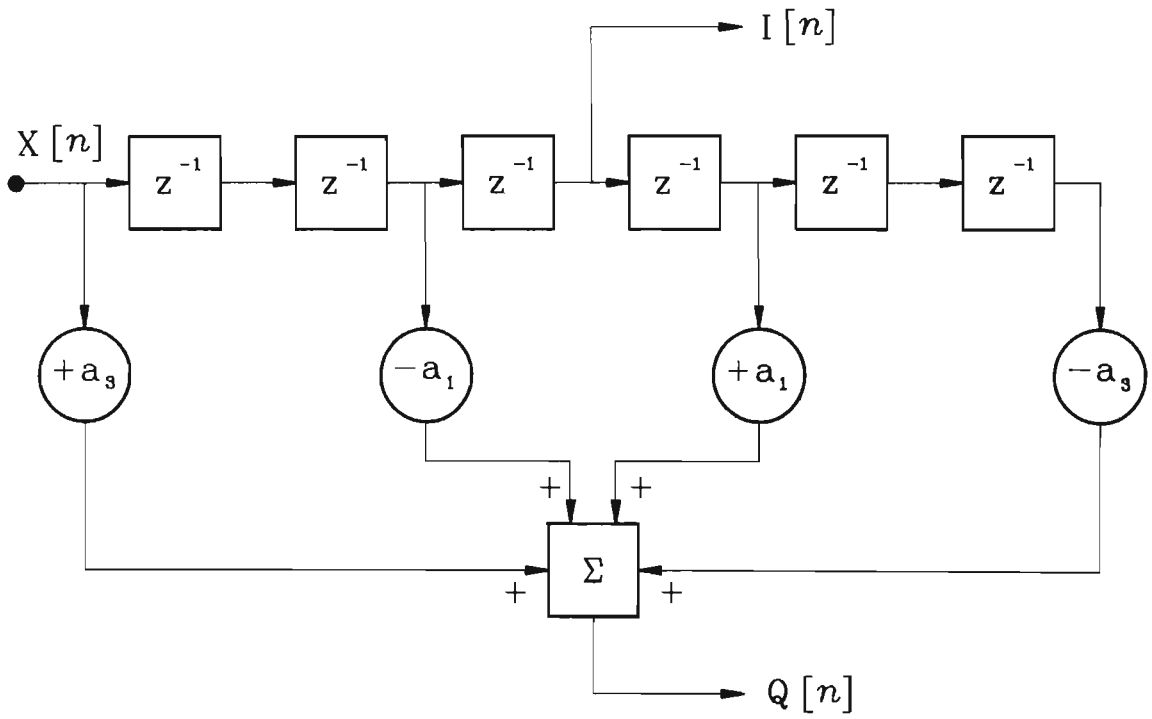

Figure 2.5 Mitchell's [1989] simplified FIR DHT filter.

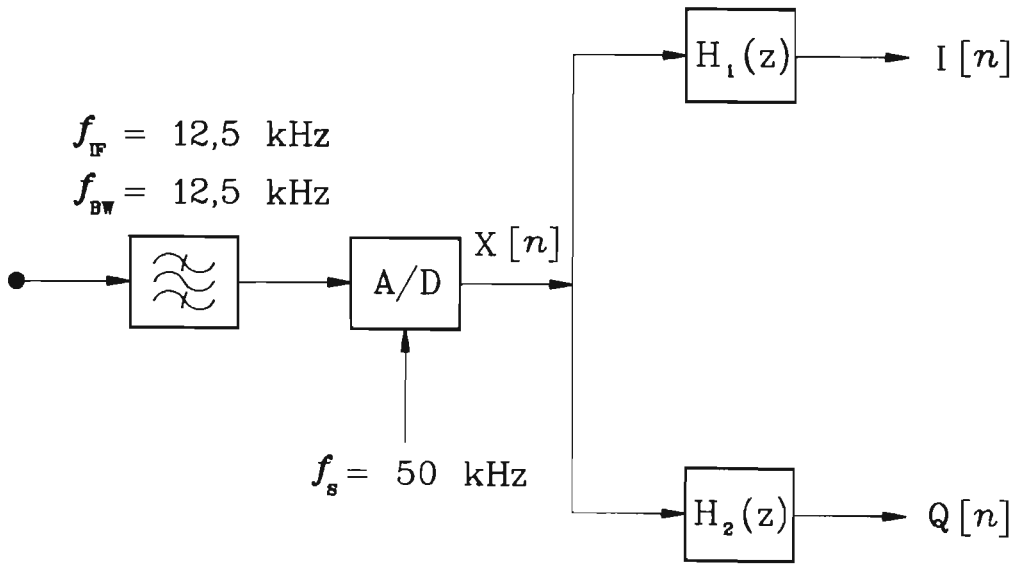

Figure 2.6 Gold & Rader's [1969] IIR DHT filter network.

found that there were a number of exploitable symmetries which reduces the two IIR filters $H_1(z)$ and $H_2(z)$ to

$$H_1(z) = z^{-1}\frac{z^{-2} - a_1^2}{1 - a_1^2 z^{-2}} \quad \text{where } a_1^2 = 0,5846832 \ , \tag{2-7}$$

and

$$H_2(z) = -\frac{z^{-2} - b_1^2}{1 - b_1^2 z^{-2}} \quad \text{where } b_1^2 = 0,1380250 \ . \tag{2-8}$$

Rader shows that further simplification occurs if baseband I and Q signals are required. By using a decimation structure which processes either the even or odd sample the network reduces to four storage elements, two multipliers and four additions as shown in figure 2.7. In applications where it is possible to take advantage of decimation the differential IIR Hilbert filter structure is simpler than Ansari's [1987] cascaded structure. Although Rader's IIR DHT is computationaly attractive, it however has a nonlinear group delay (see figure 2.8).

To conclude this discussion on filtering techniques for the creation of I and Q signals the following observations are made. Both FIR and IIR discrete Hilbert transforms can take advantage of the processing improvements offered by decimation if baseband I and Q signals are required. By careful selection of the IF frequency and sampling rate the decimation process results in a frequency translation from the IF to baseband. This is similar to mixing with a local oscillator. The difference between the two processes is that mixing creates a double frequency term which does not occur with decimation. Decimation on the other hand requires prior bandpass filtering to prevent the aliasing of unwanted out of band receiver noise which is typically greater than the A/D's quantization noise (see section 3.2.2). The bandpass filter, being the analogue image filter of the last mixer before digitization, performs this function.

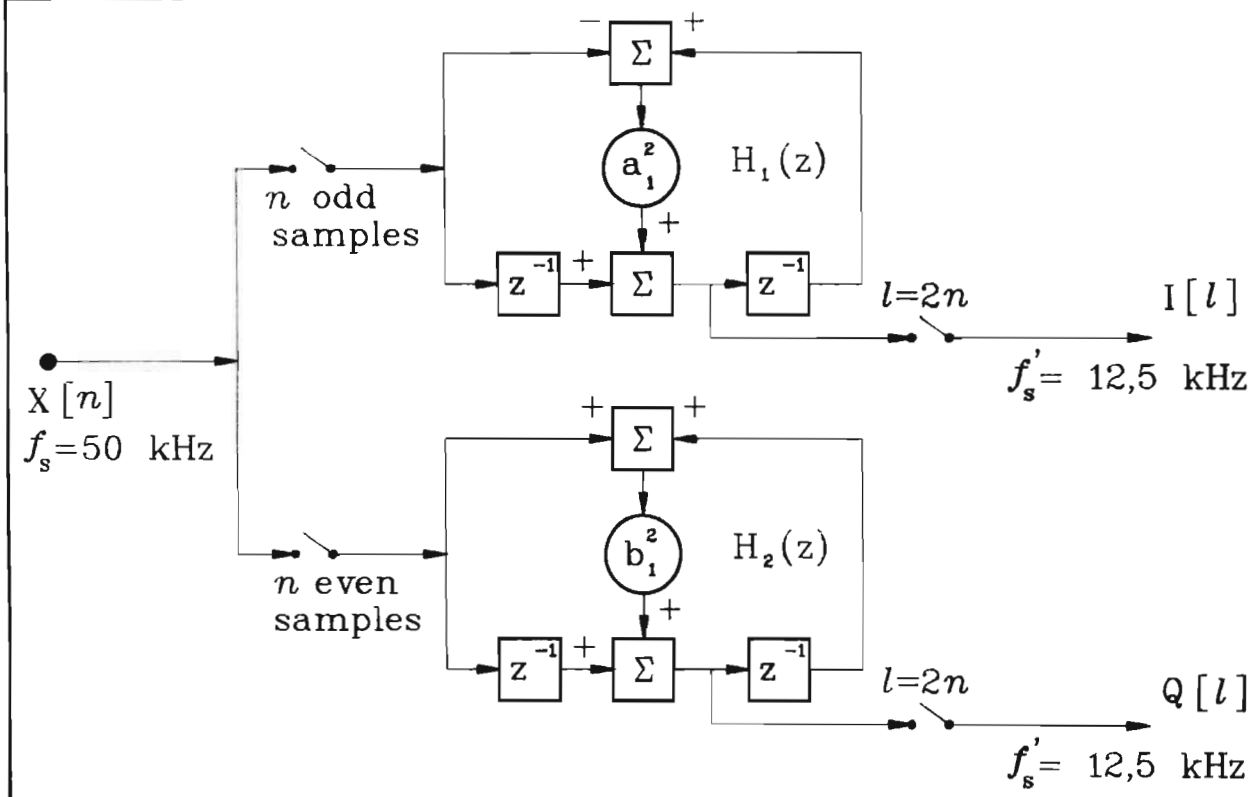

Figure 2.7 Rader's [1984] simplified IIR DHT filter network.

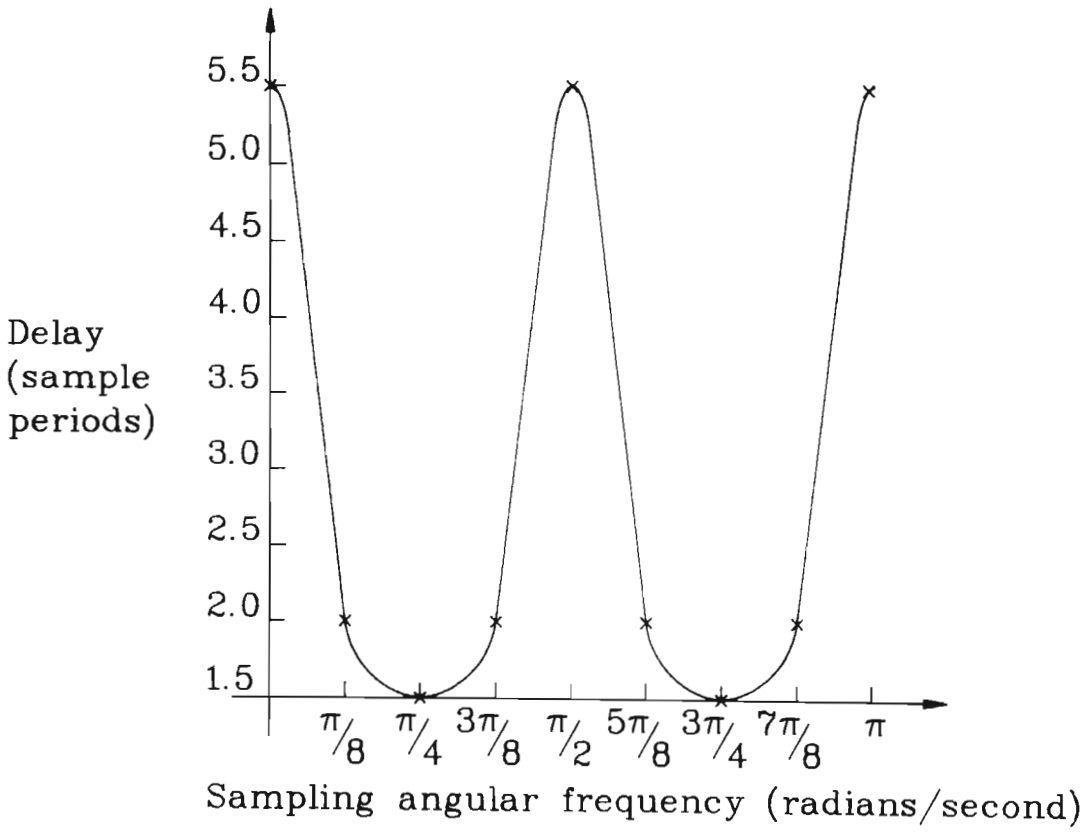

Figure 2.8 The group delay of Rader's IIR DHT filter.

2.2 TECHNIQUES TO OBTAIN THE MODULUS OF A COMPLEX NUMBER.

In AM, the information is contained in the amplitude of the carrier signal. This information can be extracted by generating the quadrature signal pair (which is essentially a complex number), and determining its magnitude. This section is a review of techniques for calculating the magnitude of a complex number. It is opportune to extend this review, en route, to include a comparison of the techniques. The basis of comparison of techniques as used by the author is the consideration of the number of divisions, multiplications and decisions required to obtain a certain percentage error. Divisions are processing intensive as they are performed on a decision based, bit-by-bit procedure, while decisions require branching in the program which disrupts the processing pipeline.

There are two general approaches to finding the modulus of the complex number. The first technique is to square, add and square root the I and Q signals, while the second approach is to approximate the modulus directly from the I and Q signals. The first technique always carries the overhead of the preceding squaring and the addition of the I and Q signals.

2.2.1 Square root techniques.

A classical technique of finding the square root of a positive number is the Newton-Raphson numerical algorithm [Kreyszig, 1979, pg. 762-768]. This is a simple, iterative procedure which progressively improves the first approximation of the root. However this technique requires a division for each iteration and has, in comparisons to both Prado & Alcantra's [1987] and Hashemian's [1990] square root algorithms, been found to be significantly slower and hence need not be analyzed in detail.

Prado & Alcantra [1987] suggest a bit-by-bit recursive technique where the speed is almost proportional to the binary length of the root. The algorithm, given in figure 2.9, uses a similar successive approximation technique as typically found in low speed, high resolution A/Ds. The algorithm uses shifts, additions, multiplications but avoids division. Operating from the most significant to the least significant bit the approximation to the root is squared and then compared with the original integer being rooted in order to set the logic level of the current bit. For a maximum percentage error of +/- 0,2% nine multiplications and seventeen decisions are required. Similar successive approximation algorithms, which are more suited to a hardware implementation, are described by Oklobdzija & Ercegovac [1982] and Zurawski & Gosling [1987].

Hashemian's [1990] square root technique, which is applicable to real numbers and integers, is based on making an initial close estimate of the square root and then using a similar successive approximation technique to improve the result. Hashemian reports that his algorithm is approximately 30% faster than Prado and Alcantra's algorithm and for a maximum percentage error of +/- 0,2% four multiplications and sixteen decisions are required.

2.2.2 Direct approximation techniques.

A well known direct approximation technique using the I and Q signals is the **coordinate rotation digital computer** (Cordic) algorithm, first proposed by Volder [1959] and is a transform from rectangular to polar coordinates. The algorithm is also suitable for other computations namely multiplication, division and conversions between binary and mixed radix number systems. The essence of the technique is a binary step-by-step process of pseudo rotations of the complex vector which results in a final angular argument of zero. The angular increments

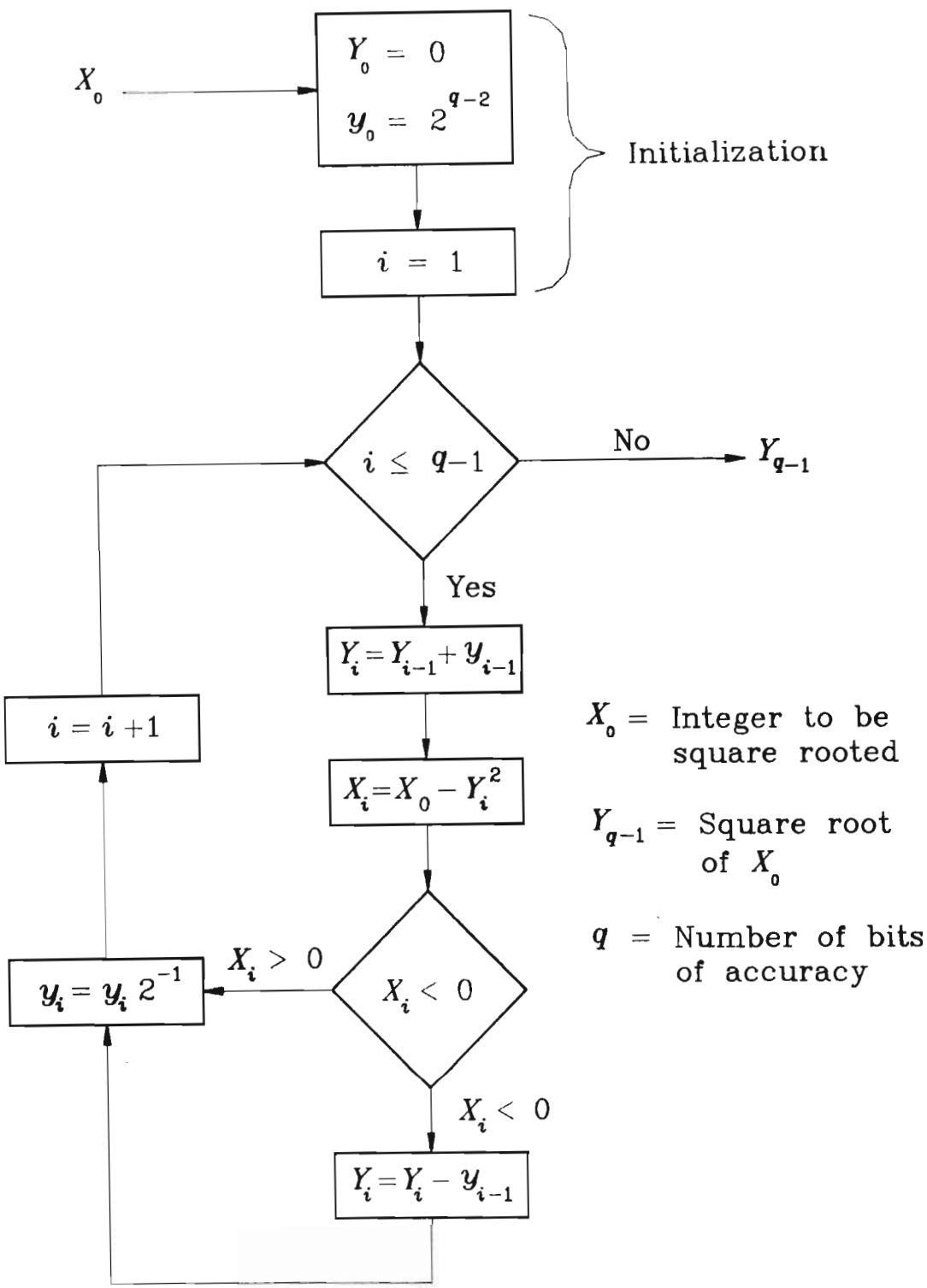

Figure 2.9 Prado & Alcantra's [1987] successive approximation technique to find the square root of an integer.

of rotation are computed in decreasing order. Volder [1959] gives an excellent derivation of his algorithm and a sample program is described in Appendix 2. The algorithm requires no multiplications, only powers of two bit shifts and 8 decisions for a maximum percentage error of +/- 0,2%. Furthermore, it is noteworthy that the algorithm can also be used to calculate the phase angle of the signal with little extra processing, which could be an advantage in certain applications.

Linear approximation of the modulus of a complex number using the relative magnitudes of the I and Q vectors was first proposed by Robertson [1971]. His proposal was further refined by Onoe [1972] who derived a range of real numbers for the linear approximation constant to obtain the best compromise between the variance and peak error. The approximation is given by

$$R = M + \kappa N \ , \tag{2-9}$$

where R is the magnitude of the complex number and κ is a constant greater than or equal to 0,2673 but less than or equal to 0,3. Furthermore the values of M and N are given by

$$M = \max(|I|, |Q|) \tag{2-10}$$

and

$$N = \min(|I|, |Q|) \ . \tag{2-11}$$

The maximum percentage error using this simple approximation is between 5 and 10% dependant on the value of the constant. Since the accuracy depends on the choice of constant Filip [1973] suggests breaking up the first quadrant into two smaller regions and Freeman [1978] extends this idea to include multiple smaller regions.

Freeman's approach (see figure 2.10) to the linear approximation of the modulus is based on rotating the complex vector $Z = I + jQ$ such that

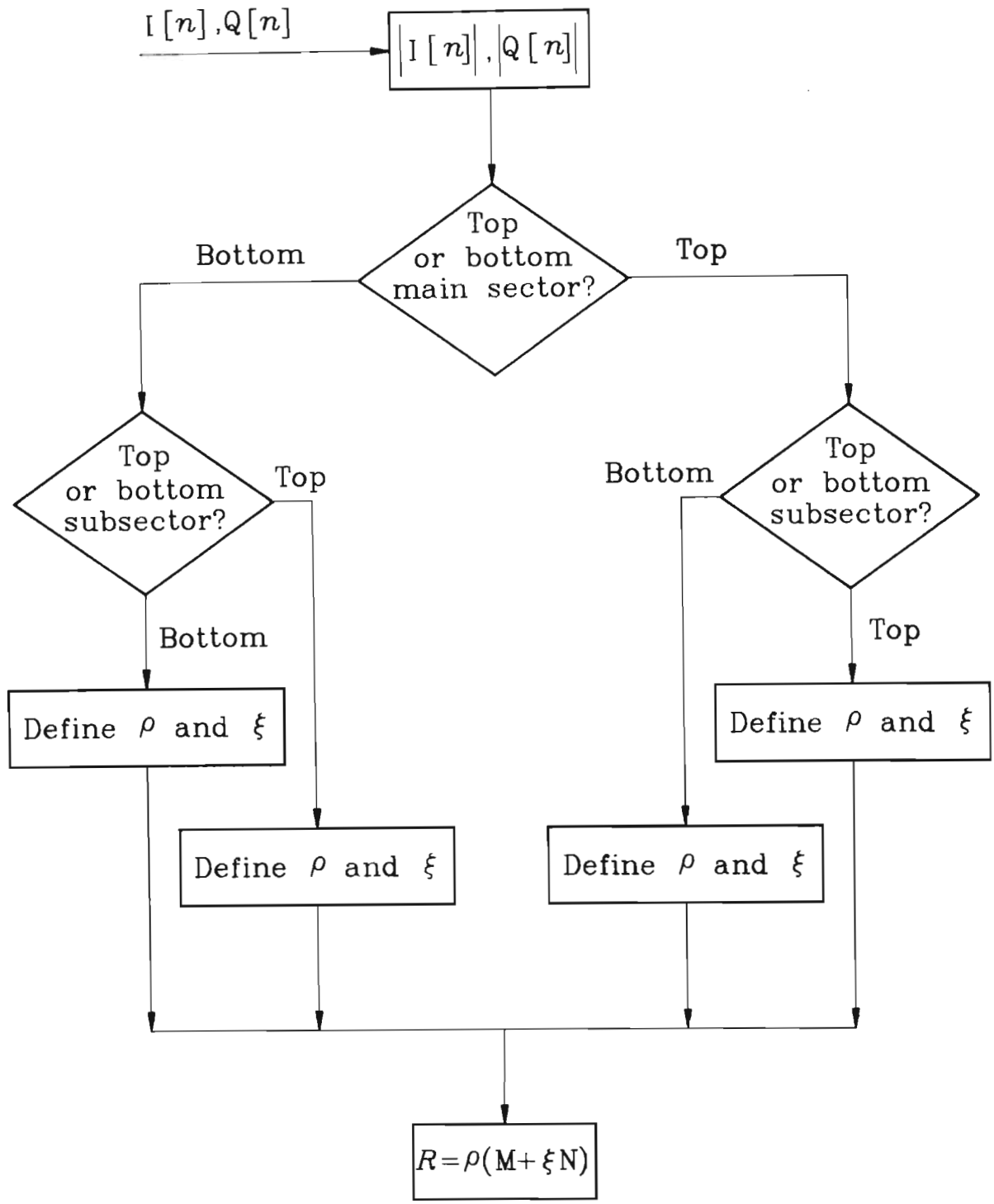

Figure 2.10 Freeman's [1978] linear approximation technique of finding the modulus of a complex number.

its argument lies in the region $0 \leq \theta \leq 0,25\pi$. The linear approximation to the modulus is given by

$$R = \rho(M + \xi N) \ . \qquad (2\text{-}12)$$

The error caused by this approximation technique is equiripple. This implies that the maximum positive and negative error deviation is equal while the average error is zero. The accuracy of the estimate is determined by the values of ρ and ξ. Freeman further subdivides the quadrant into smaller equiangular subsectors each with their own constants to improve the accuracy. The constants for the subsectors are given by

$$\rho = \sec^2\left(\frac{\psi}{4}\right)\cos\left(\chi + \frac{\psi}{2}\right) \qquad (2\text{-}13)$$

and

$$\xi = \tan\left(\chi + \frac{\psi}{2}\right) \ , \qquad (2\text{-}14)$$

where ψ is the phase angle of the subsector. For example, if the quadrant is broken into two subsectors then $\psi = 0,125\pi$. While χ is the phase at the beginning of each subsector and for the above example, $\chi = 0$ and $0,125\pi$.

The basis of the algorithm is to find in which subsector the complex point exists, this is done by comparing the relative magnitudes of the I and Q signals. Knowing this, the values for the constants may be obtained (they are pre-computed) and equation 2-12 applied. By dividing the quadrant into four subsectors results in a maximum percentage error of +/- 0,24% which requires three decisions and four multiplication operations.

From the comparison of the various algorithms to determine the modulus of the complex number it is clear that Freeman's approach is the most efficient although Volder's Cordic algorithm has the advantage of

simultaneously determining the phase of the signal with little extra processing. However to minimize the processing requirement Freeman's technique is recommended and all the results for the AM and FM demodulators are obtained using this approach.

2.3 A REVIEW OF ADAPTIVE LINE ENHANCEMENT.

Generally **automatic frequency control** (AFC) systems require the frequency estimation of a sinusoid corrupted by noise, and therefore, the trend is currently to utilize digital spectral estimation techniques (see section 5.1). A spectral estimation technique particularly suited to AFC systems is the **adaptive line enhancer** (ALE) which is essentially an adaptive filter employed to enhance the SNR of a sinusoid and provide an estimate of its frequency. The objectives of this subsection are two-fold; firstly to review the different second order **infinite impulse response adaptive line enhancer** (IIR-ALE) algorithms and secondly to provide a summary of a specific resonator IIR-ALE.

2.3.1 A comparison of different second order IIR-ALE algorithms.

Hush [1986] has shown that a suitable model for sinusoids corrupted by white noise is the **autoregressive-moving average** (ARMA) process given by the difference equation

$$Y[n] = \sum_{i=0}^{l} b_i X[n-i] - \sum_{r=1}^{m} a_r Y[n-r] \,, \qquad (2\text{-}15)$$

where $Y[n]$ is the current predicted sample, $X[n-i]$ the past observed noisy samples and $Y[n-r]$ the past predicted values. The function of an ALE is to adaptively calculate suitable values for the **moving average** (MA) b_i, and **autoregressive** (AR) a_r coefficients, so as to obtain an optimal match of the ARMA model to the corrupted sinusoids. Publications over the last ten years have included numerous examples of high order ARMA ALEs which generally differ in terms of the filter structure and adaptation algorithm. However, the order, and hence complexity, of determining the optimal ARMA process is dependent on the number of expected sinusoids, and in the simple case of a single sinusoid, a second order model suffices [Marple, 1987, pg. 296-297].

Three different second order IIR-ALE filter configurations, namely the adaptive allpass, notch and resonator filters, have been reported. These adaptive filters are generally similar in nature, while variations are introduced to suit different hardware configurations. The adaptive allpass filter, shown in figure 2.11, introduces a 180 degree phase shift at the frequency of the input sinusoid. Thus, on summation of the input and output of the allpass network, either a bandpass, or notch filter configuration, can be created with the appropriate selection of sign. Regalia [1991] reports on an implementation of the allpass IIR-ALE utilizing a lattice structure, but which is applicable to a Cordic processor. The lattice allpass structure, described by figure 2.11, but which is more suited to general purpose DSP microprocessors as it requires no computation of trigonometric functions, has been reviewed by Regalia, Mitra & Vaidyanathan [1988]. Furthermore, Cupo & Gitlin [1989] and Cho, Choi & Lee [1989] have discussed similar adaptive lattice resonator and notch IIR-ALEs.

The canonic form, unity gain, resonator IIR-ALE, see figure 2.12, was first introduced by David, Stearns, Elliott & Etter [1983] and further developed and refined by Hush [1986] with results reported in the joint paper by Hush, Ahmed, David & Stearns [1986]. Recently, Kwan & Martin [1989] have extended this second order bandpass IIR-ALE by

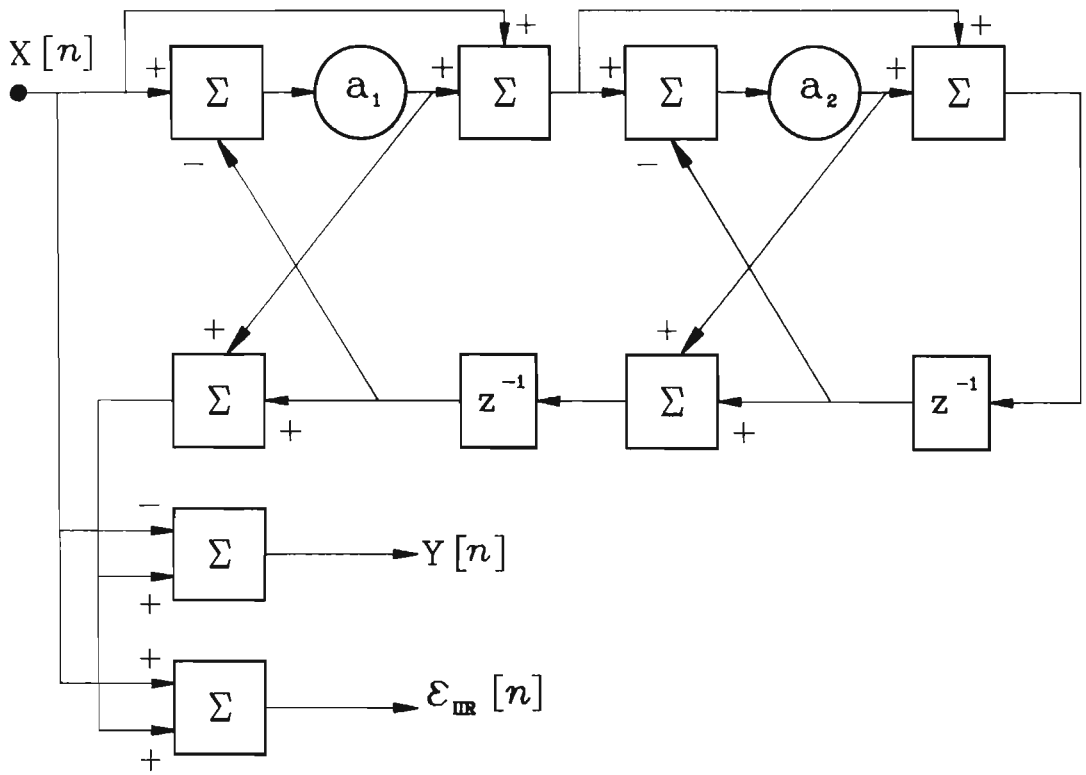

Figure 2.11 The allpass lattice IIR-ALE.

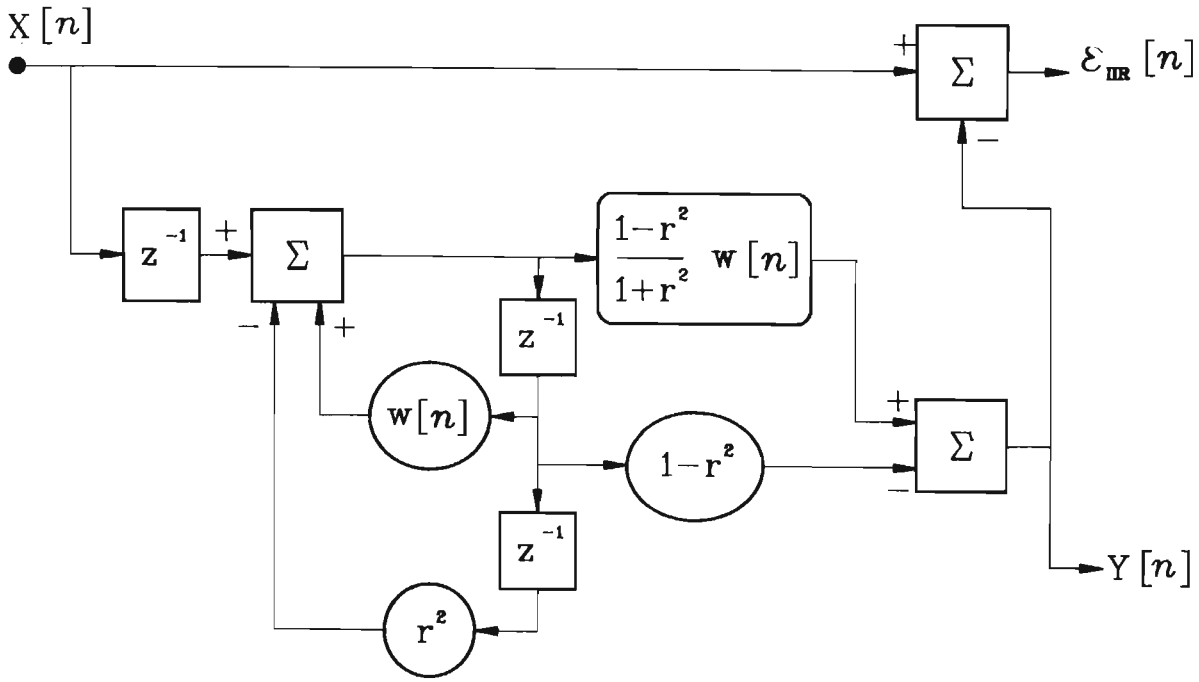

Figure 2.12 The canonic form resonator IIR-ALE.

developing adaptive constant Q and notch IIR-ALE filters. In a comparison of the various second order IIR-ALE's nodal equations, the author found that since the internal architectures of general purpose DSP microprocessors are normally optimized according to standard filter structures, the simplest second order structure for this situation, is the canonic form.

2.3.2 A second order resonator IIR-ALE algorithm.

With reference to figure 2.12 and assuming a noise decorrelation buffer of unity, the second order canonic form resonance filter proposed by David et al. [1983] is defined by the following difference equation

$$Y[n]=\left(\frac{1-r^2}{1+r^2}\right)w[n]X[n-1]-(1-r^2)X[n-2]+w[n]Y[n-1]-r^2Y[n-2]\ , \quad (2\text{-}16)$$

where $Y[n]$ is the output and $X[n]$ the input of the filter, and at the point of resonance, this filter has unity gain and zero phase shift. The -6 db bandwidth of the simple resonator is given by [Hush, 1986]

$$f_{-6BW}=\sin^{-1}\left(\frac{1-r^2}{2r}\right)\frac{f_s}{2}\ , \quad (2\text{-}17)$$

and the point of resonance occurs at

$$f_r=\cos^{-1}\left(\frac{w_{IIR}[n]}{1+r^2}\right)\frac{f_s}{2\pi}\ , \quad (2\text{-}18)$$

where $w_{IIR}[n]$ is the optimal, or steady state value of $w[n]$ following convergence. Stability of the filter is guaranteed when

$$0<r<1\ , \quad (2\text{-}19)$$

and

$$|w[n]|<2r\ . \quad (2\text{-}20)$$

Typically as $r \to 1$ the complex poles approach the unit circle and the bandwidth tends to zero. Due to the stability criteria the resonance frequency range of the IIR-ALE is limited and the lower and upper limits are given by

$$f_l = \cos^{-1}\left(\frac{2r}{1+r^2}\right)\frac{f_s}{2\pi} \ , \tag{2-21}$$

and

$$f_u = \cos^{-1}\left(\frac{-2r}{1+r^2}\right)\frac{f_s}{2\pi} \ . \tag{2-22}$$

Interestingly, as $r \to 1$, these limits increase and therefore seldom constitute a restriction in the adaptation range of the IIR-ALE.

Hush [1986] provides an excellent study of various gradient search LMS algorithms and the important features are summarized in the following paragraph. The resonator IIR-ALE operates on the principle of aligning its point of resonance with the frequency of the incoming sinusoid by adapting $w[n]$, utilizing the following update equation

$$w[n+1] = w[n] + \upsilon \epsilon_{IIR}[n]\alpha_{IIR}[n] \ , \tag{2-23}$$

where υ is the convergence parameter, $\epsilon_{IIR}[n]$ is defined as

$$\epsilon_{IIR}[n] = X[n] - Y[n] \ , \tag{2-24}$$

and the gradient of the error ($\alpha_{IIR}[n]$) has been derived as

$$\alpha_{IIR}[n] = -\frac{\partial \epsilon_{IIR}}{\partial w[n]} = \left(\frac{1-r^2}{1-r^2}\right)X[n-1] + Y[n-1] + w[n]\alpha_{IIR}[n-1] - r^2\alpha_{IIR}[n-2]. \tag{2-25}$$

The structure of the resonance filter coefficient update equation, called the **recursive least mean squares** (RLMS) algorithm, is intuitively satisfying, since the new coefficient is a function of the previous coefficient, the error in the previous coefficient prediction, and the gradient of this prediction error. The speed of convergence is dependent on the magnitude of the convergence parameter υ, but the faster the speed of convergence the greater the residual noise in the final frequency estimate. For this reason Hush [1986] proposed two techniques for speeding up the convergence which do not severely

degrade the variance of the final frequency estimate. The first technique is to use a modified form of the gradient of the error ($\alpha_{MIIR}[n]$)

$$\alpha_{MIIR}[n]=\left(\frac{1-r^2}{1-r^2}\right)X[n-1]+Y[n-1]\ . \qquad (2\text{-}26)$$

which results in a higher probability of the gradient vector taking on the correct direction of convergence. The second technique is to make the fixed convergence parameter υ variable by dividing by

$$\psi_{MIIR}[n]=\beta_F\psi_{MIIR}[n-1]+(1-\beta_F)\alpha^2_{MIRR}[n]\ , \qquad (2\text{-}27)$$

where ψ_{MIIR} is an instantaneous estimate of the power in the modified gradient vector. The parameter β_F is known as the forgetting factor and is the range of $0 \ll \beta_F < 1$. This denominator results in a large step size, away from the point of convergence, which gradually decreases as the IIR-ALE converges. Thus the final coefficient update equation, known as the **modified normalized RLMS** (MRLMS) algorithm is given by

$$w[n+1]=w[n]+\frac{\upsilon\epsilon_{IIR}[n]\alpha_{MIIR}[n]}{\psi_{MIIR}[n]}\ , \qquad (2\text{-}28)$$

The resonator IIR-ALE is a simple algorithm for tracking, enhancing and estimating the frequency of a single, noise corrupted sinusoid. In section 5.2.2 a modified fixed point implementation of the IIR-ALE which forms part of the multirate IIR-ALE/DPLL AFC system, is discussed.

2.4 THE DESIGN OF A DIGITAL PHASE-LOCKED LOOP.

Most receiver **automatic frequency control** (AFC) systems rely on tracking the frequency and phase of a suppressed carrier and in section 5.1 various classical and current AFC systems are discussed. From this review it is concluded that the **infinite impulse response adaptive line enhancer** (IIR-ALE) and the **digital phase-locked loop** (DPLL) can be combined to form a simple and robust AFC system. To address the

design of a DPLL this section is divided into two subsections. The first subsection briefly reviews relevant analogue phase-locked loop theory and the second subsection utilizes this theory to derive the DPLL via the bilinear transform.

2.4.1 Phase-locked loop design considerations.

In this subsection relevant theory is reviewed to provide a procedure for designing a **carrier wave** (CW) tracking **phase-locked loop** (PLL). Figure 2.13 gives a block diagram of the classical PLL which consists of a phase detector, loop filter and **voltage controlled oscillator** (VCO). When the loop is in lock, the phase detector provides a voltage which is proportional to the phase difference between the incoming CW signal and the VCO output. This control voltage is then filtered by the loop filter and applied to the VCO as a control signal; and any changes in the frequency and/or phase of the incoming CW signal can thus be tracked by the PLL.

The order of the PLL (determined by the loop filter), and the loop parameters are derived as a function of the expected dynamics of the received CW signal. By utilizing the final value theorem of Laplace transforms, Gardner [1979, pg. 43-53] analyzes the steady state errors caused by a phase step, frequency step and frequency ramp of the input CW signal for various orders of PLL. A phase step typically occurs on relocking after a signal fade, if the AFC system had corrected for the frequency difference between the transmitter and receiver before the signal fade. A frequency step occurs due to a Doppler frequency shift or on acquiring a new CW signal; while an accelerating mobile unit causes a frequency ramping Doppler offset. Employing the final value theorem Gardner shows that a PLL of order greater than or equal to unity, has the ability of tracking a phase step with zero steady state error. The simple first order PLL fails to track

a frequency ramped signal and loss of lock can occur. The second order loop however, has the ability to track frequency step and frequency ramped CW signals; albeit with an error. A closer analysis of these errors will show that in practice they are either corrected for by the total AFC system or are negligible for a typical mobile environment. For this reason more complex third or higher order, PLLs are not considered.

The steady state error caused by a frequency step applied to a second PLL is given by [Gardner, 1979, pg. 44]

$$\theta_v = \frac{\Delta\omega}{K_{DC}} \quad , \tag{2-29}$$

where θ_v is the static phase error, $\Delta\omega$ is the frequency step and K_{DC} is the DC loop gain. However since the DC loop gain is generally large and the function of an AFC system is to correct for frequency differences, $\Delta\omega$ tends to zero. Of greater importance is the acceleration error (θ_a), caused by a frequency ramp, which has been derived as

$$\theta_a = \frac{\Delta\dot{\omega}}{\omega_n^2} \quad , \tag{2-30}$$

where $\Delta\dot{\omega}$ is the rate of change of the CW frequency and ω_n is the natural frequency of the PLL. As an example two initially stationary mobile units which accelerate towards one another, each achieving a velocity of 120 km/hr after 15 seconds result in a $\Delta\dot{\omega}$ of 39,23 radians/sec^2 when the transmission frequency is 400 MHz. However in the specific DPLL design described in section 5.2.3, since ω_n is large enough to accommodate a fading signal, it is found that the acceleration error is only 0,18 Hz/sec^2. Classical loop filter optimization techniques include the Wiener method developed by Jaffe & Rechtin [1955]. Their loop performance criterion is the mean square error which is calculated as a combination of the phase jitter due to noise and the instantaneous phase error caused by transients. The relative ratio between these two parameters determines whether the loop filter is optimized for phase jitter (narrow loop bandwidth) or transient

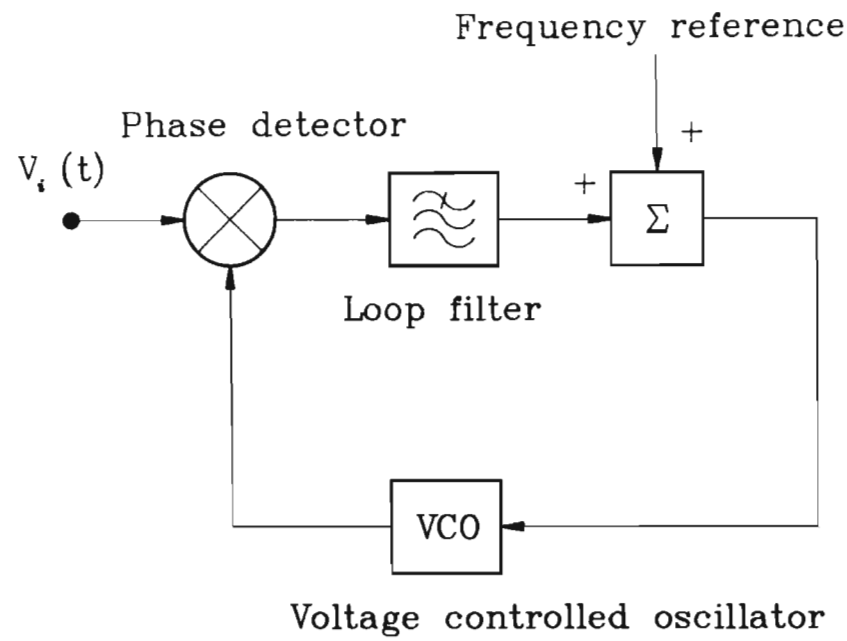

Figure 2.13 A block diagram of the PLL.

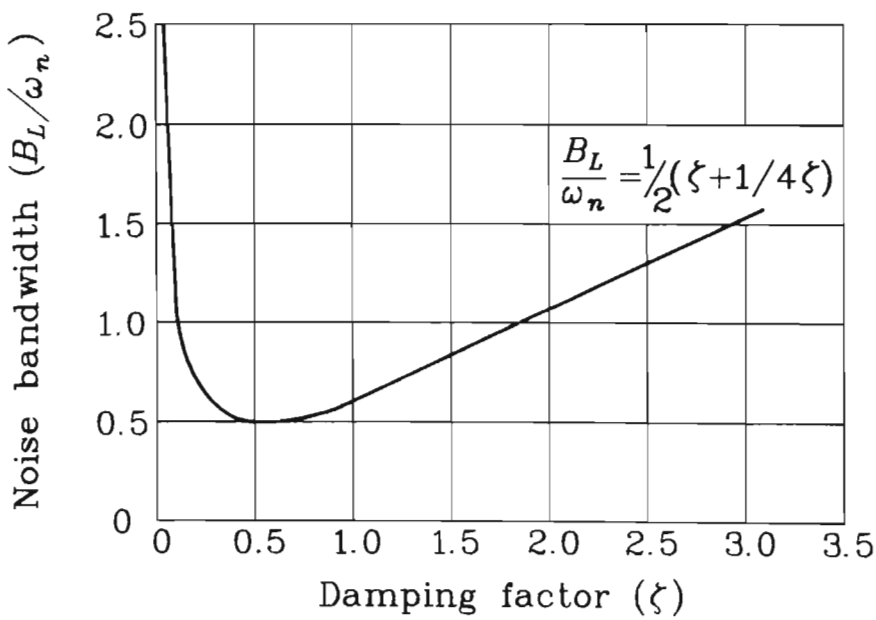

Figure 2.14 The relationship of B_L/ω_n to ζ [Gardner, 1979, pg.32].

performance (wide loop bandwidth). However, a more suitable approach for a fading signals has been developed by Weber III [1976] and in section 5.2.3 the effect of a Rayleigh fading signal on the PLL's loop bandwidth is considered.

The second order PLL's closed loop transfer function ($H_{PLL}(s)$), assuming that the second order PLL is in lock is given by [Gardner, 1979, pg. 11]

$$H_{PLL}(s) = \frac{2\zeta\omega_n s + \omega_n^2}{s^2 + 2\zeta\omega_n s + \omega_n^2} , \qquad (2\text{-}31)$$

where ζ is the damping factor and ω_n is the natural frequency of the loop. Once these two parameters have been selected it is possible to calculate the DC loop gain and loop filter coefficients needed in the design of the PLL. These two parameters, within broad limits, are generally independently selected. As discussed in the previous paragraph ω_n determines the loop bandwidth, while in the discussion that follows a motivation for the selection of ζ is provided. The second order **PLL's noise bandwidth** (B_L) which is derived from the variance of the VCO's output phase [Gardner, 1979, pg. 24-33], is given by

$$B_L = \int_0^\infty |H_{PLL}(j2\pi f)|^2 df = \frac{\omega_n}{2}\left(\zeta + \frac{1}{4\zeta}\right) . \qquad (2\text{-}32)$$

A plot of B_L/ω_n, see figure 2.14, shows that the optimum selection of ζ, to minimize the phase variance, is 0,5. However within the region of optimality the curve is relatively flat and a selection of ζ within the range of 0,25 to 1 only results in an increase of 1 dB in the phase jitter power. For this reason, and to minimize the pull in time of the second order PLL, ζ is generally selected as 0,707 [Gardner, 1979, pg. 141].

2.4.2 The derivation of a digital phase-locked loop.

There have been numerous DPLL architecture developed and the papers by Lindsey & Chie [1981] and Gupta [1975] provide excellent summaries of different structures. Often the architectures have been dependant on the digital technology available at that time, which results in a mixture of analogue and digital components and in turn affects the analyses of the PLL [Gupta, 1968]. The objectives of this subsection are to firstly motivate the architecture of the various components forming the all software DPLL and secondly to derive the loop filter's difference equation whose coefficients can be calculated once ζ and ω_n are known.

The DPLL like its analogue counterpart consists of three components, the phase detector, the loop filter and the **numerically controlled oscillator** (NCO). The implementation of the NCO is generally performed via a look-up table sine wave generation technique which utilizes the fixed point processor's full dynamic range of +1 to -1. Alternatively, Gold & Rader [1969, pg. 145-149] have developed a simple sine-cosine generator using perfect digital integrators. The structure however, is susceptible to truncation noise [Gold & Rader, 1969, pg. 147-148] and becomes unstable when frequency modulated [Carter, 1988].

Lindsey & Chie [1981] provide a summary of phase detectors applicable to variable sampling rate DPLLs and amplitude limited digital signals. Phase detectors which are applicable to sampled analogue signals include the **digital tanlock loop** (DTL), the sine function and the multiplier. The phase detector forming part of the variable sampling rate DTL, as in figure 2.15, requires I and Q signals from which the difference phase angle is calculated employing a $\tan^{-1}$ function [Lee & Un, 1982]. The structure is complex and requires a variable sampling rate, but has the advantage of a linear phase characteristic which is useful for wideband FM demodulators. The sine phase detector, given in figure 2.16, is applicable to a constant sampling rate DPLL

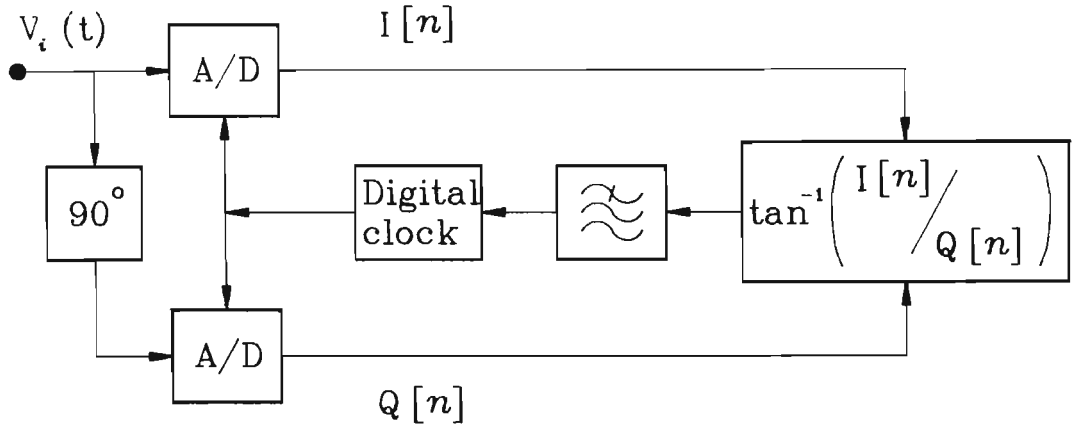

Figure 2.15 The Digital Tanlock loop [Lee & Un, 1982].

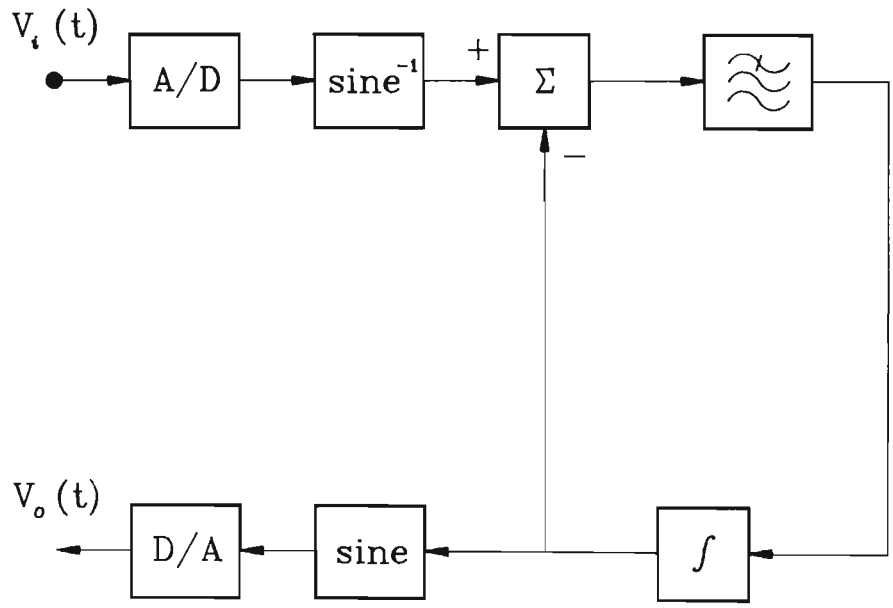

Figure 2.16 The sine DPLL [Shayan & Le-Ngoc, 1989].

architecture. The phase characteristic is also linear, but the sine and $sine^{-1}$ functions require intensive processing [Shayan & Le-Ngoc, 1989]. Although the multiplying phase detector, shown in figure 2.17, suffers from a non-linear phase response it requires minimal processing and furthermore, since the AFC system corrects for frequency differences the DPLL generally operates in the linear region of the phase detector. As described by figure 2.17 the multiplying phase detector is generally followed by a simple lowpass filter to remove the double frequency term caused by the multiplication. Insufficient filtering of the double frequency term causes unwanted sidebands at the output of the NCO. Since the loop filter defines the dynamics of the DPLL the bandwidth of the phase detector lowpass filter is designed to be greater (typically five times) than the bandwidth of the loop filter.

In the implementation of a DPLL the distribution of the gain at various stages in the loop is important. In an analogue PLL, if momentary saturation occurs, the signal within the loop experiences limiting, and although this may affect the performance of the PLL, the effect is generally not catastrophic, and the loop recovers. However if saturation occurs within a DPLL, numerical overflow results which can cause a complete loss of lock. Since numerical range checking requires further processing, it is preferable to design a DPLL which is not susceptible to overflow. As the gains of the NCO, phase detector and loop filter are combined to form the DC loop gain, it is possible to compensate (within the numerical dynamic range of the DPLL) for attenuation at a particular point in the DPLL, with gain in the next stage. With reference to figure 2.18 a block diagram of the second order DPLL, the largest signals typically occur at the phase detector and therefore it is prudent to only introduce gain after the phase detector's lowpass filter.

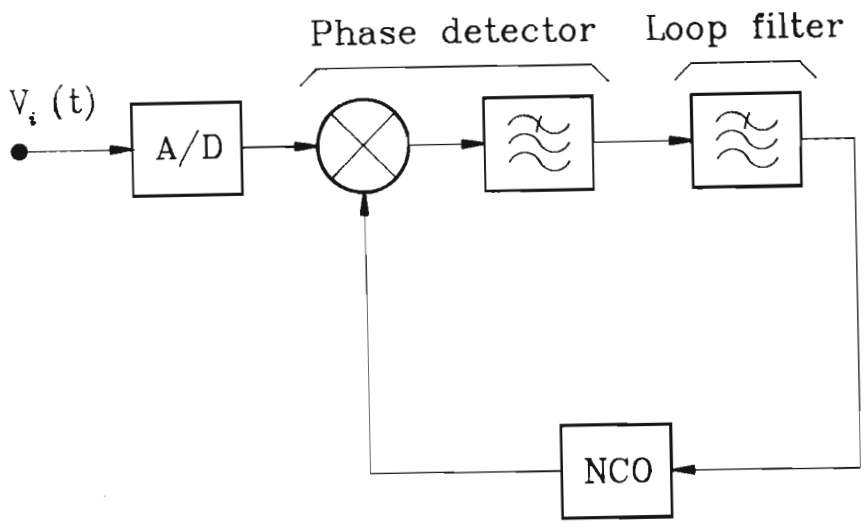

Figure 2.17 The multiplying phase detector.

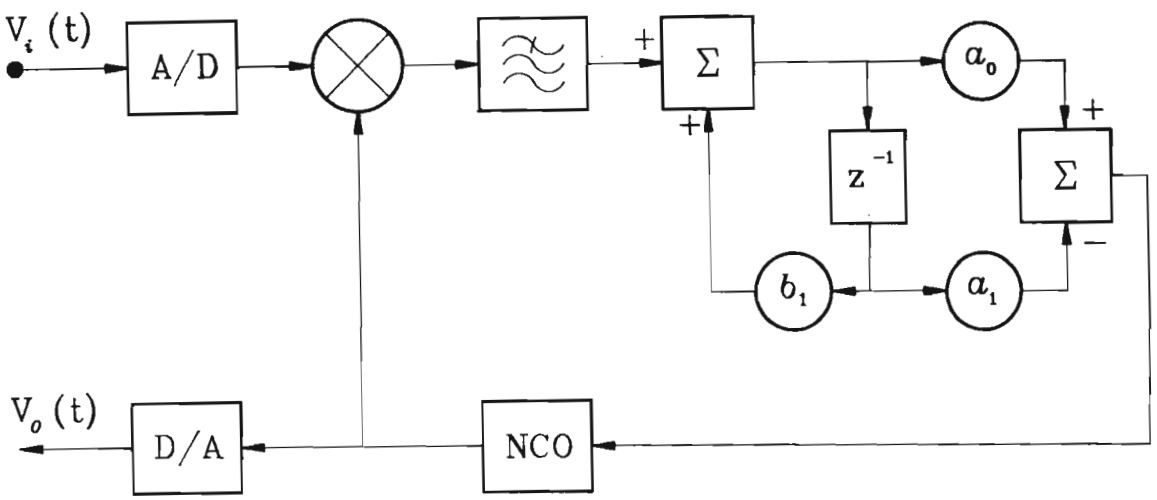

Figure 2.18 A block diagram of the second order DPLL

In analogue PLLs two alternative loop filter structures are generally employed, namely the active and passive filters, which differ in the position of the pole. Essentially the passive filter is an approximation of the ideal active loop filter [Gardner, 1979, pg. 10-11]. Both Shayan & Le-Ngoc [1989] and Schiavoni & Ray [1990] have developed DPLLs by transforming the active loop filter into its digital counterpart, this results however in small coefficient values for the zero, which essentially dampens the effect of the perfect pole. For this reason Shayan & Le-Ngoc [1989] utilized double-precision multiplications in their loop filter, to overcome the truncation effects in a fixed point processor. To circumvent the need to employ double-precision multiplications the author prefers to utilize a transformation of the non-ideal passive filter. This results in shifting the loop filter's pole slightly off the unit circle, which eases the precision requirements of the zero's coefficients.

The conventional approach to designing a loop filter, is to initially determine the natural and sampling frequency from whence a prewarping ratio is calculated. Following calculations of the prewarped filter coefficients the bilinear transform is then applied to derive the loop filter's difference equation. For the passive loop filter the natural frequency (ω_n) is given by [Gardner, 1979, pg. 10-11]

$$\omega_n = \left(\frac{K_o K_d}{\tau_1} \right)^{1/2} , \qquad (2\text{-}33)$$

where K_o is the gain of the VCO, K_d the gain of the phase detector and τ_1 the time constant of the loop filter's pole. The damping factor (ζ) has similarly been derived as

$$\zeta = \frac{\omega_n}{2} \left(\tau_2 + \frac{1}{K_o K_d} \right) , \qquad (2\text{-}34)$$

where τ_2 is the time constant of the zero. Hence if one knows ω_n, ζ, K_o and K_d, the time constants τ_1 and τ_2 can be determined. Due to the nonlinear mapping between the continuous and discrete-time domain,

the time constants must be adjusted by the ratio of ω_n/ω'_n where ω'_n is the prewarped natural frequency which is defined as

$$\omega'_n = \frac{2}{T_s}\tan\left(\frac{\omega_n T_s}{2}\right) , \qquad (2\text{-}35)$$

and T_s is the sampling period in seconds. The passive loop filter's Laplace transformation is given by

$$F(s) = \frac{s\tau_2 + 1}{s\tau_1 + 1} , \qquad (2\text{-}36)$$

and applying the bilinear transformation defined as

$$s = \frac{2}{T_s}\frac{z-1}{z+1} , \qquad (2\text{-}37)$$

results in

$$F(z) = \frac{z(2\tau'_2/T_s + 1) + (1 - 2\tau'_2/T_s)}{z(2\tau'_1/T_s + 1) + (1 - 2\tau'_1/T_s)} , \qquad (2\text{-}38)$$

where τ'_1 and τ'_2 are the respective prewarped values of τ_1 and τ_2. Finally for a fixed point processor whose dynamic range is limited to +1 to -1 this equation is normalized by the factor $2\tau'_1/T_s + 1$.

Essentially the DPLL acts as a predictor, attempting on a sample by sample basis to predict the phase of the received signal and therefore, when translating the analogue PLL to its digital counterpart, the sampling rate must be taken into consideration. Thus, to prevent a degradation in the loop tracking error and phase variance performance Lindsey & Chie [1981] have recommend that the inequality $B_L T_s < 0,1$ holds. Finally in section 5.2.3 the theory developed within this subsection is employed to derive the loop parameters for the specific DPLL which is incorporated as part of the SSB-SC AFC system.

CHAPTER 3

A NOVEL DSP MULTIRATE AM DEMODULATOR FOR SPEECH SIGNALS.

This chapter derives and assesses a simple DSP multirate AM demodulator for speech signals, beginning with a review of classical and current AM demodulators and their associated performance and digital implementation problems. From this discussion it is concluded that, generally, the quadrature envelope demodulator provides the most robust solution, although its implementation is normally complex. Based on the technical discussion in chapter 2, two suitable DSP techniques are selected, which are combined with a decimating transceiver software architecture to form a simple, robust, multirate envelope demodulator. The chapter concludes with a discussion of the implementation, a distortion analysis and an extensive performance assessment of a real time, fixed point multirate AM demodulator.

3.1 A REVIEW OF CLASSICAL AND CURRENT AM DEMODULATORS.

Historically, AM is a popular modulation mode although less efficient than SSB, due to its simplicity in generation and detection. AM implies that the information of the transmission is contained in the amplitude of a carrier signal. There are numerous roles in which AM transceivers are applied and this has resulted in differing modulation parameters, which include; modulation index, carrier accuracy and stability. If a DSP AM receiver is to have an acceptable performance it must accommodate all of these variations. There are two general classes of AM demodulators namely synchronous and envelope demodulators and the following discussion which reviews current and classical AM demodulators, is subdivided into these two categories.

3.1.1 Synchronous AM demodulators.

Figure 3.1 is a block diagram of a typical synchronous AM demodulator. There are three parts to the structure; carrier extraction, mixing and lowpass filtering. The mixer, synchronously demodulates the AM signal while the lowpass filter band limits the final signal. Carrier extraction is required due to the stability and accuracy of typical V/UHF transceiver's frequency references. The frequency reference is normally provided by a **temperature compensated crystal oscillator** (TCXO) whose accuracy is of the order of +/- 1 **part per million** (ppm). This could result, for example, in a maximum frequency difference of **+/-** (plus or minus) 800 Hz between the transmitter and receiver at 400 MHz. Furthermore, in older transceivers the problem is compounded by the frequency stability of the carrier which is sometimes frequency modulated due to poor internal circuitry isolation.

A simple technique of carrier extraction is to bandpass filter the carrier, followed by amplitude limiting in order to remove the modulation sidebands. Amplitude limiting however creates numerous harmonics which would alias in a sampled system causing distortion of the demodulated signal. Other conventional techniques of carrier tracking which do not suffer from aliasing problems as they produce a spectrally pure result, include the **phase locked-loop** (PLL) [Gardner, 1979, pg. 170-172] and Costas PLL [Lugowski, 1987]. However, since the capture range of the PLL would need to be several kHz wide, and frequency acquisition techniques add to the complexity of the PLL demodulator, adaptive filters could be applied to the problem of wideband carrier acquisition. The bandwidth of the adaptive filter may be designed to be a small fraction of the total capture range. A gradient search algorithm would then pre-steer the filter to extract and enhance the carrier. Although simple adaptive filter algorithms exist [Hush, 1986], this type of synchronous demodulator requires intensive IF processing due to the division

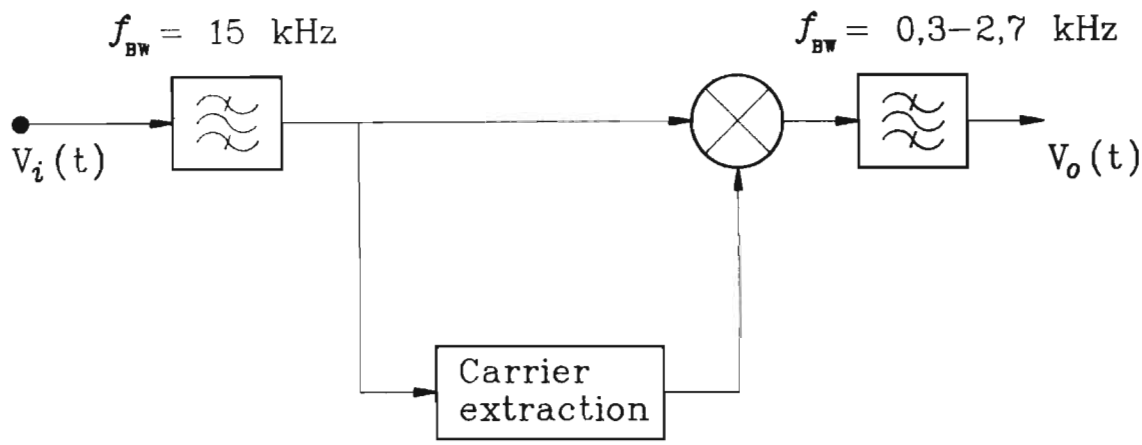

Figure 3.1 A typical synchronous AM demodulator.

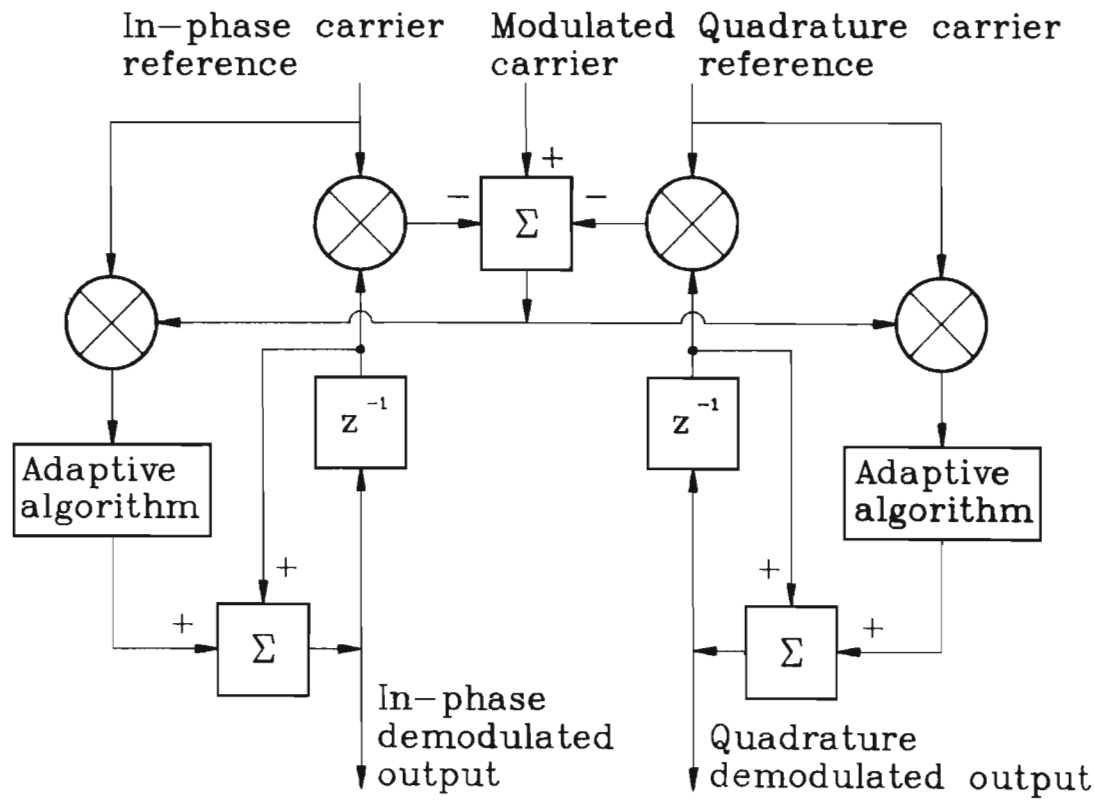

Figure 3.2 Yassa & Thompson's [1989] adaptive AM demodulator.

operation needed to speed up the convergence. A digital phase-locked loop also requires processing at the IF sampling rate. This can be avoided by making use of multirate techniques.

A recent AM demodulator based on a gradient search technique is described by Yassa and Thompson [1989] and a block diagram is given in figure 3.2. This adaptive AM demodulator corrects for phase differences between the transmitted carrier and receiver's reference and is applied as a digital demodulator [Yassa & Garverick, 1990]. It is, however, explained that frequency offsets would need to be corrected by other techniques thus adding to the complexity of the demodulator. This would typically require the inclusion of a PLL or adaptive filter which would result in a complicated demodulator structure.

In conclusion to the discussion on synchronous AM demodulators, it is often stated that they are used in preference to envelope or square law demodulators due to improved SNR detection performance, at low carrier to noise ratio, and improved distortion performance. Appendix 1 is a comparison of the SNR detection performance of the three classical AM demodulator architectures, namely the square law demodulator, the envelope demodulator and synchronous demodulator. It is apparent that for speech signals little practical advantage is gained by using synchronous AM demodulation, as a minimum SNR is required by a listener in order to understand the transmission.

A useful measure of the quality of speech signals has been defined by mobile cellular telecommunications system engineers and is generally known as "toll quality". Lee [1989, pg. 421] states that for a speech signal of toll quality the **total harmonic distortion** (THD) must be less than or equal to 2,3%. In section 3.2.2 results of the **percentage total harmonic distortion** (%THD) caused by the multirate envelope AM demodulator are discussed. For various carrier offsets, frequency deviations and modulation indices it is apparent that the percentage

distortion is typically less than 2%. Finally, it is noted that for speech, there is little advantage to synchronous AM demodulation if the demodulator architecture is more complex.

3.1.2 Envelope AM demodulators.

Envelope demodulators are popular techniques of AM detection as approximations are easy to implement with standard analogue components. Figure 3.3 is a general block diagram of an envelope demodulator. The input $V_i(t)$, which is an AM, bandpassed IF signal, is applied to a nonlinear function in order to detect the envelope of the carrier, while the lowpass filter removes any unwanted harmonics caused by the nonlinear detection.

The input $V_i(t)$ to the nonlinear demodulator is given by

$$V_i(t) = A_c(1 + m\cos\omega_m t)\cos\omega_c t \ , \qquad (3-1)$$

where ω_m is the angular frequency of the modulating signal, while A_c and ω_c are the amplitude and angular frequency of the carrier. This is Stremler's [1977, pg. 226-227] definition of a sinusoidally modulated AM signal which shall be adopted throughout the text. In Stremler's definition, m is known as the AM modulation index and is defined as

$$m = \frac{|A_m|}{|A_c|} \ , \qquad (3-2)$$

where $|A_m|$ is the modulus of the amplitude of the modulating signal.

A typical, nonlinear demodulator, for example the diode, could be modelled as a piecewise-linear device which switches at the rate of

Figure 3.3 The nonlinear envelope demodulator.

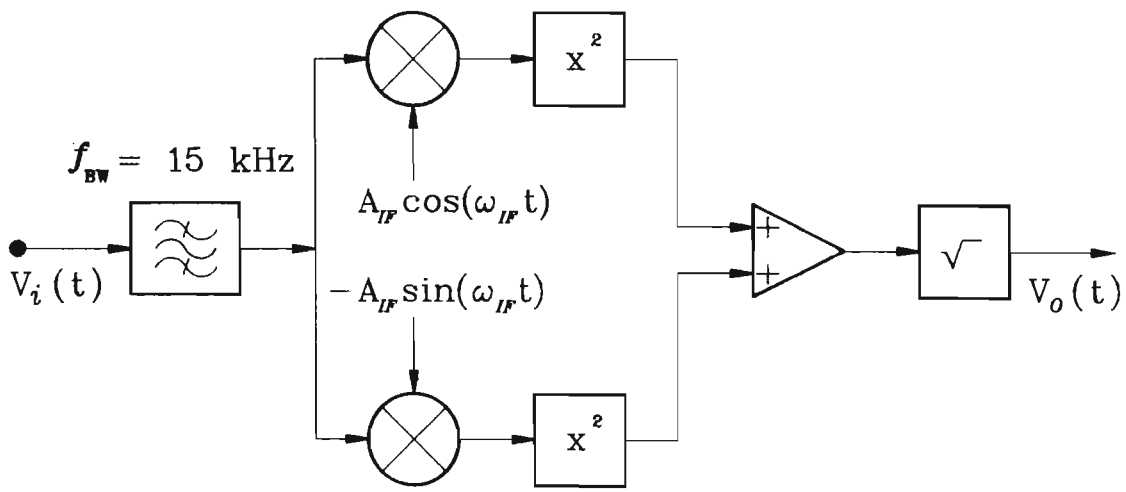

Figure 3.4 The quadrature envelope demodulator.

the carrier frequency [Schwartz, 1981, pg. 241-244] and whose output is given by

$$V_o(t) = S(t)A_c(1 + m\cos\omega_m t)\cos w_c t \ , \qquad (3\text{-}3)$$

where $S(t)$ is the switching function defined as

$$S(t) = \frac{1}{2} + \sum_{n=1}^{\infty} \frac{\sin(n\pi/2)}{n\pi/2}\cos n\omega_c t \ . \qquad (3\text{-}4)$$

The result is an infinite spectrum, with the harmonic amplitudes, decreasing with increasing frequency. Aliasing distortion results unless over sampling or interpolation of the AM signal is possible; which implies faster processing. To avoid the wideband spectrum, the switching demodulator could be replaced with a simple square law demodulator. Assuming sinusoidal modulation $A_m\cos\omega_m t$ the output of the true square law demodulator is given by

$$V_o(t) = A_c^2(1 + m\cos\omega_m t)^2\left(\frac{1}{2} + \frac{1}{2}\cos 2\omega_c t\right) \ . \qquad (3\text{-}5)$$

Following the filtering of the $\cos 2\omega_c t$ term the expression for $V_o(t)$ becomes

$$V_o(t) = \frac{A_c^2}{2} + A_c^2 m\cos\omega_m t + \frac{A_c^2 m^2}{4}\cos 2\omega_m t + \frac{A_c^2 m^2}{4} \ . \qquad (3\text{-}6)$$

This derivation shows that the square law demodulator detects the envelope of the AM signal, although distortion occurs. The distortion introduced is given by the $\cos 2\omega_m t$ term. A percentage distortion, $\%D_{SL}$, is derived from equation 3-6 by obtaining the ratio of the demodulated signal to the distortion component. The distortion is given by

$$\%D_{SL} = 25m\ \% \ . \qquad (3\text{-}7)$$

By substituting various modulation indices it is apparent that even for small indices the distortion is large. To encompass all types of operation the modulation index can vary from 0,3 to as large as 0,9.

Thus, although simple in implementation, the performance of the square law demodulator is limited by distortion which implies the need for linear envelope detection. This is achieved by using a more complex technique, namely quadrature envelope demodulation.

A quadrature envelope demodulator is shown in figure 3.4, the baseband **in-phase** (I) and **quadrature** (Q) components are generated by mixing the AM input with 90 degree phase shifted local oscillator signals. To obtain the amplitude of the carrier, the I and Q signals are squared, added and finally square rooted which is synonymous with finding the modulus of a complex number. A simplified derivation of this demodulator is;

$$V_i(t) = A_c(1 + m\cos\omega_m t)\cos\omega_c t \qquad (3-8)$$

where $V_i(t)$ is the AM input to the quadrature demodulator. Mixing with the 90 degree local oscillator signals, $A_{IF}\cos\omega_{IF}t$ and $-A_{IF}\sin\omega_{IF}t$ followed by lowpass filtering results in

$$I(t) = \frac{A_c A_{IF}}{2}(1 + m\cos\omega_m t)\cos(\omega_c - \omega_{IF})t \qquad (3-9)$$

and

$$Q(t) = \frac{-A_c A_{IF}}{2}(1 + m\cos\omega_m t)\sin(\omega_c - \omega_{IF})t \ . \qquad (3-10)$$

Squaring and adding equations 3-9 and 3-10 results in

$$V_o(t) = \frac{A_c^2 A_{IF}^2}{2}(1 + m\cos\omega_m t)^2 \ . \qquad (3-11)$$

Finding the square root and removing the DC term finally results in the demodulated signal.

An alternative notation is to consider the complex nature of the I and Q signals which is given by $r(t)\exp(j(\omega_c - \omega_{IF})t)$ where $r(t)$ is the amplitude modulation term. This ideal signal is only obtained if the gains of the I and Q paths are equal and the phase difference is exactly 90 degrees. The effect of a gain and phase imbalance, as discussed in section 3.2.2, results in an image response which is the

negative of $(\omega_c - \omega_{IF})t$. This error signal is the suppressed AM signal which has been demodulated to baseband. If a frequency offset occurs between transmitter and receiver, or the transmitter's AM signal is frequency modulated, then the suppressed carrier may fall in the demodulated signal's frequency band causing tonal interference. This type of interference is most noticeable for small AM modulation indices. The added effect of the sidebands of the suppressed AM carrier are ignored as they are relatively small compared to the carrier. It is important to note that the error image power is a function of the combined amplitude and phase imbalance. As an example of the magnitude of the effect of the errors, a maximum power imbalance ratio of 0,086 dB and maximum phase error of 1 degree between the I and Q signals is required to obtain approximately 40 dB of suppression of the error image component.

The modulus function is the second source of distortion in the quadrature envelope demodulator. From the distortion analysis in section 3.2.2 it is shown that a peak fractional error of 0,0024 results in a percentage distortion of approximately 0,12%. This distortion is in the form of harmonically related components which are more acceptable than the error image's tonal frequency distortion.

Although the quadrature envelope AM demodulator requires accurate algorithms it will be shown that by selecting a sampling frequency which is four times the carrier frequency, various symmetries are exploitable and a simple, efficient multirate demodulator results.

3.2 THE NOVEL MULTIRATE AM DEMODULATOR.

From a comparison of the different AM demodulators the author has concluded that a suitable structure is the quadrature envelope demodulator, although it requires accurate algorithms to minimize

distortion. The author starts this section by deriving the multirate AM demodulator which is essentially obtained by combining three algorithms. This is followed by a discussion on a fixed point implementation and a theoretical distortion analysis. The section is concluded with an extensive performance assessment of a fixed point implementation of the AM demodulator.

3.2.1 The derivation and implementation of the multirate AM demodulator.

Essentially the quadrature envelope AM demodulator consists of two parts. The first part creates the quadrature signals while the modulus of the complex number, forming the second part, extracts the amplitude of the carrier. This subsection begins with a brief comparison of DSP techniques which are employed in the quadrature envelope AM demodulator. This is followed by a discussion of an implementation and assessment of a multirate fixed point AM demodulator.

Three methods of obtaining quadrature signals were reviewed and compared in section 2.1. The reader is referred to this section for the list of references on this topic. The first technique is to use analogue mixers followed by sampling. This approach has practical limitations due to the difficulty of accurately balancing the amplitude and phase difference between the analogue local oscillators. To circumvent this problem sampling techniques were then developed as a second technique, although they result in a timing misadjustment between the quadrature signals. The **discrete Hilbert transform** (DHT), which is in the form of a digital filter, is the third technique of creating quadrature signals. FIR or IIR filters structures have been developed as discrete Hilbert transformers. Since it will be shown

in section 3.2.2 that decimation may be applied to AM demodulation without a degradation in the SNR performance, Rader's [1984] IIR DHT filter is preferred as it provides a processing advantage.

Section 2.2 compares different algorithms for finding the modulus of the complex number. The algorithms are categorized into two types; the square root and the direct approximation techniques. By comparing processing complexity versus accuracy the author concluded that Freeman's [1978] direct approximation technique, since complex signals are available, is the best compromise. The multirate AM demodulator, as suggested, is a combination of Rader's [1984] I and Q filter structure, Freeman's [1978] linear approximation technique and a modified version of Carter's [1988] software architecture for DSP radios. This software architecture and its application to decimation, is described in greater detail in the proceeding paragraphs, as it is an essential part of the multirate AM demodulator implementation.

Figure 3.5 gives a block diagram of the implementation of the multirate AM demodulator where the bandwidth limited IF signal is four times over sampled and a natural halving of the sample rate occurs when even and odd samples are processed alternatively in the two phase shifting filters. The z transform details of these phase shifting filters $H_1(z)$ and $H_2(z)$, are provided by equations 2-7 and 2-8 respectively. Following the filtering process the sample rate is again halved, to result in an overall four times decimation and consequently, baseband I and Q signals. The linear approximation algorithm is then applied at the four times decimated rate, to the baseband I and Q signals, to extract the amplitude of the complex number.

Figure 3.6 gives a signal processing software flowchart of the multirate AM demodulator as part of a total DSP radio. The architecture is similar to that described by Carter [1988] which is used for SSB demodulation, the difference being the addition of an extra level of decimation. There are three levels of decimation which imply three

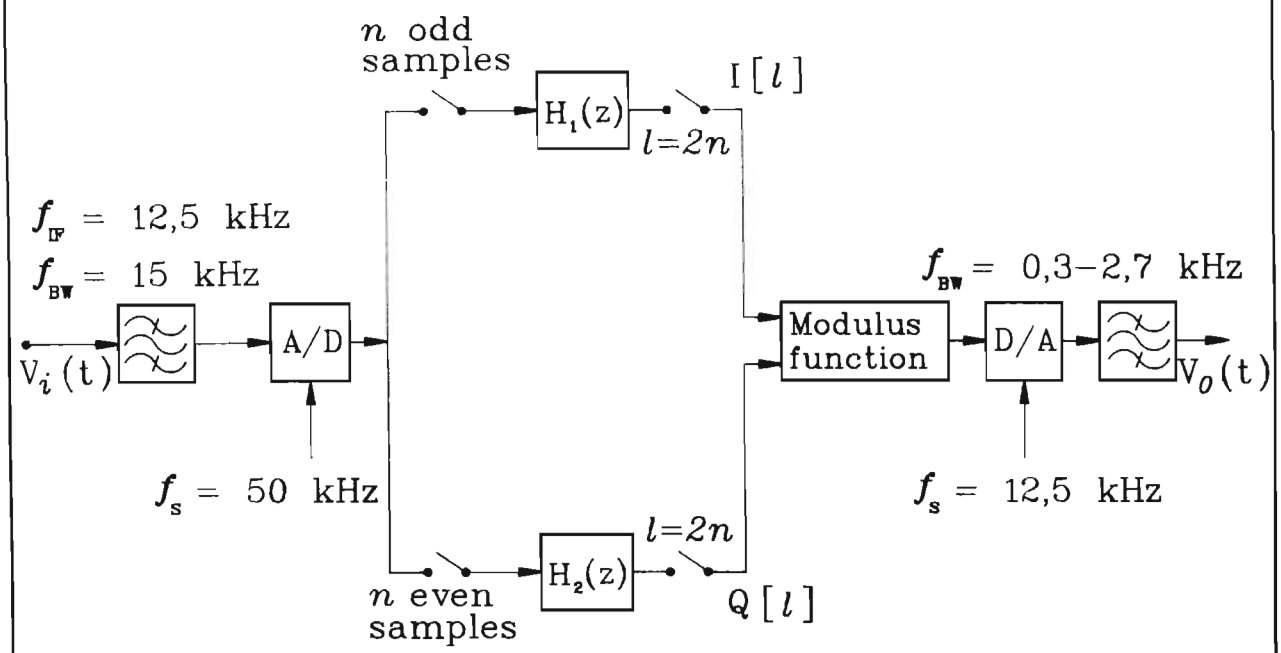

Figure 3.5 A block diagram of the multirate AM demodulator.

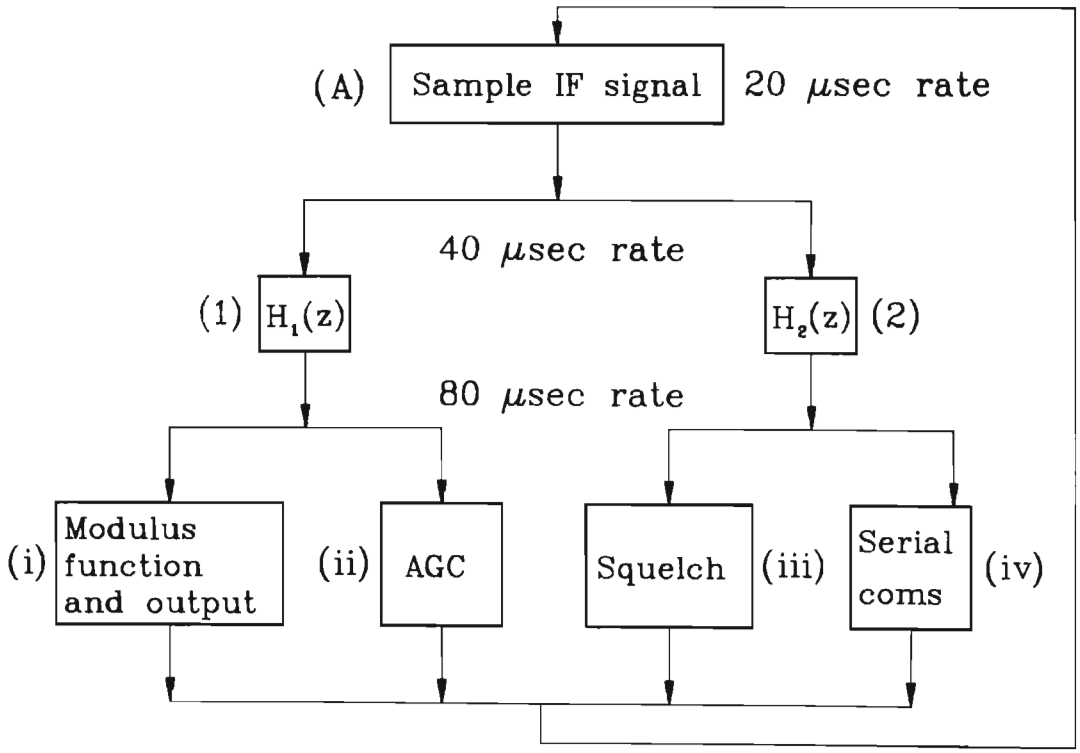

Figure 3.6 A software block diagram of the multirate AM demodulator.

different processing frequencies. The top level is typically 50 kHz which is four times the IF frequency of 12,5 kHz and in this application only includes the sampling of the IF signal. The second level of processing occurs at twice the IF frequency, or 25 kHz, and this includes the phase shifting filters; while the third level of processing occurs at 12,5 kHz and typically includes either the modulus function, automatic gain control, squelch or serial communications.

With reference to figure 3.6, each of the blocks represents a subroutine, and besides executing a signal processing function, also sets up the address of the next subroutine to be processed, which is on the same sampling rate level. For example, subroutine (1) places the address of subroutine (2) into a variable so that in the next sample period, subroutine (2) is processed in place of subroutine (1). In reciprocation subroutine (2) places the address of subroutine (1) into the variable and a simple two times decimation occurs. The execution of the various levels of subroutines occur in the following sequence which is repeated every four sample periods:-

n th period = A,1 and i subroutines.
n + first period = A,2 and ii subroutines.
n + second period = A,1 and iii subroutines.
n + third period = A,2 and iv subroutines.

At this point the cycle of four repeats itself for example.....
n + fourth period = A,1 and i subroutines ad infinitum.
Appendix 4 includes a sample program to assist in the understanding of the finer details of the multirate AM demodulator.

By combining the two algorithms into the software architecture a maximum of five decisions (two for the software architecture and three for the modulus function) and five multiplications (one for the filter and four for the modulus function) are required for a single 50 kHz processing period of the AM demodulator. Thus the multirate AM

demodulator is an attractive and simple solution for a single DSP microprocessor executing parallel tasks, in real time, for a portable transceiver.

3.2.2 A distortion analysis of the multirate AM demodulator.

In this subsection equations describing the percentage distortion caused by inaccuracies in the Hilbert transform and modulus function, which are combined to form the multirate AM demodulator, are derived.

Initially, it is shown that the filter Hilbert transform and decimating structure, as shown in figure 3.7, is equivalent to the quadrature mixing and lowpass filtering structure which is described by figure 3.8. Based on this equivalence the results of Roome's [1989] error analysis of the quadrature mixing and filtering structure are employed to determine the percentage distortion caused by the error image frequency. This part of the discussion concludes with a review of the effects of decimation on the SNR_O with special reference to AM.

The second part of this subsection considers the percentage distortion caused by the modulus operation as a function of its maximum fractional error. The subsection is concluded with a discussion of the combined effects of the two sources of distortion.

Crochiere & Rabiner [1983, pg 42-45] give the general relationship of a n sample decimation of a bandpass signal as

$$Y(\exp j\omega T'_s)=\frac{1}{n}\sum_{l=0}^{n-1} H_{BP}(\exp j(\omega T'_s-2\pi l)/n)X(\exp j(\omega T'_s-2\pi l)/n)\ , \quad (3\text{-}12)$$

where $Y(\exp j\omega T'_s)$ is the result after decimation, and T'_s is the new sampling rate after decimation. The sampled signal prior to decimation consists of the n bands of interest defined by

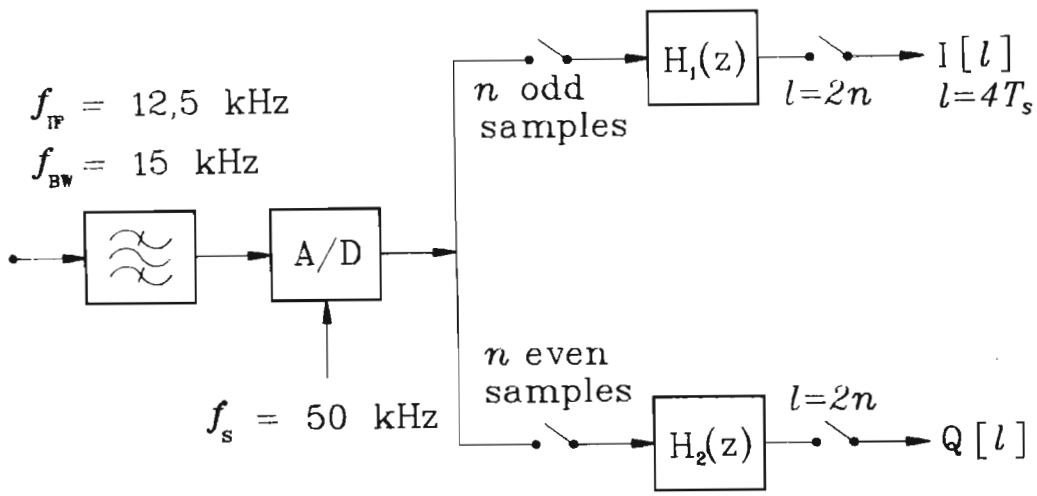

Figure 3.7 Filtering and decimation technique to obtain the I and Q signals. (AMRXPHD2.ASM).

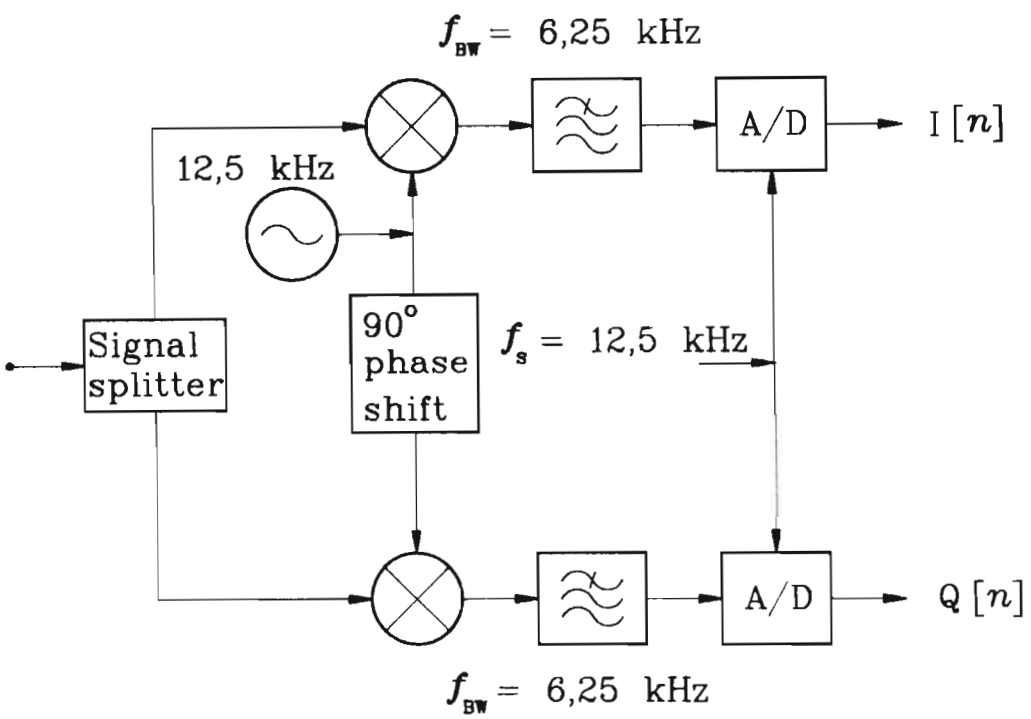

Figure 3.8 Roome's [1989] mixing and sampling technique to obtain the I and Q signals.

$H_{BP}(\exp j\omega T'_s)X(\exp j\omega T'_s)$. These bands of interest are demodulated by the $2\pi l/n$ terms due to the n sample decimation. To prevent aliasing Crochiere & Rabiner prescribe that only certain frequency bands should be allowed. These frequency bands are typically selected, after sampling, by the discrete-time bandpass filter $H_{BP}(\exp j\omega T_s)$ where

$$H_{BP}(\exp j\omega T_s) = \begin{cases} 1, \text{ for } l\frac{\pi}{n} < |\omega| < (l+1)\frac{\pi}{n} \\ 0, \text{ otherwise,} \end{cases} \qquad (3\text{-}13)$$

$l = 0, 1, 2, \ldots, n-1$ and T_s is the sampling rate before decimation.

As an example of equations 3-12 and 3-13, in a SSB system where the sampling frequency is four times the IF frequency, a four times decimation can be utilized to demodulate the signal to baseband. The lower sideband resides within the region defined by $l = 1$ and the upper sideband in the region defined by $l = 2$. Typically the DSP IF SSB sideband filter is a lowpass filter for the lower sideband and a highpass filter for the upper sideband. An analogue IF filter then restricts the receiver bandwidth to $l = 1, 2$ before IF sampling thereby creating a bandpass IF SSB filter [Carter, 1988]. Although decimation, as with mixing, results in a frequency translation it does not require post lowpass filters to remove the double frequency term. Instead, prior anti-aliasing filtering and correct selection of sampling rate of the IF is sufficient taking into consideration the bandwidth of the IF signal.

Assuming that the AM IF signal $V_i(t)$ is bandlimited to the frequency range of $\pi/4$ to $3\pi/4$ (or $l = 1, 2$) it can be defined as

$$V_i(t) = r(t) A_c \cos\{\omega_c t + \phi(t)\} , \qquad (3\text{-}14)$$

where $r(t)$ is the amplitude modulation term. Following the Hilbert transform and four sample decimation, the in-phase signal is given by

$$I(t) = r(t) \cos\{(\omega_c - \omega_{IF})t + \phi(t)\} , \qquad (3\text{-}15)$$

where $\omega_{IF} = 2\pi f_s/4$. Describing this in a complex envelope notation results in

$$I(t) = Re\{m(t)\exp j(\omega_c - \omega_{IF})t\} \ , \qquad (3\text{-}16)$$

where $m(t) = r(t)\exp j\phi(t)$ and $Re\{\}$ implies the real part of the $\exp j(\omega_c - \omega_{IF})t$ expansion. Similarly the quadrature signal is defined by

$$Q(t) = Im\{m(t)\exp j(\omega_c - \omega_{IF})t\} \ , \qquad (3\text{-}17)$$

where $Im\{\}$ implies the imaginary part of the $\exp j(\omega_c - \omega_{IF})t$ expansion. These two signals are combined to create the complex signal given by

$$V(t) = m(t)\exp j(\omega_c - \omega_{IF})t \ . \qquad (3\text{-}18)$$

The result is the same as Roome's [1989] derivation for the quadrature mixing and filtering structure, as given in figure 3.8, except for a gain difference of 0,5 caused by the mixing process. Roome completes his analysis by deriving the power ratio between the carrier and error image which is given by

$$\text{Image ratio} = 10\log_{10}(\alpha^2 + \gamma^2) - 6{,}0 - 4{,}3\alpha \ \ \text{dB}, \qquad (3\text{-}19)$$

where α is the gain error, as an amplitude ratio; while γ is the phase error in radians between the I and Q signals. The error image results in a suppressed AM signal at the frequency of $(\omega_c - \omega_{IF})t$. Roome's [1989] image power equation needs to be adjusted for the modulation index and the 0,5 gain difference in order to determine the percentage distortion caused by the error image. The adjusted equation is given by

$$P_{IM} = (\alpha^2 + \gamma^2)\left(\frac{2 + m^2}{m^2}\right)P_m \ , \qquad (3\text{-}20)$$

where P_{IM} is the error image power and P_m is the total power in the AM sidebands. It is useful to relate this result to the %THD as measured by a distortion meter. The percentage harmonic distortion caused by a phase and/or gain imbalance is derived by relating the distortion power to the demodulated signal's power

$$P_o = \left(1 + \frac{2 + m^2}{m^2}\{\alpha^2 + \gamma^2\}\right)P_m \ , \qquad (3\text{-}21)$$

where P_o is the total output power of the demodulator, ignoring any distortion contributed by the modulus function. The percentage harmonic distortion is derived from Millman's definition [1979, pg. 665], and for the quadrature signal, $\%D_{QUAD}$ is given by

$$\%D_{QUAD} = 100\sqrt{\frac{2+m^2}{m^2}\{\alpha^2+\gamma^2\}} \quad . \tag{3-22}$$

A typical peak phase error for a IIR Hilbert transform is 0,002 radians [Rader, 1984] with a negligible gain imbalance. For a modulation index of 0,9 and assuming a sinusoidal error ripple results in a $\%D_{QUAD}$ of approximately 0,37%.

Decimation is a useful signal processing technique as it matches the bandwidth of the signal to its sampling rate although prior anti-aliasing filtering is required to prevent a degradation in the SNR_O. Vaughan et al. [1991] describe this noise adding effect which occurs if the noise power in the wanted frequency band is similar to the noise power in the unwanted band.

In a receiver, when detecting a weak signal in noise, the typical spectrum is given in figure 3.9. The automatic gain control retains a constant signal and noise power and therefore there is an effective increase in the noise floor. As a result, aliasing of the noise within the bands $l = 0,1,3$ for a upper sideband signal causes a negligible effect in the **output signal to noise power ratio** (SNR_O) although this decreases as the **input signal to noise power ratio** (SNR_i) increases as shown in figure 3.10. Fortunately, however this degradation for a large SNR_i has little effect on the perceived SNR_O.

Due to the double sideband nature of AM it falls in the frequency regions defined by $l = 1,2$. Brown [1983] proves that it is possible to demodulate the signal by sampling at a frequency which is only twice the final bandwidth of the demodulated signal, if the frequency of the IF is correctly selected. No mention is made as to effect of the

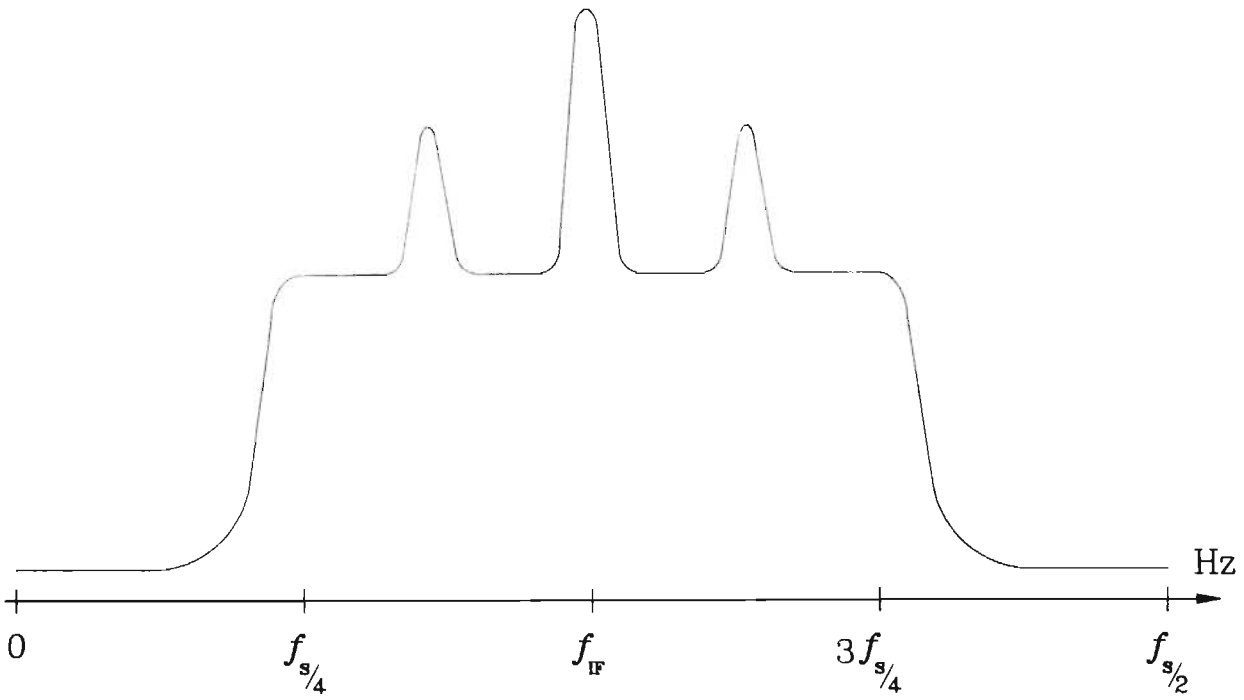

Figure 3.9 A spectral plot of a weak AM signal in noise.

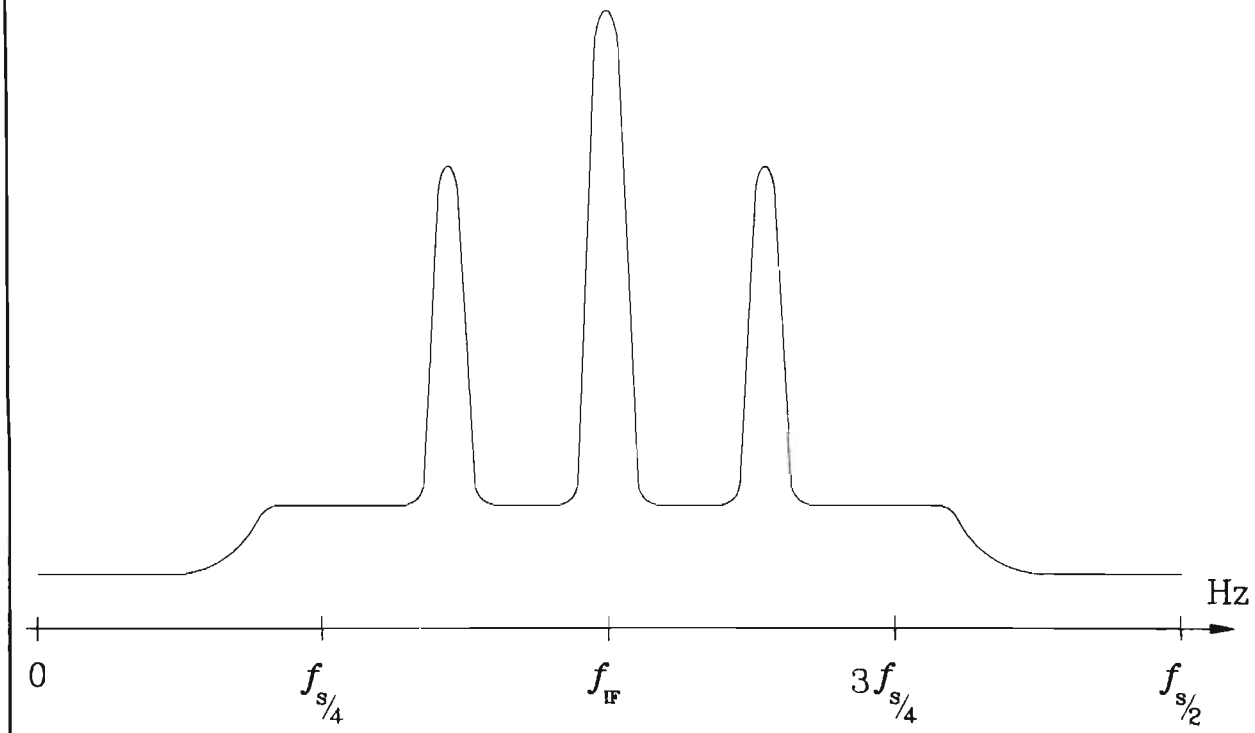

Figure 3.10 A spectral plot of a strong AM signal in noise.

final SNR_O due to the aliasing of the lower sideband on the upper sideband, however since the one sideband is a mirror of the other, and the quadrature structure corrects for any frequency offsets no degradation in the ultimate SNR_O occurs. Table 3.1 compares the SNR_O for two different quadrature demodulator architectures for a range of **input carrier to noise power ratio**'s (CNR_i) and a modulation index of 0,6. The first program, AMRXPHD2.ASM is based on the structure shown in figure 3.7 where decimation is employed to demodulate the signal so as to take advantage of the slower processing rate before applying the modulus operation. The second program AMRXPHD3.ASM, is the structure shown in figure 3.11 employs no decimation and the AM signal is demodulated by applying the modulus function directly at the IF. From the results it is apparent that no degradation occurs in the final SNR_O for a low CNR_i when applying decimation in the demodulation process.

The modulus function is the second source of distortion in the multirate AM demodulator. By neglecting the distortion effects of the quadrature signal mismatch, it is possible to determine the percentage distortion caused exclusively by the modulus function. By approximating the error ripple function of Freeman's [1978] modulus function technique by a cosinusoid, and applying a Taylor series expansion, an equation is derived, which is an estimate of the **modulus function's percentage harmonic distortion** ($\%D_{MOD}$).

The output of the modulus function which includes the **modulus function's fractional error** (ϵ_{MOD}) can be described by

$$V_o(t) = (1 + \epsilon_{MOD}) A_m \cos \omega_m t \ . \qquad (3\text{-}23)$$

Assuming that the error ripple is cosinusoidal and the rate of change of the error ripple amplitude is a function of the modulating signal then

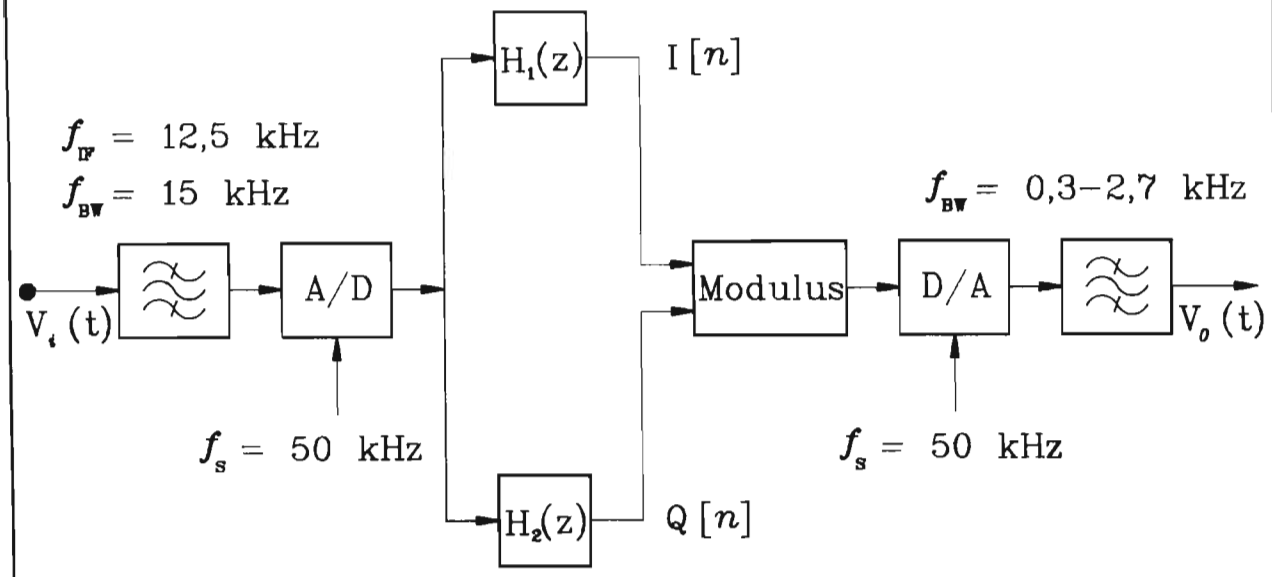

Figure 3.11 AM demodulator without decimation (AMRXPHD3.ASM).

CNR_i (dB)	SNR_o (dB) AMRXPHD2.ASM	SNR_o (dB) AMRXPHD3.ASM
21,92	14,31	14,09
18,49	11,37	11,34
15,80	7,95	8,08
13,77	6,19	5,62

Table 3.1 SNR_o for two different AM demodulator structures where the modulation index is 0,6.

$$\epsilon_{MOD} A_m \cos\omega_m t = \epsilon_{PMOD} \cos(A_m \cos\omega_m t) \ , \qquad (3\text{-}24)$$

where ϵ_{PMOD} is the modulus function's peak fractional error and is defined as

$$\epsilon_{PMOD} = \frac{A_o}{A_{ot}} - 1 \ . \qquad (3\text{-}25)$$

A_o is the actual peak amplitude, while A_{ot} is the true peak amplitude, of the demodulated signal. Using a Taylor series expansion and filtering the DC and harmonic components above the second harmonic, equation 3-24 results in

$$\epsilon_{MOD} A_m \cos\omega_m t \approx \frac{1}{4}(\epsilon_{PMOD} A_m \cos 2\omega_m t) \ . \qquad (3\text{-}26)$$

By substituting equation 3-26 into equation 3-23 and finding the power at the output of the demodulator, which includes the wanted signal and the distortion component, gives

$$P_o \approx \left(1 + \frac{\epsilon_{PMOD}^2}{4}\right) P_m \ . \qquad (3\text{-}27)$$

From this equation, the percentage harmonic distortion for the modulus function is obtained using Millman's definition [1979, pg. 665] and is given by

$$\%D_{MOD} \approx 100 \frac{(\epsilon_{PMOD})}{2} \ . \qquad (3\text{-}28)$$

A typical value for ϵ_{PMOD} is 0,0024 which results in a percentage harmonic distortion of approximately 0,12%.

The %THD of the complete AM demodulator, referred to as $\%THD_{AM}$, is the summation of the percentage distortions caused by its two parts [Millman, 1979, pg. 665].

$$\%THD_{AM} \approx 100\left(\frac{\epsilon_{PMOD}^2}{4} + \frac{2+m^2}{m^2}(\alpha^2 + \gamma^2)\right)^{1/2} \ , \qquad (3\text{-}29)$$

which is 0,39% for a modulation index of 0,9. Finally, repeating the calculations for a modulation indices of 0,6 and 0,3 results in a $\%THD_{AM}$ of 0,53% and 0,97%, respectively.

3.2.3 A performance assessment of the multirate AM demodulator.

In this section the performance of a fixed point implementation of the AM demodulator, using a 16/32 bit DSP microprocessor, is assessed. The signal to noise and the distortion performance for various operational parameters are measured and compared with expected theoretical results.

To measure the SNR performance of the AM demodulator, the demodulator was combined with an AGC algorithm and the analogue receiver utilized to limit the bandwidth of the signal and noise, which was combined and applied at the antenna. Figure 3.12 is a graph of the CNR_i versus SNR_o for two modulation indices, namely 0,9 and 0,6. The threshold of the demodulator which increases with increasing modulating index is evident. The 5 dB SNR_o value is marked and shows a close correspondence to the predicted CNR_i results predicted by Middleton [1987, pg. 539-598], the details which are described in Appendix 1. The predicted CNR_i for 5 dB SNR_o is 9 dB for a modulation index of 0,9 and 12,5 dB for a modulation index of 0,3. Unlike the limiter/ discriminator FM demodulator where the threshold is sharp and the SNR_o degrades rapidly, the quadrature envelope AM demodulator's threshold is far less pronounced and the effects much less disturbing.

Various $\%THD_{AM}$ measurements were performed to determine the robustness of the AM demodulator to various AM signal parameters. A Hewlett Packard 8904A Multifunction Synthesizer was utilized to generate the 12,5 kHz AM signal with various AM modulation indices,

carrier frequency offsets and carrier frequency modulations. The $\%THD_{AM}$ was measured with a Hewlett Packard 339A distortion meter which determines the percentage noise power plus distortion power. In these measurements the assumption was made that the distortion power was greater than the noise power. Figure 3.13 is a graph of the $\%THD_{AM}$ for three different modulation indices for various carrier frequency offsets. The measured results show close correspondence to the $\%THD_{AM}$ which were calculated in section 3.2.2. Generally the measured performance was marginally better than the calculated performance, within the passband of the Hilbert transformer. This is attributed to the design of Rader's [1984] IIR Hilbert transform where the phase error is only the bound of the design and consequently improved performance is expected at various carrier frequency offsets.

Figures 3.14 is a graph of the $\%THD_{AM}$ for a frequency modulated carrier of various frequency deviations and AM modulation indices, where the modulating frequency is 20 Hz. This waveform approximates an AM signal whose carrier frequency drifts slowly with time due to an unstable reference. Figure 3.15 is a graph of the $\%THD_{AM}$ for various carrier offsets when the carrier is frequency modulated with a deviation of 3,5 kHz and modulating frequency of 20 Hz. In both situations the $\%THD_{AM}$ for all the modulation indices is less than 1%. However, figure 3.16 is a graph of the $\%THD_{AM}$ for different frequency deviations when the modulating frequency is 1,5 kHz. This simulates the carrier instabilities in old AM transceiver's where the carrier is occasionally frequency modulated by the speech signal. The distortion increases dramatically as the frequency deviation increases, although a frequency deviation of 3 kHz can still be tolerated if toll quality is required. This distortion is attributed to the nonlinear group delay of Rader's [1984] IIR DHT and it is for this reason that a constant group delay FIR DHT is employed in the low sampling rate FM demodulator.

In conclusion the multirate speech AM demodulator is a processing efficient solution, requiring only five multiplications and five decisions for every output sample of the demodulated signal. The demodulator exhibits low distortion (typically less than 2%) for a wide range of modulation indices, carrier frequency offsets and deviations. Furthermore, the CNR_i versus SNR_o performance of the multirate speech AM demodulator exhibits a close correspondence to Middelton's [1987, pg. 539-598] theoretical analysis of the linear AM demodulator.

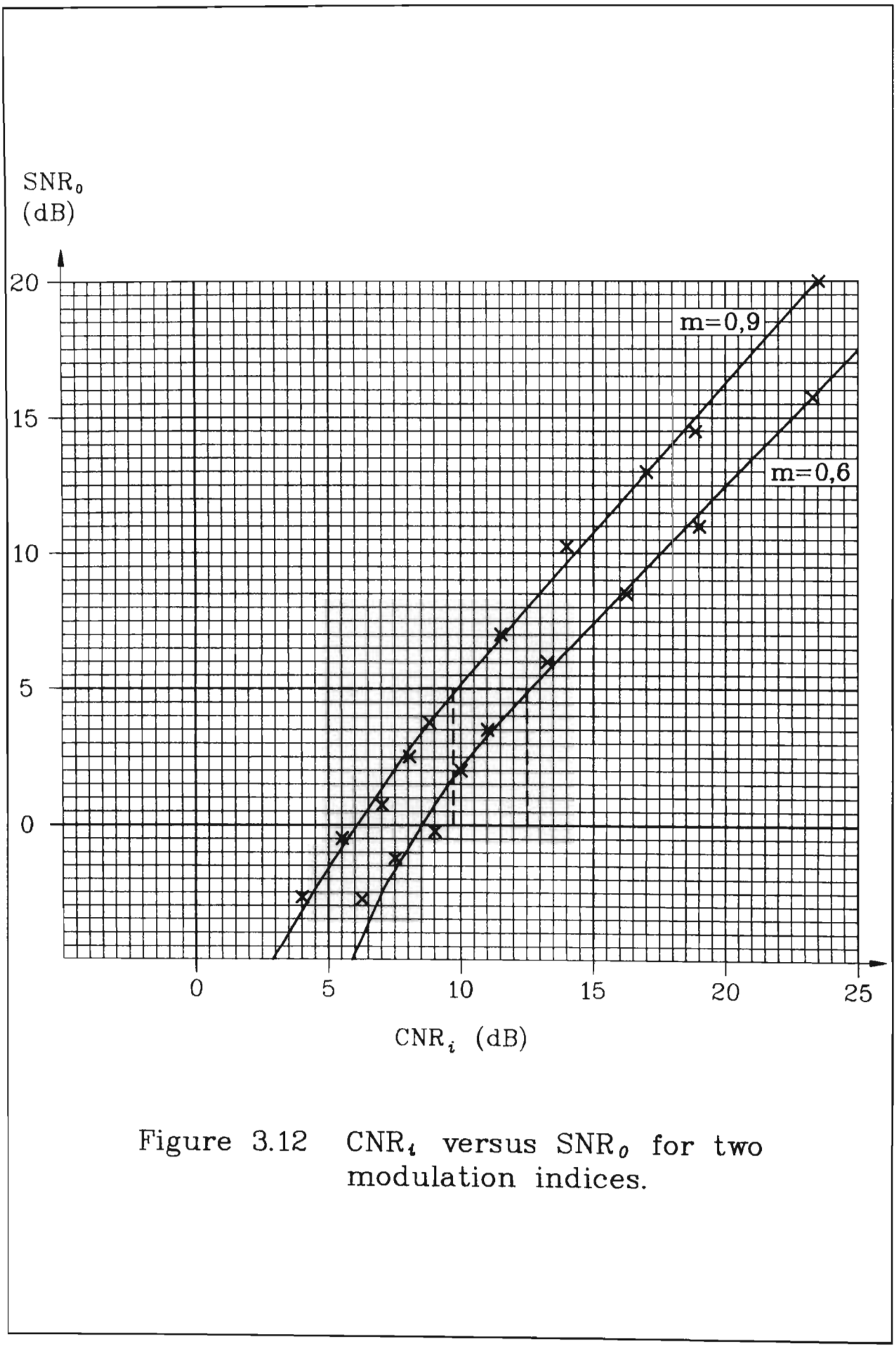

Figure 3.12 CNR$_i$ versus SNR$_o$ for two modulation indices.

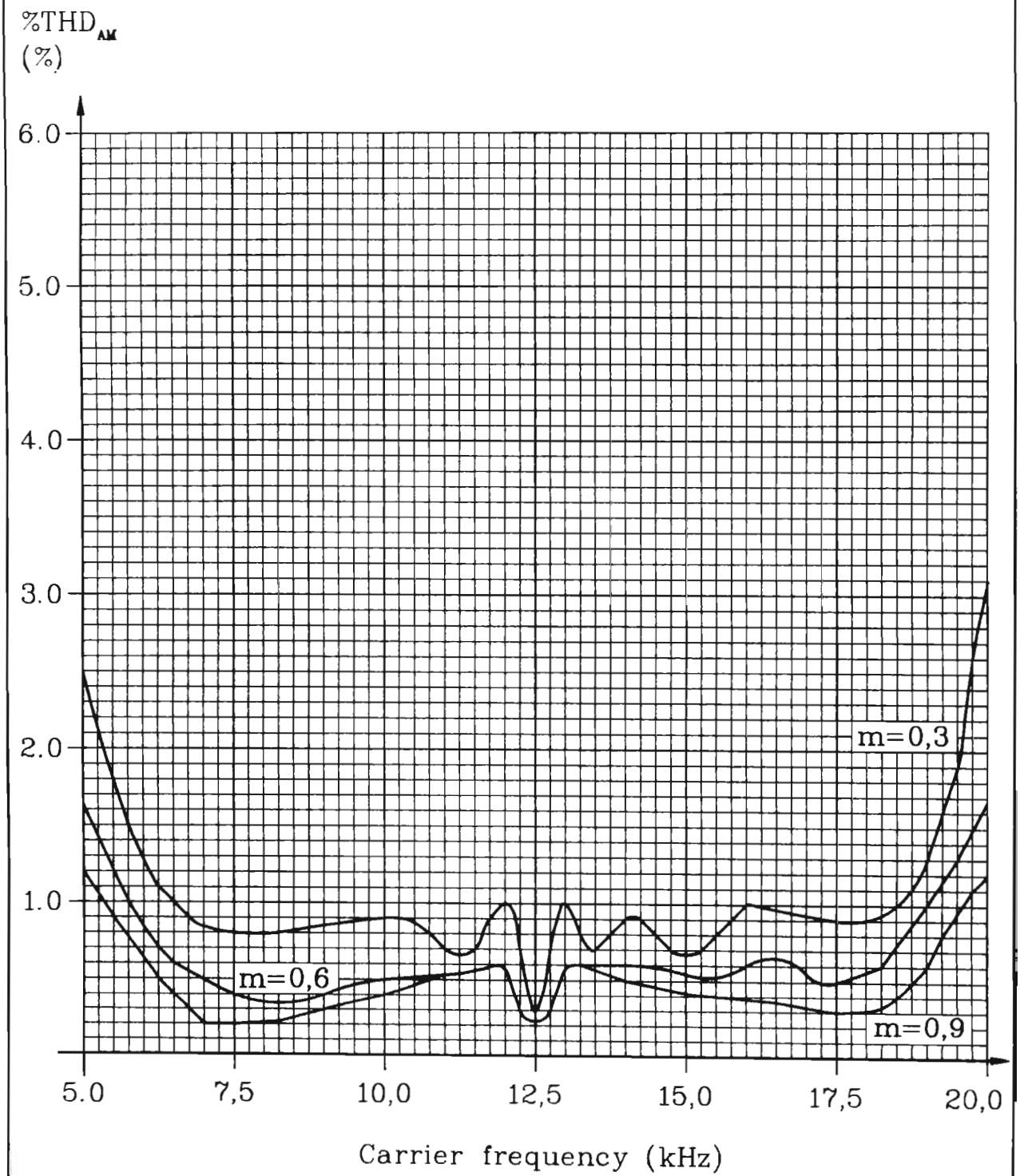

Figure 3.13 % THD_{AM} as a function of the carrier frequency.

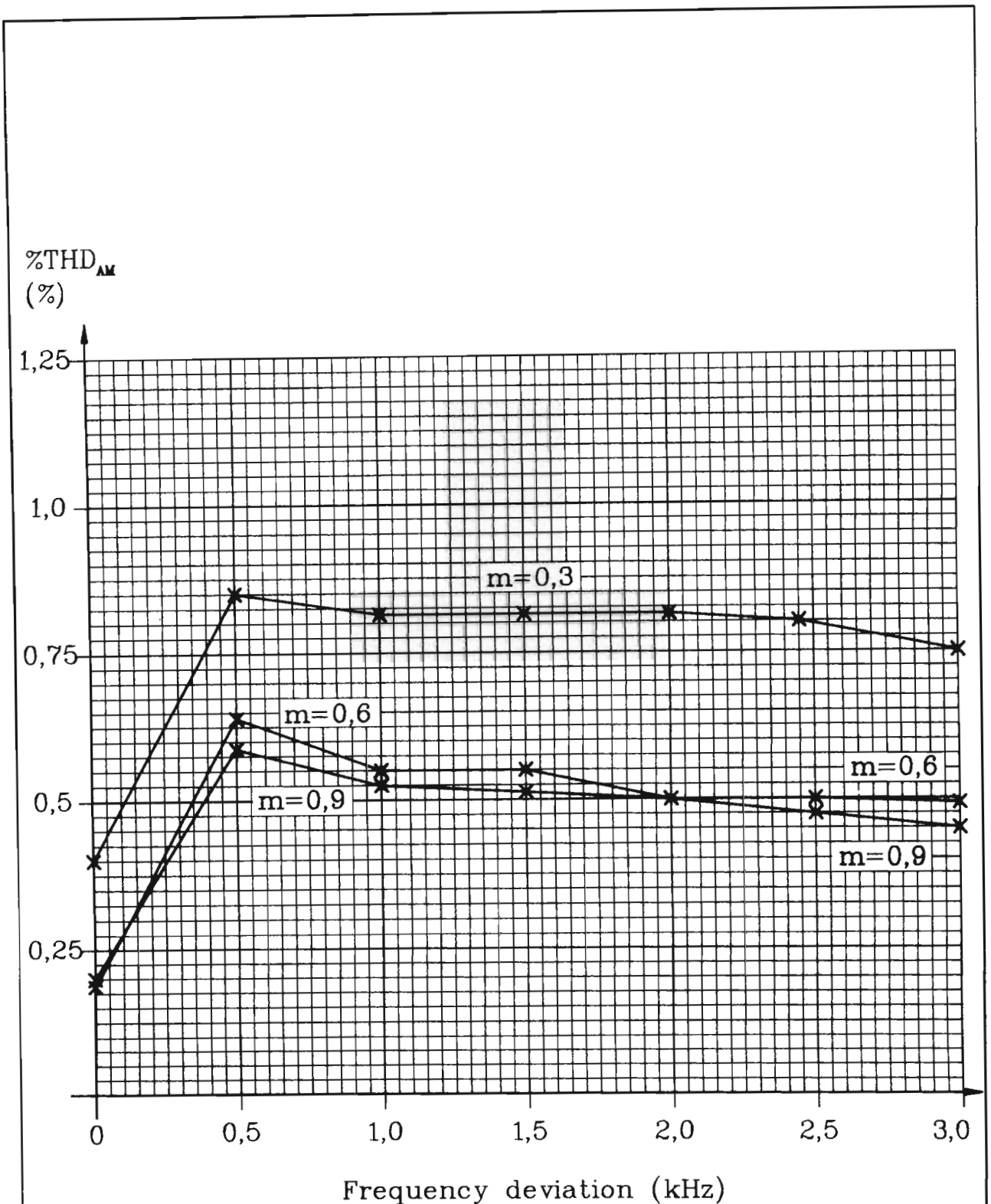

Figure 3.14 % THD$_{AM}$ for various frequency deviations and modulation indices.

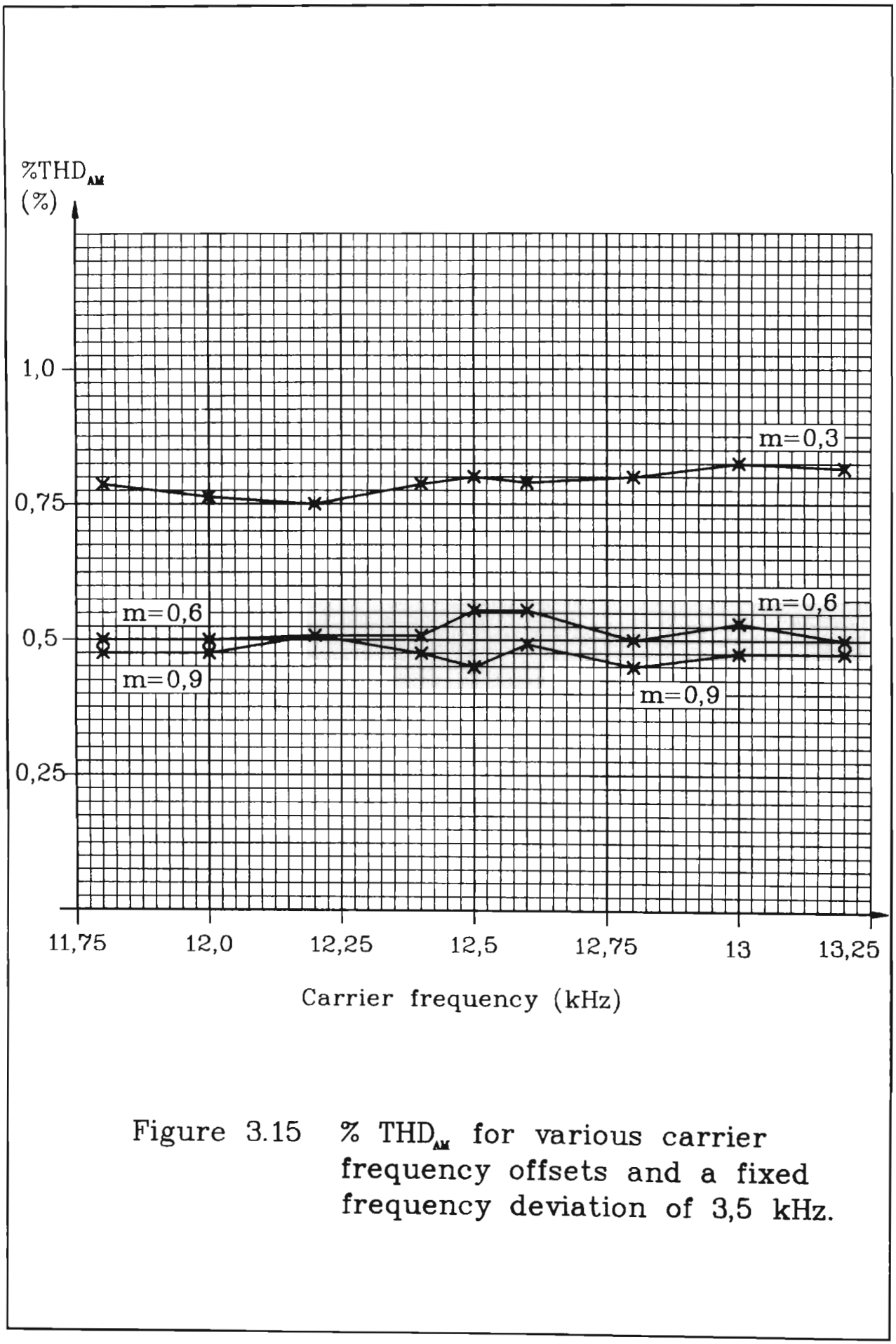

Figure 3.15 % THD_{AM} for various carrier frequency offsets and a fixed frequency deviation of 3,5 kHz.

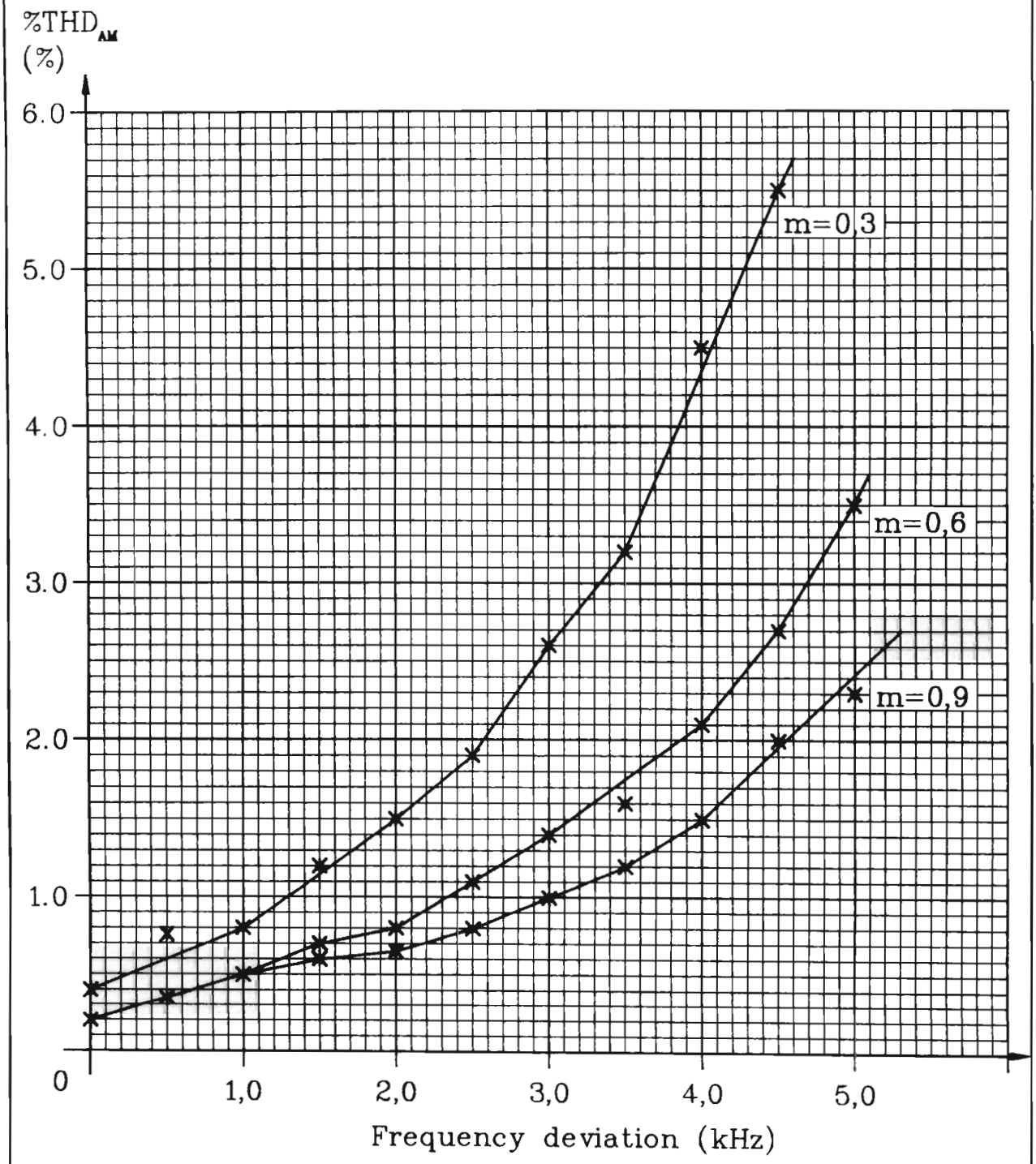

Figure 3.16 % THD_{AM} for various frequency deviations and a fixed modulation frequency of 1,5 kHz.

CHAPTER 4

A NOVEL DSP LOW SAMPLING RATE FM DEMODULATOR FOR SPEECH SIGNALS.

Within this chapter a novel DSP low sampling rate FM demodulator for speech signals is derived and assessed. The chapter begins with a review of classical and more recent VLSI FM demodulators. From this review it is concluded that the limiter/ discriminator FM demodulator is a suitable architecture when the bandwidth of the signal exceeds one quarter the sampling frequency and processing capabilities are limited. A low sampling rate FM demodulator is then derived which is essentially the combination of three DSP techniques. To allow analogue amplitude limiting of the FM signal a subharmonic sampling technique is described. This method allows interfacing at a high analogue IF frequency which simplifies the design of the post-limiter analogue filter. Following the derivation of the demodulator, the author conducts a distortion analysis. The distortion is caused by inaccuracies of the various DSP algorithms which form the sections of the low sampling rate FM demodulator. The chapter is concluded with an assessment of a fixed point implementation of the low sampling rate FM demodulator.

4.1 A REVIEW OF CLASSICAL AND CURRENT FM DEMODULATORS.

The origins of frequency modulation as a means of information transmission can be traced back to the early 1900s when it was thought that this modulation scheme could be used to compress a signal into a narrower transmission bandwidth than AM [Blachman, 1949]. Early researchers, however, disproved this theory and it was only in the mid-1930s that it was found that FM could be employed to reduce channel noise and interference by utilizing a wider transmission bandwidth

than AM does. Since that discovery, numerous schemes have been developed to demodulate FM signals and the author has chosen to categorize the various demodulators into four basic types. These four different types could be further categorized into two larger groups. The first group, are those demodulators which attempt to optimize their SNR_O performance for a low CNR_i, namely **phase-locked loop** (PLL) and **maximum a posteriori** (MAP) demodulators. The second group, which typically includes, direct conversion and limiter/ discriminator FM demodulators accept a degraded demodulation threshold in favour of a simpler architecture.

Before continuing with the review of different FM demodulators it is useful to briefly introduce the general terminology used throughout this chapter. A FM signal is defined as

$$V_i(t) = A_c \cos\left(\omega_c t + K\int_{-\infty}^{t} m(t)dt\right), \qquad (4\text{-}1)$$

where $m(t)$ is the modulating signal and K is the FM modulator constant. Assuming sinusoidal modulation, expansion of equation 4-1 results in

$$V_i(t) = A_c \cos(\omega_c t + \beta A_m \sin\omega_m t), \qquad (4\text{-}2)$$

where β is known as the FM modulation index. The FM modulation index is defined as $\Delta f / f_m$, where Δf is the peak frequency deviation and f_m is the modulating frequency, both in Hz.

4.1.1 Phase-locked loop FM demodulators.

The PLL is a classic technique of FM demodulation and in the last thirty years extensive research has been conducted into a variety of analogue and digital architectures. When operating as a FM demodulator, the PLL tracks the carrier's frequency and the driving signal to the voltage controlled oscillator is the modulating signal. PLLs have found their application in extending the FM demodulation threshold. The concept of threshold extension, which improves the SNR_O of the

demodulated signal for a low CNR_i, is described by figure 4.1. Gardner [1979, pg. 173-196] provides an excellent overview of analogue PLLs as FM demodulators and a few of his important conclusions are summarized in the following paragraphs:-

1. For a large CNR_i Gardner proves that the PLL has the same SNR_o improvement as the ordinary limiter/ discriminator.

2. The prior bandpass filter, the loop filter and the post-deemphasis filter are all essential to the optimal operation of the PLL FM demodulator.

3. The design of the PLL loop bandwidth is a compromise between noise rejection (which requires a narrow bandwidth) and carrier tracking (which requires a wide bandwidth). The optimum bandwidth is strongly dependent on the modulation parameters, hence a priori knowledge of the message statistics is required. The variation allowances in the design parameters of the PLL are small and the performance can rapidly degrade to that of a limiter/ discriminator. Enloe [1962] describes a further improvement in the SNR_o threshold performance of the PLL by employing a frequency feedback technique although a priori knowledge of the message statistics is still required.

Gardner states clearly that the analogue PLL FM demodulator is not the optimum demodulator, but only an approximation. An optimum demodulator would examine the entire message (even if it were of infinite duration) before producing the MAP estimate of the message. Since a **digital PLL** (DPLL) can be designed to incorporate signal delay it is suitable for utilization as an approximate MAP demodulator.

Concurrently in the 1970s while VLSI digital technology was rapidly being developed, research was also being conducted into techniques

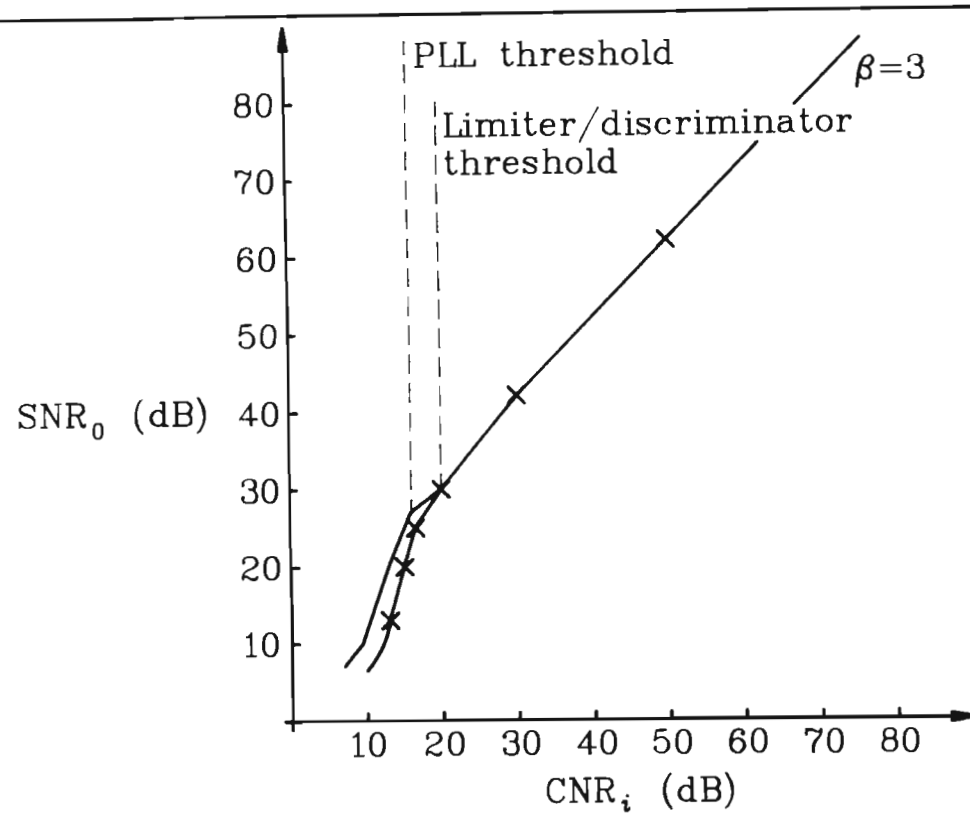

Figure 4.1 SNR_0 threshold extension of the PLL FM demodulator.

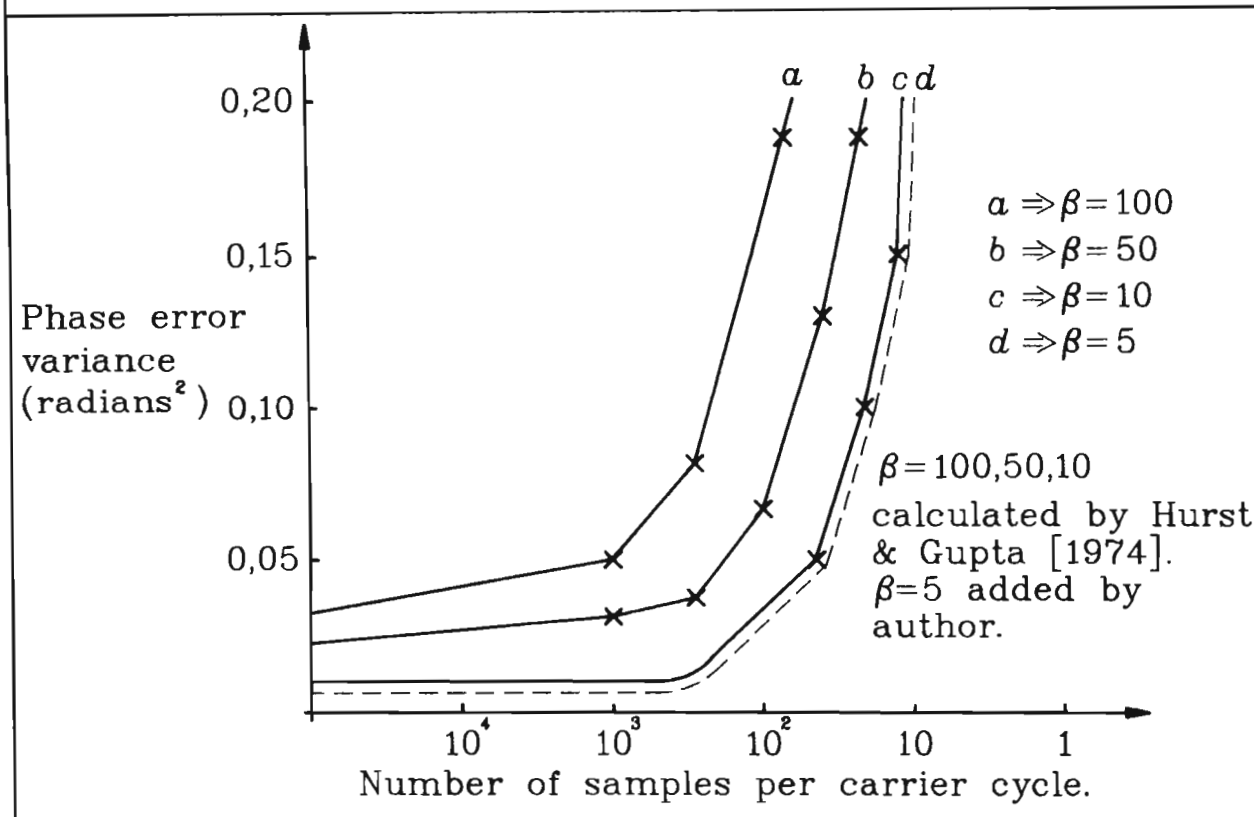

Figure 4.2 Phase error variance versus number of samples per carrier cycle [Hurst & Gupta, 1974].

of discrete-time demodulation of continuous-time signals. Kelly & Gupta [(1,2), 1972] applied nonlinear stochastic estimation theory to derive a DPLL as a near optimum FM demodulator.

McBride [1973] adopted a different approach (although also a DPLL derivative) where he employed a quadrature sampling technique to sample the FM signal at an IF frequency. The classical FM signal was translated to a discrete state-variable representation and from this model, Bayesian estimation and optimal control theory was utilized to derive a FM demodulator. The solution, which is a recursive algorithm, whose basic structure is a time varying DPLL automatically adjusts its loop gain as each sample arrives. This approach was an attempt to satisfy the conflicting requirements of a narrow loop bandwidth, to obtain a good SNR_o and wide loop bandwidth, for signal acquisition and tracking. In the optimization, the MAP criteria was used which resulted in a threshold extension of 3 dB for a $\beta = 25$. However, the nonlinear time varying gain processor results in a complex architecture.

Merritt [1989] more recently applied an iterated extended Kalman phase detector to a DPLL which resulted in a threshold extension of 6 dB for $\beta = 25$. Furthermore, the iterated extended Kalman phase detector has a reduced mean square error, and faster phase acquisition than a sinusoidal phase detector.

Although, employing DPLLs and their variations, results in improved demodulator threshold performance, they are not without practical problems and limitations:-

1. To optimize the DPLL FM demodulator a priori knowledge of the message statistics is necessary. In many applications this information is not available and would need to be calculated to prevent a degradation in performance.

2. In a DPLL the output of the numerically controlled oscillator is essentially a predictor which generates an estimate of the amplitude and phase of the carrier's current sample from previous input samples. The difference between the predicted value and the carrier's current sample results in a phase error. In all the DPLL examples it is assumed that a reasonably high sampling rate is utilized to minimize this phase error. An interesting study was carried out by Hurst & Gupta [1974] where they considered the quantization and sampling effects on a DPLL's phase error. Simple extrapolation of their results, as in figure 4.2, shows that even for a small FM modulation index of $\beta = 5$, a minimum sampling rate of approximately ten times the average carrier frequency is required. In an application where the sampling rate is only four times the average carrier frequency the resultant phase error would be significant.

3. The optimization techniques used in the development of the DPLLs result in complex FM demodulator architectures. Furthermore, high sampling rates are necessary which places this approach beyond the processing capabilities of a single DSP microprocessor solution executing multiple parallel functions.

4.1.2 Maximum a posteriori FM demodulators.

The general philosophy of MAP demodulators and DPLLs as approximate implementations, was discussed in section 4.1.1. Variations to MAP demodulators have been reported and the different schemes have been compared by Tufts & Rao [1977]. Nonlinear Bayesian estimation theory is utilized by Tam & Moore [(1,2), 1977] in the development of their MAP angle demodulator. Their demodulator is a nonlinear estimator consisting of a bank of extended Kalman filters where the signal estimate is a weighted sum of the outputs of the filters. In the limit

where the number of parallel filters becomes infinite, optimal demodulation in the minimum mean square error sense, in high noise, can be achieved. Although significant threshold extension can be achieved the demodulator is extremely complex. Furthermore, Tam & Moore show that the performance degrades rapidly as the sampling rate decreases while a priori knowledge of the message statistics is required to optimize the performance.

In concluding this discussion on PLL and MAP demodulators, it is apparent that significant threshold performance improvement is possible although this requires oversampling, complex algorithms and a priori knowledge of the message statistics. In a portable application neither the computational power nor exact message statistics are readily available. In addition, the advantage of a multimode transceiver is that alternative modulation schemes can be selected in poor SNR conditions; making the need to extend the threshold, debatable. Consequently, in the following two sections emphasis is placed on devising a FM demodulator architecture which is computationally efficient and applicable to low sampling rates, while accepting a degraded threshold performance.

4.1.3 Direct conversion FM demodulators.

Within this section two direct conversion FM demodulators are discussed. These demodulators, since they employ I and Q signals within their architecture, are alternatively known as sine-cosine demodulators. The first reference to a direct conversion FM demodulator was by Park Jr. [1970] which was later implemented on two analogue large scale integrated circuits [Goatcher, Neale & Vance, 1981]. More recently, Saulnier et al. [1990] reported the implementation and assessment of a VLSI discrete time version of the demodulator for **land mobile radio** (LMR) applications.

Park Jr.'s classic sine-cosine FM demodulator is shown in figure 4.3. The IF FM signal is mixed to baseband by quadrature local oscillator signals. Following differentiation the I and Q signals are mixed with the differentiator input signals which essentially results in synchronous AM demodulation. From the definition of the FM signal $V_i(t)$ where

$$V_i(t) = A_c \cos(\omega_c t + \phi(t)) \tag{4-3}$$

and

$$\phi(t) = K \int_{-\infty}^{t} m(t)dt \ , \tag{4-4}$$

a derivation of the demodulator is possible. Referring to figure 4.3; following mixing and lowpass filtering of the I and Q signals results in

$$I(t) = \frac{A_c}{2} \cos\phi(t) \tag{4-5}$$

and

$$Q(t) = -\frac{A_c}{2} \sin\phi(t) \ . \tag{4-6}$$

Differentiating the I and Q signals gives

$$\frac{dI(t)}{dt} = -\frac{A_c}{2} \sin\phi(t) \frac{d\phi(t)}{dt} \tag{4-7}$$

and

$$\frac{dQ(t)}{dt} = -\frac{A_c}{2} \cos\phi(t) \frac{d\phi(t)}{dt} \ . \tag{4-8}$$

The final stage of the demodulator is given by

$$V_o(t) = \frac{dI(t)}{dt} Q(t) - I(t) \frac{dQ(t)}{dt} \ . \tag{4-9}$$

Substituting equations 4-5 to 4-8 into equation 4-9 results in

$$V_o(t) = \frac{A_c^2}{4} \sin^2\phi(t) \frac{d\phi(t)}{dt} + \frac{A_c^2}{4} \cos^2\phi(t) \frac{d\phi(t)}{dt} \ . \tag{4-10}$$

and finally

$$V_o(t) = \frac{A_c^2}{4} m(t) \ . \qquad (4\text{-}11)$$

A direct DSP implementation of Park Jr.'s demodulator is possible although processing intensive, since post-mixer lowpass filtering and differentiation is required for both the I and Q signals.

More recently the literature has included descriptions of customized LMR VLSI demodulators [Saulnier et al., 1990; Saulnier & Rafferty, 1990]. Figure 4.4 is a block diagram of a typical VLSI FM demodulator [Saulnier et al., 1990] with a brief description of the circuit as follows; the bandpass, amplitude limited FM IF signal is sampled at a frequency of four times the carrier frequency. This is proceeded by a +1/-1 multiplier, or mixer, which demodulates the signal to baseband. A simple, third order FIR **discrete hilbert transform** (DHT) which is preceded by a simple DC removal circuit then generates I and Q signals, while a nonlinear sine and cosine detector finally results in a frequency to amplitude conversion [Thiel & Saulnier, 1990]. In the design a low order DHT is utilized to create the I and Q signals, as it is assumed that the bandwidth of the FM signal is small compared to the sampling rate. Furthermore, since the differentiator is a simple combination of two delays, a nonlinear frequency to amplitude transfer function results. A **read only memory** (ROM), look-up table is required to linearize the transfer function. In the application however, where the bandwidth of the FM signal exceeds a quarter of the sampling frequency, wideband techniques are required. It is also more preferable, where memory space is limited due to power consumption, to employ a higher order, linear, FIR differentiator rather than a look-up table.

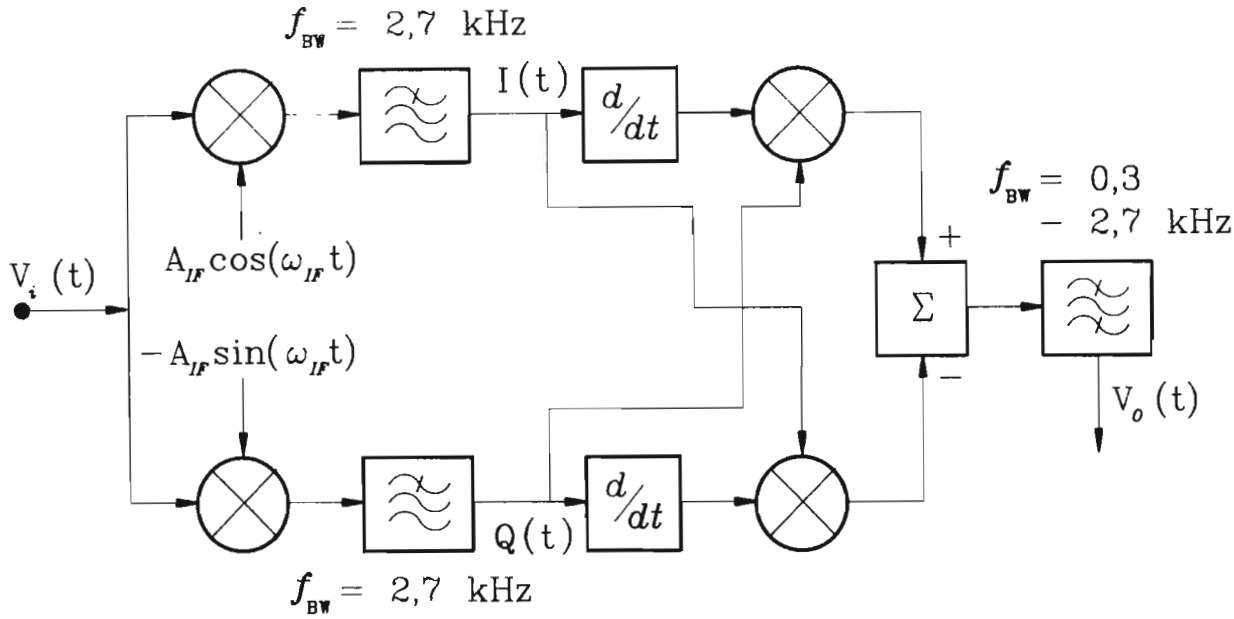

Figure 4.3 Park Jr.'s [1970] direct conversion FM demodulator.

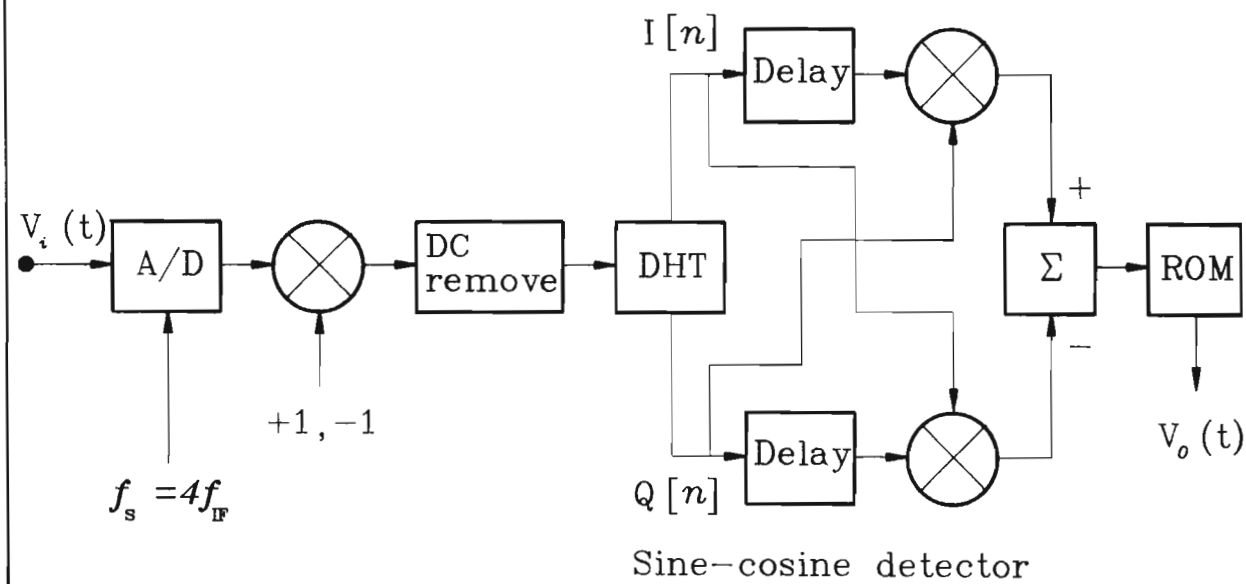

Figure 4.4 Saulnier et al.'s [1990] LMR VLSI FM demodulator.

4.1.4 Limiter/ discriminator FM demodulators.

There are three signal processing stages to a limiter/ discriminator FM demodulator, as shown in figure 4.5. The first stage is a signal limiter, which removes any amplitude fluctuations, since frequency discrimination techniques are generally amplitude dependant. The second stage is the frequency discriminator, where frequency to amplitude conversion occurs. Typical frequency discriminators include the zero crossing counter or FIR differentiator. The last stage of the limiter/ discriminator demodulator depends on the type of frequency discriminator. If a differentiator is utilized, this converts the FM signal to an AM signal (with a frequency modulating carrier), and consequently AM demodulation is the last stage of the demodulator. Frequency discrimination, using a zero crossing counter demodulator, produces a voltage proportional to the number of zero crossings of the carrier, and hence its frequency. Lowpass filtering which band-limits the final signal, would then form the last stage of the FM demodulator for this type of frequency discriminator.

Carter [1988] attempted the zero crossing counter demodulator but found difficulty in determining the exact instant in time of a zero crossing. This is due to asynchronous sampling (i.e. the sampler is not phase-locked to the carrier) and the limited number of samples per cycle of the carrier. Essentially the same problem of limited sampling time resolution is found when applying the DPLL to FM demodulation. To circumvent this problem, simple wideband DSP techniques are necessary, and within the following sections two such techniques will be applied to FM demodulation.

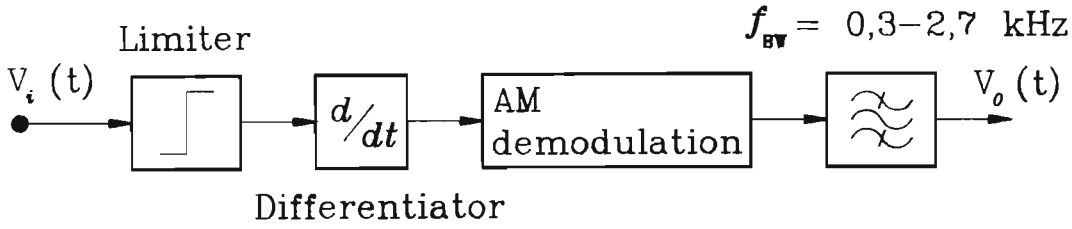

Figure 4.5 A simplified block diagram of a limiter/discriminator FM demodulator.

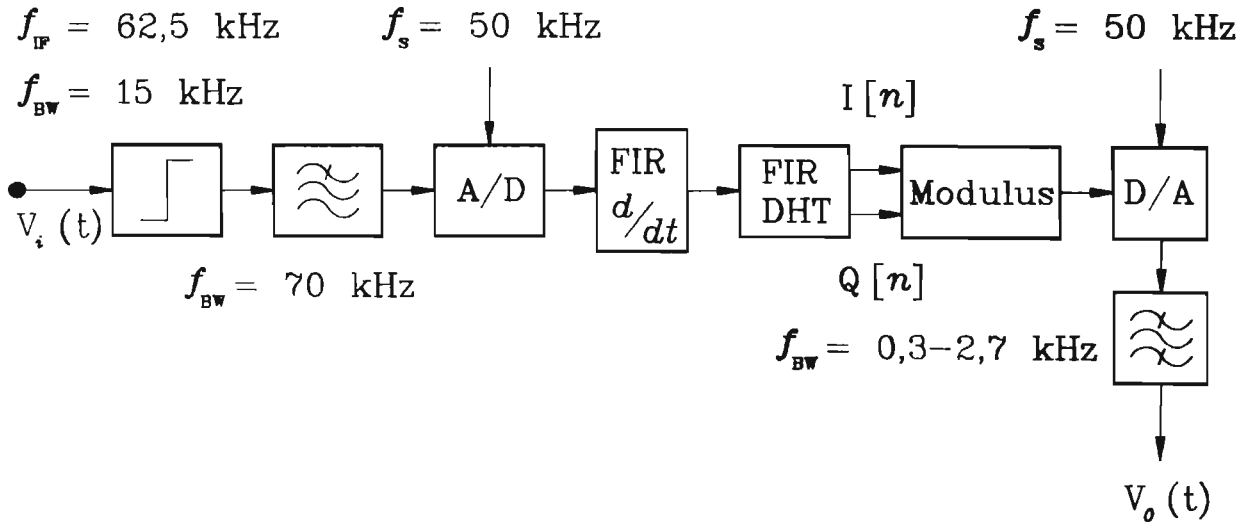

Figure 4.6 The low sampling rate DSP FM demodulator (FMRXPHD6.ASM).

4.2 THE NOVEL LOW SAMPLING RATE FM DEMODULATOR.

Within this section the author derives a simple, low distortion, low sampling rate FM demodulator for speech signals whose bandwidths exceed quarter the sampling frequency. The limiter/ discriminator demodulator is a combination of three DSP algorithms, while a subharmonic sampling technique allows interfacing with an amplitude and bandlimited, high IF, analogue FM signal. To concentrate attention on the low sampling rate demodulator no reference is made to prior modulation preemphasis filtering or post-demodulation, deemphasis filtering. Following the derivation of the low sampling rate FM demodulator the author undertakes an analysis which estimates the distortion caused by inaccuracies in the demodulator. The chapter concludes with an assessment of a real time, fixed point implementation of the FM demodulator where it is found that the measured results correspond closely to predicted results. Finally attention is drawn to appendix 5 which includes a sample program of the low sampling rate FM demodulator.

4.2.1 The implementation of the low sampling rate FM demodulator.

The low sampling rate FM demodulator, as given in figure 4.6, consists of four stages which includes a subharmonic sampler, FIR differentiator, FIR DHT and an algorithm for obtaining the modulus of the complex number. The 15 kHz, bandpass filtered FM signal is amplitude limited by an analogue limiting circuit. Lowpass filtering follows to remove high frequency harmonic components caused by the analogue limiter. Unlike the AM demodulator, where the analogue IF is situated at 12,5 kHz, or at one quarter the sampling frequency, it is necessary to increase the IF frequency for the FM demodulator to allow filtering of the harmonic components caused by the analogue limiter. Typically a transceiver's synthesizer generates local oscillator signals which

are integer multiples of a reference frequency. It is therefore possible, without the addition of extra analogue circuitry, to increase the frequency of the last IF. A multiplexor prior to the A/D selects either the AM or FM IF signal.

Saulnier et al. [1990] utilize the same technique of subharmonic sampling to interface their VLSI demodulator to a high IF frequency. Vaughan et al. [1991] provide an excellent theoretical study of subharmonic sampling which they refer to as bandpass sampling. Subharmonic sampling, if certain criteria are fulfilled, can be employed to alias a high IF to a lower IF, with no detectable degradation in the final SNR_O or added distortion [Vaughan et al. 1991]. The first criterion to prevent a degradation in the final SNR_O, is that sufficient attenuation of the out of band noise and a sufficiently small sampling aperture jitter exists. The second criterion, to prevent distortion of the aliased signal, is bandlimiting of the IF signal (which includes the filter skirts) to a maximum of half the IF sampling frequency. Finally, to ensure correct positioning of the centre frequency of the final IF the correct relationship between the present IF, final IF and sampling frequency must be established. The equation which describes this relationship, is derived from the study by Saulnier et al. [1990], and is given by

$$f_{AIF} = \frac{f_{BIF}}{2n+1} \quad , \tag{4-12}$$

where $n = 0, 1, 2, ..,$ f_{BIF} is the frequency of the IF before sampling and f_{AIF} the frequency of the IF after sampling, both in Hz. The assumption, in deriving equation 4-12, is that the sampling frequency f_s, is four times f_{AIF}. Thus, for the specific example where the sampling frequency is 50 kHz, f_{AIF} is 12,5 kHz and if $n = 2$ then f_{BIF} is 62,5 kHz. This analogue IF frequency is high enough to allow sufficient separation of the harmonics from the wanted signal, yet low enough to allow active filter design with standard operational amplifiers.

Following subharmonic sampling the FM signal is demodulated using a FIR differentiator and quadrature AM demodulator. The operation of the low sampling rate FM demodulator can best be described by the following derivation. The sinusoidally modulated FM signal is given by

$$V_i(t) = A_c \cos(\omega_c t + \beta A_m \sin \omega_m t) \ . \qquad (4\text{-}13)$$

Following differentiation this results in an AM signal whose carrier is frequency modulated

$$V_{dt}(t) = -A_c(\omega_c + \beta \omega_m A_m \cos \omega_m t)\sin(\omega_c t + \beta A_m \sin \omega_m t) \ , \qquad (4\text{-}14)$$

where $V_{dt}(t)$ is the output of the differentiator. A FIR DHT is then utilized to create I and Q signals at the 12,5 kHz IF

$$I(t) = -A_c(\omega_c + \beta \omega_m A_m \cos \omega_m t)\sin(\omega_c t + \beta A_m \sin \omega_m t) \ , \qquad (4\text{-}15)$$

and

$$Q(t) = A_c(\omega_c + \beta \omega_m A_m \cos \omega_m t)\cos(\omega_c t + \beta A_m \sin \omega_m t) \ . \qquad (4\text{-}16)$$

Finally, the baseband signal is demodulated by calculating the magnitude of the complex number,

$$V_o(t) = A_c \omega_c + 2\pi \Delta f A_m A_c \cos \omega_m t \ . \qquad (4\text{-}17)$$

Three techniques of obtaining quadrature signals, which include mixing, sampling and filtering, were reviewed and compared in section 2.1. The first technique is to use analogue mixers followed by sampling; this approach is generally limited by amplitude and phase inaccuracies between the two analogue local oscillators. Furthermore, sampling techniques the second approach, result in a timing misadjustment between the quadrature signals. For these reasons the third technique being wideband DHT filtering, is preferred, and in the following paragraphs the selection of filter structure, filter order and bandwidth is discussed.

There are two major differences between the quadrature AM demodulator, developed as a multirate structure in chapter 3, and the quadrature AM demodulator combined as part of the low sampling rate FM demodulator.

Firstly, the low sampling rate FM demodulator utilizes a FIR DHT in preference to Rader's [1984] IIR DHT and secondly it incorporates no decimation. Rader's IIR DHT although simple, has a nonlinear group delay which causes distortion when a frequency modulated carrier is applied. This group delay distortion was noted in the assessment of the multirate AM demodulator, as given in figure 3.16. Decimation is a useful DSP technique as it allows matching of the sampling frequency to the bandwidth of the signal and thereby reduces the processing requirements. However unless the signal is correctly filtered prior to decimation a degradation in the final SNR_O occurs [Vaughan et al. 1991]. The effect of the differentiator within the limiter/ discriminator FM demodulator is to parabolically shape the spectrum of the noise which provides the well known FM SNR_O enhancement in the presence of channel noise. Consequently after differentiation, as the signal is wideband, decimation as part of the post-quadrature AM demodulator degrades the possible FM noise enhancement due to aliasing. As an example of this degradation Table 4.1 is a comparison of the CNR_i versus SNR_O for two different FM demodulators. The program, FMRXPHD6.ASM is a FM demodulator where no decimation is employed, while the second program FMRXPHD7.ASM as in figure 4.7, utilizes the same FIR DHT but as part of a decimating structure which results in baseband I and Q signals.

In the design of the FIR differentiator and FIR DHT the bandwidth of the FM signal, which is defined by Carson's rule [Taub & Schilling, 1971, pg. 125], needs to be considered. Carson's rule is given by

$$f_{FM} = 2(\Delta f + f_m) \ . \qquad (4\text{-}18)$$

which gives the bandwidth required to transmit 98% of the power of a FM signal when $\beta \geq 1$. The techniques of designing FIR differentiators and FIR DHTs are similar. Both filters types may be designed to have

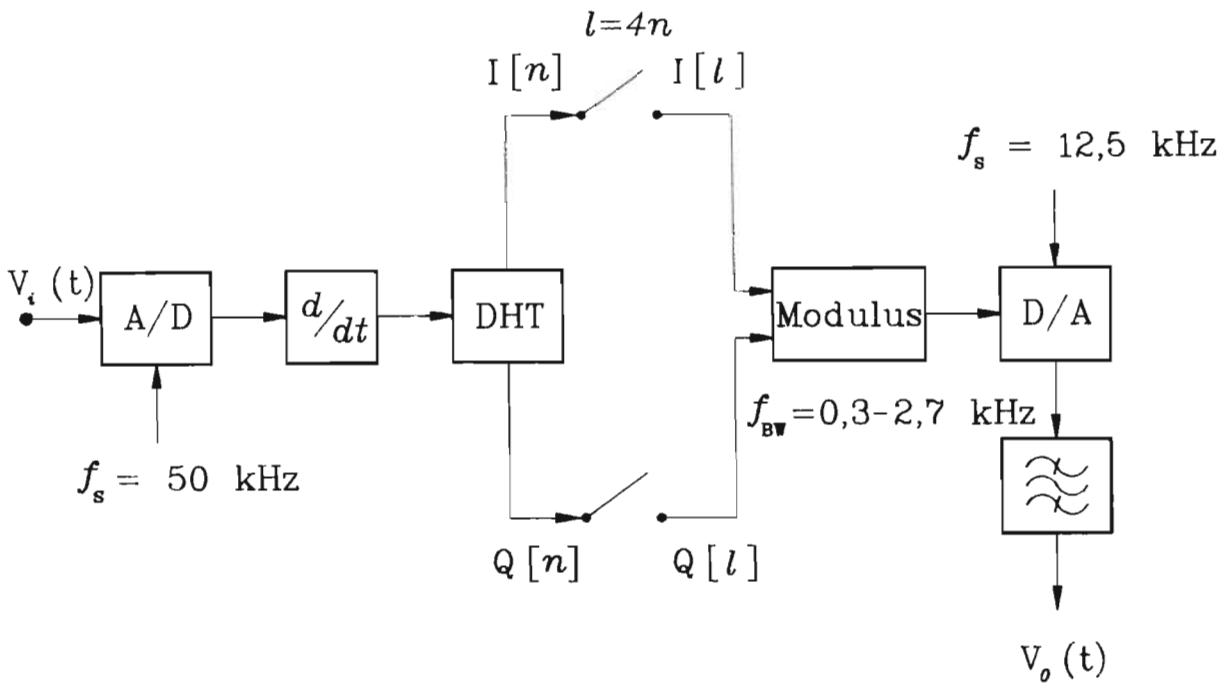

Figure 4.7 A DSP FM demodulator employing a four times decimation (FMRXPHD7.ASM).

CNR_i(dB)	SNR_o(dB) FMRXPHD6.ASM	SNR_o(dB) FMRXPHD7.ASM
23,28	37,05	29,73
24,28	38,81	31,91
25,20	40,05	32,78
27,50	43,04	36,63

TABLE 4.1 SNR_o for two different FM demodulator structures where the peak frequency deviation is 5 kHz.

a linear phase response and constant group delay, while the only error created is amplitude ripple within the passband [Rabiner & Gold, 1975, pg. 75-81].

Table 4.2 compares the filter order versus maximum percentage amplitude ripple for two different design methods of the FIR DHT. Table 4.3 is a similar comparison for the FIR differentiator where the normalized bandwidth for both filters is $\pi/4 \leq \omega \leq 3\pi/4$. The first design method is known as the Kaiser window technique. The frequency response of a digital filter is periodic and therefore can be expanded using the Fourier series. The coefficients of the Fourier series are recognizable as the impulse response of the digital filter. By employing the Kaiser window the convergence of the Fourier series can be controlled, thereby reducing the overshoot known as Gibbs phenomenon. The Kaiser window is considered to be optimal since it is of finite duration and beyond a particular frequency specified by the design, has minimum spectral energy [Rabiner & Gold, 1975, pg. 94].

The Parks-McClellan [Parks & McClellan, 1972] technique, using the Remez exchange algorithm, is the second method of designing the FIR filters which is based on a Chebyshev approximation. The solution is optimal since the peak approximation error, over the interval of approximation, is minimized. The amplitude error ripple function is sinusoidal and a weighting function is employed in the design of the FIR differentiator to obtain a constant relative amplitude error over the bandwidth of the filter. An eighth order Parks-McClellan FIR differentiator and an eleventh order Parks-McClellan FIR DHT were used in the implementation of the low sampling rate FM demodulator. Mitchell's [1989] technique, of designing odd order FIR DHTs, results in a further reduction in the necessary processing since each alternative coefficient is zero.

Filter order n (integer)	Kaiser window % ripple (%)	Parks-McClellan % ripple (%)
11	1,82	0,32
10	2,38	0,64
9	2,70	2,23
8	3,96	1,73
7	4,23	2,23
6	7,88	4,72

Table 4.2 FIR DHT maximum % amplitude ripple for different filter orders and two different design techniques.

Filter order n (integer)	Kaiser window % ripple (%)	Parks-McClellan % ripple (%)
11	3,48	0,84
10	0,16	0,04
9	13,48	2,25
8	1,20	0,12
7	31,6	6,13
6	4,88	0,43

Table 4.3 FIR differentiator maximum % amplitude ripple for different filter orders and two different design techniques.

The last stage of the low sampling rate FM demodulator requires calculating the modulus of the complex number, and in section 2.2 the different algorithms are compared. The algorithms are categorized into two types; the square root and the direct approximation techniques. By comparing processing complexity versus accuracy it is concluded that Freeman's [1978] direct approximation technique, since complex signals are available, provides the most suitable compromise. For this reason the last stage of the low sampling rate FM demodulator, where the modulus of the complex number is calculated, utilizes Freeman's [1978] algorithm.

4.2.2 A distortion analysis of the low sampling rate FM demodulator.

Within the previous subsection a low sampling rate FM demodulator for speech signals, which is the combination of three DSP techniques, was developed. Within this subsection an equation which is an estimate for the **percentage total harmonic distortion** ($\%THD_{FM}$) at the output of the FM demodulator, caused by inaccuracies in each of the DSP techniques, is derived. The percentage distortion caused by each stage of the demodulator is determined by assuming that the remaining stages have an arbitrary small effect on the total distortion. The $\%THD_{FM}$ is finally calculated by summing the distortions of the three stages.

The input to the FIR differentiator, which forms the first stage of the FM demodulator is given by,

$$V_i(t) = A_c \cos(\omega_c t + \beta A_m \sin \omega_m t) \ . \qquad (4\text{-}19)$$

Following imperfect differentiation, to create an AM signal, results in

$$V_{dt}(t) = -(1 + \epsilon_{dt}) A_c (\omega_c + \beta \omega_m A_m \cos \omega_m t) \sin(\omega_c t + \beta A_m \sin \omega_m t) \ . \qquad (4\text{-}20)$$

where ϵ_{dt} is the differentiator fractional error ripple. The FIR DHT creates I and Q signals and the modulus function demodulates the resultant AM signal. Following DC filtering the output of the demodulator is given by,

$$V_o(t) = (1 + \epsilon_{dt}) 2\pi \Delta f A_c A_m \cos \omega_m t \ . \qquad (4\text{-}21)$$

By assuming that the error ripple function is cosinusoidal over the bandwidth of the signal [Rabiner & Gold, 1975, pg. 164-168] and that the rate of change of the error ripple amplitude is a function of the modulating signal implies that ϵ_{dt} can be described as

$$\epsilon_{dt} 2\pi \Delta f A_c A_m \cos \omega_m t = \epsilon_{Pdt} \cos(2\pi \Delta f A_m A_c \cos \omega_m t) \ , \qquad (4\text{-}22)$$

where ϵ_{Pdt} is the peak differentiator fractional error ripple, and has the same definition as ϵ_{PMOD}, as given by equation 3-25. Expanding equation 4-22 using a Taylor series expansion; filtering the DC and high frequency components (above the second harmonic) and finally substituting back into equation 4-21 results in

$$V_o(t) \approx 2\pi \Delta f A_m A_c \cos \omega_m t + \frac{1}{4} \epsilon_{Pdt} 2\pi \Delta f A_m A_c \cos 2\omega_m t \ . \qquad (4\text{-}23)$$

The first component of equation 4-23 is the demodulated signal while the second component is the distortion caused by the imperfect differentiation. From equation 4-23 the **output power** (P_o), of the demodulator is given by

$$P_o \approx \left(1 + \frac{\epsilon_{Pdt}^2}{4} \right) (2\pi \Delta f A_c)^2 P_{md} \ , \qquad (4\text{-}24)$$

where P_{md} is the power in the modulating signal in watts. This equation is in the form of Millman's definition [1979, pg. 665] of fractional harmonic distortion. From this definition and equation 4-24 the **differentiator percentage harmonic distortion** ($\%D_{dt}$) is finally derived as

$$\%D_{dt} \approx 100 \left(\frac{\epsilon_{Pdt}}{2} \right) \ . \qquad (4\text{-}25)$$

The second part of the distortion analysis is to determine the **Hilbert transform's percentage harmonic distortion** ($\%D_{HIL}$) caused by its passband amplitude ripple. The distortion analysis is different to that of the DHT which forms part of the multirate AM demodulator since decimation is not applied to the FM demodulator. The derivation however is similar to the distortion analysis of the differentiator and therefore is only briefly outlined. The input to the Hilbert transform from the perfect differentiator is given by

$$V_{dt}(t) = -A_c(\omega_c + \beta\omega_m A_m \cos\omega_m t)\sin(\omega_c t + \beta A_m \sin\omega_m t) \ . \qquad (4\text{-}26)$$

The I and Q signals with the Hilbert transform's associated fractional error ripple ϵ_{HIL} are described by

$$I(t) = -A_c(\omega_c + \beta\omega_m A_m \cos\omega_m t)\sin(\omega_c t + \beta A_m \sin\omega_m t) \ , \qquad (4\text{-}27)$$

and

$$Q(t) = A_c(1 + \epsilon_{HIL})(\omega_c + \beta\omega_m A_m \cos\omega_m t)\cos(\omega_c t + \beta A_m \sin\omega_m t) \ . \qquad (4\text{-}28)$$

Obtaining the amplitude of the complex number results in

$$V_o(t) = -A_c(\omega_c + 2\pi\Delta f A_m \cos\omega_m t)$$

$$+\epsilon_{HIL} A_c(\omega_c + 2\pi\Delta f A_m \cos\omega_m t)\cos(\omega_c t + \beta A_m \sin\omega_m t) \ . \qquad (4\text{-}29)$$

Assuming a cosinusoidal error ripple, and that the rate of change of the error ripple amplitude is a function of the IF AM signal then

$$\epsilon_{HIL} A_c(\omega_c + 2\pi\Delta f A_m \cos\omega_m t)\cos(\omega_c t + \beta A_m \sin\omega_c t) =$$

$$\epsilon_{PHIL}\cos\{A_c(\omega_c + 2\pi\Delta f A_m \cos\omega_m t)\cos(\omega_c t + \beta A_m \sin\omega_c t)\} \ , \qquad (4\text{-}30)$$

where ϵ_{PHIL} is the peak Hilbert transform fractional error ripple, and has the same definition as ϵ_{PMOD}, as given by equation 3-25. $\%D_{HIL}$ is obtained by expanding equation 4-30 via a Taylor series expansion and filtering the DC and high frequency components (above the second harmonic). After algebraic manipulation and the filtering an estimate of $\%D_{HIL}$ is obtained via the same technique that $\%D_{dt}$ was derived; thus $\%D_{HIL}$ is given by

$$\%D_{HIL} \approx 100\left(\frac{\epsilon_{PHIL}}{2}\right) \ . \qquad (4\text{-}31)$$

The percentage distortion caused by the modulus function $\%D_{MOD}$, was derived in section 3.2.2 and equation 3-28 can be applied directly to the low sampling rate FM demodulator. Since the %THD of the complete FM demodulator, referred to as $\%THD_{FM}$, is the summation of the percentage distortion caused by its three parts [Millman, 1979, pg. 665] it is defined as

$$\%THD_{FM} \approx 100\left(\frac{\epsilon_{Pdt}^2}{4}+\frac{\epsilon_{PHIL}^2}{4}+\frac{\epsilon_{PMOD}^2}{4}\right)^{1/2} . \qquad (4\text{-}32)$$

This is approximately 0,21% within the IF bandwidth of $\pi/4 \leq \omega \leq 3\pi/4$ for the low sampling rate FM demodulator when $\epsilon_{PMOD} = 0,0024$; $\epsilon_{Pdt} = 0,0012$ and $\epsilon_{PHIL} = 0,0032$.

4.2.3 A performance assessment of the low sampling rate FM demodulator.

Within this section the performance of a fixed point, real time implementation of the low sampling rate FM demodulator is discussed. The measured $\%THD_{FM}$ for various values of Δf is compared with the estimated $\%THD_{FM}$ derived in section 4.2.2. The distortion measurements are then extended to include the effects of various carrier frequency offsets. Furthermore the performance of the low sampling rate FM demodulator in noise is assessed, and compared to the theoretical study in Appendix 3. A discussion of the processing requirements of the low sampling rate FM demodulator finally concludes the chapter.

To measure the $\%THD_{FM}$ a sinusoidally modulated FM signal was synthesized internally, at a 12,5 kHz IF, in the DSP microprocessor and then applied to the DSP FM demodulator. Internal synthesization of the FM signal avoided additional distortion caused by the preceding analogue circuitry. The $\%THD_{FM}$ of the demodulated, bandlimited FM signal was measured using a Hewlett Packard 339A distortion meter,

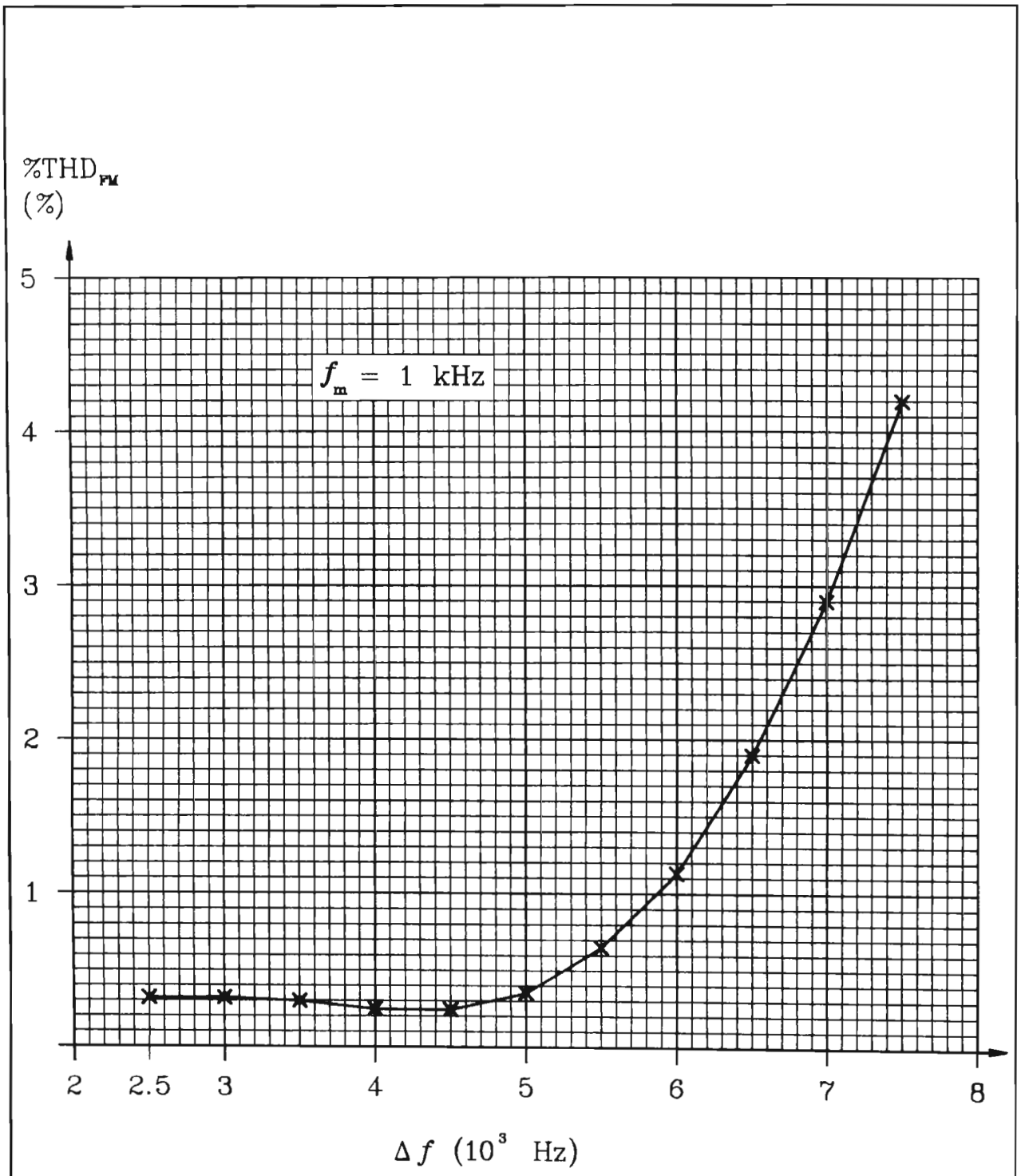

Figure 4.8 % THD_{FM} as a function of peak frequency deviation.

which determines the percentage noise power plus distortion power. In these measurements the assumption is that the distortion power is substantially greater than the noise power. Figure 4.8 is a graph of the $\%THD_{FM}$ as a function of Δf and as expected, the $\%THD_{FM}$ increases rapidly when the bandwidth of the signal exceeds the bandwidth of the FIR differentiator and FIR DHT. Within the passband of the FM demodulator, it was found that the derivation in section 4.2.2 of the $\%THD_{FM}$ is a reasonable estimate of the distortion caused by the low sampling rate FM demodulator. From Lee's [1989, pg. 421] definition of toll quality speech, where the %THD must be less than or equal to 2,3%, it is possible to determine the maximum permissible bandwidth of the FM signal. In the design of the total DSP transceiver it is also necessary to take into consideration the distortion caused by the preceding analogue circuitry. Larger values of Δf can be catered for with an increase in the sampling frequency, or increase in bandwidth of the FM demodulator.

The effect of various carrier frequency offsets on the $\%THD_{FM}$ is described by figure 4.9. From the graph it is seen that the low sampling rate FM demodulator is tolerant to small carrier frequency offsets although the $\%THD_{FM}$ degrades rapidly beyond a +500 Hz offset. Automatic frequency control to correct for a FM carrier frequency offset is simple since a DC component, which is proportional to the carrier frequency, occurs at the output of the low sampling rate FM demodulator (see equation 4-17). This DC component, after filtering and comparison to a reference, is then used to control the frequency of the TCXO within the transceiver. Although in the design of the FIR differentiator a bandwidth is specified, it functions to DC with no degradation in error ripple. For this reason, larger negative than positive carrier frequency offsets can be tolerated.

To measure the CNR_i versus the SNR_o of the low sampling rate FM demodulator the complete receiver was employed. A sinusoidally

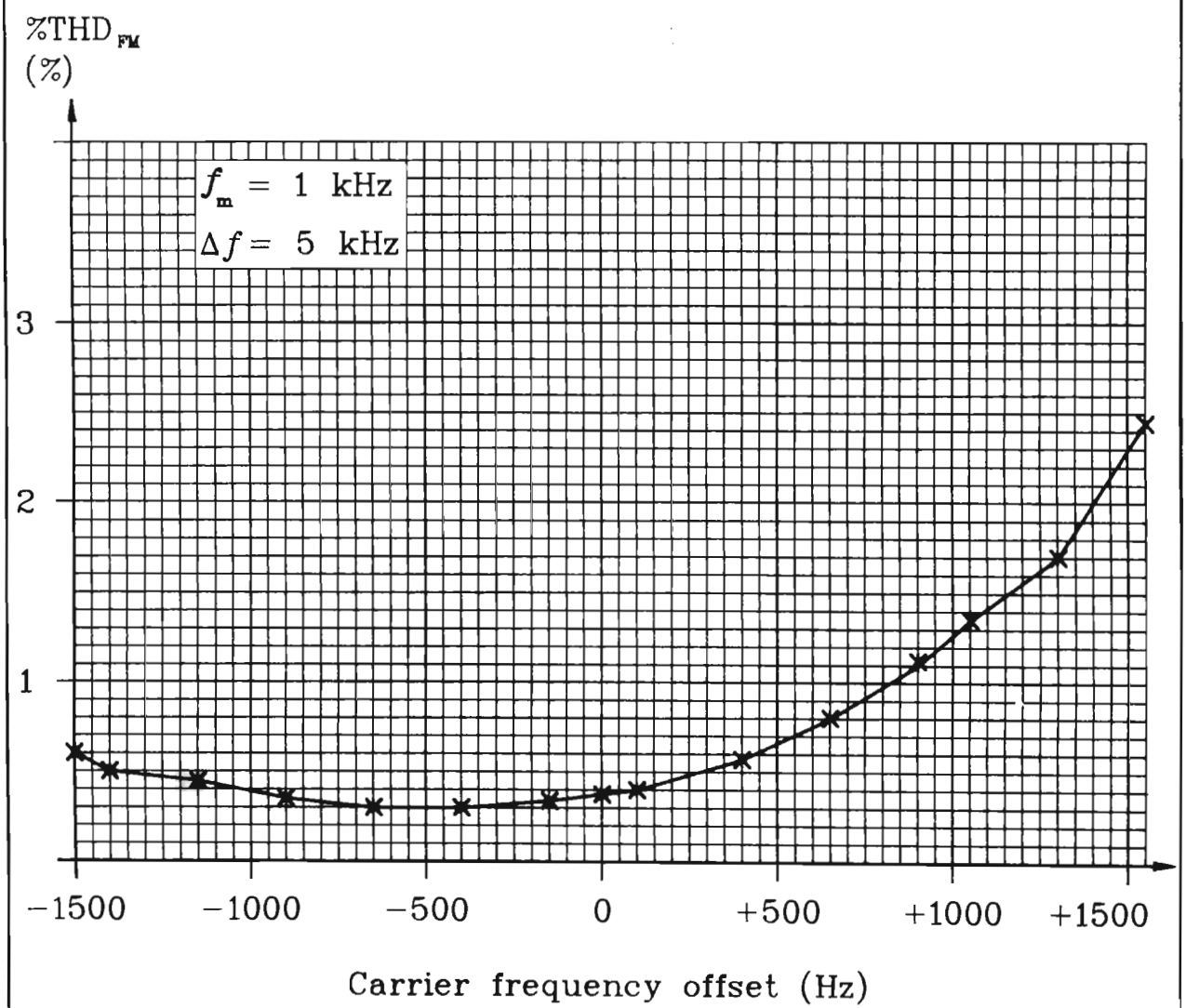

Figure 4.9 % THD_{FM} as a function of carrier frequency offset.

modulated FM signal combined with wideband noise was applied at the antenna and the CNR_i measured before the analogue limiter while the SNR_o was measured after the demodulator. Both values were adjusted for the bandwidth of the modulating signal. Figure 4.10 is a graph of the measured results for two values of β and a few observations are made. For large CNR_i's both curves flatten out thus limiting the ultimate SNR_o. This effect is caused by the phase noise generated by the transceivers' local oscillators. Lee's [1989, pg. 421] definition of toll quality speech recommends a SNR_o of at least 30 dB. Secondly although the measured CNR_i versus SNR_o performance corresponds closely to the calculated performance described by figure A.3.1 this performance can only be achieved if the received signal is not corrupted by receiver or synthesizer noise and sufficient anti-aliasing filtering prior to sampling eliminates unwanted signal components.

For the selected bandwidth and $\%THD_{FM}$ the low sampling rate FM demodulator requires eighteen multiplications and three decisions for each output sample of the demodulated signal. Although the low sampling FM demodulator requires approximately three times more processing than the multirate AM demodulator it is still a reasonably small percentage of the total processing capabilities of a single DSP microprocessor. Recently Pei & Shyu [1992] discussed the combination of a FIR differentiator and Hilbert transformer as a single structure. This approach however, does not have a significant effect on the processing requirement of the low sampling rate FM demodulator since both the I and Q signals require differentiation. In the structure proposed by Pei and Shyu only the Q signal is differentiated. Thus in conclusion, this novel low sampling rate FM demodulator is a processing efficient, low distortion demodulator for speech signals.

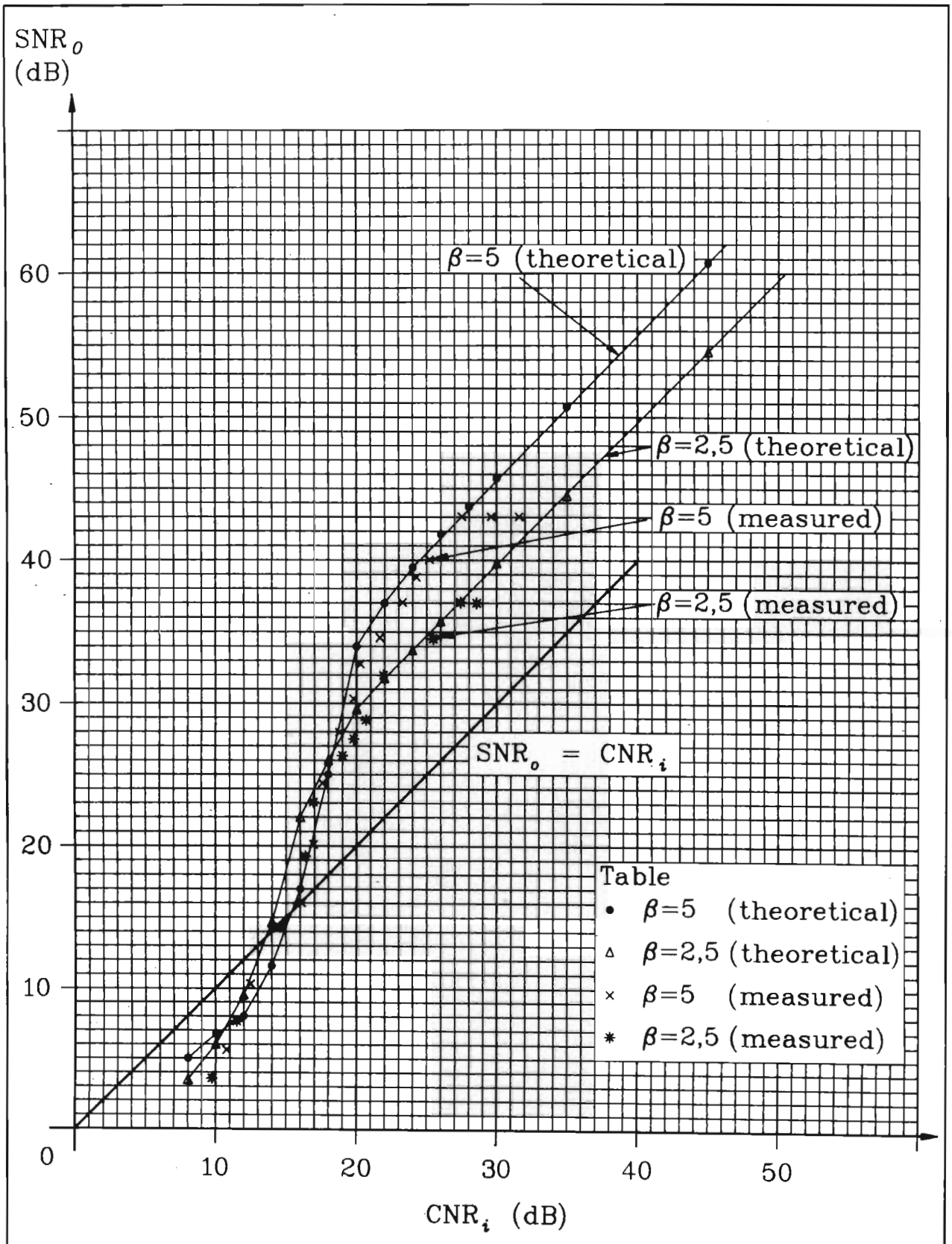

Figure 4.10 A graph of the measured CNR$_i$ versus SNR$_o$ for the low sampling rate FM demodulator.

CHAPTER 5

A NOVEL DSP MULTIRATE IIR-ALE/DPLL AFC SYSTEM FOR SSB-SC COMMUNICATIONS.

Within this chapter a novel, multirate, **automatic frequency control** (AFC) system for **single-sideband suppressed carrier** (SSB-SC) communications, is derived and assessed. The AFC system is essentially the combination of two DSP techniques. The first technique is a spectral estimation and enhancement method, namely the **infinite impulse response adaptive line enhancer** (IIR-ALE). The second technique utilizes control theory in the form of a **digital phase-locked loop** (DPLL). Both techniques are combined within a multirate SSB demodulation structure and therefore the complete algorithm is referred to as the multirate IIR-ALE/DPLL AFC system.

This chapter starts with a comparison of different digital spectral estimation techniques and current AFC system trends. From this review it is then suggested that two complementary DSP techniques be combined to form a simple, novel AFC system. The multirate IIR-ALE/DPLL AFC system is derived and assessed in the second section of the chapter and its performance compared with a classical DPLL suppressed carrier AFC system. Appendix 6 includes a discussion of various system considerations of a mobile and stationary SSB-SC communications link.

5.1 A REVIEW OF CLASSICAL AND CURRENT AFC SYSTEMS.

SSB is a bandwidth efficient modulation scheme, although it suffers from frequency difference errors between the transmitter and receiver caused by inaccuracies in their respective frequency references. Techniques for correcting these errors by analyzing the demodulated

speech signal typically include tracking the frequencies of harmonic's [Starer & Nehorai, 1986]. Since these techniques are complex it is generally accepted that a suppressed pilot tone is combined with the transmitted SSB signal to allow for the correction of frequency difference errors in the receiver [Ball & Holmes, 1981]. Besides the correction of frequency difference errors, the pilot is often filtered and employed to synchronously demodulate digital data [Cavers, (1), 1991] and employed in feedforward AGC systems to correct for short-term multipath fading [Leland & Sollenberger, 1980].

The frequency correction between a transmitter and a receiver is an important aspect in determining the ultimate performance of a communications link. It is quite possible that the performance is limited, not by the demodulation or detection scheme, but rather by an AFC system which fails in low SNR conditions or in a dynamic medium. Generally an AFC system is optimized depending on a number of criteria which include; the modulation scheme (i.e. CW, FSK, **phase-shift keying** (PSK), **quadrature amplitude modulation** (QAM)), dynamics of the received signal, required performance (i.e. capture range, capture time) and available hardware and software resources. Until recently AFC systems have been developed based on control theory techniques. Currently however, there has been a tendency to combine spectral estimation and control theory techniques into a single unified algorithm which takes advantage of the positive attributes offered by the two different approaches. The objective of this section is to review current and classical AFC systems and thereby motivate a particular structure which is a combination of an adaptive filter (spectral estimation technique) and a digital phase-locked loop (control theory technique).

5.1.1 Control Theory AFC systems.

Many of the early AFC systems, as in figure 5.1, were developed around the PLL [Ball & Holmes, 1981], as it is simple to incorporate within a receiver and furthermore, has the ability to reject channel interference. The PLL has the advantage, when applied to an AFC system, of spectrally shaping the input noise which results in the well known SNR_O advantage typically found in PLL FM demodulators. The noise spectral density ($\Gamma_c(\omega)$) appearing at the input of the **voltage control oscillator** (VCO) is given by [Gardner, 1979, pg. 177]

$$\Gamma_c(\omega) = \{\omega^2 \Gamma_n(\omega)\} \frac{|H_{PLL}(j\omega)|^2}{K_o^2} \quad , \qquad (5\text{-}1)$$

where $\Gamma_n(\omega)$ is the spectral density of the input noise, K_o is the gain of the VCO and $H_{PLL}(j\omega)$ is the closed-loop frequency response of the PLL. If the input noise is spectrally flat then the term in brackets in equation 5.1, has a parabolic spectrum. The closed-loop transfer function has the characteristic of a lowpass filter which ultimately bandlimits the noise.

Depending on the application, $H_{PLL}(j\omega)$ could include a filter external to the actual PLL, which results in further noise rejection without affecting the dynamics of the PLL. A similar concept has been reported by McGeehan & Sladen [1982] where they propose a split-loop AFC system, as in figure 5.1. This system incorporates two control loops; the short-loop is used to control the last **local oscillator** (LO), and has a faster response time than the second loop known as the long-loop. The long-loop controls the first LO, which is closest to the antenna. This concept not only prevents false-locking, caused by excessive phase shift introduced by the IF filter, but improves the spectral purity of the first LO due to the narrower bandwidth of the long-loop's filter. The IF crystal filter typically removes the adjacent channel signals and therefore places a less stringent spectral performance

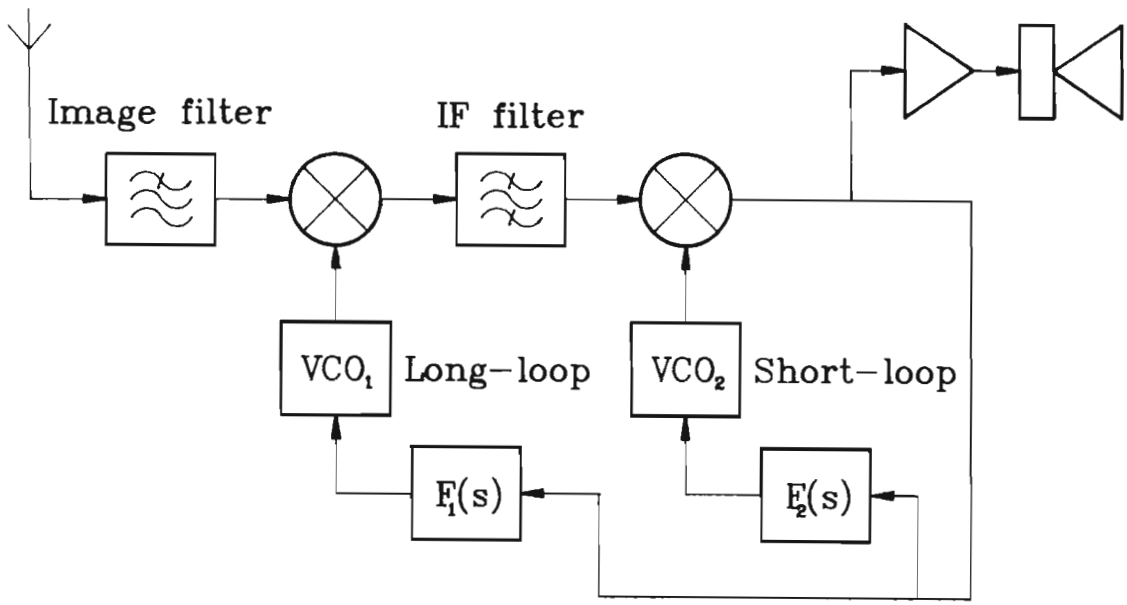

Figure 5.1 The split-loop PLL AFC system.

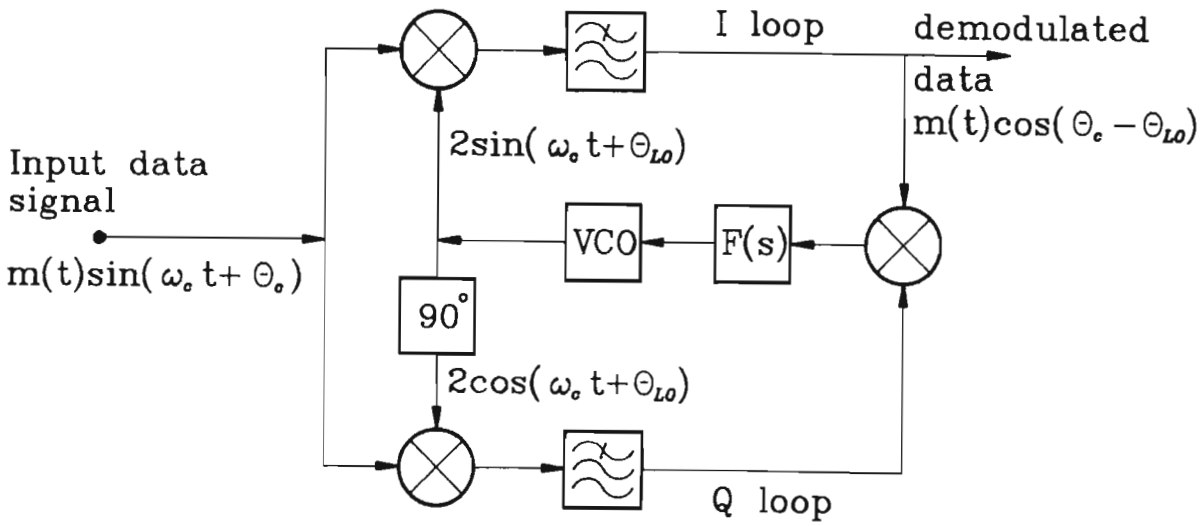

Figure 5.2 The Costas PLL.

requirement on the last LO. Thus the split-loop structure provides an improved rate of signal acquisition and pull-in range, without degrading the co-channel performance of the receiver.

In phase modulated data communications the phase variations need to be removed before applying the PLL, a process typically known as remodulation. This has resulted in numerous structures for carrier recovery which are either applied before the PLL, or as part of the PLL [Gardner, 1979, pg. 221-222]. Typical structures utilized to reconstruct the carrier include the squaring loop, Costas loop and the remodulator [Didday & Lindsey, 1968]. Although our interest is primarily CW communications it is instructive to briefly review a single structure, namely the Costas loop [Proakis, 1983, pg. 193-203]. The Costas loop, given in figure 5.2 incorporates a quadrature VCO configuration to correct for frequency and phase errors and it simultaneously demodulates the data. Essentially the Q loop acts as a PLL to correct for frequency and phase errors while the I loop acts as the data demodulator. By combining the two loops the effect of the phase variations on the VCO's control voltage is removed. The Costas loop is a versatile structure and has been applied to many different modulation schemes [Natali, 1984].

A PLL AFC system for CW applications, typically SSB-SC, is simple to implement as no correction for phase modulation is required. The disadvantage of PLL AFC systems is that they suffer from a compromise between noise rejection (which requires a narrow loop bandwidth), and wideband signal acquisition (requiring a wide loop bandwidth) [Gardner, 1979, pg. 137-164]. The **temperature controlled oscillator** (TCXO) which forms the frequency reference in a transceiver suffers from inaccuracies due to temperature variations and aging. Although these errors are small they are compounded by a frequency multiplication effect when communications occur at **ultra high frequencies** (UHF). Typically, for a possible TCXO error of +/- 1 ppm, a maximum frequency difference of +/- 800 Hz between the transmitter and receiver can occur at 400

MHz. The initial capture range of the PLL would need to be large (1,6 kHz); however, once signal acquisition has occurred the wide bandwidth is unnecessary even for severe Doppler effects, and therefore, degraded phase variance performance at low SNRs would occur.

Numerous techniques have been proposed for assisting the PLL in initial carrier acquisition including frequency sweeping, frequency steering via discrimination and bandwidth widening [Gardner, 1979, pg. 72-91]. Frequency sweeping requires ramping the VCO's control voltage until frequency lock is detected. A frequency steering PLL, employing a discriminator, relies on the large DC loop gain of the phase-locked loop section of the circuit to take control once frequency acquisition has occurred, as shown in figure 5.3. Bandwidth widening requires switching in a wide loop bandwidth to assist in acquisition. Once the signal is acquired a narrower loop filter is selected. A more recent technique, which is suited to the reacquisition and instantaneous phase tracking of a **quadrature phase-shift keying** (QPSK) signal in a fast fading channel, was proposed by Satio & Suzuki [1989]. Their circuit, referred to as the Adaptive Carrier Tracker, is combined with a Costas PLL and digitally controls the reference phase (after the VCO output). Although all these techniques improve the acquisition capabilities of the PLL they tend to be limited either by the SNR_i, signal dynamics or reliable loop lock detectors.

The DPLL is applicable to a DSP implementation and Lindsey & Chie [1981] provide an excellent tutorial reference of different architectures. Since the performance of these algorithms suffer from similar limitations as their analogue counterparts they are not considered in any detail here. However, a derivative of these algorithms is the delay-locked loop [Cernuschi-Frias & Rocha, 1981], as in figure 5.4, which is used to estimate the period of the signal. This algorithm adapts the sampling rate in order to correlate an estimated one period delay and the first difference (approximated derivative) of the signal from which the frequency of the sinusoid can be derived. This in turn

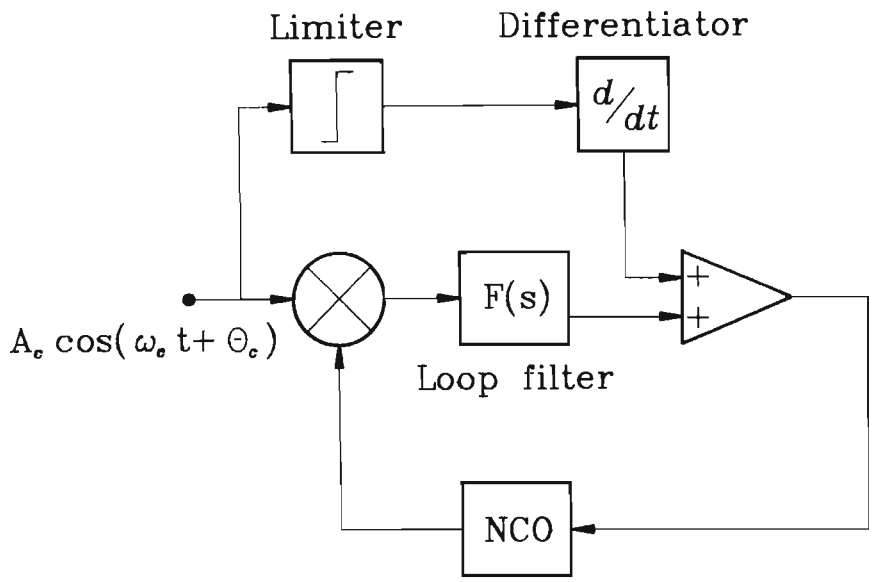

Figure 5.3 Frequency steering via frequency discrimination.

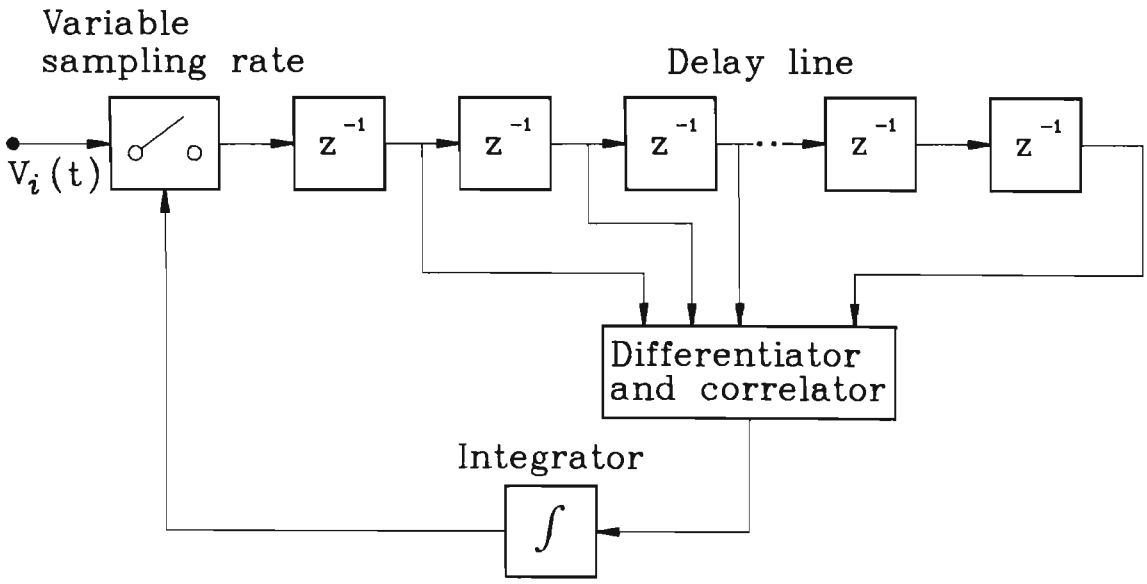

Figure 5.4 A simplified block diagram of Cernuschi-Frias & Rocha's [1981] delay-locked loop.

would provide the error signal to control the receiver's frequency reference. Non-periodic sampling rates however are difficult to implement within a fixed sampling rate system. A different approach but based on a similar structure is described by Etter & Hush [1987] where they utilize a variable delay element and a gradient search technique to obtain an estimate of the frequency of a sinusoid. However, to minimize the bias in the frequency estimate a high degree of oversampling is required.

5.1.2 Digital spectral estimation AFC systems.

Modern digital spectral analysis has made rapid advances over the last thirty years and many recent DSP applications (e.g. speech coding and signal classification) find their origins in this theory. Spectral estimation techniques are ideally suited to AFC applications since knowledge of the parameters of the signal makes it possible to correct for frequency and phase errors. Since these techniques only determine the parameters of the signal, they are generally included as part of a frequency control loop, typically a frequency or phase-locked loop. Marple [1987] defines three classes of spectral estimators; classical (e.g. **fast Fourier transform** (FFT)), parametric (e.g. adaptive filters and Prony) and non-parametric (e.g. minimum variance and **multiple signal classification** (MUSIC)). However due to the simple model required to describe CW type signals in noise [Hush, 1986], and the relative processing complexity of the different algorithms [Marple, 1987, pg. 381], only classical and certain parametric techniques have been applied to AFC systems. This section includes a brief historical review of classical, and certain parametric spectral estimation methods which is used to support the discussion of current AFC systems recently developed for specialized applications (i.e. high data rate modems, airborne and mobile communications).

Humans have always had, of necessity, to predict the cyclic behavior of natural phenomena, and the origins of modern spectral analysis can be traced back to Pythagoras, who in the sixth century B.C., developed a formula which described the periodic motion of a length of string of fixed tension. Later historical milestones included the work of Sir Isaac Newton, who, in the seventeenth century, introduced the concept of a spectrum when observing white light passed through a prism. Later Bernoulli and Euler derived solutions to the wave equation, which was further developed by Fourier as the Fourier series analysis. Early Fourier analysis, which forms the basis of classical spectral analysis, was employed to predict the tides within harbors, and sunspot numbers. Researchers in the early part of this century found however, that periodograms (a windowed power spectrum) calculated by using noisy data often produced erratic results and it was only later that averaging of periodograms was proposed [Marple, 1987, pg. 1-24]. A useful summary of the effects of windowing, averaging, and overlapping multiple periodogram calculations is provided by Hush [1986].

An early reference to **discrete Fourier transform** (DFT) AFC systems is given by Natali [1984] where he describes two configurations. Since the structure and performance of the two algorithms are similar only the DFT AFC is discussed. This algorithm, with structure as in figure 5.5, is suitable for CW and **differential phase shift keying** (DPSK) modulation schemes. A **numerically controlled oscillator** (NCO) creates quadrature signals which are mixed with the input to form I and Q signals. These quadrature signals are used to compute the DFT. The spectrum of a DPSK signal is similar to a **double-sideband suppressed carrier** (DSB-SC) and therefore by establishing the difference between the power in adjacent cells centered around the suppressed carrier, a loop control voltage is generated. For CW modulation, the control is simpler, as all the frequency bins around the correct bin must be zero. Although the implementation of the DFT or the FFT is normally processing and data memory intensive (depending on the frequency resolution), it is interesting to observe a more general structure

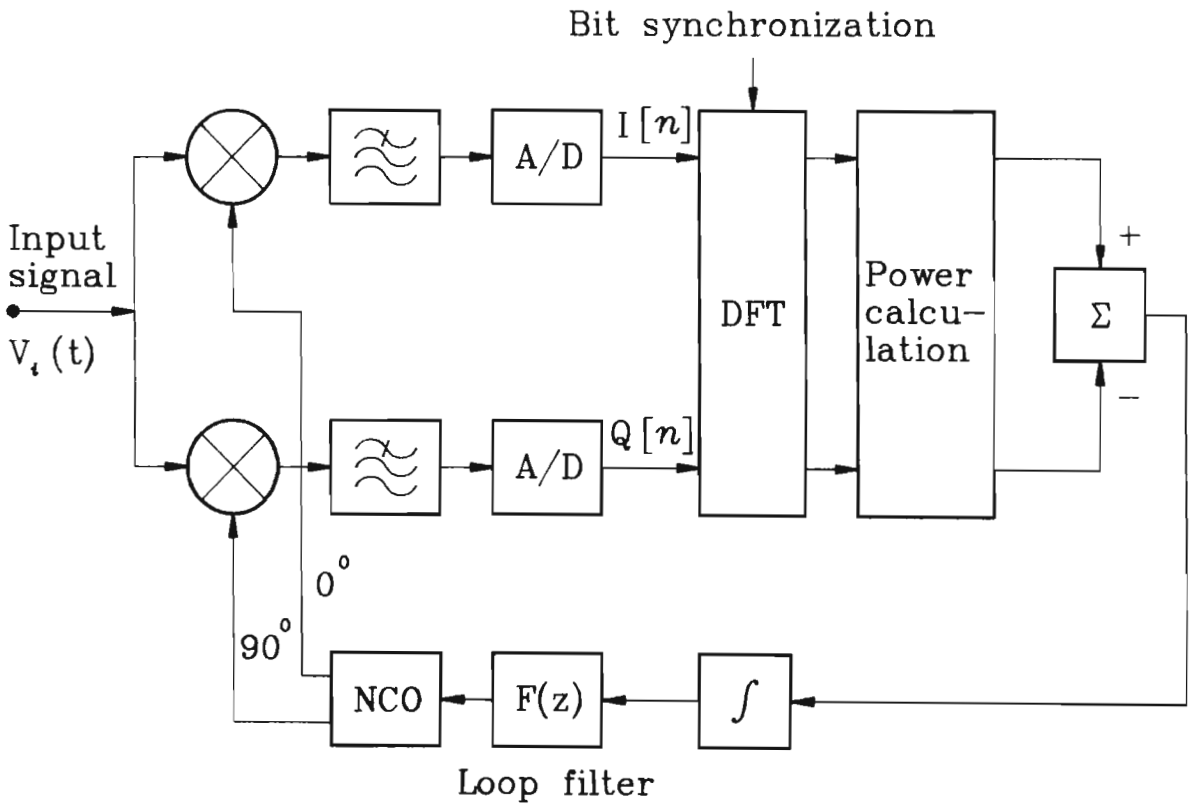

Figure 5.5 Natali's [1984] DFT AFC system.

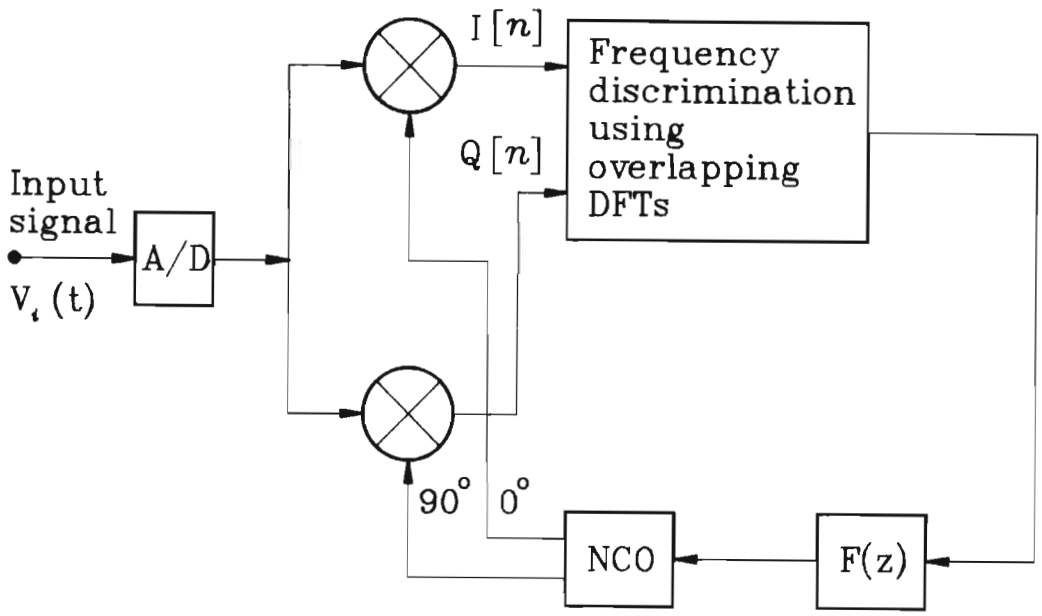

Figure 5.6 Aguirre & Hinedi's [1989] overlapping DFT AFC system.

hidden within the DFT AFC. A simple method of calculating a single point of the DFT is the Goertzel algorithm. This is essentially a second order bandpass resonator with poles on the unit circle at the desired frequency of calculation. Thus an alternative structure is to replace the DFT with a single, second order, adaptive spectral estimator, as part of, or before, the loop control.

Tran, Mathews & Rushforth [1988] present a carrier frequency estimator for FSK and PSK signals. Their structure, although complex, as it requires calculating the Hilbert transform, FFT and inverse FFT is advantageous, as a single algorithm can be applied to multiple modulation schemes. Tran et al. conduct a useful comparison between their algorithm and carrier frequency estimation using either zero crossings or linear regression. A more recent airborne CW AFC system based on overlapping DFTs, given in figure 5.6, is described by Aguirre & Hinedi [1989]. Essentially, by operating on the skirt of a low resolution DFT a frequency discrimination transfer function is achieved, and after loop filtering this error control voltage is applied to the NCO. Aguirre and Hinedi compare the performance of this simple DFT AFC system with a more complex **Extended Kalman filter** (EKF), when subjected to a highly dynamic signal profile typically found in an airborne global positioning application. Although, as expected the adaptive EKF AFC system has an improved tracking performance, the simpler system's performance is comparable which can in turn be attributed to the wide bandwidth of the DFT based frequency discriminator. Generally, the Kalman filter's improved performance is at the expense of complex processing [Tan & Kyriakopoulos, 1988].

Motivated by the limitations of the periodogram, Yule introduced a different technique when he proposed modeling a time series using linear regression analysis in order to predict the periodicity of sunspot numbers [Marple, 1987, pg. 1-24]. Yule developed a simple difference equation using past samples of noisy data to predict the current sample of the signal, an approach known today as **linear**

prediction (LP). Yule's equation contained two unknowns, namely the periodicity of the sequence and a random error component and the solution to this equation has formed the basis of parametric spectral analysis. Three different time series models have been proposed for solving the LP problem and these models can be described by using a single equation [Hush, 1986]

$$Y[n] = \sum_{i=0}^{l} b_i X[n-i] - \sum_{r=1}^{m} a_r Y[n-r] \ , \qquad (5-2)$$

where $Y[n]$ is the current predicted sample, $X[n-i]$ the past observed noisy samples and $Y[n-r]$ the past predicted values. The first time series model, called the **autoregressive moving-average** (ARMA) model, assumes that both the observed noisy samples (i.e. input samples to the filter) and past predicted values (i.e. previous filter output samples) are utilized to predict the current signal's sample. If only observed noisy samples are utilized then the second model is referred to as **moving-average** (MA). The **autoregressive** (AR) or third model utilizes the single current noisy data sample and previous predicted values. The signal model is a discrete time filter employing either poles and zeros (ARMA), zeros (MA) or just poles (AR) [Honig & Messerschmitt, 1984, pg. 11-16]. The objective of a probabilistic LP approach is to match the filter to the signal by adapting the filter coefficients a_r and b_i, and hence these time varying filters are generally known as adaptive filters. The quality of the match, or the prediction error, is determined by using a performance criterion typically the **mean square error** (MSE).

Since adaptive filters have the ability to track non-stationary sinusoids in noise, and their filter coefficients can be utilized to derive information concerning the signal, they are ideally suited to perform signal to noise enhancement and frequency estimation [Orfanidis & Vail, 1986]. A study, conducted by Kumar & Pal [1990], assesses the tracking performance of different ARMA and AR adaptive filter structures. Although the performance of these structures is dependant

on various parameters, (e.g. adaptation step size, forgetting factor, filter selectivity and SNR_i), typical performance includes tracking of a sinusoid whose frequency varies at a rate of 15 to 20 Hz per second. Generally, for the correct selection of adaptation step size, the variance of the filter coefficients and therefore the frequency estimate, is small even for input SNRs as low as -10 to -15 dB. Furthermore, adaptive filters display a graceful degradation in performance as the SNR_i degrades, where as the PLL provides little useful information once phase-lock is lost.

Other probabilistic performance criteria, besides the classical least squares approach, which could be used to measure the quality of the prediction include MAP, **maximum likelihood** (ML) or **minimum variance** (MV) estimation. The advantage of the MSE based algorithms is that they are generally simple to implement as they require little statistical knowledge of the signal [Giordano & Hsu, 1985, pg. 7-12]. Generally there are two criteria used to assess the performance of spectral estimators, namely the bias in the estimate, and the mean square error. If zero estimate bias exists then the mean squared error is the variance of the estimate [Marple, 1987, pg. 113]. Giordano & Hsu [1985, pg. 11] show that the estimate obtained by minimizing the MSE criterion is unbiased and of minimum variance. There are numerous filter coefficient update algorithms based on minimizing the MSE (e.g. **least mean square** (LMS) and **recursive least squares** (RLS)) which often require approximations to reduce the computational complexity, and which in turn, affect the rate of adaptation, estimate bias and variance.

An interesting phase synchronizer, which corrects for frequency and phase errors, employing a least squares performance criteria was proposed by Hagiwara & Nakagawa [1989]. Essentially they suggest replacing the loop filter and NCO of a DPLL with a least squares frequency and phase estimator, as in figure 5.7. The output of the frequency and phase predictor is used to control a counter and a phase

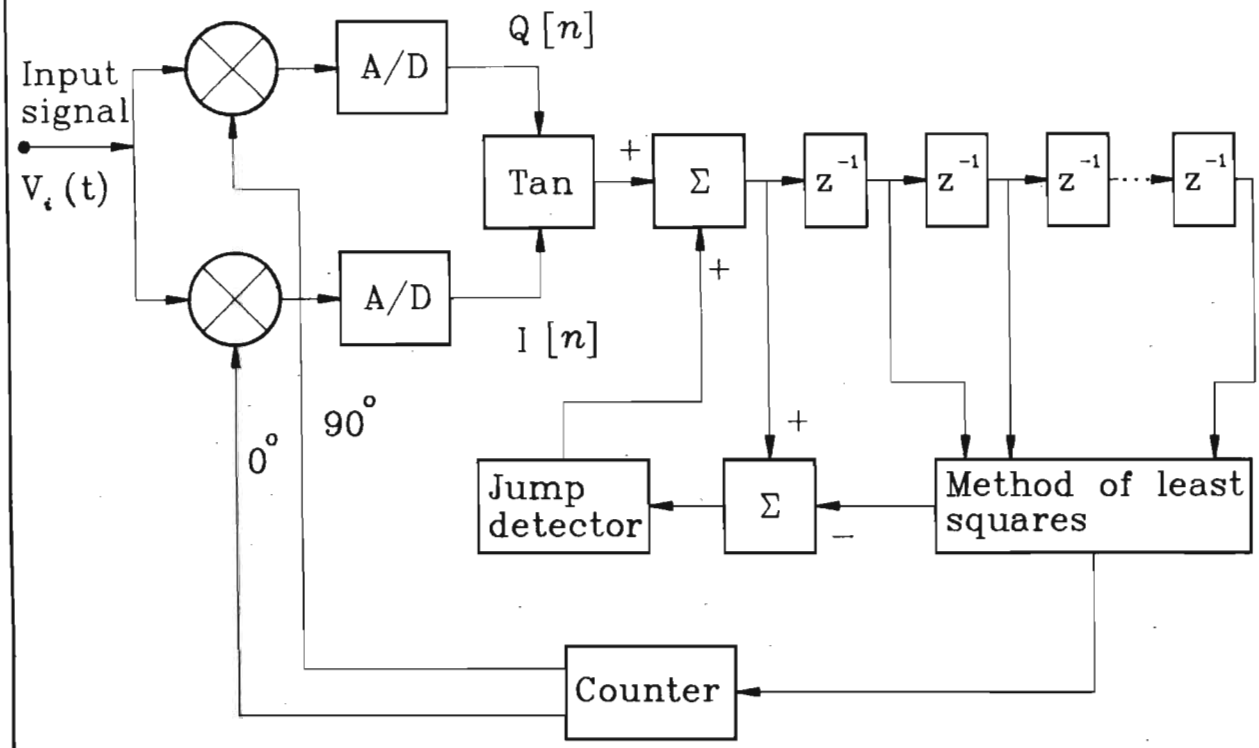

Figure 5.7 Hagiwara & Nakagawa's [1989] least squares AFC system.

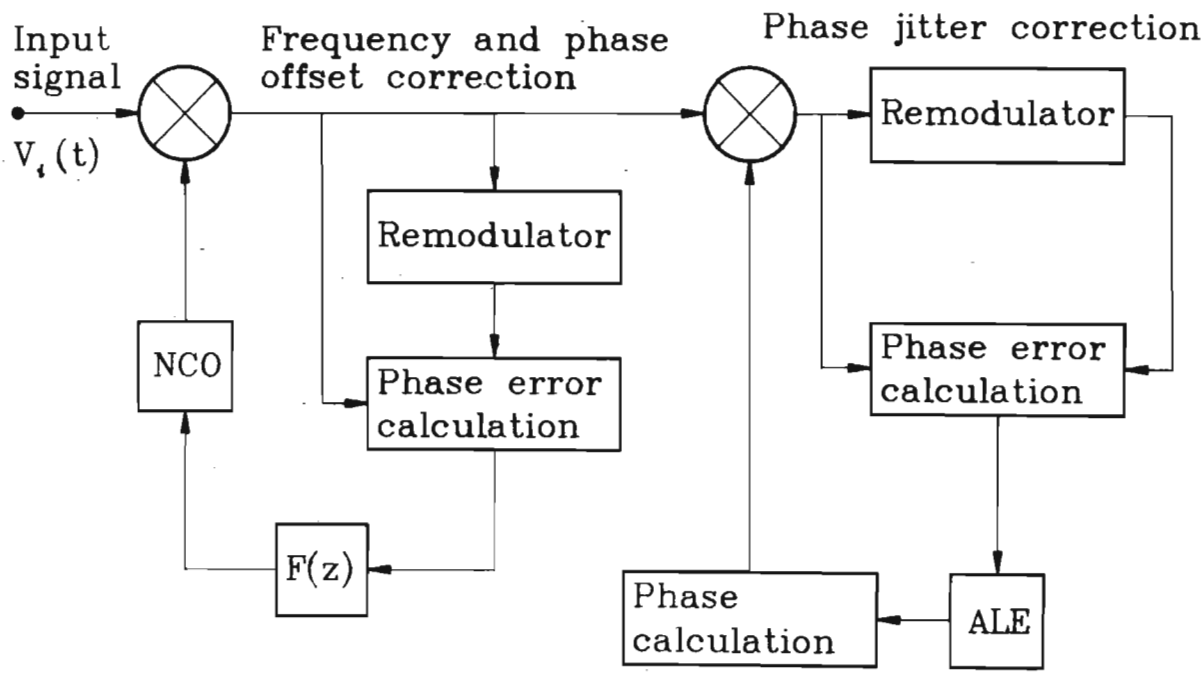

Figure 5.8 Cupo & Gitlin's [1989] adaptive carrier recovery system.

jump detector. The authors conclude that their algorithm can satisfy phase tracking and noise suppression simultaneously, with a wider capture range than the conventional DPLL. Recently they evaluated their algorithm for Rayleigh fading channels [Sano, Hagiwara & Nakagawa, 1990] and found that the method of least squares is a robust technique of phase estimation for these conditions. The structure however is complex as it requires, besides matrix computations and divisions, two trigonometry calculations and is generally more suited to a floating point processor.

Cupo & Gitlin [1989] recently described a carrier recovery system for very bandwidth efficient QAM modems, typically 7 **bits per second per Hertz** (bits/s/Hz) for a 19,2 **kilobits per second** (Kbits/s) voiceband modem application. The carrier recovery system, shown in figure 5.8, consists of a non-adaptive data-directed DPLL which is followed by an adaptive lattice IIR-ALE. The performance of the DPLL for QAM carrier recovery schemes requires a compromise between wide bandwidth, to track fast carrier phase jitter, and narrow bandwidth, to minimize the output noise. In Cupo and Gitlin's algorithm the non-adaptive data-directed DPLL corrects for frequency and phase errors between the transmitter and receiver, and also provides a fixed bandwidth phase jitter filter. For this reason the DPLL is followed by an IIR-ALE to adaptively filter the phase jitter. Cupo and Gitlin compare three ALE structures namely the FIR-ALE, Hush et al.'s [1986] resonator IIR-ALE and a lattice IIR-ALE, where all the adaptive filters employ a simple LMS algorithm to update the filter coefficients. They preferred the lattice IIR-ALE due to finite precision limitations of their hardware configuration.

In Cupo and Gitlin's application the SNR_j is typically 23 dB or greater and the frequency difference errors between the transmitter and receiver are small; of the order of a few Hz. In a UHF SSB-SC application where frequency difference errors up to +/- 800 Hz, and CW SNRs as low as -5 dB (within a 300 Hz to 2,7 kHz bandwidth) are possible, it

is advantageous to rather reverse the structure and precede the DPLL with an ALE, as the ALE has better acquisition and tracking abilities for these conditions. The next section includes further motivation and a discussion on the implementation of the multirate IIR-ALE/DPLL AFC system.

5.2 THE NOVEL MULTIRATE IIR-ALE/DPLL AFC SYSTEM.

Within this section the author derives, and assesses a multirate IIR-ALE/DPLL AFC system for SSB-SC communications. The first subsection discusses and motivates the structure of the IIR-ALE/DPLL AFC system and how it is combined with the multirate SSB demodulator architecture proposed by Carter [1988]. Following the motivation of the structure of the AFC system the second subsection considers the implementation of Hush et al.'s [1986] resonator IIR-ALE from whence suitable adaptation and bandwidth parameters are selected. The third subsection, based on the derivations in section 2.4, considers in detail the design of the DPLL which follows the IIR-ALE. This section concludes with a performance assessment of the IIR-ALE/DPLL AFC system for stationary and mobile SSB-SC communication links.

5.2.1 The implementation of the multirate IIR-ALE/DPLL AFC system.

From the review of current and classical AFC systems the observed trend is to combine spectral estimation and control theory techniques so as to utilize the advantages of both approaches. The IIR-ALE/DPLL AFC system proposed adopts a similar philosophy where a spectral estimation and enhancement technique (the IIR-ALE) precedes a control theory technique (the DPLL). The discussion on the implementation of the IIR-ALE/DPLL AFC system is broken into four different subsections.

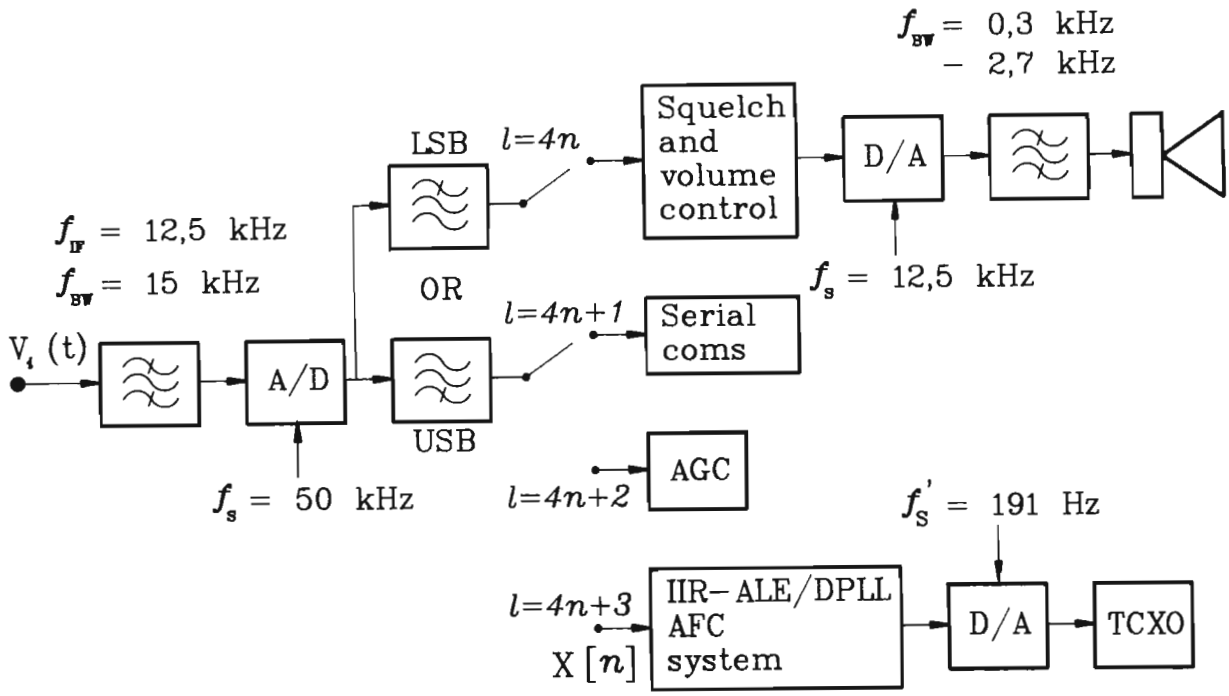

Figure 5.9 A block diagram of the multirate SSB demodulator.

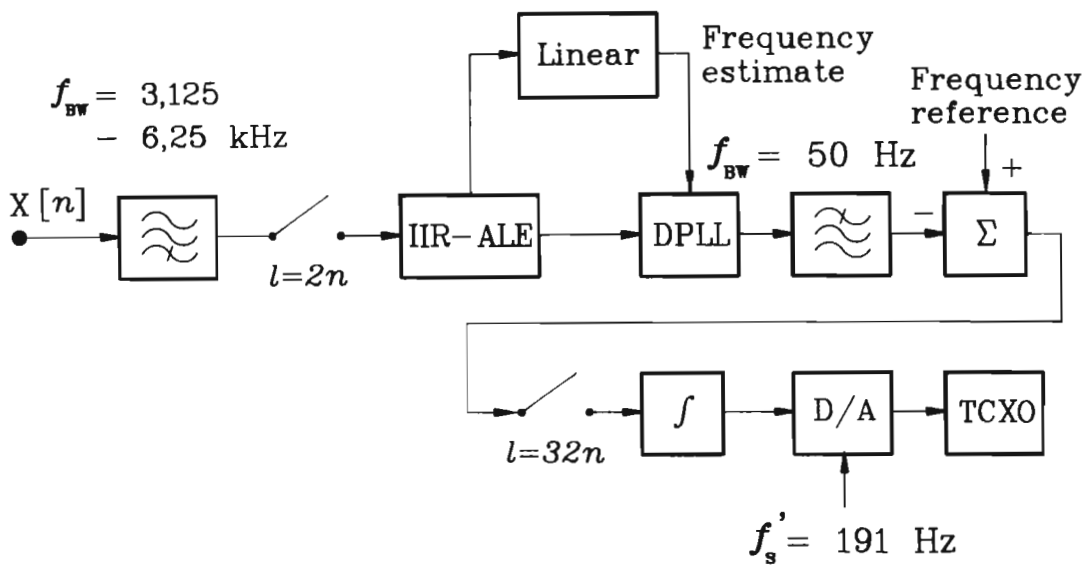

Figure 5.10 A block diagram of the multirate IIR–ALE/DPLL AFC system.

The first subsection describes how the IIR-ALE/DPLL AFC system forms part of a typical multirate SSB demodulator while the second subsection provides an overview of the AFC system. The third subsection includes a discussion on a few of the finer details of the IIR-ALE/DPLL AFC system. Finally in the last subsection a motivation for the IIR-ALE/DPLL AFC system's architecture and its configuration is provided.

Figure 5.9 is a block diagram of a typical multirate SSB demodulator [Carter, 1988] and section 3.2.2 provides an explanation of AM and SSB demodulation performed by decimation. To describe how the IIR-ALE/DPLL AFC system forms part of this structure, a brief description of the multirate SSB demodulator is provided. The bandlimited IF signal is sampled at a frequency of $4f_{IF}$ and highpass or lowpass IF digital filters select either the upper or lower sidebands. Following the sideband filtering a four times decimation demodulates the SSB signal to baseband. This multirate structure is suited to processing signals at different rates and hence bandwidths. The final sampling rate at baseband is f_{IF}, and thus the time period between baseband samples is four times that of IF samples. This implies that four different baseband subroutines can be processed every four IF samples, and therefore this structure is advantageous for processing separate baseband tasks as shown in figure 5.9. These baseband tasks typically include speech in noise detection (or squelch), serial communications with a host microprocessor, AGC and AFC functions.

The block diagram of the IIR-ALE/DPLL is described in figure 5.10 and a comprehensive description is provided by figure 5.11. The AFC system consists of four sections, a highpass filter, an IIR-ALE, a DPLL and the TCXO control. The SSB-SC **tone-above-band** (TAB) signal is sampled at a frequency of f_{IF} following which the carrier (typically 4,6 kHz) is filtered from the speech (300 Hz to 2,7 kHz) via a highpass filter. The carrier signal is then applied to the IIR-ALE whose primary function is to track and enhance the SNR of the carrier. The IIR-ALE's adapting resonance frequency provides a coarse frequency estimate

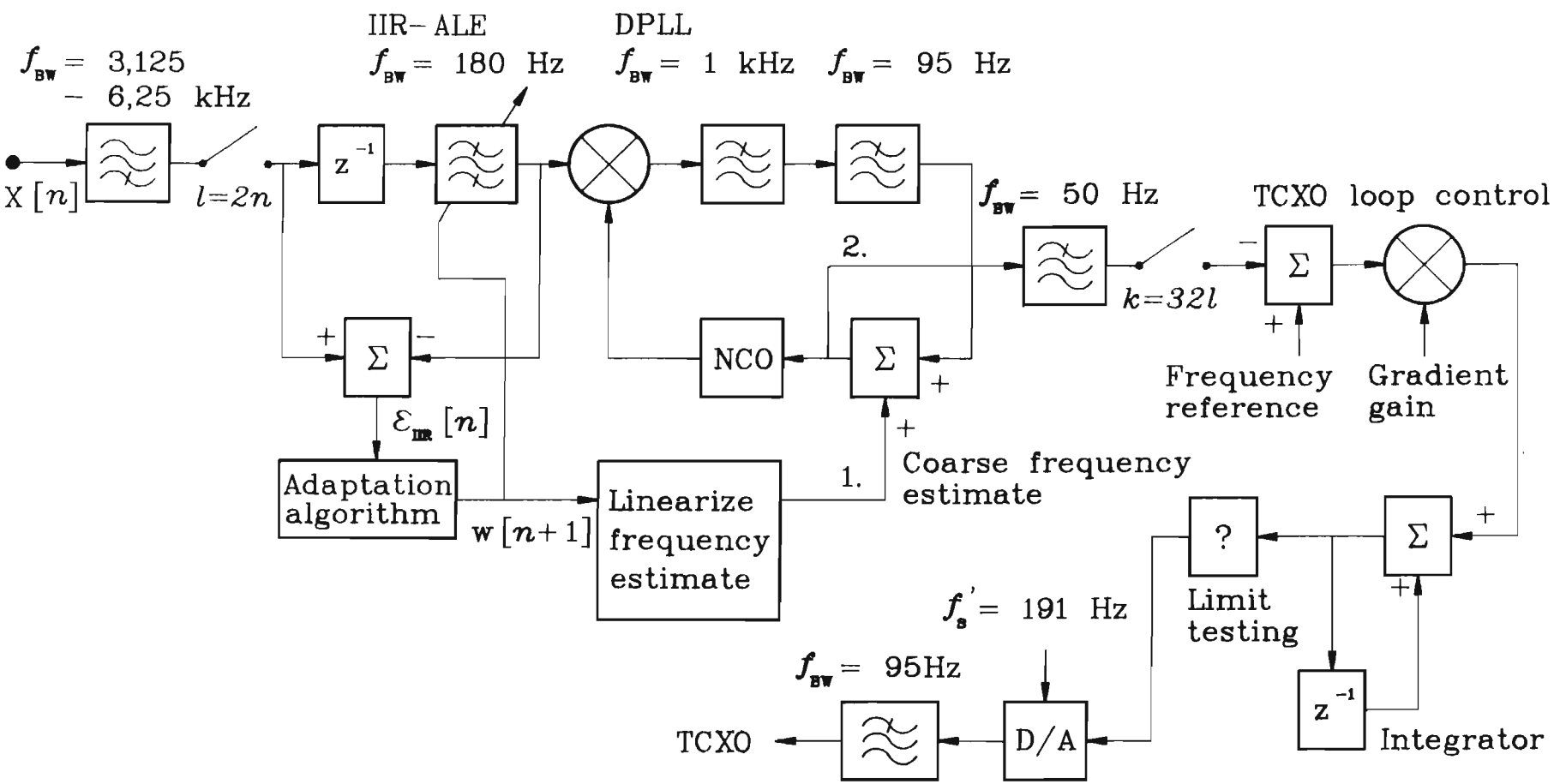

Figure 5.11 A detailed block diagram of the multirate IIR–ALE/DPLL AFC system.

which is utilized to presteer the DPLL. The IIR-ALE's frequency estimate (see section 5.2.2) is a nonlinear function of the carrier frequency and a simple straight line approximation is employed to linearize the estimate to presteer the DPLL's NCO. The enhanced carrier is then applied to the DPLL which further improves the accuracy of the frequency estimate of the carrier.

The IIR-ALE/DPLL AFC system has two control loops. The DPLL contains the short-loop where the NCO output can be utilized for coherent demodulation. The long-loop which forms the last stage of the AFC system generates the control voltage to the TCXO. With reference to figure 5.11, the post DPLL lowpass filter performs two important functions, firstly it bandlimits the NCO's control voltage and secondly it acts as an anti-aliasing filter prior to the TCXO control. Due to the multiplication effect of the frequency reference at ultra high frequencies the update rate of the TCXO's control voltage is minimized to prevent a degradation in the local oscillator sideband and phase noise performance. A typical update frequency of 191,4 Hz implies a 32 times decimation. The bandlimited control voltage is subtracted from a frequency reference and the error signal is amplified to match the gradient's of the voltage to frequency transfer functions of the NCO and TCXO. The gained error signal is then applied to a perfect integrator whose initial value is determined when calibrating the transceiver's TCXO. Finally, the value of the integrator is the TCXO's control voltage and simple limit testing determines whether the AFC loop is beyond the necessary suppressed carrier capture range and should be reset.

Within this paragraph a few finer details of the architecture of the IIR-ALE/DPLL AFC system are discussed. The highpass filter before the IIR-ALE includes a two times decimation process and combined these two operations perform three functions simultaneously. The first, as described in an earlier paragraph, is to separate the speech from the TAB carrier signal. The second, is to match the bandwidth of the

signal to approximately half the sampling frequency. The bandwidth of the signal is determined predominantly by the accuracy of the transceiver's reference. As described in section 3.1.1 a maximum difference of +/- 800 Hz between the transmitter and receiver can occur at 400 MHz; this implies a suppressed carrier signal bandwidth of 1,6 kHz. The third, less apparent function, is to prewhiten the spectrum before applying the signal to the IIR-ALE. The IIR-ALE operates on the principle of enhancing the signal component containing autocorrelative properties. Thus, with reference to figure 5.11, to decorrelate the noise, a delay is inserted between the input of the IIR-ALE and the bandpass filter. If the noise is white (ie: constant spectral density between 0 Hz and $f_s/2$), a simple single delay is required to decorrelate the noise [Hush, 1986]. Assuming that the spectrum after the highpass filter, which is not white, is limited to the region of $f_s/4$ to $f_s/2$. The decimation process after the highpass filter then aliases this frequency band to lie in the region of 0 Hz to $f'_s/2$, where $f'_s/2$ is the sampling frequency after decimation, and this whitens the spectrum. Thus, assuming an IF sampling frequency f_s of 50 kHz, the prewhitening filter is processed at a sampling frequency $f_s/4$ or 12,5 kHz, and the IIR-ALE and DPLL (including the TCXO control) in two separate subroutines, each at $f_s/8$ or 6,25 kHz.

Cupo & Gitlin [1989] in their AFC system place the IIR-ALE after the DPLL since the expected SNR is large and the frequency offsets small. However in SSB-SC communications the converse; low SNR and large frequency offsets, often occurs. There are five advantages, described in the following paragraphs, to reverse this operation and place the IIR-ALE before the DPLL. The first two advantages also motivate for the inclusion of the IIR-ALE in the AFC system while the last three provide motivation for the DPLL.

1. Kumar & Pal [1990] have shown that bandpass IIR-ALEs, if the correct bandwidth and adaptation parameters are selected, are capable of acquiring and tracking sinusoids at low input SNRs,

typically -10 dB and less. This is unlike the PLL which requires a loop SNR of between 0 and 6 dB to acquire lock [Gardner, 1979, pg. 81].

2. As the SNR decreases, the variance in the IIR-ALE's frequency estimate increases relatively slowly; unlike the PLL where the VCO's control voltage contains no frequency information once phase-lock is lost.

3. The third advantage is found in the mechanism of the update in the position of the IIR-ALE's resonance frequency which is given by

$$w[n+1] = w[n] + \frac{\upsilon \epsilon_{IIR}[n]\alpha_{MIIR}[n]}{\psi_{MIIR}[n]} \quad , \tag{5-3}$$

where $w[n]$ is the filter's coefficient which is a function of the resonance frequency. The rate of convergence is controlled by υ, and $\epsilon_{IIR}[n]$ is the error signal. The variable $\alpha_{MIIR}[n]$ is the gradient of the error signal and $\psi_{MIIR}[n]$ an estimate of its instantaneous power. This structure is in the form of single pole lowpass filter where the z transform has been derived as [Ogata, 1970, pg. 651-652]

$$\frac{Y(z)}{X(z)} = \frac{1-\exp(-T_s/\tau_{RC})}{1-\exp(-T_s/\tau_{RC})z^{-1}} \quad , \tag{5-4}$$

and τ_{RC} is the time constant of the filter. From this transfer function it is observed that the gain increases as the input frequency approaches DC, and thus, if used to control the TCXO, creates close-in local oscillator noise. Decreasing the bandwidth to reduce this close-in noise adversely affects the time response of the complete AFC system. This is unlike the PLL where the noise spectral density ($\Gamma_c(\omega)$) appearing at the input of the **voltage control oscillator** (VCO) is given by [Gardner, 1979, pg. 177]

$$\Gamma_c(\omega) = \{\omega^2 \Gamma_n(\omega)\} \frac{|H_{PLL}(j\omega)|^2}{K_o^2} \quad , \tag{5-5}$$

where $\Gamma_n(\omega)$ is the spectral density of the input noise, K_o is the gain of the VCO and $H_{PLL}(j\omega)$ is the closed-loop frequency response of the PLL. Hence the noise is spread away from the DC point, and easily filtered by a post DPLL lowpass filter. Thus by applying the frequency estimate of the IIR-ALE to the DPLL the noise is then preshaped, allowing for filtering without degrading the dynamic performance of the AFC system. As an example of this effect figure 5.12 (a) is a spectral plot of the IIR-ALE's frequency estimate (see figure 5.11 point 1) where a lowpass noise distribution is apparent. Figure 5.12 (b) is a similar spectral plot of the NCO's control voltage (see figure 5.11 point 2) where preshaping of the noise is evident.

4. If the IIR-ALE was to track rapid Doppler frequency variations the time constant of the update equation would need to be small. This is equivalent to increasing the bandwidth of the update equation which would in turn increase the variance of the IIR-ALE's frequency estimate. Hence the fourth advantage to following the IIR-ALE with a DPLL, is to design the bandwidth of the IIR-ALE filter to be sufficiently large to pass the Doppler frequency variations which are then tracked by the DPLL. Thus the IIR-ALE is responsible for correcting the initial frequency offsets and tracking the long-term frequency variations.

5. Finally, the fifth advantage is that due to the lowpass filter nature of the coefficient update algorithm; the rate of convergence decreases as the IIR-ALE approaches the optimal value. However, since the DPLL acquires the signal within this region it improves the overall acquisition time of the IIR-ALE/DPLL AFC system.

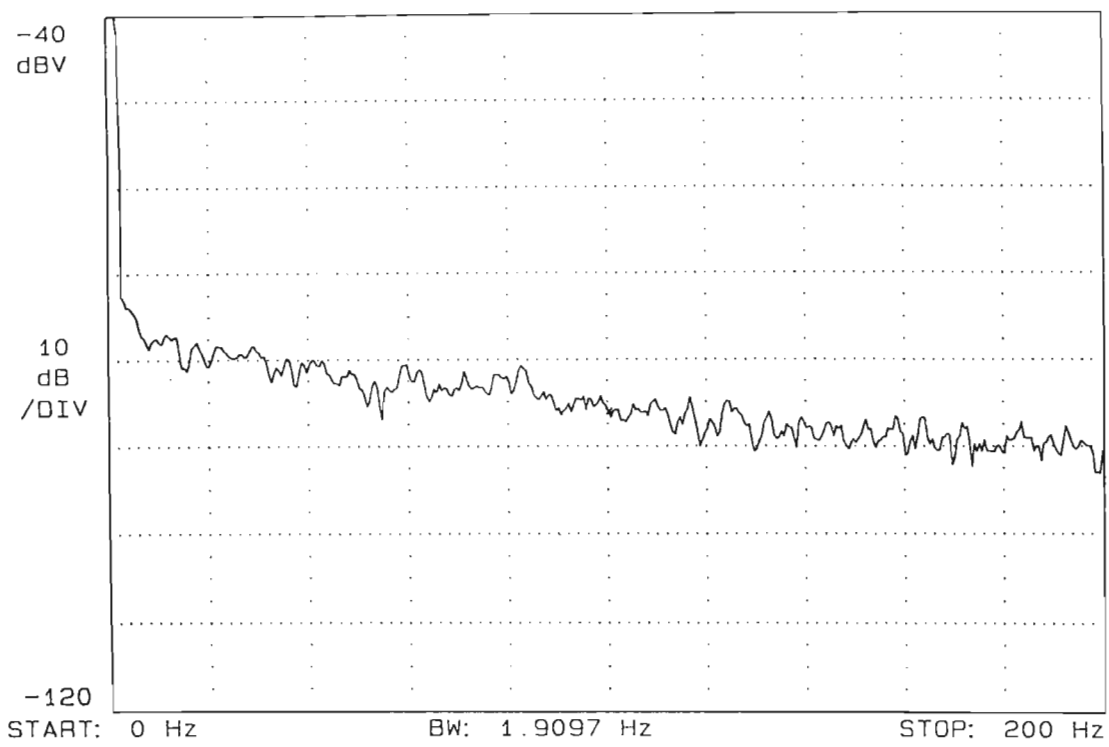

Figure 5.12(a) Spectral plot of the IIR-ALE's frequency estimate (point 1, figure 5.11).

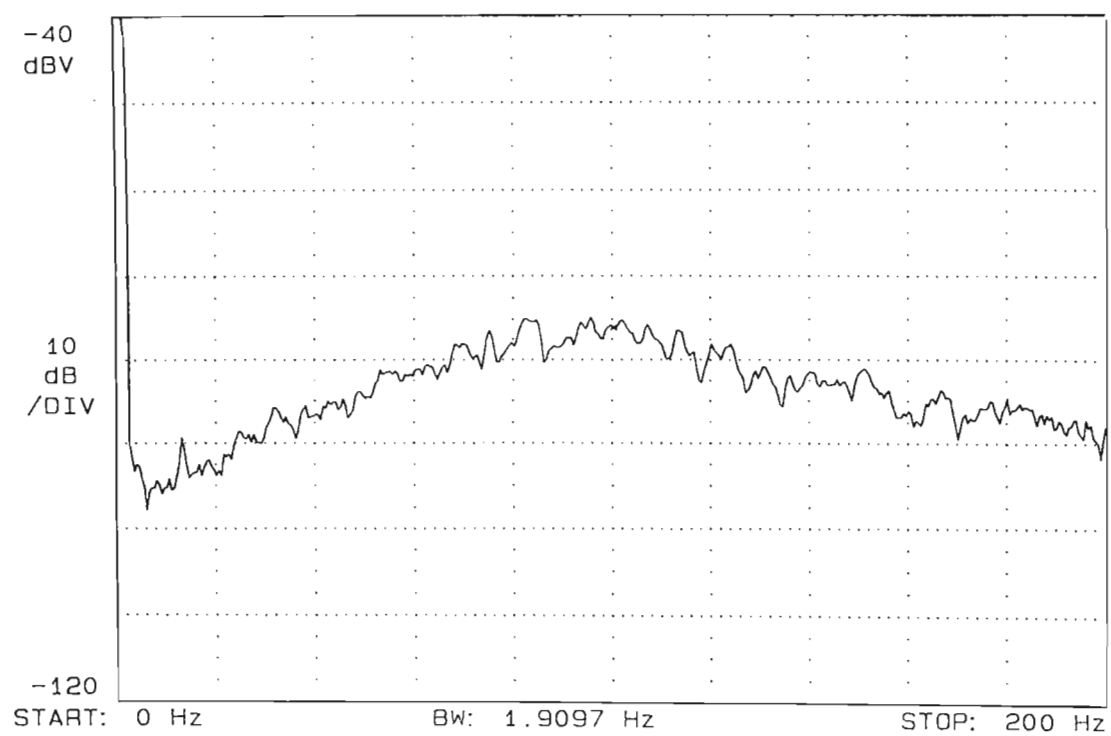

Figure 5.12(b) Spectral plot of the DPLL's NCO's control voltage (point 2, figure 5.11).

5.2.2 The performance evaluation of the IIR-ALE.

This subsection discusses the implementation and performance evaluation of the resonator IIR-ALE, which forms part of the IIR-ALE/DPLL AFC system. Further, a simple technique for improving the rate of convergence without increasing the variance of the DPLL's coarse frequency estimate, is introduced. Due to the recursive nature of IIR-ALE's, they are difficult to analyze and a rigorous analysis of their transient and convergence behavior is often unavailable [Hush, 1986]. Hence, for the purpose of this brief discussion, the effects of the various algorithm parameters, specific to the IIR-ALE/DPLL AFC system, are determined via computer simulation methods.

Section 2.3 is a review of various second order IIR-ALE structures where it is concluded that Hush et al.'s [1986] resonator algorithm provides the simplest nodal equations and therefore is utilized in the IIR-ALE/DPLL AFC system. In section 2.3.2 the salient aspects of the resonator IIR-ALE were introduced and a motivation for the modified gradient search adaptation algorithm provided. To summarize this review the resonator IIR-ALE can be described by the following five difference equations. Referring to figure 5.13, and assuming a noise decorrelation buffer of unity, the second order canonic form resonance filter proposed by David et al. [1983] is defined by the following difference equation

$$Y[n]=\left(\frac{1-r^2}{1+r^2}\right)w[n]X[n-1]-(1-r^2)X[n-2]+w[n]Y[n-1]-r^2Y[n-2]\ , \qquad (5\text{-}6)$$

where $Y[n]$ is the output and $X[n]$ the input of the filter. The bandwidth of the bandpass resonator is determined by r and the point of resonance by $w[n]$. To align the point of resonance with the frequency of the incoming sinusoid Hush [1986] suggests employing a gradient-based search algorithm known as the **modified normalized RLMS** (MRLMS) algorithm which is given by

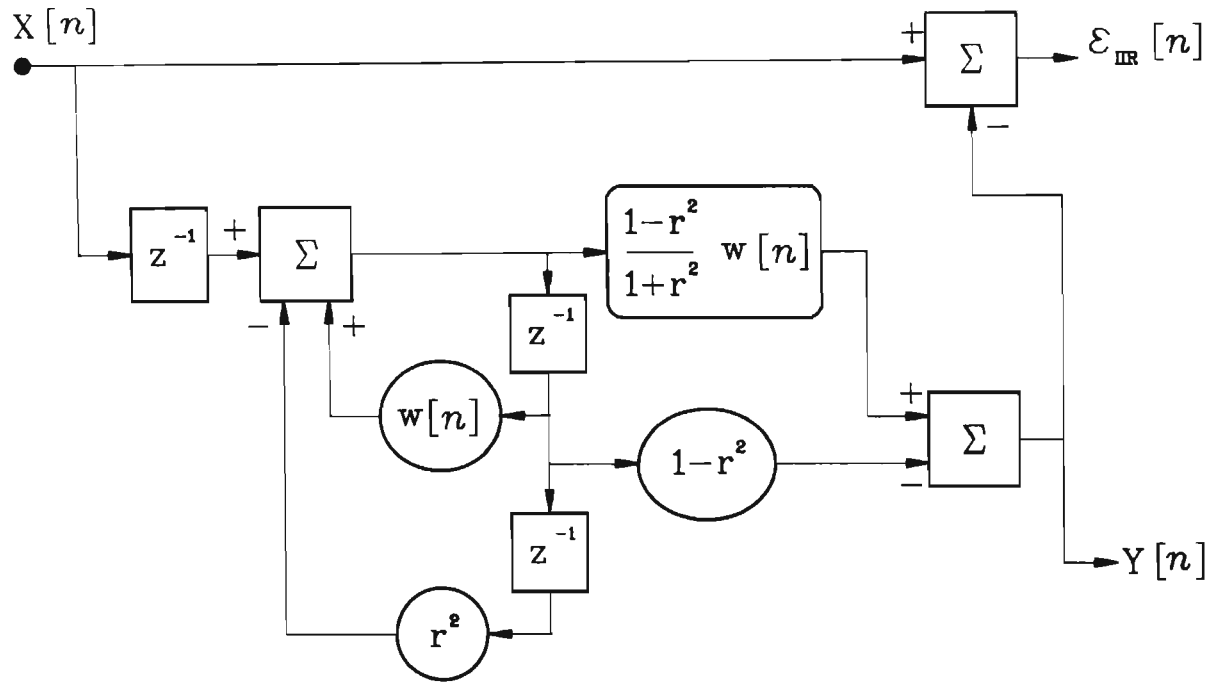

Figure 5.13 The canonic form resonator IIR–ALE.

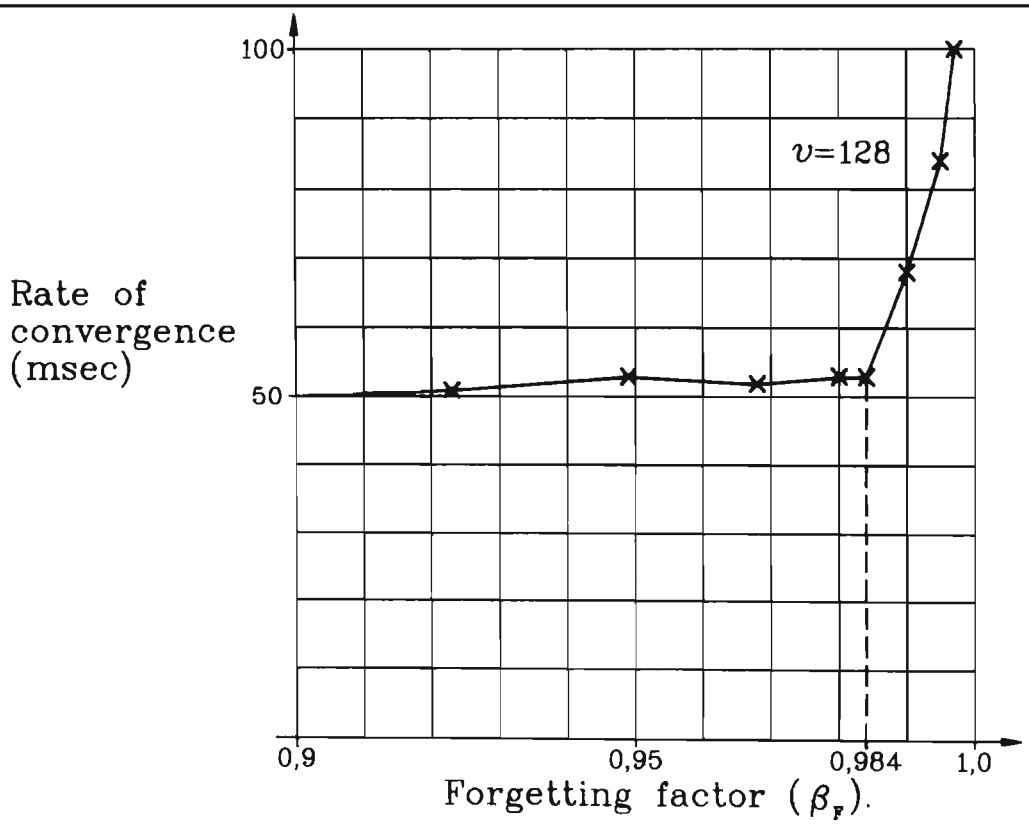

Figure 5.14 The rate of convergence versus forgetting factor (β_F).

$$w[n+1] = w[n] + \frac{\upsilon \epsilon_{IIR}[n]\alpha_{MIIR}[n]}{\psi_{MIIR}[n]} \quad , \tag{5-7}$$

where υ is known as the convergence parameter and $\epsilon_{IIR}[n]$ is the error signal defined as

$$\epsilon_{IIR}[n] = X[n] - Y[n] \quad , \tag{5-8}$$

The modified form of the gradient of the error ($\alpha_{MIIR}[n]$) is given by

$$\alpha_{MIIR}[n] = \left(\frac{1-r^2}{1-r^2} \right) X[n-1] + Y[n-1] \quad , \tag{5-9}$$

from whence $\psi_{MIIR}[n]$, an instantaneous estimate of the power in the gradient vector, is calculated as

$$\psi_{MIIR}[n] = \beta_F \psi_{MIIR}[n-1] + (1-\beta_F)\alpha^2_{MIRR}[n] \quad , \tag{5-10}$$

where β_F is known as the forgetting factor and is the range of $0 \ll \beta_F < 1$. From these five difference equations it is apparent that there are three parameters which need to be determined, r, υ and β_F.

The function of the IIR-ALE is to correct for the long-term frequency variations of the carrier and hence the bandwidth should be large enough to pass the peak doppler frequency offset (f_{PD}). In section 5.2.3 f_{PD} is calculated as being approximately 90 Hz, hence a -3 dB power bandwidth of 180 Hz caters for a possible instantaneous change in sign of the doppler frequency and thus $r = 0,925$. The optimum value of $w[n]$, known as $w_{IIR}[n]$, occurs when $\epsilon_{IIR}[n]$ is minimized, or alternatively the IIR-ALE has converged to its steady state value. The relationship between $w_{IIR}[n]$ and the carrier frequency f_c is given by [Hush, 1986]

$$w_{IIR}[n] = (1+r^2)\cos\left(\frac{2\pi f_c}{f_s} \right) \quad , \tag{5-11}$$

where f_s is the sampling frequency. However, a simple straight line approximation where $w_{IIR}[n]$ is directly employed to obtain a equiripple coarse frequency estimate to presteer the DPLL makes it unnecessary to calculate the $\cos^{-1}$ function.

The rate of convergence of the IIR-ALE is a function of υ and in the next paragraph the effects of this parameter is determined. However, since the calculation of the power of the modified gradient vector $\psi_{MIIR}[n]$ relies on its previous values it is important that the time constant of this difference equation does not affect the overall convergence rate of the IIR-ALE. Figure 5.14 is a graph of the rate of convergence for various values of β_F and an assumed maximum value of υ. It is apparent from figure 5.14 that, below a value of $\beta_F = 0,984$ (or equivalently a time constant of 10 milliseconds) the time response of the calculation of $\psi_{MIIR}[n]$ has little or no effect on the overall rate of convergence of the IIR-ALE when $\upsilon = 128$.

Although the rate of convergence is improved by employing an adaptive step size in the form of $\upsilon/\psi_{MIIR}[n]$ this parameter is still dependant on the magnitude of υ. Figure 5.15 is a graph of the rate of convergence for typical values of υ when a frequency step of 800 Hz (f_s = 6,25 kHz) is applied to the IIR-ALE. However, with reference to figure 5.16, increasing the value of υ results in a larger steady state adaptive step size, where $\pi/2$ is the steady state condition. The larger steady state adaptive step size implies an increase in the variance of the DPLL's course frequency reference, and hence a compromise is generally required between the rate of convergence and the residual noise in the parameter $w_{IIR}[n]$. To overcome this compromise a simple variation to the adaptation algorithm is proposed by making the fixed parameter υ adaptive by employing the simple update equation

$$\upsilon[n+1] = \upsilon[n] - 1 \quad . \tag{5-12}$$

The power in the gradient vector, $\psi_{MIIR}[n]$, is then used as a measure of the frequency offset between the current value of $w[n]$ and the received carrier. If the frequency difference is large (i.e. $\psi_{MIIR}[n]$ is small) then υ is preset to a maximum value and once the IIR-ALE has began adaptation υ slowly converges (at a rate much less than the overall rate of convergence) to a preset minimum value. The upper limit of υ is dependant on the required maximum rate of convergence

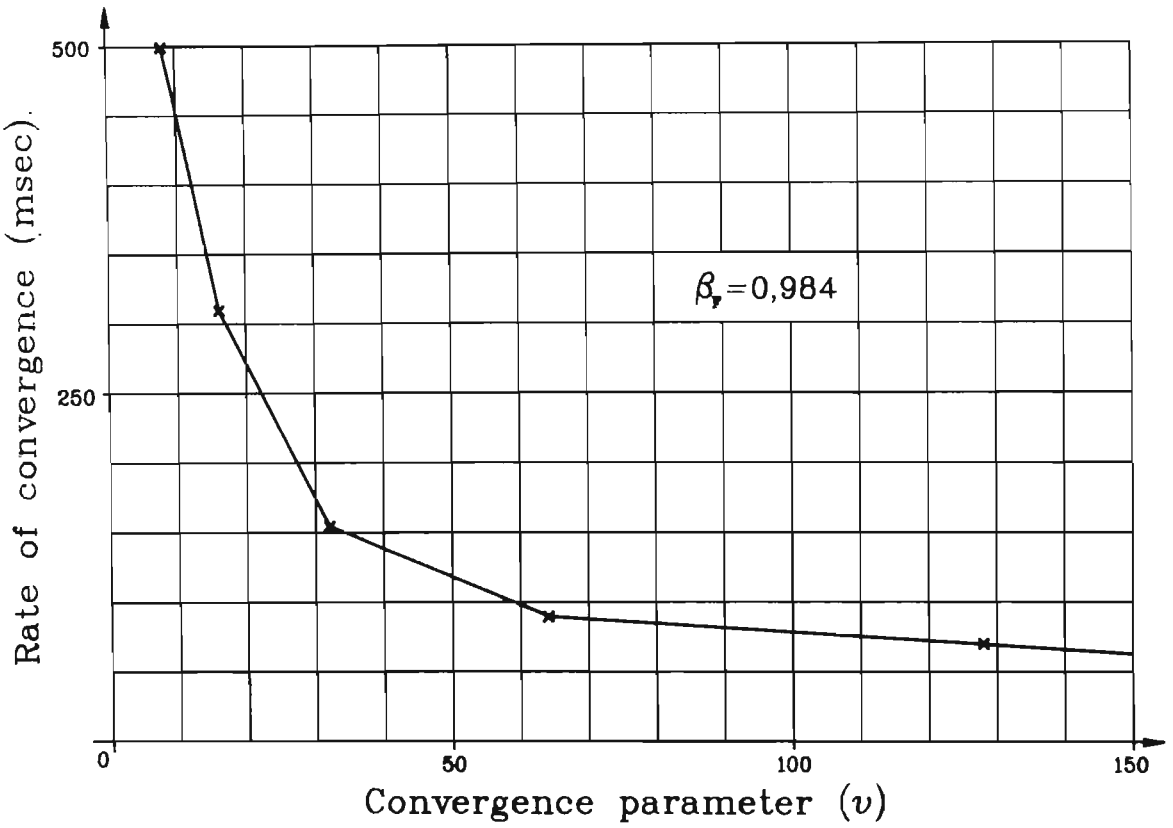

Figure 5.15 Rate of convergence versus convergence parameter (υ).

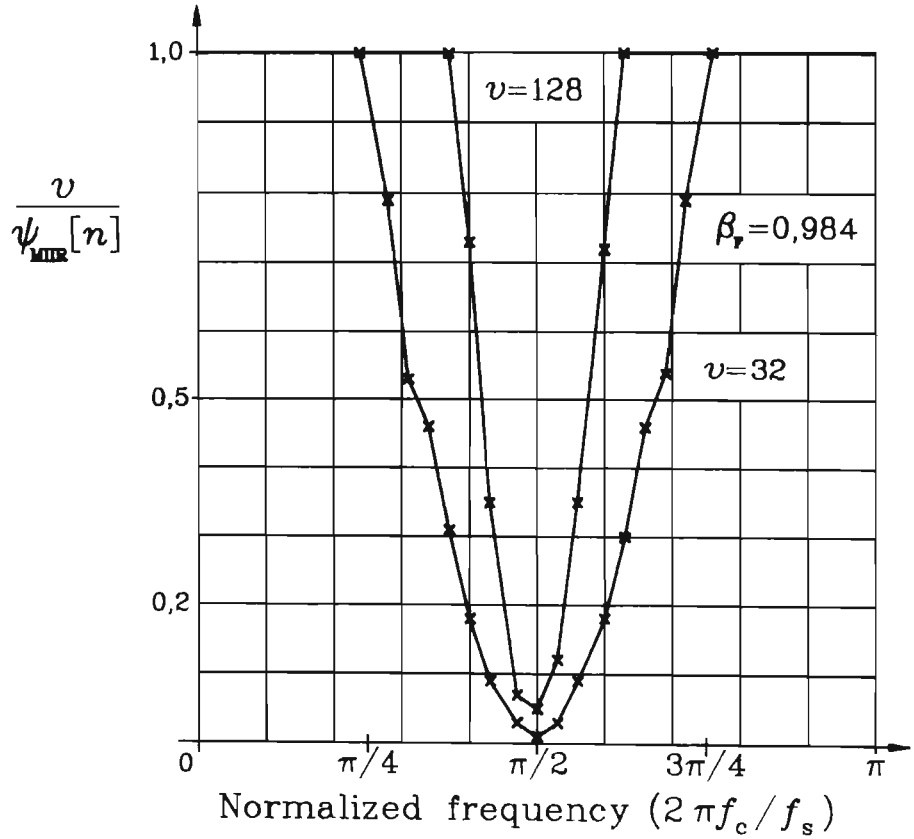

Figure 5.16 $\upsilon/\psi_{MIIR}[n]$ versus normalized frequency.

while the lower limit determines the ability of the IIR-ALE to track slow frequency variations of the received carrier. There are numerous possible combinations in the limits of υ and threshold values of $\psi_{MIIR}[n]$, but to assess the performance of the IIR-ALE/DPLL AFC system, typical values are proposed and utilized in section 5.2.4.

5.2.3 Performance optimization of the DPLL.

Within this subsection the DPLL's parameters are calculated taking into consideration the effects of a Rayleigh fading signal. In section 2.4, the structure of the DPLL was motivated, and the discrete time loop filter given. Essentially the only information required to complete a specific design is a derivation of the loop bandwidth (B_L), from whence the natural frequency (ω_n) and damping factor (ζ) can be calculated by applying the formula [Gardner, 1979, pg. 24-33]

$$B_L = \frac{\omega_n}{2}\left(\zeta + \frac{\zeta}{4}\right) . \qquad (5\text{-}13)$$

Generally the performance analyses of PLLs have been for constant amplitude signals corrupted by additive white Gaussian noise [Gardner, 1979, pg. 25-42]. In radio communications however, variations in the channel affect the received signal power, which in turn alter the loop gain and hence the PLL's performance. There are three approaches to combatting the effects of signal fading; firstly, to employ a limiter to remove amplitude fluctuations, secondly to precede the PLL with an **automatic gain control** (AGC), and thirdly to alter the loop bandwidth to accommodate the fading rate. Signal limiting however causes harmonics and hence aliasing distortion, while Leland & Sollenberger [1980] have shown that the fading cancellation abilities of TAB AGC systems are limited, and therefore, it is necessary to design the DPLL to accommodate signal power fluctuations.

Weber III [1976] has considered the effects of Rice-Nakagami, Rayleigh and lognormal fading channels on the phase variance performance of a first order PLL. Biswas, Ray & Bhattacharya [1979] later extended this study to consider signal acquisition for the same statistical channel models and concluded that higher order PLLs can provide a closer approximation to the channel model. A graph provided by Weber III [1976], given in figure 5.17, essentially sets a lower bound for the loop bandwidth as a function of the maximum fading rate; which in turn is determined by the peak Doppler frequency (f_{PD}). In figure 5.17, different curves are plotted for various ratios of B_L/f_{PD} for different average loop SNRs. To prevent the PLL from loosing lock during a fade, Weber III [1976] concluded that this ratio should be a maximum of unity. Increasing the loop bandwidth however, degrades the ultimate phase variance and hence a ratio of 0,95 is selected as a compromise between the two requirements. For example, in the extreme situation of two mobile units travelling directly towards one another, each at a velocity of 120 km/hr, a f_{PD} of approximately 90 Hz results when the transmission frequency is 400 MHz and thus, the minimum loop bandwidth (B_L) is calculated as being 95 Hz. Furthermore, knowing B_L it is confirmed that Lindsey & Chie's [1981] inequality (see section 2.4.2), $B_L T_s < 0,1$, holds for a sampling frequency of 6,25 kHz and therefore no degradation in the phase variance or tracking performance is expected due to the sampling process.

Multipath propagation causes both destructive and constructive interference, and this increase in signal amplitude can result in numerical overflow if the signal level is not correctly adjusted before processing. From figure A.6.3 it is concluded that there is a 0,1% probability that the signal power, subjected to Rayleigh fading, will exceed the average signal power by 10 dB. By calculating the input signal level required to give a power of -10 dB less than the NCO's power, and adjusting the gain of the multiplying phase detector to account for the halving caused by the multiplication, results in a phase detector gain (K_d) of 0,316 volts/ radians. Similarly the

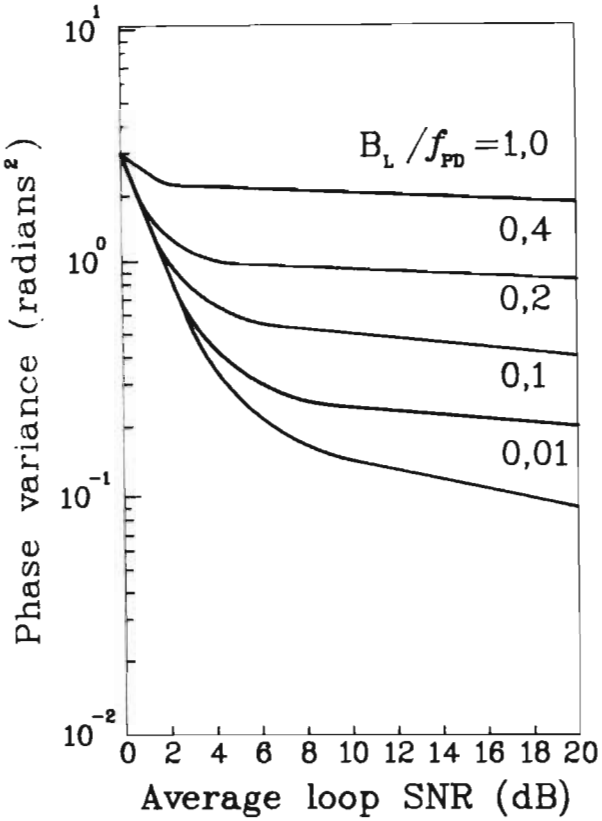

Figure 5.17 Graph of phase variance versus average SNR for a Rayleigh fading signal [Weber III, 1976].

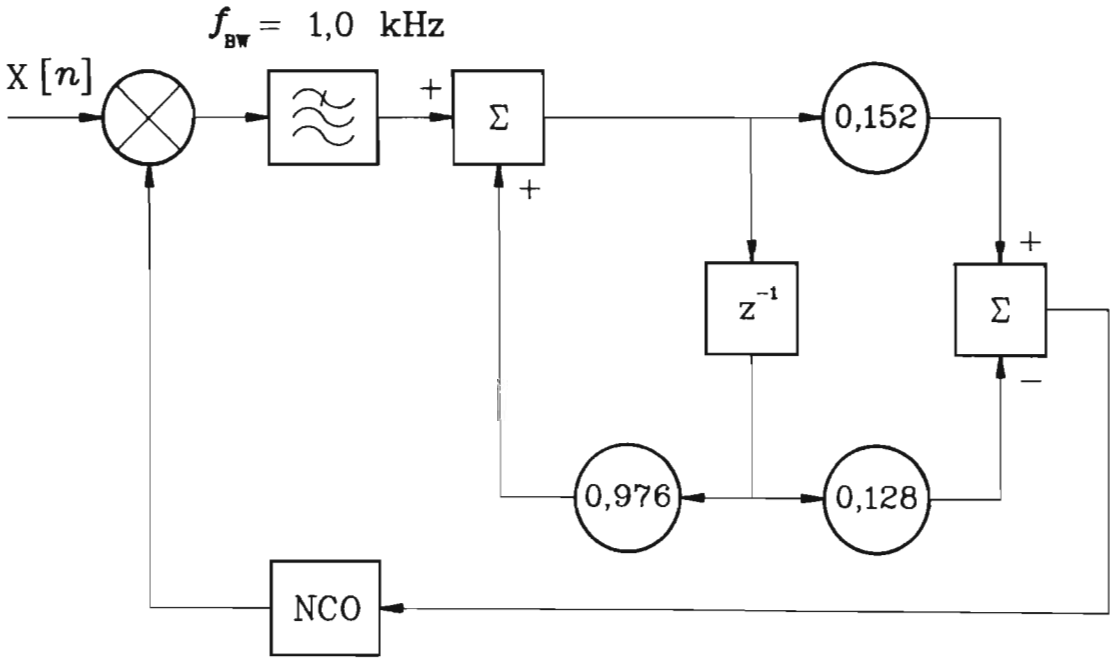

Figure 5.18 The IIR-ALE/DPLL AFC system's second order DPLL.

table look-up NCO's frequency range is from 0 to $1/2T_s$ for an input numerical range of 0 to 0,5. For a sampling frequency of 6,25 kHz this implies a NCO gain (K_o) of 39,27 x 10^3 radians/ second volt. Thus assuming a ζ of 0,707, which is a compromise between the phase variance and signal acquisition, results in an $\omega_n/2\pi$ of 214,9 Hz from equation 5-13. By applying the design procedure outlined in section 2.4.2 and substituting for K_o, K_d, ω_n and ζ finally results in the DPLL's normalized loop filter, see figure 5.18, which is given by

$$F(z)=\frac{0.152-0.128z^{-1}}{1-0.976z^{-1}} \quad . \tag{5-14}$$

5.2.4 A performance assessment of the multirate IIR-ALE/DPLL AFC system.

In this subsection the multirate IIR-ALE/DPLL AFC system's performance is assessed and compared to a classical wideband DPLL AFC system, for three different channel models. The first model is a stationary channel which typically occurs in a portable role. The second model assumes a simple amplitude fading signal, as a first measure of the AFC systems' performance in a multipath environment; while the third model, is a Rayleigh fading channel, a statistical model which is representative of a mobile communications channel. In Appendix 6.1 various SSB-SC system considerations are reviewed which includes the effects of multipath propagation on the amplitude and phase of the received carrier.

Figure 5.19 is a block diagram of the classical wideband DPLL AFC system used in the comparison between the two AFC systems. The two systems are similar except that the IIR-ALE/DPLL is replaced by a wideband DPLL. The wideband DPLL's loop filter designed, using the procedure outlined in section 2.4.2, assumes a ζ of 0,707, and an

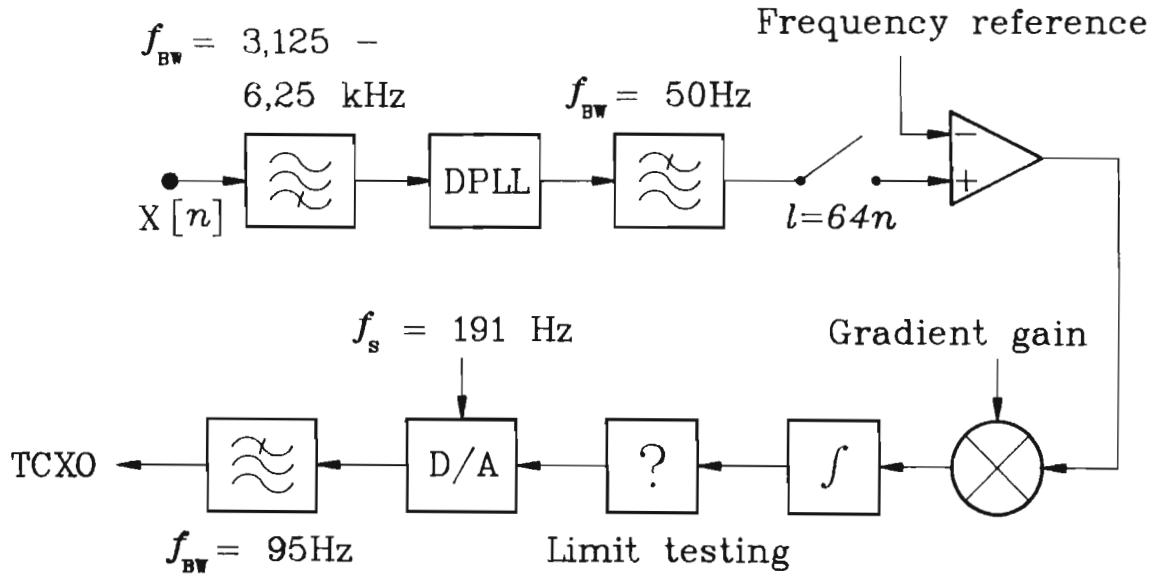

Figure 5.19 The classical DPLL AFC system.

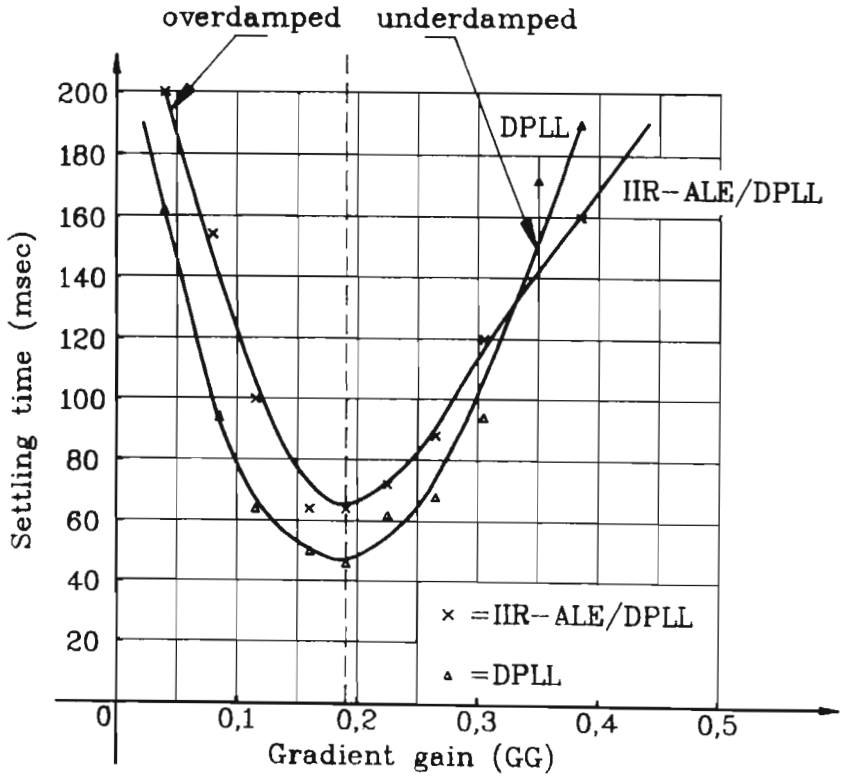

Figure 5.20 The settling time versus gradient gain.

$\omega_n/2\pi$ of 900 Hz. Due to the wider loop bandwidth it is necessary to increase the sampling rate and hence there is little computational advantage to the classical wideband DPLL AFC system. For a large CNR_i (greater than 30 dB), a frequency capture range of +/- 1,08 kHz was measured, for the wideband DPLL. The degradation in the anticipated frequency capture range of +/- 1,3 kHz, is attributed to the sinusoidal phase detector, a result observed by Mengali [1973] who studied the effects of different phase detectors on signal acquisition. The degradation in wideband signal acquisition performance is more pronounced for larger loop bandwidths, and thus a linear phase detector, albeit with increased processing, is strictly necessary. However in the comparison of the two AFC systems the sinusoidal phase detector is utilized to ensure a reasonably fair comparison in performances.

For evaluation purposes the two AFC systems were integrated into the SSB demodulator structure described by figure 5.9, which includes a feedback **automatic gain control** (AGC) system. Based on the discussion in section 5.2.2 the following IIR-ALE parameters were selected; $\beta_F = 0.984$, $32 < \upsilon < 128$ and υ was set at its maximum value if the calculation of $\psi_{MIIR}[n]$ indicated a frequency offset of greater than 200 Hz. In order to determine the dynamics of the transceiver's synthesizer a 350 MHz carrier signal (at 30 dB SNR) was frequency modulated by a 1 Hz square wave with a frequency deviation of 200 Hz; which represents a frequency step of 400 Hz. Figure 5.20 is a graph of the settling time versus **gradient gain** (GG) where the gradient gain (see figure 5.11) is defined as

$$GG = \frac{G_{ACT}}{G_{UNI}} \quad . \tag{5-15}$$

G_{UNI} is the numerical value which results in unity gain between the NCO's and TCXO's voltage to frequency relationships while G_{ACT} is the actual numerical value utilized. From the results described by figure 5.20 the following two observations are made. The longer settling

time of the IIR-ALE/DPLL AFC system is caused by the time constants in the adaptation algorithm since this system requires a finite period to perceive a change in frequency. Normally a random "walk about" occurs prior to signal acquisition which reduces the time difference. For gradient gains less than 0,15 both AFC systems become overdamped while for values greater than 0,25 the systems are underdamped. The settling time is increased in both situations due to a slow step response (overdamped) and unnecessary ringing (underdamped).

In portable communications the emphasis is on minimizing the power consumption, hence the importance of operating at low SNRs. Figure 5.21 is a graph of the maximum frequency step acquisition versus CNR_i, which is adjusted for a 300 Hz to 2,7 kHz bandwidth. The measurement assumes a stationary communications link and is a function of three different gradient gains, where the carrier frequency is 380 MHz and is frequency modulated with a 1 Hz square wave with various frequency deviations. Although the improved frequency acquisition capabilities of the IIR-ALE/DPLL AFC system is apparent, of importance is the relative degradation in capture range as the CNR_i decreases. Pollack & Pickett [1959] have shown that for a 5 dB SNR speech signal 75% word recognition is possible and the author assumes this to be the minimum tolerable SNR for SSB communications. Furthermore, the carrier power is typically transmitted -10 dB below the peak envelope power [Ball & Holmes, 1981], and hence, it is important to consider the relative degradation in frequency acquisition for a -5 dB CNR_i. Assuming a gradient gain of 0,192 and a CNR_i of -5 dB, the frequency step acquisition of the IIR-ALE/DPLL degrades by 25% while the wideband DPLL degrades by 72%.

Bandwidth and power efficiency are the two primary reasons for employing SSB rather than FM or AM modulation schemes. In commercial SSB mobile communications the emphasis is on speech quality, hence operation at low SNRs seldom occurs and SSB is rather employed for its bandwidth considerations. In a paramilitary application the emphasis is on

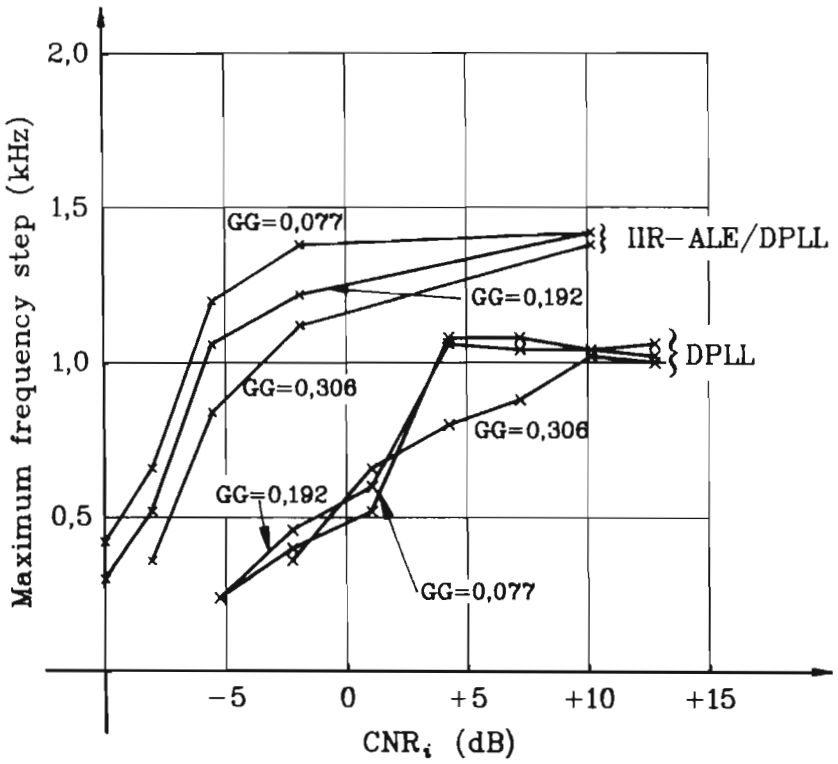

Figure 5.21 Maximum frequency step acquisition versus CNR$_i$ at different gradient gains (GG).

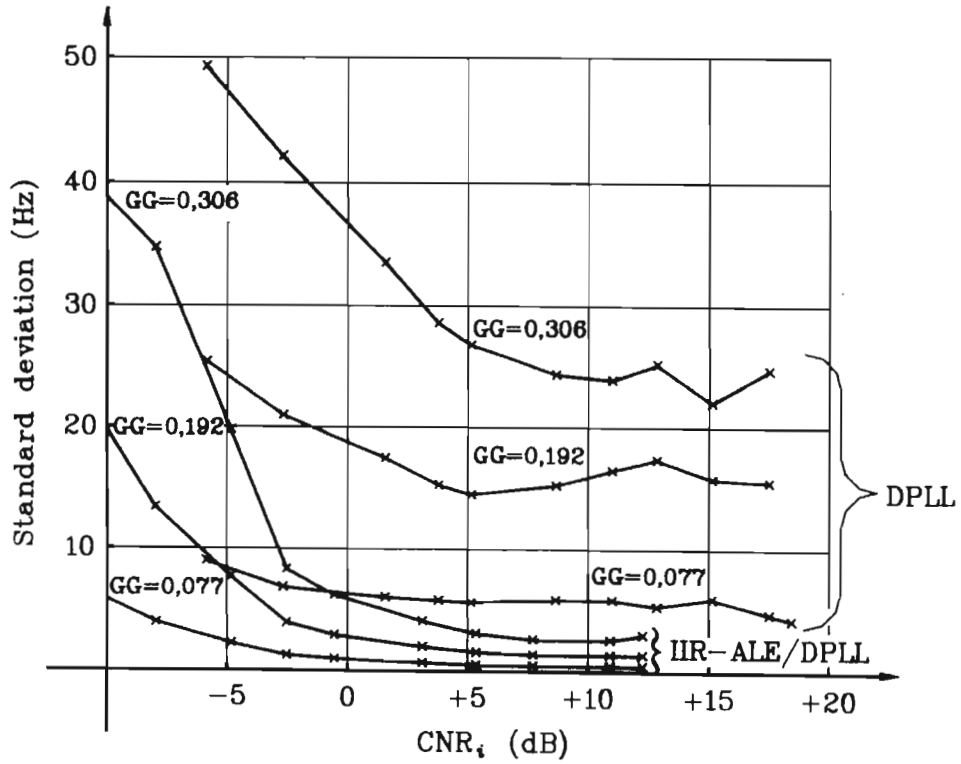

Figure 5.22 The standard deviation of the frequency estimate for a stationary link.

avoidance of detection and power efficiency, thus it is important that the system operates successfully at small CNRs. As the CNR_i degrades, so does the frequency estimate provided by the AFC system which results in a "warbling" effect as the speech is frequency modulated by narrowband noise. This problem is compounded since the speech is already severely degraded by the channel noise. Figure 5.22 is a graph of the **standard deviation** (SD) of the frequency estimate, of the two AFC systems, as a function of the CNR_i for three different gradient gains. The carrier frequency is 380 MHz and a stationary communications link is assumed. The frequency estimate standard deviation was calculated for a period of approximately 8 seconds to 64 bits of precision utilizing the following equation

$$SD = \left\{ \frac{1}{1536} \sum_{k=1}^{1536} E[n-k]^2 - \left(\frac{1}{1536} \sum_{k=1}^{1536} E[n-k] \right)^2 \right\}^{\frac{1}{2}}, \qquad (5\text{-}16)$$

where $E[n]$ is the frequency estimate applied to the TCXO's D/A converter. It was found by listening to a noise corrupted sinusoid applied to the IIR-ALE/DPLL AFC system that for a frequency estimate standard deviation of 9 Hz, and less, no frequency modulation is perceived. Between 10 and 15 Hz frequency modulation is perceived although not objectionable, while above 16 Hz the performance of the communications link would be severely degraded. Similar results were obtained during field evaluations of the IIR-ALE/DPLL AFC system where it was found by several listeners that for frequency estimate standard deviations of less than 10 Hz no perceived degradation in the speech quality and no frequency modulation was detected.

Figure 5.23 is a graph of the standard deviation of the frequency estimate versus average CNR_i for an amplitude fading signal. A 380 MHz 100% amplitude modulated signal with various modulating frequencies was applied to both AFC systems with a fixed gradient gain of 0,192. This simple fading signal typically simulates the effects of a rural environment where there is a single dominant multipath component due to a reflection from the road surface. In a rural environment higher

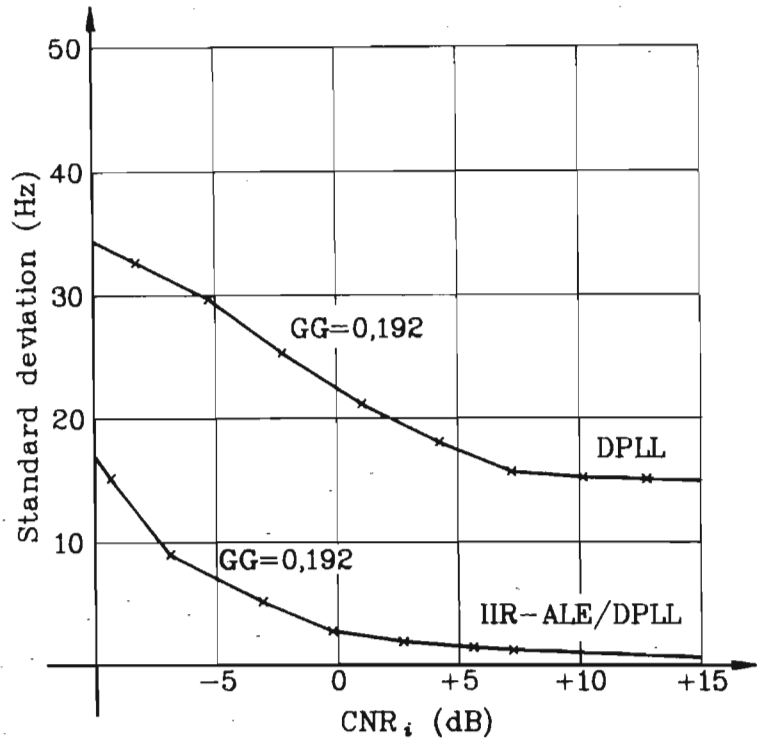

Figure 5.23 The standard deviation of the frequency estimate for an amplitude fading signal.

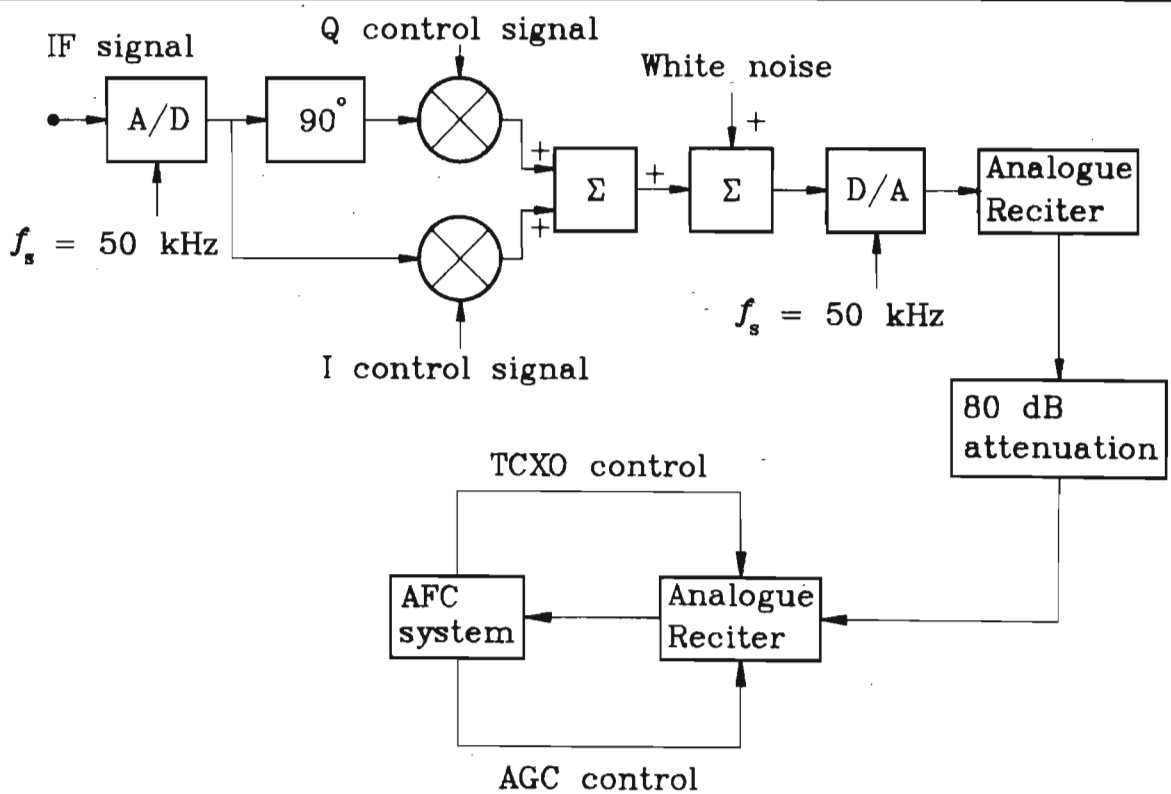

Figure 5.24 A block diagram of the Rayleigh channel simulation system.

mobile velocities are expected and hence fading frequencies of 32 Hz (90 km/hr), 42 Hz (120 km/hr) and 84 Hz (240 km/hr) were applied to the two different algorithms where a carrier frequency of 380 MHz is assumed. From figure 5.23 it is observed that the various fading rates have little effect on the frequency estimate standard deviation of either system; this is attributed to the simple fading model which does not include any form of phase modulation. Due to the small spread of results the frequency estimate standard deviation for the 42 Hz fading signal is indicated; generally however the higher Doppler frequency (84 Hz) resulted in a slightly larger standard deviation than the lower Doppler frequency (32 Hz).

To assess the performance of the two AFC systems for a mobile communications channel the Rayleigh channel simulator proposed by Jakes [1974, pg. 65-78] was implemented using the wideband DSP transceiver. Recently Casas & Leung [1990] have reported a similar implementation of this channel simulator and found through measurements that the resultant carrier signal statistics exhibit a close correspondence to a Rayleigh distribution. Figure 5.24 is a block diagram of the test system used to evaluate the two AFC systems. The first transceiver performed the function of Jake's channel simulator; the DSP third IF sampled a carrier signal whose frequency was offset by 12,5 kHz and by using a FIR Hilbert transformer, quadrature 12,5 kHz IF signals were created. Eight NCOs of varying relative amplitudes and frequencies were summed to obtain in-phase and quadrature fading control signals which were used to modulate the carrier signal. The modulated in-phase and quadrature signals were then summed to create the 12,5 kHz IF Rayleigh fading signal. Noise with a flat spectral density between 0 Hz and $f_s/2$ where f_s is 50 kHz was then added to the fading signal to alter the SNR of the carrier signal. The resultant 12,5 kHz IF signal was then modulated by the analogue **reciter** (receiver/ exciter) and transmitted to a second wideband DSP transceiver which incorporated either of the two AFC systems. Attenuation between the two transceivers prevented saturation of the second transceiver's analogue front end

amplifiers. Although the noise was bandlimited to 15 kHz by the second IF's crystal filter its bandwidth was larger than the bandwidth of the two AFC systems and hence was assumed to be white for the purpose of the AFC algorithms' evaluation. Figure 5.25 is a spectral plot of a typical noise corrupted Rayleigh fading signal created by the DSP IF stage. From Jake's [1974, pg. 20-26] discussion on the moments of the radio frequency spectra it is possible to calculate the standard deviation of the frequency of the carrier signal when subjected to Rayleigh fading. From the derivation of the second moment of the electric field, the standard deviation of the frequency of the carrier signal is given by

$$SD = 0,612 f_{PD} \ , \qquad (5\text{-}17)$$

When observing the resultant Rayleigh fading spectrum described by figure 5.25 the result is intuitively satisfying since there is an obvious bias towards the peak Doppler frequency.

Figure 5.26 describes the IIR-ALE/DPLL AFC system's standard deviation of the frequency estimate versus average CNR_i (measured in a 300 Hz to 2,7 kHz bandwidth) for three fading frequencies and two gradient gains. The fading frequencies of 10 Hz, 21 Hz and 35 Hz simulated the urban velocities of 30 km/hr, 60 km/hr and 90 km/hr respectively, for a carrier frequency of 380 MHz. From the results a number of interesting observations are made. For a gradient gain of 0,192 the frequency estimate standard deviations for the three fading frequencies, at a 5 dB average CNR_i, are 4,8 Hz, 8 Hz and 11,8 Hz. From equation 5-17 it is apparent that these results are less than the calculated standard deviations of 6,1 Hz, 12,6 Hz and 21,4 Hz for the three fading frequencies of 10 Hz, 21 Hz and 35 Hz. By increasing the gradient gain to 0,230 the standard deviation of the frequency estimate for the three fading frequencies at a 5 dB average CNR_i became 6,8 Hz, 12,8 Hz and 18 Hz. Since increasing the gradient gain degrades the

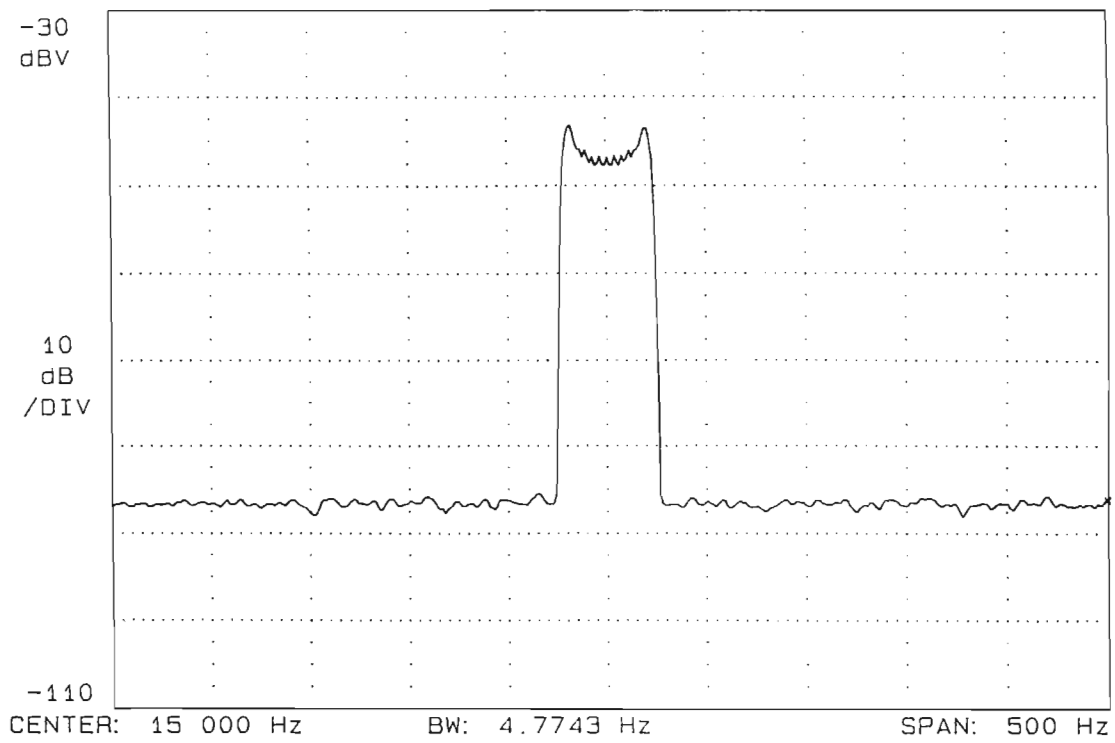

Figure 5.25 The spectrum of a typical Rayleigh fading signal (f_{PD} = 21 Hz).

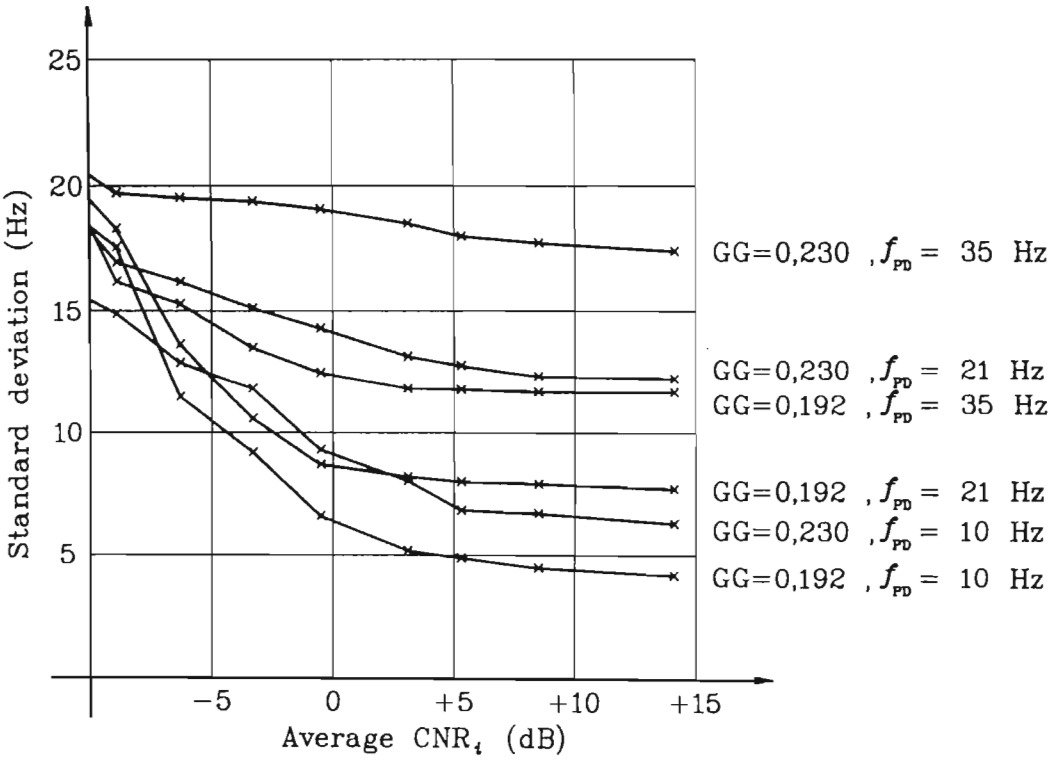

Figure 5.26 The IIR−ALE/DPLL AFC system's standard deviation of the frequency estimate for a Rayleigh fading signal.

standard deviation of the frequency estimate for a stationary communications link generally a compromise between the two situations is reached. However an improvement in the overall performance could be achieved by relating the gradient gain to the standard deviation of the frequency estimate which is a function of the peak Doppler frequency. For a gradient gain of 0,192 the IIR-ALE/DPLL AFC system's standard deviation starts to increase below a -3 db average CNR_i which is similar to the results of the stationary communications link described by figure 5.22. This is unlike the DPLL AFC system whose standard deviation of the frequency estimate increased rapidly, irrespective of the fading frequency, for an average CNR_i of less than or equal to 7 dB. For the stationary communications channel the DPLL AFC system's standard deviation of the frequency estimate only started to increase for a CNR_i of less than 3 dB.

Besides the controlled laboratory evaluation the IIR-ALE/DPLL AFC algorithm was also subjected to extensive field tests. The field evaluations were primarily concerned with the subjective assessment of various dynamic channel conditions on the IIR-ALE/DPLL AFC system and its affect on the received speech quality. The first transceiver was located at a fixed point while the second transceiver was installed in a mobile unit. The mobile unit's velocity varied between 30 and 90 km/hr in the urban environment while velocities in the order of 120 km/hr were achieved in the rural environment. The majority of the transmissions took place at 390 MHz although the system was also tested at lower frequencies. For the field trials a gradient gain of 0,2 was utilized while the TAB carrier's power was preset at -10 dB below the power of a transmitted 1 kHz audio tone. During the mobile and stationary tests the AFC algorithm was also subjected to intermittent power line and the mobile unit's impulse interference. The received audio signal varied from approximately 25 to 0 dB SNR for both the stationary and mobile communication links. In all conditions the IIR-ALE/DPLL AFC algorithm acquired the carrier within a maximum time period of approximately 200 milliseconds (which included

the settling time of the receiver's AGC) and no discernable frequency modulation was detected. It was determined that the acquisition period had little or no affect on the operation of the speech communications link. Interestingly the author has found that experienced radio amateurs, even under marginal conditions (0 to 5 dB SNR) can differentiate between the predominant amplitude modulation effects of multipath propagation and the frequency modulation effects of a failing AFC system.

In conclusion, besides the performance advantage the IIR-ALE/DPLL AFC system has over a conventional wideband DPLL AFC system, due to the two times decimation, the processing requirements of both systems is similar (see figures 5.19 and 5.11). Furthermore it has been found that the IIR-ALE/DPLL AFC system is suitable for low data rate applications (< 1 kbits/sec) which is utilized when synchronizing a frequency hopping network. In this application, since a one shot synchronization technique is often employed, it is necessary to simultaneously perform speech and data demodulation to retain speech communications while setting up the network.

CHAPTER 6

CONCLUSIONS AND RECOMMENDATIONS.

The objective of the research described in this dissertation, is the derivation of three optimized digital signal processing algorithms for application in radio communication. Optimized, as implied by the author, is a suitable compromise between performance, complexity and numerical processing efficiency. Besides the derivation of the algorithms, necessary classical and current research is reviewed and, where applicable, compared. The three algorithms derived and assessed are:-

1. A multirate speech amplitude modulation demodulator which exhibits low distortion (typically less than 2%) for a wide range of modulation indices, carrier frequency offsets and deviations. The demodulator is processing efficient and requires only five multiplications and five decisions for every output sample.

   Although the distortion is minimal, a significant portion is caused by the nonlinear group delay of the infinite impulse response Hilbert transformer when the amplitude modulated carrier experiences frequency modulation. It is therefore recommended that if a significant carrier frequency deviation relative to the sampling frequency is expected, that the infinite impulse response Hilbert transformer be replaced with a decimating finite impulse response Hilbert transformer, although this structure is slightly less processing efficient.

2. A low sampling rate speech frequency modulation demodulator for signals whose bandwidth exceed a quarter of the sampling frequency.

The demodulator exhibits low distortion (typically less than 2%) and is processing efficient, requiring eighteen multiplications and three decisions for every output sample.

In tactical communications intermediate frequency speech processing [Carter, 1988] is often employed in the transmitter to improve the intelligibility of the received signal when corrupted by channel noise. Speech processing relies on predistorting the transmitted signal and hence the need for a low distortion demodulator in this application is questionable. In this special situation it is recommended that Lee's [1989, pg. 421] distortion criteria be relaxed to reduce the processing requirement of the low sampling rate frequency modulation demodulator.

3. A multirate single-sideband suppressed carrier automatic frequency control system which involves the combination of a simple second order infinite impulse response adaptive line enhancer and a digital phase-locked loop. The tone-above-band automatic frequency control system is evaluated for stationary and mobile communication channels and is suitable for applications where the average carrier to noise power ratio exceeds -5 dB within a 300 Hz to 2,7 kHz bandwidth. Due to the multirate structure the processing requirement of the automatic frequency control system is similar to a classical digital phase-locked loop system.

   Recently the technique of employing a pilot tone as a phase and amplitude reference for demodulation on a mobile fading channel has again received the attention of researchers. Generally a narrow bandwidth pilot filter is used to extract the reference; the bandwidth however is a compromise between pilot signal distortion and additive noise present in the Doppler-spread tone. Li & Cavers [1991] describe a technique whereby the bandwidth of the pilot

filter is adapted depending on the peak Doppler frequency. Their system however, does not cater for the initial frequency offset between the transmitter and receiver.

A recommendation of an alternative approach is the incorporation of a bandpass pilot filter into the automatic frequency control system whose center frequency is determined by the adaptive line enhancer's optimum coefficient value. The pilot filter's bandwidth would then be calculated employing the standard deviation of the frequency estimate which has been shown to be directly related to the peak Doppler frequency.

In conclusion, digital signal processing offers numerous advantages over conventional analogue techniques. Once functional algorithms and techniques have been developed and combined with low cost integrated circuits, this technology should become the radio communication technology of the immediate future.

REFERENCES.

Aguirre S. & Hinedi S., (1989), "Two Novel Automatic Frequency Tracking Loops", IEEE Transactions on Aerospace and Electronic Systems, Vol. 25, No. 5, September, 1989, pg. 749-760.

Anderson D.T. & Whikehart J.W., (1985), "A Digital Signal Processing HF Receiver", Third International Conference on HF Communication Systems and Techniques, Electronics Division of the IEE, London, England, February 26-28, 1985, pg. 89-93.

Ansari R., (1987), "IIR Discrete-Time Hilbert Transformers", IEEE Transactions on Acoustics, Speech, and Signal Processing, Vol. ASSP-35, No. 8, August, 1987, pg. 1116-1119.

Antoniou A., (1979), "Digital Filters: Analysis and Design", McGraw-Hill Book Company, New York, United States of America, 1979.

Bagwell D.J. & Considine V., (1985), "Digital Processing Architectures for HF Radio Receivers", Third International Conference on HF Communication Systems and Techniques, Electronics Division of the IEE, London, England, February 26-28, 1985, pg. 86-88.

Ball J.R. & Holmes D.W.J., (1981), "An SSB with pilot receiver for Mobile Radio", Clerk Maxwell Commemorative Conference on Radio Receivers and Associated Systems, Institution of Electronic and Radio Engineers, University of Leeds, Proceedings No. 50, 7-9 July, 1981, pg. 429-435.

Biswas B.N., Ray S.K., Bhattacharya A.K., (1979), "Phase Locked Loop Acquisition for a Fading Signal in a Noisy Environment", IEEE Transactions on Communications, Vol. COM-27, No. 1, January, 1979, pg. 170-176.

Blachman N.M., (1949), "The Demodulation of a Frequency-Modulated Carrier and Random Noise by a Discriminator", Journal of Applied Physics, Volume 20, October, 1949, pg. 976-983.

Brown, Jr., J.L., (1979), "On Quadrature Sampling of Bandpass Signals", IEEE Transactions on Aerospace and Electronic Systems, Vol. AES-15, No. 3, May, 1979, pg. 366-371.

Brown, Jr., J.L., (1980), "First-Order Sampling of Bandpass Signals. A New Approach", IEEE Transactions on Information Theory, Vol. IT-26, No. 5, September, 1980, pg. 613-615.

Brown, Jr., J.L., (1983), "On Uniform Sampling of Amplitude Modulated Signals", IEEE Transactions on Aerospace and Electronic Systems, Vol. AES-19, No. 4, July, 1983, pg. 633-635.

Brown R.A., Dewey R.J. & Collier C.J., (1986), "Limitations in a Direct Conversion Radio on AM reception", Conference on Radio Receivers and Associated Systems, Institution of Electronic and Radio Engineers, University College of North Wales, Bangor, Wales, Publication No. 68, July 1-4, 1986, pg. 191-197.

Carter A.J.A., (1986), "A High Frequency Digital Transceiver: Discussion of the Results", Fourth South African Symposium on Digital Signal Processing, University of Pretoria, Pretoria, South Africa, June 27, 1986, pg. 4.3.1 - 4.3.5.

Carter A.J.A., (1988), "Digital Signal Processing Applied to Radio Communications", M.Sc. Eng. Thesis, University of Natal, Durban, South Africa, 1988.

Casas E. & Leung C., (1990), "A Simple Digital Fading Simulator for Mobile Radio", IEEE Transactions on Vehicular Technology, Vol. 39, No. 3, August, 1990, pg. 205-212.

Cavers J.K., (1), (1991), "Performance of Tone Calibration with Frequency Offset and Imperfect Pilot Filter", IEEE Transactions on Vehicular Technology, Vol. 40, No. 2, May, 1991, pg. 426-434.

Cavers J.K., (2), (1991), "The Performance of Phase Locked Transparent Tone-in-Band with Symmetric Phase Detection", IEEE Transactions on Communications, Vol. 39, No. 9, September, 1991, pg. 1389-1399.

Cernuschi-Frias B. & Rocha L.F., (1981), "A Delay-Lock Period Estimator", IEEE Transactions on Acoustics, Speech, and Signal Processing, Vol. ASSP-29, No. 4, August, 1981, pg. 912-914.

Cho N.I., Choi C. & Lee S.U., (1989), "Adaptive Line Enhancement by Using an IIR Lattice Notch Filter", IEEE Transactions on Acoustics, Speech, and Signal Processing, Vol. 37, No. 4, April, 1989, pg. 585-589.

Churchill F.E., Ogar G.W. & Thompson B.J., (1981), "The correction of I and Q Errors in a coherent Processor", IEEE Transactions on Aerospace and Electronic Systems, Vol. AES-17, No. 1, January, 1981, pg. 131-137.

Claasen T., Mecklenbrauker W., Peck J. & Van Hurck N., (1980), "Signal Processing Method for Improving the Dynamic Range of A/D and D/A converters", IEEE Transactions on Acoustics, Speech, and Signal Processing, Vol. ASSP-28, No. 5, October, 1980, pg. 529-537.

Crochiere R.E. & Rabiner L.R., (1983), "Multirate Digital Signal Processing", Prentice-Hall, Inc., Englewood Cliffs, New Jersey, United States of America, 1983.

Cupo R.L. & Gitlin R.D., (1989), "Adaptive Carrier Recovery Systems for Digital Data Communications Receivers", IEEE Journal on Selected Areas in Communications, Vol. 7, No. 9, December, 1989, pg. 1328-1339.

Davarian F., (1987), "Mobile Digital Communications via Tone Calibration", IEEE Transactions on Vehicular Technology, Vol. VT-36, No. 2, May, 1987, pg. 55-62.

David R.A., Stearns S.D., Elliot G.R. & Etter D.M., (1983), "IIR Algorithms for Adaptive Line Enhancement", IEEE International Conference on Acoustics, Speech, and Signal Processing (ICASSP), Boston, April, 1983, pg. 12-20.

Didday R.L. & Lindsey W.C., (1968), "Subcarrier Tracking Methods and Communication System Design", IEEE Transactions on Communications Technology, Vol. COM-16, No.4 , August, 1968, pg. 541-550.

Enloe L.H., (1962), "Decreasing the Threshold in FM by Frequency Feedback", Proceedings of the IRE, Vol. 50, January, 1962, pg. 18-30.

Etter D.M. & Hush D.R., (1987), "A New Technique for Adaptive Frequency Estimation and Tracking", IEEE Transactions on Acoustics, Speech, and Signal Processing, Vol. ASSP-35, No. 4, April, (1987), pg. 561-564.

Filip A.E., (1973), "Linear Approximations to $\sqrt{x^2+y^2}$ having Equiripple Error Characteristics", IEEE Transactions on Audio and Electroacoustics, Vol. AU-21, December, 1973, pg. 554-556.

Freeman D.F., (1978), "Equal Ripple Approximation for Envelope Detection", IEEE Transactions on Acoustics, Speech and Signal Processing, Vol. ASSP-26, No. 3, June, 1978, pg. 254-256.

Gardner F.M., (1979), "Phaselock Techniques", Second Edition, John Wiley and Sons, New York, 1979.

Garner P.J & Gibson R.W., (1981), "SSB systems for Land Mobile use", Clerk Maxwell Commemorative Conference on Radio Receivers and Associated Systems, Institution of Electronic and Radio Engineers, University of Leeds, Proceedings No. 50, 7-9 July, 1981, pg. 373-381.

Giordano A.A. & Hsu F.M., (1985), "Least Square Estimation with Applications to Digital Signal Processing", John Wiley & Sons, New York, United States of America, 1985.

Goatcher J.K., Neale M.W. & Vance I.A.W., (1981), "Noise considerations in an integrated circuit VHF radio receiver", Clerk Maxwell Commemorative Conference on Radio Receivers and Associated Systems, Institution of Electronic and Radio Engineers, University of Leeds, Proceedings No. 50, 7-9 July, 1981, pg. 49-59.

Gold B. & Rader C.M., (1969), "Digital Processing of Signals", Malabar, Fla.: Robert E. Krieger Publishing Co., 1983, originally published by McGraw-Hill International Book Company, Mexico, 1969.

Grace O.D. & Pitt S.P., (1968), "Quadrature Sampling of High-Frequency Waveforms", The Journal of the Acoustical Society of America, Vol. 44, Num. 5, 1968, pg. 1453-1454.

Grace O.D. & Pitt S.P., (1970), "Sampling and Interpolation of Bandlimited Signals by Quadrature Methods", The Journal of the Acoustical Society of America, Vol. 48, Num. 6 (Part 1), 1970, pg. 1311-1318.

Gupta S.C., (1968), "On Optimum Digital Phase-Locked Loops", IEEE Transactions on Communication Technology (Concise Papers), Vol. 16, No. 2, April, 1968, pg. 340-344.

Gupta S.C., (1975), "Phase-Locked Loops", Proceedings of the IEEE, Vol. 63, No. 2, February, 1975, pg. 291-306.

Hagiwara M. & Nakagawa M., (1989), "DSP type novel Phase Synchronizer with the method of Least Squares", IEEE Transactions on Consumer Electronics, Vol. 35, No. 4, November, 1989, pg. 814-819.

Hamilton N.C., (1991), "Aspects of Direct Conversion Receiver Design", Fifth International Conference on HF Radio Systems and Techniques, Institute of Electrical Engineers, Heriot-Watt University, Edinburgh, United Kingdom, July 22-24, 1991, pg. 299-303.

Hart P., (1990), G3SJX, "Kenwood TS-950S Digital HF Transceiver Review", Radio Communication, April, 1990, pg. 35-37.

Hashemian R., (1990), "Square Rooting Algorithms for Integer and Floating-Point Numbers", IEEE Transactions on Computers, Vol. 39, No. 8, August, 1990, pg. 1025-1029.

Hayes D.F, (1987), "An Integrated Voice/Data Architecture For HF Tactical Communications", MILCOM 1987, 1987 IEEE Military Communications Conference, Washington, D.C., October 19-22, 1987, pg. 2.6.1-2.6.4.

Hladik S.M., Saulnier G.J. & Rafferty W., (1989), "A Tone-aided Dual Vestigial Sideband System for Digital Communications on Fading Channels", MILCOM 1989, 1989 IEEE Military Communications Conference, Boston, MA, October 15-18, 1989, pg. 39.4.1-39.4.6.

Honig M.L. & Messerschmitt D.G., (1984), "Adaptive Filters: Structures, Algorithms, and Applications", Kluwer Academic Publishers, Boston, United States of America, 1984.

Hurst G.T. & Gupta S.C., (1974), "Quantizing and Sampling Considerations in Digital Phase-Locked Loops", IEEE Transactions on Communications (Concise Papers), Vol. COM-22, January, 1974, pg. 68-72.

Hush D.R., (1986), "Adaptive schemes for enhancement, detection, and identification of narrowband signals in broadband noise", Ph.D. Dissertation, University of New Mexico, Albuquerque, May, 1986.

Hush D.R., Ahmed N., David R. & Stearns S.D., (1986), "An Adaptive IIR structure for sinusoidal Enhancement, Frequency Estimation, and Detection", IEEE Transactions on Acoustics, Speech, and Signal Processing, Vol. ASSP-34, No. 6, December, 1986, pg. 1380-1389.

Jaffe R. & Rechtin E.C., (1955), "Design and Performance of Phase-Lock Loops Capable of Near-Optimum Performance Over a Wide Range of Input Signal and Noise Levels", IRE Transactions on Information Theory, IT-1, March, 1955, pg. 66-76.

Jakes, Jr., W.C., (1974), "Microwave Mobile Communications", John Wiley & Sons, New York, United States of America, 1974.

Kelly C.N. & Gupta S.C., (1), (1972), "The Digital Phase-Locked Loop as a Near-Optimum FM Demodulator", IEEE Transactions on Communications (Concise Papers), Vol. COM-20, June, 1972, pg. 454-462.

Kelly C.N. & Gupta S.C., (2), (1972), "Discrete-Time Demodulation of Continuous-Time Signals", IEEE Transactions on Information Theory, Vol. IT-18, No. 4, July, 1972, pg. 488-493.

Kohlenberg A., (1953), "Exact interpolation of band-limited functions", Journal of Applied Physics, Vol. 24, No. 12, December, 1953, pg. 1432-1436.

Kreyszig E., (1979), "Advanced Engineering Mathematics", Fourth Edition, John Wiley & Sons, New York, United States of America, 1979.

Kruger J.P., (1986), "Enkelsybanddemodulasie met behulp van syferseinverwerking", M.Ing Verhandeling, Randse Afrikaanse Universiteit, Johannesburg, South Africa, 1986.

Kumar R.V.R & Pal R.N., (1990), "Tracking of Bandpass Signals Using Center-Frequency Adaptive Filters", IEEE Transactions on Acoustics, Speech, and Signal Processing, Vol. 38, No. 10, October, 1990, pg. 1710-1721.

Kwan T. & Martin K., (1989), "Adaptive Detection and Enhancement of Multiple Sinusoids Using a Cascade IIR Filter", IEEE Transactions on Circuits and Systems, Vol. 36, No. 7, July, 1989, pg. 937-947.

Lee W.C.Y., (1982), "Mobile Communications Engineering", McGraw-Hill Book Company, New York, United States of America, 1982.

Lee W.C.Y., (1989), "Mobile Cellular Telecommunications Systems", McGraw-Hill Book Company, New York, United States of America, 1989.

Lee J.C. & Un C.K., (1982), "Performance Analysis of Digital Tanlock Loop", IEEE Transactions on Communications, Vol. COM-30, No. 10, October, 1982, pg. 2398-2411.

Leland K.W. & Sollenberger N.R., (1980), "Impairment Mechanisms for SSB Mobile Communications at UHF with Pilot-based Doppler/Fading Correction", The Bell System Technical Journal, Vol. 59, No. 10, December, 1980, pg. 1923-1942.

Li H.W. & Cavers J.K, "An Adaptive Filtering Technique for Pilot-Aided Transmission Systems", IEEE Transactions on Vehicular Technology, Vol. 40, No. 3, August, 1991, pg. 532-545.

Lindsey W.C. & Chie C.M., (1981), "A Survey of Digital Phase-Locked Loops", Proceedings of the IEEE, Vol. 69, No. 4, April, 1981, pg. 410-431.

Liu H., Ghafoor A. & Stockmann P.H., (1989), "A New Quadrature Sampling and Processing Approach", IEEE Transactions on Aerospace and Electronic Systems, Vol. 25, No. 5, September, 1989, pg. 733-747.

Loper R.K., (1990), "A Tri-Phase Direct Conversion Receiver", MILCOM 1990, 1990 IEEE Military Communications Conference, Monterey, California, September 30 - October 3, 1990, pg. 61.1.1 - 61.1.5.

Lugowski A.N., (1987), "A proposed Stereophonic System for AM broadcasting", IEEE Transactions on Broadcasting, Vol. BC-33, No. 2, June, 1987, pg. 43-47.

Marple Jr., S.L., (1987), "Digital Spectral Analysis with Applications", Prentice-Hall INC., Englewood Cliffs, New Jersey, United States of America, 1987.

Masterton J., Benn H., Dolman G., Roberts A., Breakenridge E. & Rambaut M. (1991), "A Low Cost Digitally Implemented Marine HF Band Receiver", Fifth International Conference on HF Radio Systems and Techniques, Institute of Electrical Engineers, Heriot-Watt University, Edinburgh, United Kingdom, July 22-24, 1991, pg. 295-298.

McBride A.L., (1973), "On Optimum Sampled-Data FM Demodulation", IEEE Transactions on Communications, Vol. COM-21, No. 1, January, 1973, pg. 40-50.

McGeehan J.P. & Bateman A.J., (1984), "Phase-Locked Transparent Tone-in-Band (TTIB): A New Spectrum Configuration Particularly Suited to the Transmission of Data Over SSB Mobile Radio Networks", IEEE Transactions on Communications, Vol. COM-32, No. 1, January, 1984, pg. 81-87.

McGeehan J.P. & Lymer A., (1981), "Problem of speech pulling and its implementation for the design of phase-locked SSB radio systems" IEE Proceedings, Vol. 128, Pt. F, No. 6, November, 1981, pg. 361-369.

McGeehan J.P. & Sladen J.P.H., (1982), "Elimination of False-Locking in Long Loop Phase-Locked Receivers", IEEE Transactions on Communications, Vol. COM-30, No. 10, October, 1982, pg. 2391-2397.

Mengali U., (1973), "Acquisition Behavior of Generalized Tracking Systems in the Absence of Noise", IEEE Transactions on Communications, Vol. COM-21, No. 7, July, 1973, pg. 820-826.

Merritt S.A., (1989), "The Iterated Extended Kalman Phase Detector", IEEE Transactions on Communications, Vol. 37, No. 5, May, 1989, pg. 522-526.

Middleton D., (1987), "Introduction to Statistical Communication Theory", Peninsula Publishing, Los Alto, California, United States of America, 1987.

Millman J., (1979), "Microelectronics: Digital and Analog Circuits and Systems", McGraw-Hill International Book Company, Mexico, 1979.

Mitchell R.L., (1989), "Creating Complex Signal Samples from a Band-Limited Real Signal", IEEE Transactions on Aerospace and Electronic Systems, Vol. 25, No. 3, May 1989, pg. 425-427.

Natali F.D., (1984), "AFC Tracking Algorithms", IEEE Transactions on Communications, Vol. COM-32, No. 8, August, 1984, pg. 935-947.

Ogata K., (1970), "Modern Control Engineering", Prentice-Hall Electrical Engineering Series, Prentice-Hall, Inc., Englewood Cliffs, New Jersery, United States of America, 1970.

Ohno K. & Adachi F., (1990), "Performance Evaluation of Various Decision Schemes for Frequency Demodulation of Narrow-Band Digital FM Signals in Land Mobile Radio", IEEE Transactions on Vehicular Technology, Vol. 39, No. 2, May, 1990, pg. 109-116.

Oklobdzija V.G. & Ercegovac M.D., (1982), "An On-Line Square Root Algorithm", IEEE Transactions on Computers (Correspondence), Vol. C-31, No. 1, January, 1982, pg. 70-75.

Onoe M., (1972), "Fast Amplitude Approximation Yielding either Exact Mean or Minimum Deviation for Quadrature Pairs", Proceedings of the IEEE, Vol. 60, July 1972, pg. 921-922.

Oppenheim A.V. & Schafer R.W., (1975), "Digital Signal Processing", Prentice Hill Inc., Englewwod Cliffs, New Jersey, 1975.

Orfanidis S.J. & Vail L.M., (1986), "Zero-Tracking Adaptive Filters", IEEE Transactions on Acoustics, Speech and Signal Processing, Vol. ASSP-34, No. 6, December 1986, pg. 1566-1572.

Park Jr. J.H., (1970), "An FM Detector for low S/N", IEEE Transactions on Communication Technology, Vol. COM-18, No. 2, April 1970, pg. 110-118.

Parks T.W. & McClellan J.H., (1972), "Chebyshev Approximation for Nonrecursive Digital Filters with Linear Phase", IEEE Transactions on Circuit Theory, Vol. CT-19, March, 1972, pg. 189-194.

Partridge E., (1966), "Origins - A Short Etymological Dictionary Of Modern English", Routledge & Kegan Paul, London, England, 1966.

Pei S.C. & Shyu J., (1992), "Relationships Among Digital One/ Half Band Filters, Low/ High Order Differentiators, and Discrete/ Differentiating Hilbert Transformers", IEEE Transactions on Signal Processing, Vol. 0, No. 3, March, 1992, pg. 694-700.

Pengelley R., (1992), "Practical tactical radio systems from South Africa", International Defense Review, Vol. 25, January, 1992, pg. 55-57.

Pollack I. & Pickett J.M., (1959), "Intelligibility of Peak-Clipped Speech at High Noise Levels", The Journal of the Acoustical Society of America, Vol. 31, No. 1, January, 1959, pg. 14-16.

Prado J. & Alcantra R., (1987), "A Fast Square-Rooting Algorithm Using a Digital Signal Processor", Proceedings of the IEEE, Vol. 75, No. 2, February, 1987, pg. 262-264.

Proakis J.G., (1983), "Digital Communications", McGraw-Hill International Book Company, Mexico, 1983.

Rabiner L.R. & Gold B., (1975), "Theory and Application of Digital Signal Processing", Prentice-Hall, INC., Englewood Cliffs, New Jersey, United States of America, 1975.

Rader C.M., (1984), "A Simple Method for Sampling In-Phase and Quadrature Components", IEEE Transactions on Aerospace and Electronic Systems, Vol. AES-20, No. 6, November, 1984, pg. 821-824.

Rafferty W., Anderson J.B., Saulnier G.J. & Holm J.R., (1987), "Laboratory Measurements and a Theoretical Analysis of the TCT Fading Channel Radio System", IEEE Transactions on Communications, Vol. COM-35, No. 2, February, 1987, pg. 172-180.

Regalia P.A., (1991), "An Improved Lattice-Based Adaptive IIR Notch Filter", IEEE Transactions on Signal Processing, Vol. 39, No. 9, September, 1991, pg. 2124-2128.

Regalia P.A., Mitra S.K. & Vaidyanathan P.P., (1988), "The Digital All-Pass Filter: A Versatile Signal Processing Building Block", Proceedings of the IEEE, Vol. 76, No. 1, January, 1988, pg. 19-37.

Rice D.W. & Wu K.H., (1982), "Quadrature Sampling With High Dynamic Range", IEEE Transactions on Aerospace and Electronic Systems, Vol. AES-18, No. 4, November, 1982, pg. 736-739.

Robertson G., (1971), "Fast amplitude approximation for quadrature pairs", Bell System Technology Journal, Vol. 50, October, 1971, pg. 2849-2852.

Roome S.J., (1989), "Analysis of quadrature detectors using complex envelope notation", IEE Proceedings, Vol. 136, Pt. F, No. 2, April, 1989, pg. 95-100.

Roome S.J. & Griffin C., (1991), "Digital surveillance receivers", Electronics and Communication Engineering Journal, April, 1991, pg. 81-87.

Sano H., Hagiwara M. & Nakagawa M., (1990), "Phase Synchronizer for Fading Channels with the Modified Method of Least Squares", IEEE International Conference on Acoustics, Speech, and Signal Processing (ICASSP), 1990, D11.6, pg. 1659-1662.

Satio S. & Suzuki H., (1989), "Fast Carrier-Tracking Coherent Detection with Dual-Mode Carrier Recovery Circuit for Digital Land Mobile Radio Transmission", IEEE Journal on selected areas in Communications, Vol. 7, No. 1, January, 1989. pg. 130-139.

Saulnier G.J. & Rafferty W., (1990), "A Novel Demodulator/Detector for Digital and Analog Signals on LMR Channels", IEEE Transactions on Vehicular Technology, Vol. 39, No. 1, February, 1990, pg. 6-16.

Saulnier G.J., Puckette IV. C. McD., Gaus Jr. R.C., Dunki-Jacobs R.J. & Thiel T.E., (1990), "A VLSI Demodulator for Digital RF Network Applications: Theory and Results", IEEE Journal on Selected Areas in Communications, Vol. 8, No. 8, October, 1990, pg. 1500-1511.

Schiavoni M.T. & Ray R.T., (1990), "Simulation of a QPSK High Data Rate Receiver: Modelling of Tracking Loops and Adaptive Equalizer", MILCOM 1990, 1990 IEEE Military Communications Conference, Monterey, California, September 30 - October 3, 1990, pg. 29.5.1-29.5.5

Shayan Y.R. & Le-Ngoc T., (1989), "All digital phase-locked loop: concepts, design and applications", IEE Proceedings, Vol. 136, Pt. F, No. 1, February, 1989, pg. 53-56.

Schwartz M., (1981), "Information Transmission, Modulation and Noise", Third Edition, Mc Graw-Hill International Book Company, Mexico, 1981.

Simon M.K., (1986), "Dual-Pilot Tone Calibration Technique", IEEE Transactions on Vehicular Technology, Vol. VT-35, No. 2, May, 1986, pg. 63-70.

Stremler F.G., (1977), "Introduction to Communication Systems", Addison-Wesley Publishing Company, Second Edition, Massachusetts, United States of America, 1977.

Starer D. & Nehorai A., (1986), "Adaptive SSB Carrier Offset Determination", Fourth South African Symposium on Digital Signal Processing, University of Pretoria, Pretoria, South Africa, June 27, 1986, pg. 2.3.1 - 2.3.4.

Swannell J., (1986), "The Little Oxford Dictionary", Oxford University Press, Oxford, England, 1986.

Tam P.K.S. & Moore J.B., (1), (1977), "A Gaussian Sum Approach to Phase and Frequency Estimation", IEEE Transactions on Communications, Vol. COM-25, No. 9, September, 1977, pg. 935-942.

Tam P.K.S. & Moore J.B., (2), (1977), "Improved Demodulation of Sampled FM Signals in High Noise", IEEE Transactions on Communications, Vol. COM-25, No. 9, September, 1977, pg. 1052-1054.

Tan J. & Kyriakopoulos N., (1988), "Implementation of a Tracking Kalman Filter on a Digital Signal Processor", IEEE Transactions on Industrial Electronics, Vol. 35, No. 1, February, 1988, pg. 126-134.

Taub H. & Schilling D.L., (1971), "Principles of Communication Systems", McGraw-Hill International Book Company, Tokyo, Japan, 1971.

Thiel T.E. & Saulnier G.J., (1990), "Simplified Complex Digital Sampling Demodulator", Electronic Letters, Vol. 26, No. 7, 29th March, 1990, pg. 419-421.

Tran T.H., Mathews V.J. & Rushforth C.K., (1988), "A New Carrier Frequency Estimator for Modem signals", IEEE International Conference on Acoustics, Speech, and Signal Processing (ICASSP), 1988, D11.9, pg. 1886-1889.

Tufts D.W. & Rao R.M., (1977), "Frequency Tracking by MAP Demodulation and by Linear Prediction Techniques", Proceedings of the IEEE (Letters), Vol. 65, August, 1977, pg. 1220-1221.

Vaughan R.G., (1986), "Signals in Mobile Communications: A Review", IEEE Transactions on Vehicular Technology, Vol. VT-35, No. 4, November, 1986, pg. 133-145.

Vaughan R.G., Scott N.L. & White D.R., (1991), "The Theory of Bandpass Sampling", IEEE Transactions on Signal Processing, Vol. 39, No. 9, September, 1991, pg. 1973-1984.

Volder J.E., (1959), "The CORDIC Trigonometric Computing Technique", IRE Transactions on Electronic Computers, Vol. EC-8, No. 3, September, 1959, pg. 330-334.

Weber III W.J., (1976), "Performance of Phase-Locked Loops in the Presence of Fading Communication Channels", IEEE Transactions on Communications, Vol. COM-2, No. 5, May, 1976, pg. 487-499.

Yassa F.F. & Thompson B.A., (1989), "Adaptive Phase-Insensitive Amplitude Demodulator for noncoherent DSBSC signals", IEEE International Conference on Acoustics, Speech, and Signal Processing (ICASSP), 1986, D8.12, pg. 1231-1234.

Yassa F.F. & Garverick S.L., (1990), "A Multichannel Digital Demodulator for LVDT/RVDT Position Sensors", IEEE Journal of Solid-State Circuits, Vol. 25, No. 2, April 1990, pg. 441-450.

Ziemer R.E. & Tranter W.H., (1976), "Principles of Communications", Houghton Mifflin Company, London, England, 1976.

Zurawski J.H.P. & Gosling J.B., (1987), "Design of a High-Speed Square Root Multiply and Divide Unit", IEEE Transactions on Computers, Vol. C-36, No. 1, January, 1987, pg. 13-23.

APPENDIX 1 A COMPARISON OF THE SIGNAL TO NOISE PERFORMANCE OF THREE CLASSICAL AM DEMODULATORS.

This appendix is a comparison of the demodulated signal to noise power to the input carrier signal to noise power for three different classical AM demodulators. The three AM demodulators are the square law demodulator, the linear demodulator and the synchronous demodulator. Use is made of the signal to noise performance curves for the linear and square law AM demodulators provided by Middelton [1987, pg. 539-598].

An interesting study carried out by Pollack & Pickett [1959] on the intelligibility of speech in high noise levels shows that for a 5 dB **signal to noise power ratio** (SNR) 75% word recognition is possible. Based on this study, the subjective assumption is made that this is the maximum error that can be tolerated in a message. In certain applications lower signal to noise ratios are usable.

Assuming that a listener requires a minimum 5 dB SNR at the output of the demodulator in order to understand the transmission, it is shown that for this condition the linear AM demodulator operates above its theoretical threshold and thus has the same signal to noise performance as a synchronous AM demodulator. The measured **output signal to noise power ratio** (SNR_O) performance of the linear, quadrature, multirate AM demodulator is described in section 3.2.3 and shows excellent correspondence with Middelton's theoretical analysis.

An AM signal sinusoidally modulated is defined as

$$V_i(t) = A_c(1 + m\cos\omega_m t)\cos\omega_c t \ . \qquad (A.1\text{-}1)$$

Assuming a 1 ohm load the total average power is given by

$$\overline{V}_i(t)^2 = \frac{A_c^2}{2} + \frac{m^2 A_c^2}{4} \ . \qquad (A.1\text{-}2)$$

from whence the efficiency μ in the transmission is derived. The efficiency μ is defined as the ratio of the power in the sidebands to the total signal power and is given by

$$\mu = \frac{m^2}{2+m^2} \ . \qquad \text{(A.1-3)}$$

Hence for $m = 1$, 33% of the total power is transmitted in the sidebands and 67% in the carrier. The total power in the sidebands is then 3 dB less than the power in the carrier and hence for 5 dB SNR_o an 8 dB **carrier to noise power ratio** (CNR_i) is required. The SNR_o and CNR_i are defined by equations A.1-4 and A.1-5 as follows,

$$SNR_o = 10\log\frac{P_o}{N_o} \ \text{dB.} \qquad \text{(A.1-4)}$$

P_o is the output demodulated signal power in watts while N_o is the total output noise power in watts within the demodulated signal's bandwidth, typically 300 Hz to 2,7 kHz.

$$CNR_i = 10\log\frac{C_i}{N_i} \ \text{dB,} \qquad \text{(A.1-5)}$$

where C_i is the input carrier signal power in watts while N_i is the total input noise power in watts within the demodulated signal's bandwidth, typically 300 Hz to 2,7 kHz. A similar analysis for $m = 0,6$ results in 12 dB CNR_i for 5 dB SNR_o.

Taken from Middelton [1987, pg 568 & 573], figure A.1.1 is the theoretical SNR_o performance of the linear AM demodulator while figure A.1.2 describes the SNR_o performance of the square law demodulator. The graphs clearly indicate the threshold effect caused by the demodulator structures. Essentially, synchronous AM demodulation results in straightening the curves which would then be parallel with the line added, which passes through the origin. For a demodulator SNR_o of 5 dB or greater it is apparent from figure A.1.1 that the linear demodulator operates well above its theoretical threshold (ie: for a modulation index of 1, a CNR_i of 8 dB is required for a 5 dB SNR_o). However, as shown in figure A.1.2, the square law demodulator

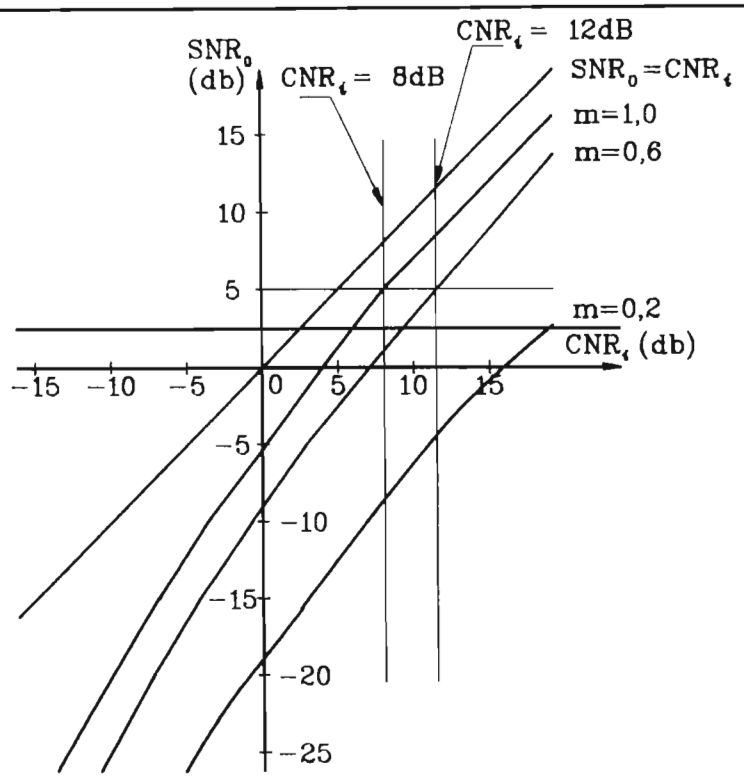

Figure A.1.1 SNR_o versus CNR_i for a sinusoidally modulated carrier in noise through a linear AM demodulator.

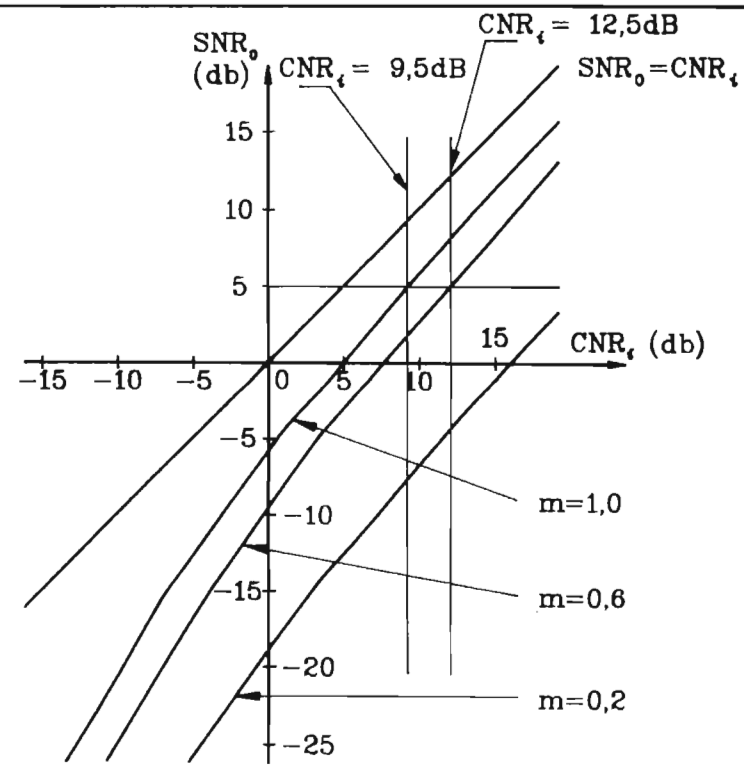

Figure A.1.2 SNR_o versus CNR_i for a sinusoidally modulated carrier in noise through a square law AM demodulator.

operates in the region of its threshold and a degradation of approximately 1 to 2 dB is expected (ie: for a modulation index of 1 a CNR_i of 9,5 dB results in a 5 dB SNR_o). Generally analogue demodulators (ie: the diode) are an approximation to either the linear or square law demodulator and normally a degraded performance is experienced.

APPENDIX 2 A SAMPLE PROGRAM OF THE CORDIC ALGORITHM TO OBTAIN THE MODULUS OF THE COMPLEX NUMBER.

Due to the multi-option structure of the Cordic algorithm it is easier to understand the algorithm by following pseudo-code rather than a flowchart.

```
*
* The program begins here, the I signal is in the variable
* IND1 and the Q signal is in the variable QND1. XST1, XST2,
* YST1 and YST2 are general variables. "*" indicates a comment
* within the program.
*
            BRANCH to L0POS IF IND1 is greater than zero
            ELSE continue
*
* The section of code if the Y vector is negative
*
L0NEGF      XST1 = -IND1              * First level of accuracy
            YST1 =  QND1
            BRANCH to L1POSF IF YST1 is greater than zero
            ELSE continue
*
L1NEGF      XST2 = XST1 - YST1        * Second level of accuracy
            YST2 = YST1 + XST1
            BRANCH to L2POSF IF YST2 is greater than zero
            ELSE continue
*
L2NEGF      XST1 = XST2 - YST2/2      * Third level of accuracy
            YST1 = YST2 + XST2/2
            BRANCH to L3POSF IF YST1 is greater than zero
            ELSE continue
*
L3NEGF      XST2 = XST1 - YST1/4      * Fourth level of accuracy
```

```
            YST2 = YST1 + XST1/4
            BRANCH to L4POSF IF YST2 is greater than zero
            ELSE continue
*
L4NEGF      XST1 = XST2 - YST2/8        * Fifth level of accuracy
            YST1 = YST2 + XST2/8
            BRANCH to L5POSF IF YST1 is greater than zero
            ELSE continue
*
L5NEGF      XST2 = XST1 - YST1/16       * Sixth level of accuracy
            YST2 = YST1 + XST1/16
            BRANCH to L6POSF IF YST2 is greater than zero
            ELSE continue
*
L6NEGF      XST1 = XST2 - YST2/32       * Seventh level of accuracy
            YST1 = YST2 + XST2/32
            BRANCH to L7POSF IF YST1 is greater than zero
            ELSE continue
*
L7NEGF      XST2 = XST1 - YST1/64       * Eighth level of accuracy
            YST2 = YST1 + XST1/64
            BRANCH to VECOUF
*
* The Section if the Y vector is positive
*
L0POSF      XST1 = IND1                 * First level of accuracy
            YST1 = -QND1
            BRANCH to L1NEGF IF YST1 is less than zero
            ELSE continue
*
L1POSF      XST2 = XST1 + YST1          * Second level of accuracy
            YST2 = YST1 - XST1
            BRANCH to L2NEGF IF YST2 is less than zero
            ELSE continue
```

```
*
L2POSF      XST1 = XST2 + YST2/2        * Third level of accuracy
            YST1 = YST2 - XST2/2
            BRANCH to L3NEGF IF YST1 is less than zero
            ELSE continue
*
L3POSF      XST2 = XST1 + YST1/4        * Fourth level of accuracy
            YST2 = YST1 - XST1/4
            BRANCH to L4NEGF IF YST2 is less than zero
            ELSE continue
*
L4POSF      XST1 = XST2 + YST2/8        * Fifth level of accuracy
            YST1 = YST2 - XST2/8
            BRANCH to L5NEGF IF YST1 is less than zero
            ELSE continue
*
L5POSF      XST2 = XST1 + YST1/16       * Sixth level of accuracy
            YST2 = YST1 - XST1/16
            BRANCH to L6NEGF IF YST2 is less than zero
            ELSE continue
*
L6POSF      XST1 = XST2 + YST2/32       * Seventh level of accuracy
            YST1 = YST2 - XST2/32
            BRANCH to L7NEGF IF YST1 is less than zero
            ELSE continue
*
L7POSF      XST2 = XST1 + YST1/64       * Eighth level of accuracy
            YST2 = YST1 - XST1/64
*
* The end of the calculation, the modulus in stored in
* location XST2.
*
```

```
VECOUF        MOD = XST2
*
END.
```

APPENDIX 3 A SIGNAL TO NOISE PERFORMANCE ANALYSIS OF THE LIMITER/ DISCRIMINATOR FM DEMODULATOR.

Within this appendix a graph is presented for the expected signal to noise performance of the limiter/ discriminator FM demodulator for two FM modulation indices. Ziemer & Tranter [1976, pg. 285-289] derive an equation which approximates the SNR_o of the limiter/ discriminator as a function of the modulation index (β) and the ratio of the carrier power (C_i) to noise power (N_i). The equation, which does not include the effects of preemphasis or deemphasis filtering, assumes sinusoidal modulation and is given by

$$SNR_o \approx 10\log\left\{\frac{(3\beta^2(C_i/N_i))/2}{1+(12\beta/\pi)(C_i/N_i)(\exp(-(C_i/N_i)/2(\beta+1)))}\right\} . \quad (A.3\text{-}1)$$

SNR_o is the output SNR of the demodulated signal, which when measured, is defined as

$$SNR_o = 10\log\frac{P_o}{N_o} , \quad (A.3\text{-}2)$$

where P_o is the output demodulated signal power in watts while N_o is the total output noise power in watts within the demodulated signal's bandwidth, typically 300 Hz to 2,7 kHz. The CNR_i at the input to the limiter is defined as

$$CNR_i = 10\log\frac{C_i}{N_i} , \quad (A.3\text{-}3)$$

where C_i is the input unmodulated carrier signal power in watts while N_i is the total input noise power in watts adjusted for the demodulated signal's bandwidth, typically 300 Hz to 2,7 kHz.

Figure A.3.1 is a graph of equation A.3-1 for two values of β. The graph clearly exhibits the FM noise enhancement when the CNR_i is large, however as the CNR_i decreases the exp function in the denominator of equation A.3-1 becomes dominant which implies a demodulator threshold. In section 4.2.3 figure A.3.1 is compared to the measured performance of the low sampling rate DSP FM demodulator.

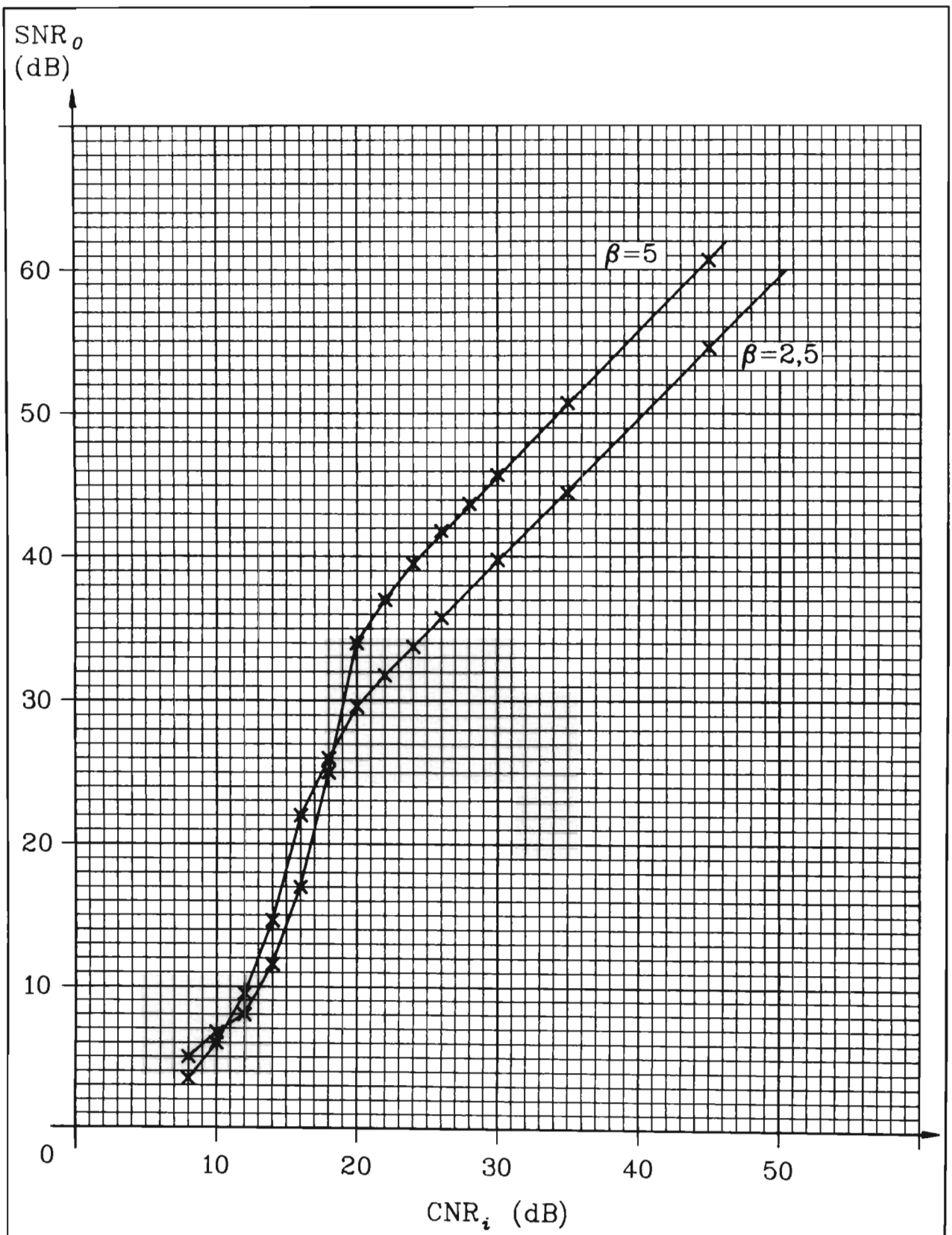

Figure A.3.1 A graph of the calculated CNR_i versus SNR_o through a limiter/discriminator FM demodulator.

APPENDIX 4 A SAMPLE PROGRAM OF THE MULTIRATE AM DEMODULATOR.

Within this appendix a pseudo-code program of the multirate AM demodulator is presented. The program's general software block diagram is described by figure 3.6. The initialization is included as correct sequencing of the subroutines is important. The same naming convention of the subroutines, as described by figure 3.6, is employed in the pseudo-code.

```
*
* The program begins here with initialization.
* The initialization includes setting up the addresses of the
* first decimation subroutines. DEC1 is a variable which contains
* the address of the subroutine for the first level of decimation
* ie: decimation by two. DEC2 is a similar variable for the second
* level of decimation ie: decimation by four.
*
            STORE (1) in DEC1
            STORE (i) in DEC2
            ENABLE interrupts          * Enable sampling interrupt
*
WAIT        BRANCH to WAIT             * Wait for the interrupt
*
* The main interrupt routine execute every 20 microseconds.
*
INTER       SAMPLE the A/D             * Subroutine (A) sample A/D
            BRANCH to subroutine specified by DEC1
            BRANCH to subroutine specified by DEC2
            ENABLE interrupts
            RETURN to wait loop.
*
* The two subroutines in the first level of decimation.
* These subroutines include the two filters H1(z)
* and H2(z). IFSIG is the 50 kHz sampled AM signal.
```

```
*
* The filter H2(z) where QND1 and QFD1 are storage
* variables. TEMP is a temporary variable.
*
(1)          TEMP = IFSIG + QND1          * The filter.
             QND1 = TEMP x B^2 - QFD1
             QFD1 = IFSIG
             STORE (2) in DEC1            * Setting up the decimation
             RETURN to INTER              * address.
*
* The filter H1(z) where IND1 and IFD1 are storage
* variables. TEMP is a temporary variable.
*
(2)          TEMP = IFSIG + IND1          * The filter.
             IND1 = TEMP x A^2 + IFD1
             IFD1 = IFSIG
             STORE (1) in DEC1            * Setting up the decimation
             RETURN to INTER              * address.
*
* The next group of four subroutines is the second level
* of decimation ie: decimation by four.
*
* The FIRST subroutine includes finding the modulus of the complex
* number. MAX and MIN are temporary variables and the
* demodulated AM signal is stored in AMDEM.
*
(i)          MAX = |IND1|
             MIN = |QND1|
             TEMP = MAX - MIN             * Test which half of circle.
             BRANCH to TESTOK if TEMP is greater than zero
             ELSE continue
*
             TEMP = MIN                   * Swop if test failed.
             MIN = MAX
```

```
            MAX = TEMP
*
TESTOK      TEMP = MAX x 0,414 - MIN  * Test for quadrant.
            BRANCH to AMRH1 if TEMP is greater than zero
            ELSE continue
*
* The second quadrant
*
AMRH2       TEMP = MAX x 0,668 - MIN  * Test for subsector
            BRANCH to AMRQ3 if TEMP is greater than zero
            ELSE continue
*
* Fourth subsector
*
AMRQ4       AMDEM = MAX x 0,774 + MIN x 0,635
            STORE (ii) in DEC2        * Setting up the decimation
            RETURN to INTER           * address.
*
* Third subsector
*
AMRQ3       AMDEM = MAX x 0,884 + MIN x 0,472
            STORE (ii) in DEC2        * Setting up the decimation
            RETURN to INTER           * address.
*
* The first quadrant.
*
AMRH1       TEMP = MAX x 0,198 - MIN  * Test for subsector
            BRANCH to AMRQ1 if TEMP is greater than zero
            ELSE continue
*
* Second subsector
*
AMRQ2       AMDEM = MAX x 0,959 + MIN x 0,290
            STORE (ii) in DEC2        * Setting up the decimation
```

```
            RETURN to INTER             * address.
*
* First subsector
*
AMRQ1       AMDEM = MAX x 0,997 + MIN x 0,098
            STORE (ii) in DEC2          * Setting up the decimation
            RETURN to INTER             * address.
*
* The SECOND subroutine which includes the AGC.
*
(ii)        AGC function.
            STORE (iii) in DEC2         * Setting up the decimation
            RETURN to INTER             * address.
*
* The THIRD subroutine which includes the Squelch.
*
(iii)       Squelch function
            STORE (iv) in DEC2          * Setting up the decimation
            RETURN to INTER             * address.
*
* The FOURTH subroutine which includes the Serial
* communications with host.
*
(iv)        Serial communications
            STORE (i) in DEC2           * Setting up the decimation
            RETURN to INTER             * address.
*
END.
```

APPENDIX 5 A SAMPLE PROGRAM OF THE LOW SAMPLING RATE FM DEMODULATOR.

This appendix includes the pseudo-code of the low sampling rate FM demodulator while the block diagram of the program is described by figure 4.6.

```
*
* The program begins here. Once the microprocessor
* is interrupted it branches from the WAIT loop to the
* INTER subroutine which is the FM demodulator.
*
WAIT        BRANCH to WAIT
*
* The interrupt routine which is processed every 20
* microseconds.
*
INTER       SAMPLE the A/D
*
* The eighth order FIR differentiator.
* TEMP is a temporary variable and FMDIF7 to FMDIF0
* are the FIR differentiator variables.
*
            TEMP = 0
            TEMP = TEMP + FMDIF7 x 0,0054
            FMDIF7 = FMDIF6
            TEMP = TEMP + FMDIF6 x -0,0212
            FMDIF6 = FMDIF5
            TEMP = TEMP + FMDIF5 x 0,0913
            FMDIF5 = FMDIF4
            TEMP = TEMP + FMDIF4 x -0,9899
            FMDIF4 = FMDIF3
            TEMP = TEMP + FMDIF3 x 0,9899
            FMDIF3 = FMDIF2
```

```
            TEMP = TEMP + FMDIF2 x -0,0913
            FMDIF2 = FMDIF1
            TEMP = TEMP + FMDIF1 x 0,0212
            FMDIF1 = FMDIF0
            TEMP = TEMP + FMDIF0 x -0,0054
            FMDIF0 = IFSIG
*
* The eleventh order FIR DHT.
* FMSIG is the input into the FIR DHT and FMDHT10 to
* FMDHT0 are the FIR DHT variables.
*
            FMSIG = TEMP
            TEMP = 0
            TEMP = TEMP + FMDHT10 x -0,0261
            FMDHT10 = FMDHT9
            FMDHT9 = FMDHT8
            TEMP = TEMP + FMDHT8 x -0,1276
            FMDHT8 = FMDHT7
            FMDHT7 = FMDHT6
            TEMP = TEMP + FMDHT6 x -0,6032
            FMDHT6 = FMDHT5
            FMDHT5 = FMDHT4
            TEMP = TEMP + FMDHT4 x 0,6032
            FMDHT4 = FMDHT3
            FMDHT3 = FMDHT2
            TEMP = TEMP + FMDHT2 x 0,1276
            FMDHT2 = FMDHT1
            FMDHT1 = FMDHT0
            TEMP = TEMP + FMDHT0 x 0,0261
            FMDHT0 = FMSIG
*
* Finding the modulus of the complex number.
* MAX and MIN are temporary variables and the demodulated
* FM signal is stored in FMDEM.
```

```
*
            MAX = |TEMP|
            MIN = |FMDHT6|
            TEMP = MAX - MIN          * Test which half of circle.
            BRANCH to TESTOK if TEMP is greater than zero
            ELSE continue
*
            TEMP = MIN                * Swop if test failed.
            MIN = MAX
            MAX = TEMP
*
TESTOK      TEMP = MAX x 0,414 - MIN  * Test for quadrant.
            BRANCH to FMRH1 if TEMP is greater than zero
            ELSE continue
*
* The second quadrant
*
FMRH2       TEMP = MAX x 0,668 - MIN  * Test for subsector
            BRANCH to FMRQ3 if TEMP is greater than zero
            ELSE continue
*
* Fourth subsector
*
FMRQ4       FMDEM = MAX x 0,774 + MIN x 0,635
            OUTPUT FMDEM              * Output to D/A.
            RETURN to WAIT            * End of computation.
*
* Third subsector
*
FMRQ3       FMDEM = MAX x 0,884 + MIN x 0,472
            OUTPUT FMDEM              * Output to D/A.
            RETURN to WAIT            * End of computation.
*
* The first quadrant.
```

```
*
FMRH1       TEMP = MAX x 0,198 - MIN  * Test for subsector
            BRANCH to FMRQ1 if TEMP is greater than zero
            ELSE continue
*
* Second subsector
*
FMRQ2       FMDEM = MAX x 0,959 + MIN x 0,290
            OUTPUT FMDEM              * Output to D/A.
            RETURN to WAIT            * End of computation.
*
* First subsector
*
FMRQ1       FMDEM = MAX x 0,997 + MIN x 0,098
            OUTPUT FMDEM              * Output to D/A.
            RETURN to WAIT            * End of computation.
END.
```

APPENDIX 6 SSB-SC SYSTEM CONSIDERATIONS.

The purpose of this appendix is to introduce pertinent system considerations which affect the SSB-SC IIR-ALE/DPLL AFC algorithm. The first subsection discusses the statistical nature of a stationary and mobile communication link. A simple mobile communications channel model is presented which allows the assessment of the AFC algorithm in a short-term fading environment as a first measure of the performance of the SSB-SC AFC algorithm. The second subsection compares the different suppressed carrier configurations. It is concluded that tone-above-band is the most suitable compromise when simple, transparent SSB-SC communications is required.

6.1 THE MOBILE COMMUNICATIONS CHANNEL.

A signal transmitted to a mobile unit suffers propagation path losses; these are caused by the direct-path attenuation and the topography of the surrounding terrain. Generally for a mobile unit the signal is subjected to both long-term and short-term fading. Long-term fading is caused by radiation path losses and small variations in the surrounding topography; while short-term fading occurs due to stationary and moving signal scatterers and is therefore known as multipath fading. Since all the communication between a base station and a mobile unit occurs at ground level, and often within an urban environment, multipath fading is an important consideration [Lee, 1982, pg. 15-21]. A typical graph of the received signal power as a mobile unit travels through an urban environment is given in figure A.6.1. As the vehicle travels further from the source the general trend of the received power is to decrease. Within the sensitivity limits of the receiver these slow signal power fluctuations are corrected for by a slow responding feed back automatic gain control system.

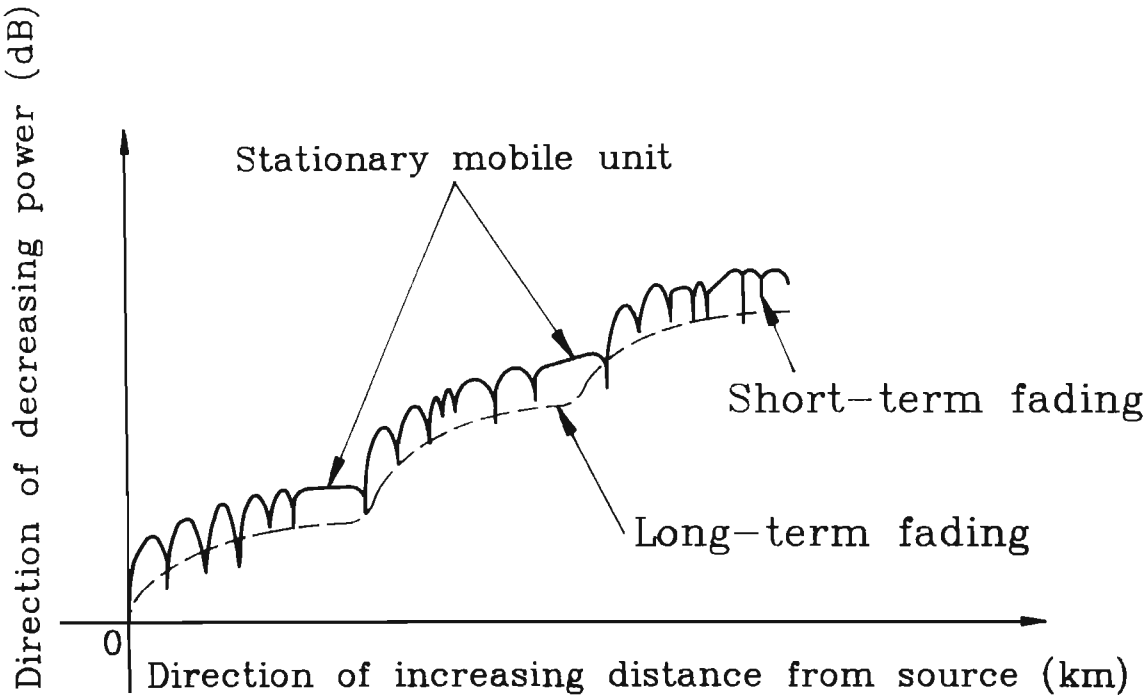

Figure A.6.1 The typical trend of the received power for a mobile unit.

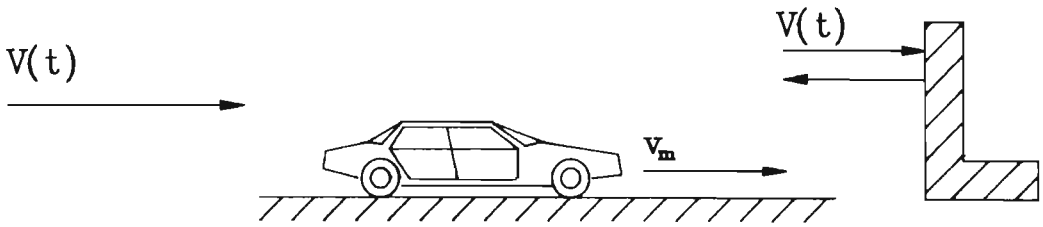

Figure A.6.2(a) A single signal scatterer.

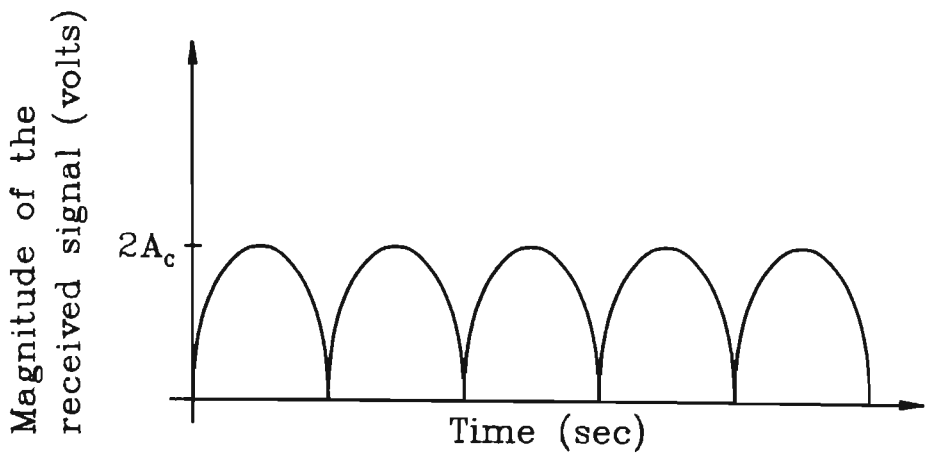

Figure A.6.2(b) The signal fading caused by a standing wave [Lee, 1982, pg. 29].

Of equal importance are the short-term signal power variations superimposed on the general trend, which are reviewed in greater detail in the following paragraphs.

When considering multipath fading caused by signal scatterers Lee [1982, pg. 25-33] suggests three situations. Firstly the mobile unit and surrounding scatterers are stationary, which is similar to the portable role of a transceiver. Secondly the mobile unit is stationary but the surrounding scatterers are in motion and thirdly the mobile unit and scatterers are in motion. In the first situation he shows that since constant propagation paths are established the received signal's amplitude and phase remains unchanged in time. Even in a portable application this is the perfect situation, and therefore it is preferably assumed that the received signal's amplitude and phase varies slowly with respect to time. In the second situation, where it is assumed that the motion of the surrounding scatterers is random, the amplitude and phase of the received signal are corrupted with the statistics of narrowband thermal noise [Lee, 1982, pg. 33-40]. Since this condition essentially occurs when both the mobile unit and surrounding scatterers are in motion the third situation is considered in greater detail.

In the situation where the mobile unit and scatterers are in motion Lee [1982, pg. 28-30] again considers three situations. Firstly the absence of scatterers, secondly a single scatterer and thirdly many scatterers in the vicinity of the mobile unit. In the situation of no scatterers the signal received by a mobile unit is given by

$$V_r(t) = A_c \cos(\omega_c t + \phi - 2\pi f_D t) \ , \qquad \text{(A.6-1)}$$

where $A_c \cos(\omega_c t + \phi)$ is the carrier signal. From equation A.6-1 it is apparent that an additional frequency component is added as a result of the motion of the mobile unit, which is referred to as the Doppler frequency and is defined as

$$f_D = f_{PD} \cos\theta_D \ , \qquad \text{(A.6-2)}$$

where f_{PD} is the peak Doppler frequency given by

$$f_{PD} = \frac{v_m}{\lambda_c} , \qquad (A.6\text{-}3)$$

and v_m is the velocity of the mobile unit, and $\lambda_c$the wavelength of the carrier. The angle of incidence of the received signal is defined by $\cos\theta_D$ and where multiple scatterers are found θ_D assumes a random distribution, resulting in a Doppler frequency spread. It is instructive, see figure A.6.2 (a), to consider the special situation of a single, perfect reflecting scatterer, whose reflection has a zero angle of incidence. Lee [1982, pg. 29] derives the envelope of the received signal which is plotted in figure A.6.2 (b). The magnitude of the signal is given by

$$|V_i(t)| = |2A_c \sin(2\pi f_{PD} t - \omega_c T_p/2)| , \qquad (A.6\text{-}4)$$

where T_p is the time for the wave to travel to the scatterer and return to the mobile unit. The fade rate of the received signal is determined by the Doppler frequency and perfect cancellation occurs when $2\pi f_{PD} t = n\pi + \omega_c T_p/2$, which results in infinite depth power nulls. In reality, since multiple scatterers are present, perfect cancellation seldom occurs, and power nulls are typically of the order of -5 to -30 dB, relative to the average received signal power [Lee, 1982, pg. 175]. Although this simplified fading model does not take into consideration the statistical nature of the multipath fading or the random phase changes, it is a useful as the first measure of a SSB-SC AFC algorithm's performance.

Lee [1982, pg. 169-184] derives the **probability density function** (pdf) of the envelope of a short-term fading signal by assuming that the multiple scatterers are random, Gaussian and independent processors. The pdf ($p(A_c)$) is given by

$$p(A_c) = \frac{A_c}{\sigma^2} \exp\left(-\frac{A_c^2}{2\sigma^2}\right) , \qquad (A.6\text{-}5)$$

where A_c is the instantaneous magnitude of the short-term time varying envelope of the received signal and σ is the standard deviation of a Gaussian distribution. This derivation is based on the removal of the long-term fading component of the signal which requires calculating the running mean of the received signal. Interestingly, Lee suggests [1982, pg. 103-105] that a sample window of between 40 and 200 wavelengths be utilized to calculate the running mean, and this essentially determines the required time response of a feedback automatic gain control system for a mobile communications link.

Equation A.6-5 describes the Rayleigh probability density function and it is generally assumed by mobile communication engineers that the statistics of the envelope of the received signal, suffering from multipath short-term fading, match this pdf [Cavers, (1), 1991]. A direct line-of-sight from the transmitter to the receiver or an effective reflector normally results in a dominant single incident signal. Under these conditions the envelope pdf varies from a Rayleigh to a Rician distribution [Vaughan, 1986]. Figure A.6.3 is a graph of the percentage probability that the amplitude of the received signal is less than a particular reference, typically taken as the average power (0 dB) of the Rayleigh fading signal. From the graph it is seen that the probability of deep fades, greater than -20 dB is less than 1%. A second important result derived from the pdf of the Rayleigh fading signal is the level crossing rate. Figure A.6.4 is a graph describing the expected number of level crossings per second (normalized by the Doppler frequency) versus the signal level relative to the average signal power (0 dB). For example, only 20% of the total number of fades for a Rayleigh fading signal are greater than -15 dB.

The effect of the channel on the received signal's phase results in a uniform distribution between 0 and 2π. The absolute phase prescribes a random walk with frequent steps of random polarity. Generally the absolute phase of the received signal is unimportant but rather its first derivative with respect to distance travelled.

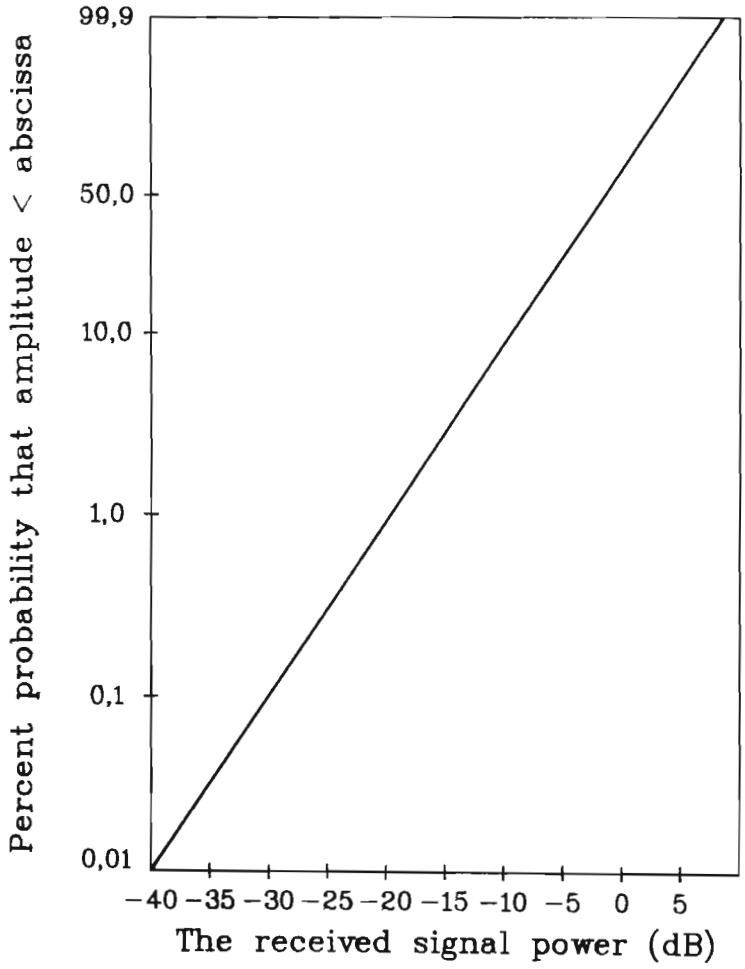

Figure A.6.3 The statistical properties of a Rayleigh fading signal [Lee, 1982, pg. 175].

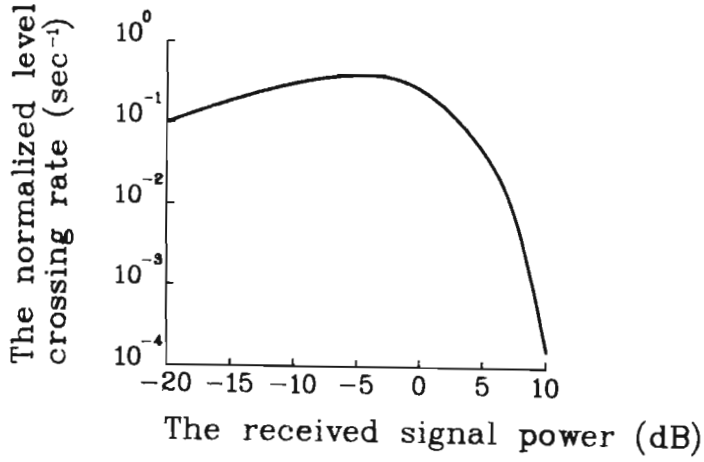

Figure A.6.4 The level crossing rate of a Rayleigh fading signal [Lee, 1982, pg. 183].

The random phase polarity steps, which are associated with the deep signal fades, result in random FM independent of SNR_i. However, as the envelope pdf tends towards a Rician distribution the occurrence of the random phase polarity steps, decreases [Vaughan, 1986]. It is apparent from the discussion of the statistical nature of the mobile communications channel that the simple amplitude fading model described by equation A.6-4 is limited. There are two accepted approaches to determine the performance of a system for a mobile communications channel. The first approach is to use samples of the signal applied to an actual channel; this approach has obvious limitations in terms of repeatability of the experiment and the need for numerous samples taken under various conditions. The second approach is channel simulation which also has its limitations depending on the channel model selected, although the results are repeatable. For this reason the SSB-SC AFC system described in chapter 5 is evaluated for three conditions; a portable (or stationary) communications link, the simple amplitude fading model describe by equation A.6-4 and a Rayleigh fading model employing Casas & Leung's [1990] channel simulator.

6.2 WHICH CONFIGURATION; PC, TIB, TAB, TTIB....?

Current research in SSB-SC mobile communications has generally focused on the following system parameters; position of the pilot, the bandwidth and spectral shape of the carrier filter and the relative amplitude of the pilot. Early research was more preoccupied with SSB speech communications [Garner & Gibson, 1981], however the current research emphasis is on SSB data communications and the effect that the system parameters have on the bit error rate [Rafferty, Anderson, Saulnier & Holm, 1987]. Pilot based SSB communication configurations are generally grouped into three different categories namely, **pilot carrier** (PC), **tone-in-band** (TIB) and **tone-above-band** (TAB) and they differ in the positioning of the pilot, as shown in figure A.6.5. Consequently

the objective of this section is to review and compare the advantages and disadvantages of the different proposed system configurations, and thereafter select the most suitable option.

Garner & Gibson [1981] provide an early reference to PC SSB communications where they describe some of the practical advantages of this configuration as being:-

1. The configuration is compatible with AM, and asynchronous demodulation (albeit the audio signal is distorted) with existing receivers is possible.

2. Filtering of the demodulated pilot is simple as it results in a DC component, and the pilot's frequency position does not interfere with the demodulated audio signal.

However the disadvantages of the PC configuration include:-

1. In modern transceivers the synthesizer creates discrete LO frequencies and typically the resolution determines the channel spacing. Leakage of these LO components result in spurious, low level signals at the PC frequency. In AM transmission, due to the modulation index, these components are relatively small and hence cause no interference. However, in suppressed carrier transmission, the pilot power is typical 10 dB less than the **peak envelope power** (PEP) of the transmitted audio signal [Ball & Holmes, 1981] and thus, in marginal conditions, these spurious components cause interference.

2. The differential group delay at the edges of a typical SSB crystal filter is greater than at the centre of the filter. This results in a timing mismatch between the PC and audio signal if a feedforward AGC is employed to reduce the effects of multipath fading.

3. The correlation between the PC and the audio signal also decreases as the frequency difference increases, due to the limited coherence bandwidth of the channel [Lee, 1982, pg. 44-45].

To overcome these problems researchers have suggested various TIB configurations, but the tone within the audio band introduces a host of other problems which include:-

1. In SSB speech communications the TIB signal is filtered by a narrowband notch filter to prevent audio interference. Loss in pilot acquisition, which can occur during fading, causes interference to the listener [Garner & Gibson, 1981]. Furthermore, McGeehan & Lymer [1981] discuss the interference effects of the speech on a phase-locked receiver which are compounded by a TIB configuration.

2. TIB has gained popularity for coherent terrestrial and satellite-aided data mobile communications [Davarian, 1987]. The pilot is conveniently placed within the audio band and it is assumed that the fading impairments on the data and pilot are the same. In the receiver the pilot is then extracted, amplitude normalized and used as a coherent reference in a synchronous data demodulator. Although frequency offsets between the transmitter and receiver need to be corrected [Cavers, (1), 1991], phase-locking becomes unnecessary as the pilot is the coherent reference. The pilot signal is normally placed in a null created by Manchester encoding of the data signal [Rafferty, Anderson, Saulnier & Holm, 1987]. However the problem with encoding the data signal is that it generally increases the transmission bandwidth. Hladik, Saulnier & Rafferty [1989] proposed a Tone-Aided Dual Vestigial Sideband configuration to reduce the bandwidth but with added demodulator complexity and phase-locking in the receiver.

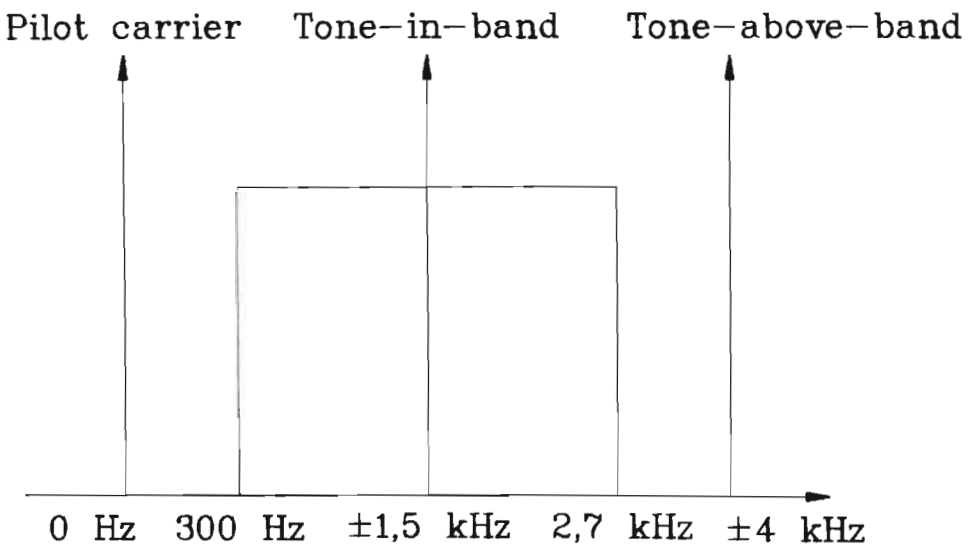

Figure A.6.5 The relative position of PC, TIB and TAB pilot signals.

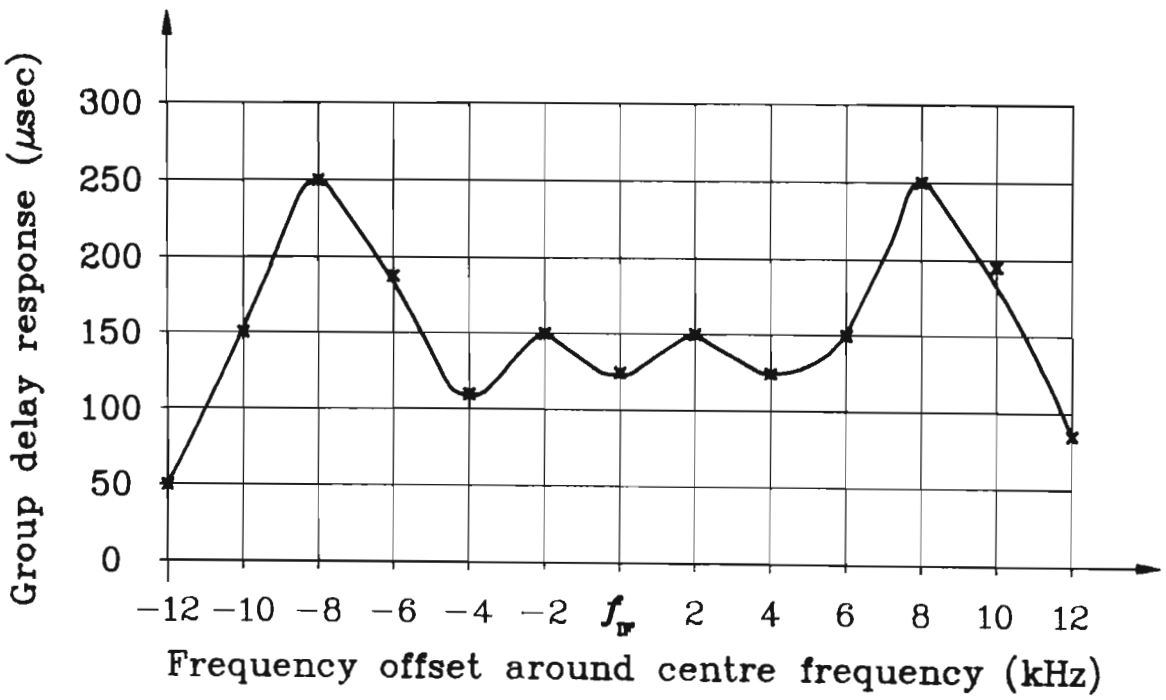

Figure A.6.6 The group delay response of a typical FM IF crystal filter.

Simon [1986] discusses a **dual-pilot tone calibration** (DPTCT) scheme where he places a pilot above and below the data spectrum in order to reduce the bandwidth requirement. However, this scheme is less power efficient than single carrier schemes and more susceptible to IF SSB filter differential group delay distortion.

3. A further problem with a TIB configuration is that it is not transparent to other peripheral communication equipment. Two schemes which overcome this problem are **Transparent Tone-in-Band** (TTIB) and **pilot symbol assisted modulation** (PSAM). TTIB was first proposed by McGeehan & Bateman [1984] and later adapted for data signals by Cavers [(2), 1991]. TTIB requires splitting the audio spectrum into two discrete frequency bands using filters and mixers. The pilot is inserted in the null created, and in the receiver the pilot is used to phase-lock a LO which, after filtering, recombines the two sidebands. The PSAM system requires the transmission of periodic data words which are used in the receiver to correct for the frequency and phase errors. However both systems increase both the complexity of the transmitter, and receiver.

TAB, which is the third group of suppressed carrier schemes, suffers from similar limitations as the PC configuration. These limitations include; degraded differential group delay response at the edges of the SSB IF crystal filter, increase in the transmitted signal's bandwidth, and degraded correlation between the pilot and the audio signal due to limited channel coherence bandwidth.

In the design of a multimode transceiver, the bandwidth and differential group delay response of the analogue second IF crystal filter is defined by the modulation scheme which requires the widest bandwidth, namely FM. Figure A.6.6 is a graph of the group delay response of a typical FM crystal filter which is relatively constant except for the edges of the filter. The SSB filtering then occurs within the DSP IF stage [Carter, 1988] and therefore the differential group delay of

the digital IF filter can be minimized by employing suitable IF filter design techniques, structures or simple static group delay equalization. Furthermore, as the SSB filter is implemented in software no variation in the filter performance occurs between different transceivers.

The channel coherence bandwidth is considered in detail by Leland & Sollenberger [1980] in their design of a mobile UHF feedforward AGC. They derive an equation for the complex envelope correlation (C_E) which is a function of the RF angular frequency separation (ω_{cs}) and the urban time delay spread (T_{Dt}) and is given by

$$C_E^2 = \frac{1}{1 + \omega_{cs}^2 T_{Dt}^2} \quad . \qquad (A.6\text{-}6)$$

This results in a correlation of 0,995, for a separation of 5 kHz and a 3 microsecond urban time delay spread. This time delay spread is considered to be a "worst case" condition for an urban environment and has a 1% probability of occurrence. Thus, although a TAB configuration increases the transmitted signal's bandwidth, it is recommended, since it has little effect on the transmitter's architecture and results in a simple transparent communications link.